STRATEGIC PLANNING FOR SERVICE-BASED ADVANCED AIR MOBILITY SYSTEMS UNDER UNCERTAINTY: MODELS, METHODS AND APPLICATIONS

ZHONGYI JIN

PhD

The Hong Kong Polytechnic University

2025

The Hong Kong Polytechnic University

Department of Aeronautical and Aviation Engineering

Strategic Planning for Service-Based Advanced Air Mobility Systems Under Uncertainty: Models, Methods and Applications

Zhongyi Jin

A thesis submitted in partial fulfillment of the requirements for the degree of Doctor of Philosophy

March 2025

CERTIFICATE OF ORGINALITY

I hereby declare that this thesis is my own work and that, to the best of my knowledge and belief, it reproduces no materials previously published or written, nor material that has been accepted for the award of any other degree or diploma, except where due acknowledgement has been made in the text.

_____ (Signed)

JIN Zhongyi (Name of student)

Abstract

National Aeronautics and Space Administration's Advanced Air Mobility (AAM) initiative is set to transform our communities by enabling the movement of people and goods from the ground to the sky. This new transportation system will revolutionize both urban mobility and cargo delivery services. In the context of urban transportation, this concept is commonly known as Urban Air Mobility (UAM), which focuses on enabling low-altitude aerial travel for passengers using electric vertical take-off and landing vehicles. UAM aims to alleviate traffic congestion, shorten commute times, and offer an environmentally sustainable alternative to traditional ground transportation. In the cargo delivery domain, particularly in humanitarian logistics, AAM provides critical advantages in disaster response through the use of drones. Drones can rapidly deliver goods to isolated or hard-to-reach regions, bypassing blocked roads and ensuring timely aid. This ability to quickly and flexibly deliver supplies to disaster-stricken areas provides an indispensable tool for humanitarian organisations. This thesis focuses on the strategic planning of service-based AAM systems under uncertainty, with a particular emphasis on the application of UAM and drone-supported last-mile humanitarian logistics.

The first study introduces an integrated optimisation problem aimed at addressing decision-making processes related to the strategic planning and service operations of UAM systems, considering both demand uncertainty and spatial equity. We introduce a spatial equity metric and establish a bi-objective optimisation model to balance the

trade-off between service profitability and spatial equity considerations. We employ a scenario-based robust optimisation framework that incorporates the interval robust method to capture the demand uncertainty, enhancing resilience against uncertain factors. We evaluate the model performance through numerical experiments and a practical case study based on a megalopolis in southern China and propose valuable policy recommendations for UAM service providers.

The second study focuses on drone-supported last-mile humanitarian logistics planning under demand uncertainty, specifically in scenarios where the uncertainty is realised sequentially. We propose a drone-supported last-mile humanitarian logistics system planning problem. To capture the demand uncertainty, we establish a multistage stochastic programming model incorporating nonanticipativity constraints to make decisions at each stage without knowledge of the demand information in future time periods. The Benders decomposition algorithm is then employed to derive exact solutions. We validate the proposed optimisation models and solution methods through a case study of the Lushan earthquake in China. This research contributes to the field of humanitarian logistics by providing a comprehensive framework for planning drone-supported last-mile humanitarian logistics systems.

In the third study, we examine a scenario in which historical demand data is lacking and distribution information is only partially available. We investigate a novel drone-supported relief facility location problem and apply a distributionally robust optimisation (DRO) framework, utilising box, polyhedral, and ellipsoidal ambiguity sets to address demand uncertainty. To overcome the computational challenges, we reformulate the DRO models into computationally tractable forms. The DRO approach ensures superior out-of-sample performance in the face of partial demand information, thereby supporting effective decision-making in humanitarian logistics. Finally, we also validate the proposed optimisation models through a case study of the Lushan earthquake in China and offer valuable managerial implications to support decision-making

processes for humanitarian organisations.

The models and methods proposed in this thesis pave the way for innovative practices in strategic planning for service-based AAM systems.

Chief supervisor: Prof. Kam K.H. Ng

Co-supervisor: Prof. Gangyan Xu

Publications

***: Corresponding author.**

Journal Papers (Arising from the Thesis)

1. **Jin, Z.**, Ng, K. K.*, Zhang, C., Wu, L., Li, A. (2024). Integrated optimisation of strategic planning and service operations for urban air mobility systems. **Transportation Research Part A: Policy and Practice**, 183, 104059.
2. **Jin, Z.**, Ng, K. K., Zhang, C.*, Chan, Y., Qin, Y. (2025). A multistage stochastic programming approach for drone-supported humanitarian last-mile logistics system planning. **Advanced Engineering Informatics**, 65, 103201.
3. **Jin, Z.**, Ng, K. K.*, Zhang, C., Liu, W., Zhang, F., Xu, G. (2024). A risk-averse distributionally robust optimisation approach for drone-supported relief facility location problem. **Transportation Research Part E: Logistics and Transportation Review**, 186, 103538.

Journal Papers (Others)

1. **Jin, Z.**, Ng, K. K., Wang, H.*, Wang, S., Zhang, C. (2025). Electric airport ferry vehicle scheduling problem for sustainable operation. **Journal of Air Transport Management**, 123, 102711.
2. **Jin, Z.**, Ng, K. K.*, Zhang, C. (2024). Robust optimisation for vertiport location problem considering travel mode choice behaviour in urban air mobility systems. **Journal of the Air Transport Research Society**, 2, 100006.

3. Wang, H., Wang, W., **Jin, Z.*** (2024). Mechanism for allocating delay to constituent activities in project management. **Computer & Industrial Engineering**, 110603.

4. Zhang, C., **Jin, Z.**, Ng, K. K.*, Tang, T., Tang, R. (2025). Distributionally robust optimisation approach for aircraft sequencing and scheduling with learning-driven arrival and departure time predictions. **Omega: The International Journal of Management Science**, 103415.

5. Zhang, C., **Jin, Z.**, Ng, K. K.*, Tang, T., Zhang, F., Liu, W. (2025). Predictive and prescriptive analytics for robust airport gate assignment planning in airside operations under uncertainty. **Transportation Research Part E: Logistics and Transportation Review**, 195, 103963.

6. Zhang, C., Ng, K. K.*, **Jin, Z.**, Sun, X., Qin, Y. (2025). Benders decomposition for the risk-averse two-stage stochastic gate assignment problem. **Computer & Industrial Engineering**, 111269.

7. Zhang, C., Ng, K. K.*, **Jin, Z.**, Yao, S., Qin, Y. (2025). Learning-driven exact and meta-heuristic algorithms for the robust gate assignment problem. **Advanced Informatics Engineering**, 67, 103551.

8. Li, X., Wu, L.*, Lang, H., **Jin, Z.**, He, P. (2025). A critical literature review on layout designs and handling technology in traditional and automated container terminals. **Transport Economics and Management**.

9. Guo, J., Wang, W.*, Philip K., Peng, Y., **Jin, Z.**, Pei, Z., Chen, Z., Yang, Y. (2025). Predicting recoverable ship ballast water using machine learning: Implications for port and maritime sustainability. **Transportation Research Part D: Transport and Environment**, in press.

Under Review Papers

1. **Jin, Z.**, Zhang, C., Ng, K. K.*, Tian, X., Wang, H., Xu, G. Humanitarian logistics planning under uncertain demand and third-party supply capacity: A distri-

butionally robust optimisation approach. Submitted to **International Journal of Production Research**, under third-round review.

2. Zhang, C., **Jin, Z.**, Ng, K. K.*, Liu, Y., Wu, L. Stabilised branch-and-check method for optimising multi-runway aircraft landing problem modelled through stochastic programming with learning-driven arrival time predictions. Submitted to **Transportation Research Part E: Logistics and Transportation Review**, under second-round review.

Conference Papers

1. **Jin, Z.**, Wang, H., Ng, K. K., Wang, S. (2024). Electric ferry vehicle scheduling problem for sustainable airport operation. **The 27th ATRS World Conference**, Lisbon, Portugal.

2. **Jin, Z.**, Zhang, C., Ng, K. K. (2024). An improved variable neighbourhood search for the gate assignment problem with time windows. **AIAA AVIATION Forum 2024**, Las Vegas, USA.

3. **Jin, Z.**, Ng, K. K., Zhang, C.(2023). Robust optimisation for the vertiport location problem in urban air mobility system. **The 26th ATRS World Conference**, Kobe, Japan.

Contents

Acknowledgements

First and foremost, I would like to express my deepest gratitude to my supervisor, Prof. Kam Hung Ng, for his unwavering support, valuable guidance, and continuous encouragement throughout my doctoral journey. Prof. Ng consistently demonstrated a genuine willingness to assist me when I get in trouble in doing research and in daily life. He provided me with valuable opportunities to attend international conferences and academic exchange. This thesis would not have been possible without him. Heartfelt thanks go to my host supervisor at HEC Montréal, Canada, Prof. Okan Arslan. I had a wonderful time in Canada, and I am deeply grateful for his support during my transition to a new life and work environment, as well as for our collaboration on the research.

Second, I would like to express my gratitude to the Board of Examiners: Prof. Wen-Hua CHEN from PolyU, Prof. Wei Liu from PolyU, Prof. Yong-Hong KUO from the University of Hong Kong, and Prof. Yang Liu from National University of Singapore for their valuable comments, which have greatly improved the quality of the thesis. Sincere thanks are also due to my co-supervisor, Prof. Gangyan Xu from PolyU. I would also like to express my heartfelt gratitude to Prof. Lingxiao Wu for his support during my research and for his efforts in providing me with valuable advice. I extend my appreciation to Prof. Wenyi Xia at HEC Montréal and Prof. Kun Wang from PolyU for their strong support in conducting research in transport economics. I am also grateful to all of the faculty and administrative members of AAE for creating

a supportive environment for learning and research.

A heartfelt thank you to all the members of my research group, Air Transportation Management Research Group: Qinbiao, Chenliang, Nana, Ye, Mengtao, Senna, Xin, Dave, Alan, James, Yipeng, Congcong, Changxin, Rong, Qinyu, Yuanyuan, and Terrence. The days spent in FJ005 were filled with laughter and brought me immense joy. I feel incredibly fortunate to have met all of you during my doctoral journey. I am especially grateful to my exceptional collaborator, Dr. Chenliang Zhang, for his assistance throughout this time. Whenever I faced challenges, he was always there to support me and comfort me. Many thanks also go to my friends, both those from far away and those I have met at PolyU, for bringing joy to my leisure time and supporting me throughout the journey.

Finally, I would like to dedicate this thesis to my parents for their endless love and support.

List of Figures

List of Tables

Abbreviations

AAM	Advanced Air Mobility
CVaR	Conditional Value-at-Risk
DRO	Distributionally robust optimisation
DLHLSP	Drone-Supported Last-mile Humanitarian Logistics System Planning
DSRFLP	Drone-Supported Relief Facility Location Problem
DSP	Dual Formulation of Primal Subproblem
eVTOL	Electric Vertical Takeoff and Landing
FAA	Federal Aviation Administration
GBA	Guangdong-Hong Kong-Macao Greater Bay Area
GDP	Gross Domestic Product
LB	Lower Bound
MCVaR	Mean-Conditional Value-at-Risk
MP	Master Problem
NASA	National Aeronautics and Space Administration
OD	Origin-Destination
PDR	Price of Distributional Robustness
PSP	Primal Subproblem
UAM	Urban Air Mobility
UAV	Unmanned Aerial Vehicle

UB	Upper Bound
UTM	Unmanned Aircraft System Traffic Management
WCVaR	Worst-case Conditional Value-at-Risk
WMCVaR	Worst-case Mean-Conditional Value-at-Risk

Chapter 1

Introduction

1.1 Research Background

The rapid advancement of aviation technologies has led to the emergence of a new transportation paradigm: Advanced Air Mobility (AAM). This initiative, spearheaded by the National Aeronautics and Space Administration (NASA), has the potential to dramatically reshape how we think about urban transportation and cargo logistics (Johnson and Silva, 2022).

The integration of AAM into urban transportation systems offer numerous benefits, particularly with the development of electric vertical takeoff and landing (eVTOL) aircraft (Jin et al., 2024a; Coppola et al., 2024). These innovative vehicles promise to alleviate congestion on city roads by providing an alternative mode of transport that operates above ground level (Al Haddad et al., 2020). As urban populations continue to grow, the demand for efficient and sustainable transportation solutions becomes increasingly critical (Sun et al., 2018). According to the Federal Aviation Administration (FAA), Urban Air Mobility (UAM) is a critical component of the broader AAM framework in urban transportation. UAM has the potential to significantly reduce travel times, enhance connectivity between urban centres and suburban areas, and

decrease the environmental impact associated with traditional ground transportation (Zhao et al., 2025). Currently, numerous cities are actively working towards the deployment of UAM systems, aiming to provide better options for both intra-city and inter-city commutes (Wang and Qu, 2023; Wang et al., 2023). For instance, Dubai is expected to offer UAM services catering to tourists; Singapore plans to introduce air taxis for commercial routes connecting Marina Bay and Sentosa, with plans to expand this service to include cross-border travel, encompassing destinations such as Indonesia and Malaysia. In China, Shenzhen is implementing the UAM system in collaboration with various commercial enterprises. In the near future, it is anticipated to provide faster, more efficient, and more environmentally friendly transportation services to revolutionise urban transportation compared with conventional ground-based transportation modes (Zhao and Feng, 2025; Chen et al., 2022).

In addition to revolutionising passenger transport, AAM plays a crucial role in advancing cargo logistics, particularly in the context of last-mile humanitarian logistics (Purtell et al., 2024; Ziakkas and Natakusuma, 2025). This phase is a critical component of the overall humanitarian logistics system, serving as a pivotal stage in facilitating disaster relief efforts (Lebcir and Roy, 2023). It ensures that aid reaches those in need promptly and effectively. However, last-mile humanitarian logistics planning faces various challenges (Kovács and Spens, 2009). One major obstacle is the vulnerability of ground transportation networks in disaster areas, which are often susceptible to disruptions (Akbari et al., 2021). The extent of damage to physical transportation infrastructure is often unforeseeable in terms of its nature, scale, and extent, potentially impeding the delivery of critical relief items. For example, the magnitude-9.0 earthquake that struck Japan on 11 March 2011, generated a massive tsunami, destroying extensive coastal infrastructure and severely affecting transportation and rescue efforts. In this incident, approximately 29 railway stations, 78 bridges, and 4,000 road segments were estimated to have been damaged (Zhang et al., 2021).

To address these challenges, integrating drone technology into last-mile humanitarian logistics has emerged as a promising solution (Chowdhury et al., 2017). Drone technology is a notable trend in Industry 5.0, offering a revolutionary tool for reshaping various industries including transportation and logistics (Moshref-Javadi and Winkenbach, 2021; Yi et al., 2021). In particular, the utilisation of drones for last-mile delivery of relief supplies—such as medicine, blood, and vaccines—provides unprecedented advantages in tackling the logistical challenges inherent in both natural and human-made disaster situations. For instance, drones provide a versatile and rapid means of transportation, capable of navigating difficult terrain and bypassing damaged infrastructure (Yin et al., 2023b). This capability not only expedites delivery times but also enhances the flexibility and responsiveness of relief efforts, particularly in remote or inaccessible areas. Drones have become increasingly deployed in relief operations across numerous emergency and disaster scenarios in real-world applications. Examples include Typhoon Haiyan in 2013 (Meier, 2014), terrorist attacks in the United States on 11 September 2011 (Bravo et al., 2019), Turkey–Syria earthquakes in 2023 (Kandavel, 2023), and vaccine delivery during the COVID-19 pandemic (Crabtree, 2021).

Therefore, establishing AAM systems is imperative to provide high-quality travel services for passengers and efficient humanitarian logistics services for relief organisations. Uncertainty is an inherent characteristic that cannot be ignored when planning AAM systems, as it can significantly influence decision-making processes (Noyan et al., 2022; Ben-Tal et al., 2011). In particular, demand uncertainty stands out as a critical factor that should be carefully considered, both in the context of urban transportation and humanitarian logistics (Wang et al., 2021a; Farahani et al., 2020; Chen and Liu, 2023). In particular, in the field of humanitarian logistics, the chaotic nature of disaster environments often leads to a lack of historical data. As a result, two distinct scenarios need to be considered: one in which demand uncertainty information is realised sequentially, and another where historical data is scarce and only partial information

is available.

Overall, this thesis aims to propose a comprehensive framework for the strategic planning of service-based AAM systems under uncertainty. Specifically, three critical areas are explored within AAM systems: designing a profit-maximising and equitable spatially UAM system under demand uncertainty; developing a drone-supported last-mile humanitarian logistics system when demand uncertainty information is realised sequentially; and optimising drone-supported last-mile humanitarian logistics decisions to address the challenges posed by limited historical data. This thesis contributes valuable managerial insights and provides enhanced support for the practical implementation and operation of AAM systems in both urban transportation and humanitarian logistics contexts.

1.2 Research Scope and Objectives

In recent years, the aviation landscape has experienced a transformative shift, driven by the rapid advances in electric vertical take-off and landing (eVTOL) and Unmanned Aerial Vehicle (UAV) technology (Gong et al., 2023; Garrow et al., 2021). This paradigm shift has propelled the AAM concept into the forefront of urban transportation and logistics discussions (Haan et al., 2021; Gu et al., 2023). Therefore, this thesis aims to explore the strategic planning decisions of AAM systems under demand uncertainty, proposing optimisation models, solution methods, and applications to validate the proposed approaches. The thesis is organised into three studies:

In the first study, we delve into an integrated optimisation problem aimed at addressing decision-making processes related to the strategic planning and service operation of UAM systems, considering both demand uncertainty and spatial equity. The problem encompasses various decision components, including parking stand numbers at vertiports and vertistops, eVTOL fleet sizing as well as eVTOL fleet allocation

and operations. Additionally, we introduce a spatial equity metric and establish a bi-objective optimisation model to balance the trade-off between service profitability and spatial equity considerations. We transform the bi-objective optimisation model to a tractable single-objective formulation using ε-constraint approach and linearisation technique. In this study, we employ a scenario-based robust optimisation framework that incorporates the interval robust method to capture the demand uncertainty, enhancing resilience against uncertain factors. We evaluate the model performance using a small-scale example and further validate the proposed model through a real-world case study. Numerical analysis results demonstrate that the scenario-based robust optimisation framework can ensure the robustness of decision-making against the effect of uncertain conditions. Furthermore, numerical experiments reveal a trade-off between profitability and spatial equity, potentially requiring a partial sacrifice of profit to attain a desired equity level. Finally, we propose valuable policy recommendations to guide the decision-making processes of UAM service providers.

In the second study, we plan drone-supported last-mile humanitarian logistics when precise knowledge of the demand uncertainty information is realised sequentially. This study introduces a novel approach to address these challenges by proposing a drone-supported last-mile humanitarian logistics system planning (DLHLSP) problem. The DLHLSP problem involves decision-making for both pre-disaster and post-disaster phases, taking into account the unique characteristics of drone-based delivery operations and uncertain demands. In the pre-disaster phase, decisions include determining drone-supported relief facility locations, drone deployment strategies, and drone visit schedules to disaster sites. Post-disaster decisions focus on inventory management, relief item procurement, and drone-based delivery operations. To capture the demand uncertainty in the chaotic disaster environment, we establish a multistage stochastic programming model incorporating nonanticipativity constraints to make decisions at each stage without knowledge of the demand information in future time periods. Next,

we employ the Benders decomposition algorithm to obtain exact solutions. Furthermore, we perform numerical experiments to verify the exact algorithm using randomly generated numerical instances. The results show that the algorithm significantly outperforms the Gurobi solver and could solve the problem on a practical scale. Finally, the study validates the proposed model based on a case study of the Lushan earthquake in China and provides several managerial implications and insights. Overall, this research contributes to the field of humanitarian logistics by offering a comprehensive framework for the planning of drone-supported last-mile humanitarian logistics systems.

In the third study, we plan drone-supported last-mile humanitarian logistics when the historical data is insufficient and the demand distribution information is partial and incomplete. We present a novel drone-supported relief facility location problem (DSRFLP) to plan the drone-supported last-mile humanitarian logistics system. This problem aims to facilitate joint decision-making for both pre-disaster and post-disaster phases, taking into account factors such as the characteristics of drone-based delivery operations and uncertain demands. Pre-disaster decisions encompass the selection of relief facility locations, inventory prepositioning, drone assignments, and allocation to demand sites. Post-disaster decisions focus on determining delivery quantities. To manage incomplete demand distribution information, we propose a DRO model that considers the risk-averse attitude of relief organisers. This model employs three ambiguity sets (box, ellipsoidal, and polyhedral) to depict demand ambiguity. We then reformulate the DRO models under three ambiguity sets into two mixed-integer linear programming models and one second-order cone programming model to make the models computationally tractable. Through validation through small-scale and large-scale case studies of the Lushan earthquake in China, we demonstrate the superior performance of the proposed DRO model in mitigating the impact of incomplete distributions. Drawing from experimental results, we provide valuable managerial implications and

insights. Finally, we introduce two extended models considering multiple relief items and equity constraints, conducting numerical experiments to address various real-world disaster scenarios.

1.3 Organisation of the Thesis

After a brief introduction in chapter 1, the subsequent chapters of this thesis are structured as follows:

In chapter 2, we review the existing literature on UAM and humanitarian logistics system planning and identify the research gaps in these areas. In chapter 3, we develop an optimisation approach to solve an integrated decision-making problem that encompasses both strategic planning and operational service decisions for UAM systems. This study incorporates considerations of demand uncertainty and spatial equity. In chapter 4, we focus on a DLHLSP problem. To address the challenge of sequential realisation of demand uncertainty, we propose a multistage stochastic programming model with non-anticipativity constraints and apply the Benders decomposition algorithm to obtain exact solutions. In chapter 5, we address the scenario of insufficient historical data and propose a DRO model that accounts for the risk-averse attitudes of relief organisations. This model uses three ambiguity sets—box, ellipsoidal, and polyhedral—to capture demand uncertainty. We then reformulate the DRO models under these ambiguity sets into computationally tractable forms. Finally, in chapter 6, we present the conclusions and contributions of this thesis on the planning of the AAM system. This chapter also outlines future directions and highlights the limitations of the thesis.

Chapter 2

Literature Review

2.1 Strategic Planning for UAM Systems

According to the FAA, the UAM system is a subset of AAM, which includes components such as air mobility operators, vertiport infrastructure, and air traffic management. The literature explores various aspects of the UAM system to enhance its planning and management (Straubinger et al., 2020). Most studies focused on vertiport location decisions and macro-level system analysis. Some research also concentrated on the aspects of air traffic management of UAM systems.

In terms of determining vertiport locations, Lim and Hwang (2019) presented a K-means clustering algorithm to optimise the vertiport locations in the Seoul metro area. Gonzalez (2020) conducted a rooftop-place suitability analysis to identify suitable rooftop surfaces for UAM operations. Additionally, some literature extended the traditional hub location problem to solve the vertiport location problem based on optimisation techniques. For instance, Chen et al. (2022) proposed an optimisation model for selecting vertiport locations for air taxi operations. This study modelled the discrete demand within a grid graph and excluded the forbidden grids which cannot be selected as the vertiports. Shin et al. (2022) presented a vertiport location model con-

sidering traffic congestion. The objective function of the model was minimising the travel time cost, fixed vertiport opening costs, flight service cost, and collision risk cost. In another study, Rath and Chow (2022) proposed a hub location problem considering choice-constrained user choice behaviour. Wu and Zhang (2021) presented a mathematical model to obtain the optimal vertiport locations after identifying the potential locations based on Geographic Information Systems tools. On the other hand, the vertiport location problem was also addressed by extending other classic operations research problems. For instance, Rimjha et al. (2021) investigated a mathematical model to maximise UAM demand coverage. Ale-Ahmad and Mahmassani (2021) established an optimisation model to solve a capacitated location-allocation-routing problem considering time windows. Noteworthily, a recent study by Wang et al. (2022b) attracted our attention due to its holistic exploration of the UAM system planning. This research adopted an optimisation-based approach and delved into joint decisions of strategic deployment and tactical operations, including vertiport location and capacity determinations, sizing of eVTOL fleet, as well as effective route planning and repositioning strategies. Furthermore, the paper incorporated crucial factors such as battery charging dynamics and passenger pooling into the mathematical model. This is a comprehensive study in the field of UAM system operations and management.

Furthermore, there is also some literature on the macro-level analysis of UAM systems. For instance, Li et al. (2020) conducted a series of simulation-driven feasibility and scalability analyses to estimate the capacity and throughput. This research aimed to obtain UAM ecosystem design guidelines and effective operational policies. Vascik et al. (2018) explored potential operational limitations that might emerge during the deployment and expansion of a UAM system. Vascik and Hansman (2018) investigated the fundamental mechanisms of UAM systems, such as air traffic control, ground infrastructure, and noise.

Finally, in terms of air traffic flow management of UAM systems, He et al. (2022) proposed a route network planning approach to design aerial routes in a complex urban environment. Song and Yeo (2021) proposed three scheduling strategies: branch queuing approach, sequence-based approach, and sequence-based approach with moving circles. The strategies were assessed by comparing the on-time performance with hovering time and ground time. Wang et al. (2022c) introduced an air traffic assignment framework tailored for 3D air transport networks within urban airspace. The purpose was to facilitate UAM operations to meet anticipated demand levels in the future. Veytia et al. (2022) investigated three separation management concepts with varying degrees of centralisation for urban aerial mobility. Kleinbekman et al. (2018) developed an optimisation model to have a determination of the required arrival time, ensuring safe separation and minimising delays.

Furthermore, equity consideration is an important issue in transportation systems, including urban, air, rail transportation systems, etc. In the urban transportation system, Caggiani et al. (2020) proposed an equitable bike-sharing station location problem to minimise inequality as well as ensure accessibility and coverage level. Chen et al. (2023) proposed a target-based DRO model to achieve optimal service efficiency and spatial equity in docked bike-sharing systems considering uncertain demands. Wu et al. (2015) established an optimisation model for synchronising timetables, aiming to minimise the total waiting time of passengers and maintain the waiting time equitable across all transfer stations in the subway system. Ruiz et al. (2017) presented an optimisation model to obtain the bus frequency, which ensures the harmonisation between the service level and social equity in the bus system. In the realm of air transportation systems, Guo et al. (2022a) proposed different equity metrics and established both deterministic and robust bi-objective optimisation models to ensure efficiency and equity for the decision-making process of air traffic flow managers. Zografos and Jiang (2019) introduced an equity metric of slot scheduling and proposed a bi-objective optimisation

model to obtain solutions that consider equity and efficiency simultaneously. For the rail transportation system, Shao et al. (2022) proposed a novel formulation to estimate equity performance and an integrated optimisation model to make decisions on train timetables and stop planning for the suburban railway system. In particular, in the context of UAM systems, there are also some studies that consider equity. For example, Chin et al. (2021) formulated the air traffic flow management of Unmanned Aircraft Systems operations considering the equity of delay assignment. Chin et al. (2023) established an optimisation model to locate drone bases to respond rapidly and cover as large an area as possible. Besides, this study assessed variations in the accessibility levels across distinct regions.

2.2 Strategic Planning for Drone-Supported Humanitarian Logistics

In humanitarian logistics, it is crucial to deliver relief items to disaster sites as quickly and securely as possible. However, there are many inherent uncertain factors that will have a significant influence on the delivery process. As stated by Tofighi et al. (2016), inherent uncertainties cannot be neglected because they affect the efficiency of the humanitarian logistics system. Therefore, much literature focuses on humanitarian logistics planning, considering various uncertain factors and aiming to design an efficient and rapid-response system to save lives and support people in need.

Stochastic programming has been widely adopted as a methodology to address humanitarian logistics planning problems, given the inherent significance of uncertainty. In the stochastic programming model, the precise distributions of the uncertain parameters are known perfectly. Currently, there is widespread utilisation of a two-stage stochastic programming framework with discrete probability distributions to tackle demand uncertainty. For instance, Moreno et al. (2018) proposed a two-stage stochastic

programming model to solve a combined location-transportation problem within disaster relief contexts. Shu et al. (2023) established a chance-constrained stochastic programming model to obtain facility location, inventory pre-positioning, and assignment of relief facility to disaster areas considering the uncertainty of demand. Particularly, a joint chance constraint is added to assess the responsiveness of the humanitarian relief network. Rath et al. (2016) introduced a stochastic programming model to obtain optimal decisions of intermediate depot locations and vehicle acquisition, considering the uncertainty of accessibility of the road network in disaster relief operations. Hu et al. (2017) investigated a stochastic model to optimise the pre-disaster inventory quantity and post-disaster procurement planning considering demand uncertainty. Manopiniwes and Irohara (2017) established a multi-objective model to optimise relief operations during the preparedness and response phases based on the stochastic programming framework. Hu et al. (2019) considered heterogeneous vehicles and incorporated the uncertainty of road network state into a two-stage stochastic programming framework to solve a relief distribution problem. The uncertain road state was represented by dynamic road capacity. Wang and Nie (2022) integrated pre-disaster decisions regarding emergency supply and transportation network mitigation, along with post-disaster decisions involving dynamical transportation planning considering traffic congestion effects based on the stochastic programming approach. Elçi and Noyan (2018) established a chance-constrained two-stage stochastic programming model to address a novel risk-averse relief network design problem considering the uncertainty of demand. Alem et al. (2016) developed a two-stage network flow model to make decisions during both the preparedness and response stages. This model can promote effective strategies for promptly delivering humanitarian aid to disaster victims. Paul and Zhang (2019) developed a two-stage stochastic programming model to address decision-making regarding supply location and transportation planning during hurricane scenarios. The objective in their model was to optimise the deprivation and logistics costs. Ahmadi

et al. (2015) introduced a multi-depot location-routing model for last-mile distribution after earthquakes, considering network failures, multiple vehicle uses, and relief time constraints. The model determined the locations of local depots and routing for last-mile distribution after an earthquake. Furthermore, this study extended to a two-stage stochastic programming to determine distribution centre locations under random travel times. Oksuz and Satoglu (2020) established a two-stage stochastic programming model to address the critical problem of locating temporary medical centres during disasters. This model was developed to optimise temporary medical centre locations while minimising setup and transportation costs. Wang et al. (2024) addressed the challenge of optimising resource allocation in disaster rescue, considering the uncertainties associated with multiple secondary hazards. A two-stage stochastic optimisation model was proposed to allocate rescue teams, warehousing items, and medical resources effectively.

Furthermore, there is limited literature focusing on the application of multistage stochastic programming approaches in the field of humanitarian logistics. For example, Zahiri et al. (2017) established a novel multistage possibilistic stochastic programming model, incorporating fuzzy probabilities along the arcs of scenario trees, and applied this approach to relief distribution planning. Hu et al. (2023a) introduced a dynamic pre-positioning problem for humanitarian relief operations based on a multistage stochastic programming framework to optimise procurement and return decisions. Siddig and Song (2021) proposed a fully adaptive multistage stochastic programming model integrated with a Markov chain approach for optimising logistics planning in disaster relief efforts amid uncertain demand forecasts due to impending hurricanes.

The aforementioned literature has assumed the distributions of uncertain parameters are known perfectly. However, this may not be possible in most real-world scenarios. Aiming at this problem, a robust optimisation method was proposed to avoid negative impacts on the decision-making process due to a lack of accurate information

on uncertain parameter distribution (Bertsimas and Sim, 2004; Gorissen et al., 2015). Hence, there is much literature that focuses on obtaining optimal decisions in humanitarian logistics based on the robust optimisation method. For instance, Ni et al. (2018) proposed a min-max robust model to determine the facility location, inventory pre-positioning, and delivery operations considering the uncertainties of the proportions of the usable inventories, demand, and road capacities. Yahyaei and Bozorgi-Amiri (2019) designed a network for relief logistics considering the facility disruption risks in order to distribute resources timely and hedge against uncertain environments based on the robust optimisation approach. Avishan et al. (2023) presented an adaptable robust optimisation model to address a humanitarian logistics problem considering uncertain travel time. This model made joint decisions regarding routing and the service times of the disaster sites for relief logistics teams. Furthermore, Sun et al. (2021) introduced a robust optimisation model to minimise total cost while also reducing injury severity scores.

The empirical distribution estimated from the historical data is always partial and inaccurate in stochastic programming. At the same time, the decisions obtained from the robust optimisation are always too conservative due to a lack of distribution information on the uncertain parameter. To address the limitations of stochastic programming and robust optimisation, DRO has emerged as a promising methodology, which offers a solution to handle the uncertainty without the need for complete distribution information of the uncertain parameter (Delage and Ye, 2010). Additionally, this methodology can mitigate the overly conservative nature of the solutions obtained from the robust optimisation method (Goh and Sim, 2010). This methodology has been gradually applied to make crucial decisions in humanitarian logistics planning. Zhang et al. (2022) investigated a DRO model to minimise total cost and time while simultaneously maximising the equitable distribution of relief supplies. Additionally, a DRO model was established by Wang et al. (2022a) to address a relief logistics

problem considering lateral transhipment strategy. Yang et al. (2023) addressed a location-allocation problem in humanitarian logistics considering the dynamic relief facility location and relief distribution based on the DRO approach. Additionally, Shehadeh and Tucker (2022) proposed a DRO model to obtain optimal locations and inventory prepositioning of opened warehouses and joint decisions on the procurement and distribution decisions of relief items.

There has been a significant increase in the utilisation of drones for disaster relief operations. Drones offer unique advantages in relief efforts, including their ability to access hard-to-reach areas and deliver critical supplies swiftly. As a result, an increasing number of literature has focused the efforts on optimising drone operations for disaster relief scenarios.

Currently, some literature is investigating the application of a synchronised truck-drone delivery system in humanitarian logistics. For instance, Yin et al. (2023b) investigated a vehicle routing problem with drones under uncertain demands and travel times for resource transport in the aftermath of disasters. This study proposed a robust optimisation model using budgeted uncertainty sets and an enhanced branch-and-price-and-cut algorithm. Lu et al. (2022) introduced a multi-objective humanitarian pickup and delivery vehicle routing problem with drones, focusing on cooperative delivery in humanitarian logistics. This study aimed to minimise maximum cooperative routing time and maximise the minimum fulfillment rate of demand nodes. Najy et al. (2023) addressed an inventory-routing problem by integrating collaborative truck-and-drone delivery strategies to optimise transportation and holding costs. Zhang et al. (2021) proposed a collaborated truck-and-drone system to perform the assessment task in the humanitarian relief network.

Furthermore, some research exclusively investigates drone-supported relief operations rather than synchronised transportation operations involving both trucks and drones. Ghelichi et al. (2022) proposed a chance-constrained programming model

aimed at determining the optimal locations for drone launching platforms. This model took into account the uncertainties in demand arising from disasters, thus providing a framework for decision-making in disaster scenarios. Kim et al. (2019) investigated an optimisation model for relief facility location and drone delivery assignments across multiple time periods in disaster scenarios. Notably, this study integrated a chance constraint to account for uncertainties in drone flight distances. Dukkanci et al. (2023) addressed the relief distribution problem using drones in post-disaster scenarios considering uncertainties in demand and road networks, aiming to minimise total unsatisfied demand within time constraints. This study employed a two-stage stochastic programming and scenario decomposition algorithm and was validated through a case study in Istanbul, Turkey. Ghelichi et al. (2022) presented a stochastic optimisation approach for efficiently deploying drone fleets to deliver aid packages to disaster-affected areas with uncertain demand, utilising chance-constrained programming to minimise total disutility. Zhu et al. (2022) introduced a two-stage robust facility location problem with drones for post-disaster drone-based humanitarian relief operations, addressing demand uncertainty and incorporating realistic drone electricity consumption models. Chauhan et al. (2019) proposed a maximum coverage facility location problem with drones and established an integer linear programming formulation to maximise coverage while considering drone energy consumption and range constraints. Rabta et al. (2018) investigated an optimisation model for drone-based last-mile relief distribution with the installation of charging stations.

2.3 Summary of the Literature Review and Research Gaps

Firstly, to the best of our knowledge, there is currently a lack of existing literature that provides a comprehensive framework of strategic planning and service operations con-

sidering equity and demand uncertainty in the context of the UAM system planning. Therefore, this thesis focuses on addressing the following specific gaps. Firstly, there is a scarcity of research that focuses on the strategic deployment of the eVTOL parking stands of vertiports and vertistops while considering equitable service operation optimisation. Secondly, the evaluation of the spatial equity performance of the UAM system lacks a well-defined metric. Thirdly, a mathematical model is lacking to simultaneously address both profit-based and equity-based considerations while accounting for the demand uncertainty in the UAM systems. Hence, we propose an integrated optimisation problem in the context of UAM systems, which involves making joint decisions on strategic planning and service operations, including the determination of parking stand numbers at vertiports and vertistops, eVTOL fleet size as well as eVTOL fleet allocation and operations. Additionally, we introduce a spatial equity metric and establish a bi-objective optimisation to simultaneously ensure the operating profit and spatial equity. Finally, to address the issue of demand uncertainty consideration and enhance the model robustness, we adopt a scenario-based robust optimisation framework incorporating the interval robust optimisation model to this problem.

Secondly, although significant research has been conducted on optimising disaster response operations under uncertainty, there remains a notable gap in the comprehensive planning of drone-supported last-mile humanitarian logistics systems. Additionally, the demand information during the entire planning horizon becomes realised after decisions regarding the first-stage problem have been made in the previous literature. This is not in line with the real-world practice. Therefore, this thesis fills these gaps by proposing a holistic approach to planning a drone-supported last-mile humanitarian logistics system. We make integrated decisions encompassing drone-supported relief facility location, drone deployment, drone visit scheduling, delivery operations, inventory management, and procurement. Moreover, we utilise multistage stochastic programming to effectively model the uncertain demand characteristics in

different stages during the planning horizon. In the proposed model, the demand information for a particular stage becomes known only after decisions have been made for the preceding stage, which can more precisely reflect the uncertain environments in this problem. This thesis can lead to a more efficient and drone-supported last-mile humanitarian logistics system, improving the overall effectiveness and responsiveness of humanitarian relief efforts.

Finally, there is currently a lack of existing literature on the drone-supported last-mile humanitarian logistics system planning based on the DRO approach. Therefore, this thesis contributes to the research agenda by addressing specific gaps. First, no previous research has made integrated decisions regarding drone-supported relief facility location, the inventory of relief items, drone assignment to the relief facility and allocation to disaster demand sites, and delivery quantities given battery and payload weight requirements in the field of drone-supported last-mile humanitarian logistics planning. Second, the application of the DRO approach in this field is limited. Current research in this field is unavailable to address the conservative nature of robust optimisation and the difficulty in obtaining accurate distribution information in stochastic programming. Third, within the context of drone-supported last-mile humanitarian logistics planning, there is a lack of literature that considers the risk-averse attitudes of decision makers to hedge the potential risk of the system. To fill these gaps, we introduce a novel risk-averse DRO model adopting the risk criterion under three ambiguity sets, namely box, ellipsoidal, and polyhedral, to address the DSRFLP to obtain joint decisions.

Overall, this thesis investigates a novel and comprehensive framework for the strategic planning of service-based AAM systems under uncertainty.

Chapter 3

Integrated Optimisation of Strategic Planning and Service Operations for Urban Air Mobility Systems

With the rapid development of novel vehicle technologies, eVTOL vehicles are becoming a new transport servicing model to achieve better UAM systems. The UAM systems can efficiently utilise low-altitude airspace resources, providing a solution to alleviate congestion in urban ground traffic. This study delves into an integrated optimisation problem aimed at addressing decision-making processes related to the strategic planning and service operation of UAM systems, considering both demand uncertainty and spatial equity. The problem encompasses various decision components, including parking stand numbers at vertiports and vertistops, eVTOL fleet sizing, and eVTOL fleet allocation and operations. Additionally, we introduce a spatial equity metric and establish a bi-objective optimisation model to balance the trade-off between service profitability and spatial equity considerations. We transform the bi-objective optimisa-

tion model to a tractable single-objective formulation using the ε-constraint approach and linearisation technique. In this study, we employ a scenario-based robust optimisation framework incorporating the interval robust method to capture the demand uncertainty, enhancing resilience against uncertain factors. We evaluate the model performance using a small-scale example and further validate the proposed model through a real-world case study. Numerical analysis results demonstrate that the scenario-based robust optimisation framework can ensure the robustness of decision-making against the effect of uncertain conditions. Furthermore, numerical experiments reveal a trade-off between profitability and spatial equity, potentially requiring a partial sacrifice of profit to attain a desired equity level. Finally, we propose valuable policy recommendations to guide the decision-making processes of UAM service providers.

3.1 Introduction

As defined by the Federal Aviation Administration (FAA), UAM is a pivotal component within the framework of AAM. An integrated UAM system comprises various components, including air mobility operators, the infrastructure (station), the Unmanned Aircraft System Traffic Management (UTM) system, and other essential elements. Among these, foundational infrastructure assumes critical significance. Firstly, it provides dedicated spaces for the specialised take-off and landing operations required by eVTOLs and facilitates the embarkation and disembarkation of passengers. Secondly, the infrastructure construction serves as an indispensable prerequisite in shaping the UAM systems (Brunelli et al., 2023). Only with the establishment of infrastructures can a comprehensive UAM service network be realised. Notably, Rajendran and Srinivas (2020) underscored the existence of two distinctive infrastructure types in UAM systems: vertiports and vertistops. A vertiport serves as a central station, encompassing multiple landing and take-off facilities equipped with essential amenities such

as charging stations and maintenance services. A vertistop is typically smaller and more compact, functioning as a single-purpose station for passenger embarkation and disembarkation, and features a lone helipad (Clarke, 2022). In terms of vertiports and vertistops, the parking stands are crucial resources which influence the capacity of the aerial hubs and the ability to accommodate the fleet of eVTOLs. From the perspective of UAM service providers, strategic deployment of parking stands becomes a pivotal element in enhancing the operational efficiency of vertiports and vertistops. In the previous literature on vertiport infrastructure planning, significant attention has been directed toward design and location decisions (Wang et al., 2022b; Preis, 2021). These studies play a pivotal role in establishing high-efficiency UAM systems. However, it is noteworthy that the literature is relatively limited when addressing the issue of deploying parking stands for both vertiports and vertistops. As a matter of fact, the deployment of parking stands is of distinctive significance. Unlike the well-explored facets of design and location decisions, the determination of parking stand deployment operates at a more macro-level, representing a prerequisite strategic decision that significantly influences the planning of both vertiports and vertistops. This strategic decision precedes and profoundly impacts the subsequent choices related to vertiport location and design. As elucidated by Rajendran and Srinivas (2020) in their literature, prior to finalising a site location, it is imperative to pre-determine the sizing of related facilities of vertiports and vertistops to enhance the service level and service profitability. Hence, this study concentrates on the decision-making regarding the deployment of parking stands for both vertiports and vertistops. As mentioned earlier, the crucial distinction in the parking stands between vertiports and vertistops is that the parking stands at vertiports are equipped with charging facilities, while those at vertistops lack such amenities. Given the distinct features of parking stands at vertiports and vertistops, we consider their deployments separately. Meanwhile, given the inseparable connection between strategic planning and service operations, the decisions pertaining

to strategic planning and service operations should be considered simultaneously. This integrated consideration aims not only to bolster the overall efficiency of the enterprise but also to contribute to profit growth. Additionally, another crucial aspect that needs consideration is people's attitudes towards equality. The concept of equity holds particular significance within the context of urban transportation (Li et al., 2022). It is imperative to emphasise that, within the realm of urban transportation, equity encompasses various dimensions, such as accessibility equity, environmental equity, and spatial equity (Chen et al., 2023; Feitelson, 2002; Chen et al., 2019). Among these dimensions, spatial equity, which focuses on the equitable distribution of transportation resources across different regions, plays a pivotal role in ensuring that the benefits of transportation systems are accessible and fairly distributed across diverse districts. Therefore, we adopt the concept of spatial equity into the realm of UAM systems. An effective management of spatial equity not only fosters enhanced social welfare but also contributes to the long-term development of the enterprise. Hence, it becomes imperative to consider both service profitability and equity simultaneously. Nonetheless, a perpetual conflict exists between profit and equity; prioritising profit often results in fewer considerations for equity. This delicate balance arises as pursuing optimal service profit tends to cover a substantial share of demand, while service equity ensures equal access to the system across diverse regions. Addressing equity concerns proves challenging, and operational managers of public transportation systems often lack awareness of this issue in reality. Therefore, we address this problem by introducing an optimisation approach to guide long-term strategic planning and service operations of UAM systems. Specifically, we present an integrated optimisation problem considering both demand uncertainty and spatial equity, encompassing decisions in both strategic planning and service operations of UAM systems. In strategic planning, our considerations span the determination of parking stand numbers at vertiports and vertistops. Delving into operational service levels, we address decisions related to eVTOL fleet sizing as

well as allocation and operations. To solve this problem, we propose a spatial equity metric and establish a bi-objective optimisation model that aims to strike a balance between service profit and spatial equity. To sum up, the main contributions of this study are summarised as follows:

(1) We introduce an integrated optimisation problem that addresses the strategic planning and service operations of UAM systems while considering both demand uncertainty and spatial equity. This problem aims to make joint decisions, including the determination of the number of parking stands at vertiports and vertistops, eVTOL fleet sizing, eVTOL fleet allocation, and operations. This study represents the initial endeavour to comprehensively address these combined decisions within the domain of UAM system operations and management.

(2) We introduce a novel spatial equity metric and propose a bi-objective optimisation model designed to balance the service profit and spatial equity. In this optimisation model, we aim to maximise total profit while simultaneously optimising the spatial equity metric, subject to various constraints such as the investment budget and management capacity of low-altitude urban airspace, among others. To yield the Pareto solution set, we employ the ε-constraint approach and linearisation technique to effectively transform the model into a tractable single-objective one.

(3) In this study, we employ a scenario-based robust optimisation framework that integrates the interval robust method to address demand uncertainty effectively. Additionally, we assess the model performance through a small-scale instance, followed by a comprehensive case study to validate the proposed model thoroughly. The numerical outcomes demonstrate that the scenario-based robust optimisation framework can generate solutions resilient to uncertain factors. Lastly, we provide insightful policy recommendations to empower UAM service providers in guiding their future decision-making processes. The remainder of this study is organised as follows. In Section 3.2, we introduce a spatial equity metric and present a bi-objective optimisation model.

Additionally, the ε-constraint approach is adopted to achieve the model transformation, and the scenario-based robust optimisation model that incorporates the interval robust optimisation model considering demand uncertainty is proposed. In Section 3.3, we evaluate the model performance through a small-scale example, and a case study is conducted to further validate our proposed model. Additionally, the policy recommendations are proposed to help UAM service providers make decisions. Ultimately, conclusions are illustrated in Section 3.4.

3.2 Problem Description and Mathematical Formulation

In this section, we first describe the research problem and present assumptions to build a foundation for the model establishment in subsection 3.2.1. Then, we introduce a spatial equity metric in subsection 3.2.2. In subsection 3.2.3, we construct a bi-objective optimisation model that aims to maximise system profit while considering spatial equity. Subsequently, in subsection 3.2.4, the bi-objective optimisation model is transformed into a single-objective optimisation model using the ε-constraint approach and linearisation technique. Finally, subsection 3.2.5 presents an interval robust optimisation model is presented in Subsection 3.2.5, and in subsection 3.2.6, we establish a scenario-based robust optimisation model that incorporates the interval robust optimisation model.

3.2.1 Problem description and notations

The emergence and progression of UAM systems mark a revolutionary paradigm shift within the transportation sector, introducing the potential for unparalleled transformations in the urban mobility landscape. As the UAM system undergoes development,

numerous challenges have emerged that urgently require solutions. Therefore, this study delves into an integrated optimisation problem that addresses both strategic planning and service operations of UAM systems, considering the inherent uncertainty in demand. Additionally, recognising the social responsibility of UAM service providers to enhance overall social welfare, we introduce spatial equity considerations into the research problem.

In this subsection, we provide a thorough overview of the research problem and subsequently introduce a mathematical model to address this issue. Our modelling framework incorporates decision-making regarding both strategic planning and service operations and employs a bi-objective optimisation approach, aiming to achieve a harmonious balance between profitability and spatial equity considerations. Specifically, we divide the research region into discrete independent zones. Let K denote the set of zones. Furthermore, the daily operational planning horizon of UAM systems is composed of a finite number of time periods. We let T represent the set of time periods. For the decisions regarding strategic planning, we consider the determination of parking stand numbers at vertiports and vertistops, as well as the sizing of the eVTOL fleet. For each $k \in K$, we introduce the non-negative integer decision variable x_k as the number of opening eVTOL parking stands with charging facilities at vertiports in zone k, and the non-negative integer decision variable y_k as the number of opening eVTOL parking stands without charging facilities at vertistops in zone k. For each opening parking stands at vertiports and vertistops, there exists a unit opening cost denoted by non-negative parameters F^1 and F^2, respectively. However, due to the limited financial investment in infrastructure construction, there is an investment budget for opening parking stands represented by a non-negative parameter H. Additionally, the land area resources allocated for opening vertiports and vertistops are also limited. Therefore, we define the non-negative parameter C_k^1 and C_k^2 as the maximum number of opening parking stands with charging facilities at vertiports in zone k and the

maximum number of opening parking stands without charging facilities at vertistops in zone k, respectively.

Furthermore, we determine the service operation decisions, including the sizing of the eVTOL fleet, eVTOL fleet allocation and operations. We let S denote the set of scenarios and $s \in S$. For each scenario $s \in S$, the occurrence probability is denoted by a non-negative parameter Pr_s. Regarding the uncertain parameter, for each $k \in K$, $p \in K \backslash \{k\}$, $t \in T$, and $s \in S$, we let D^s_{kpt} indicate the travel demand between origin zone k and destination zone p in time period t under scenario s. For each demand, UAM service providers can generate revenue denoted by a non-negative parameter R^{V}. Specifically, for each $t \in T$ and $s \in S$, we define the non-negative integer decision variable Ω^s_t as the operational eVTOL fleet size of the UAM system in time period t under scenario s. We are tasked to allocate the homogeneous eVTOL fleet to zones. Therefore, for each $k \in K$, $t \in T$ and $s \in S$, we introduce the non-negative integer decision variable z^s_{kt} as the number of eVTOL allocated to zone k at the start of time period t under scenario s. Furthermore, there are some unique characteristics that need to be considered for the UAM systems. Firstly, two kinds of eVTOL operation states should be considered, including in-service and repositioning (Wang et al., 2022b). Therefore, for each $k \in K$, $p \in K \backslash \{k\}$, $t \in T$, and $s \in S$, we let the non-negative integer decision variable q^s_{kpt} express the number of in-service eVTOLs from origin zone k to destination zone p in time period t under scenario s. Meanwhile, for each $k \in K$, $p \in K \backslash \{k\}$, $t \in T$, and $s \in S$, we let the non-negative integer decision variable r^s_{kpt} denote the number of repositioning eVTOLs from origin zone k to destination zone p in time period t under scenario s. The unit cost of the in-service operation and repositioning operation are respectively denoted as non-negative parameters c^{Q} and c^{R}. Additionally, for each $k \in K$, $p \in K \backslash \{k\}$, $t \in T$, and $s \in S$, we let the non-negative integer decision variable w^s_{kpt} denote the unsatisfied demand between origin zone k and destination zone p in time period t under scenario s. The unit penalty

cost of unsatisfied demand is represented as a non-negative parameter ω. Secondly, the UAM system needs low-altitude air traffic control systems to coordinate the air traffic in the aerial routes. Therefore, the management capacity is susceptible to weather conditions and the service level of air traffic control (Wang and Qu, 2023). Here, we denote the low-altitude urban airspace management capacity as a non-negative parameter J. Specifically, the low-altitude airspace management capacity refers to the maximum number of eVTOLs that the air traffic control system can handle under current environmental conditions, akin to the concept of sector capacity in civil aviation systems. Thirdly, we need to consider the charging requirement of the UAM system (Guo et al., 2022b). Hence, we present the eVTOL battery depletion rate within a unit flying distance as a non-negative parameter b^{D}. The flying distance from origin zone k to destination zone p is expressed as l_{kp}. Finally, we define a non-negative parameter B^{C} as the unit charging capacity of a parking stand with charging facilities at vertiports. We summarise the notations in Table 3.1.

To establish a rigorous mathematical model, we introduce some assumptions. Firstly, we assume that each zone is characterised by a single central point, and the distances between zones are calculated based on the distances between these central points (Chen and Liu, 2023). In essence, this assumption postulates that the vertiports and vertistops within each zone cluster around a central location, disregarding potential variations of distances caused by the spatial distribution. The rationale behind this assumption aligns with a practical understanding of urban settings and UAM systems. Within certain urban zones, it is conceivable that a core business or activity area serves as the economic centre. Besides, as eVTOLs are characterised by rapid flying speeds, their ability to efficiently connect various points within a zone further bolsters the viability of this premise. Secondly, ride-sharing is not considered in this study. Thirdly, we do not incorporate the impact of congestion into our study (Rath and Chow, 2022). Finally, this model does not keep track of the individual state of charge for each eVTOL

(Wang et al., 2022b). Our attention is concentrated on the charging issue concerning the charging capacity of the overall system from a macro-level perspective.

3.2.2 Spatial equity metric

The concept of equity has received considerable attention in transportation systems. In this study, our primary focus revolves around spatial equity among different zones. Spatial equity plays a crucial role in achieving long-term sustainable profits (Chen et al., 2023). We define the spatial equity ratio here as the ratio of the proportion of the satisfied demand to the proportion of the total demand for each original-destination (OD) pair. Subsequently, equity requirement is achieved by ensuring that all zones have similar spatial equity ratios. Hence, we have the spatial equity ratio of OD pair (k, p) under scenario s, which is expressed as Eq.(3.1).

$$\varrho_{kp}^{s} = \frac{\frac{\sum_{t\in T} q_{kpt}^{s}}{\sum_{t\in T}\sum_{k'\in K}\sum_{p'\in K\backslash\{k'\}} q_{k'p't}^{s}}}{\frac{\sum_{t\in T} D_{kpt}^{s}}{\sum_{t\in T}\sum_{k'\in K}\sum_{p'\in K\backslash\{k'\}} D_{k'p't}^{s}}}, \quad \forall k \in K, \quad \forall p \in K\backslash\{k\}, \quad \forall s \in S, \tag{3.1}$$

where the numerator denotes the proportion of the satisfied demand from zone k to zone p to the total satisfied demand of the UAM system, while the denominator means the proportion of the user demand from zone k to zone p to the total demand of the UAM system. Note that if $\varrho_{kp}^{s} = 1$, OD pair (k, p) is a fairly treated pair under scenario s; if $\varrho_{kp}^{s} > 1$, OD pair (k, p) is a favoured pair under scenario s; if $\varrho_{kp}^{s} < 1$, OD pair (k, p) is a disfavoured pair under scenario s.

Using Eq.(3.1), the spatial equity metric for scenario s, defined Ψ_s, can be proposed as follows:

$$\Psi_s = \max_{k\in K, p\in K\backslash\{k\}} \mid \varrho_{kp}^{s} - \overline{\varrho_{kp}^{s}} \mid, \quad \forall s \in S, \tag{3.2}$$

where $\overline{\varrho_{kp}^{s}}$ is the average value of ϱ_{kp}^{s}. Note that a similar equity metric has been applied in many decision-making problems, such as the decision of air traffic flow management

Table 3.1: Notations of UAM system planning problem

Notation	Definition
Sets	
K	Set of zones, $k \in K$.
T	Set of time periods, $t \in T$.
S	Set of scenarios, $s \in S$.
Parameters	
D^s_{kpt}	The demand between origin zone $k \in K$ and destination zone $p \in K$ in time period t under scenario s.
C^1	The maximum number of opening parking stands with charging facilities at vertiports in zone k.
C^2	The maximum number of opening parking stands without charging facilities at vertiports in zone k.
F^1	The unit cost of opening a parking stand with charging facilities at vertiports.
F^2	The unit cost of opening a parking stand without charging facilities at vertiports.
J	The low-altitude urban airspace management capacity.
H	The investment budget for opening parking stands.
B^{C}	The unit charging capacity of a parking stand with charging facilities at vertiports.
R^{V}	The unit revenue of each demand.
c^{R}	The unit cost of repositioning operation.
c^{Q}	The unit cost of in-service operation.
ω	The unit penalty cost of unsatisfied demand.
l_{kp}	The flying distance from zone k to zone p.
Pr_s	The occurrence probability of scenario s.
Variables	
x_k	The number of opening eVTOL parking stands with charging facilities at vertiports in zone k.
y_k	The number of eVTOL opening parking stands without charging facilities at vertistops in zone k.
z^s_{kt}	The number of eVTOLs allocated to zone k at the start of time period t under scenario s.
q^s_{kpt}	The number of in-service eVTOLs from origin zone k to destination zone p in time period t under scenario s.
w^s_{kpt}	The unsatisfied demand from origin zone k to destination zone p in time period t under scenario s.
r^s_{kpt}	The number of repositioning eVTOLs from origin zone k to destination zone p in time period t under scenario s.
Ω^s_t	The operational eVTOL fleet size of the UAM system in time period t under scenario s.

(Guo et al., 2022a; Zografos and Jiang, 2019).

3.2.3 Bi-objective optimisation model

The bi-objective optimisation model can be formulated as follows:

$$\max_{\boldsymbol{q},\boldsymbol{r},\boldsymbol{w}} \quad \sum_{s\in S} p_s \left[\sum_{t\in T} \sum_{k\in K} \sum_{p\in K\backslash\{k\}} (R^{\mathrm{V}} - c^{\mathrm{Q}}) q^s_{kpt} \right]$$

$$- \sum_{s\in S} p_s \left[\sum_{t\in T} \sum_{k\in K} \sum_{p\in K\backslash\{k\}} c^{\mathrm{R}} r^s_{kpt} - \omega \sum_{t\in T} \sum_{k\in K} \sum_{p\in K\backslash\{k\}} w^s_{kpt} \right] \tag{3.3}$$

$$\min_{\boldsymbol{\Psi}} \quad \sum_{s\in S} p_s \Psi_s \tag{3.4}$$

s.t. $$z^s_{kt} \leq x_k + y_k, \ \ \forall k \in K, \ \forall t \in T, \ \forall s \in S, \tag{3.5}$$

$$x_k \leq C^1_k, \ \ \forall k \in K, \tag{3.6}$$

$$y_k \leq C^2_k, \ \ \forall k \in K, \tag{3.7}$$

$$\sum_{k\in K} F^{\mathrm{P}} x_k + \sum_{k\in K} F^{\mathrm{S}} y_k \leq H, \tag{3.8}$$

$$q^s_{kpt} + w^s_{kpt} = D^s_{kpt}, \ \ \forall k \in K, \ \forall p \in K\backslash\{k\}, \ \forall s \in S, \ \forall t \in T, \tag{3.9}$$

$$\sum_{k\in K} z^s_{kt} \leq \Omega^s_t, \ \ \forall t \in T, \ \forall s \in S, \tag{3.10}$$

$$z^s_{kt} + \sum_{p\in K\backslash\{k\}} r^s_{pkt} - \sum_{p\in K\backslash\{k\}} r^s_{kpt} \geq \sum_{p\in K\backslash\{k\}} q^s_{kpt}, \ \ \forall k \in K, \ \forall t \in T, \ \forall s \in S, \tag{3.11}$$

$$z^s_{kt} = z^s_{k(t-1)} + \sum_{p\in K\backslash\{k\}} r^s_{pk(t-1)} - \sum_{p\in K\backslash\{k\}} r^s_{kp(t-1)} + \sum_{p\in K\backslash\{k\}} q^s_{pk(t-1)} - \sum_{p\in K\backslash\{k\}} q^s_{kp(t-1)},$$

$$\forall k \in K, \ \forall t \in T\backslash\{0\}, \ \forall s \in S, \tag{3.12}$$

$$\sum_{k\in K} \sum_{p\in K\backslash\{k\}} r^s_{kpt} + \sum_{k\in K} \sum_{p\in K\backslash\{k\}} q^s_{kpt} \leq J, \ \ \forall t \in T, \ \forall s \in S, \tag{3.13}$$

$$\sum_{k\in K} \sum_{p\in K\backslash\{k\}} b^{\mathrm{D}} l_{kp} r^s_{kpt} + \sum_{k\in K} \sum_{p\in K\backslash\{k\}} b^{\mathrm{D}} l_{kp} q^s_{kpt} \leq B^{\mathrm{C}} \sum_{k\in K} x_k, \ \ \forall t \in T, \ \forall s \in S,$$

$$\tag{3.14}$$

$$x_k,\ y_k \in \mathbb{Z}^+,\ \ \forall k \in K, \tag{3.15}$$

$$z^s_{kt},\ q^s_{kpt},\ r^s_{kpt},\ w^s_{kpt},\ \Omega^s_t \in \mathbb{Z}^+,\ \ \forall t \in T,\ \ \forall k \in K,\ \forall p \in K\backslash\{k\},\ \forall s \in S. \tag{3.16}$$

The objective function (3.3) maximises the total profit of the UAM system. The objective function (3.4) minimises the spatial equity metric. Constraint (3.5) means that the number of eVTOLs assigned at any given time period should not exceed the capacity of parking stands. Constraints (3.6) and (3.7) guarantee that the number of opening parking stands at vertiports and vertistops cannot exceed the limit imposed by available land or infrastructure. Constraint (3.8) indicates that the total cost of opening the vertiports or vertistops cannot exceed the investment budget. Constraint (3.9) gives a balanced formulation, that is, the number of satisfied demands plus the respective unsatisfied quantity is equivalent to the corresponding total demand for any OD pairs. Constraint (3.10) calculates the eVTOL fleet sizing. Constraint (3.11) ensures the number of idle eVTOLs after the repositioning operation can meet the travel demand. Constraint (3.12) ensures the conservation of traffic flow in each zone. In other words, the number of eVTOLs located in each zone at the time period equals the sum of rebalanced and in-service eVTOLs flying to that zone minus eVTOLs leaving the zone. Constraint (3.13) indicates that the capacity of low-altitude airspace of UAM systems is limited due to some factors, including weather conditions and service level of air traffic control. Specifically, the total number of rebalanced and in-service eVTOLs within the entire airspace must not exceed the management capacity of low-altitude urban airspace. Constraint (5.41) stipulates at a strategic level that the overall electricity consumption must not exceed the total electricity capacity that the entire UAM system can provide. Constraints (3.15) and (3.16) define the domain of the variables respectively.

3.2.4 Model transformation based on ε-constraint approach

The proposed mathematical model involves two objective functions. Typically, there is no single solution that optimises all objectives simultaneously. Therefore, the bi-objective optimisation lies in finding the optimal trade-off among objectives to help decision makers select the most favourable solution (Tang et al., 2022). It is widely recognised that a good solution should not be dominated by other feasible alternatives. The set of non-dominated solutions is known as the Pareto-optimal solution set.

Multiple methods exist to solve the bi-objective optimisation models, including ε-constraint approach, weighted sum, and goal programming method (Demir et al., 2014). In this study, we choose to adopt the ε-constraint approach to solve the proposed bi-objective optimisation model due to its numerous advantages. A key strength of this method is that it can generate a complete and well-distributed set of Pareto-optimal solutions, even when the Pareto front is non-convex–a scenario where traditional weighted-sum methods often fail. Furthermore, it offers the decision-maker significant control over the resolution of the Pareto front by adjusting the value of ϵ, allowing for a more focused exploration of regions of interest. Moreover, this method eliminates the need for cumbersome a priori normalization or weighting, which might be an issue with other methods like the weighted sum method (Mavrotas, 2009).

The general framework of this method for two minimisation objective functions is given as the following equations. This approach keeps one of the objective functions and transforms the other one as a constraint.

$$\begin{aligned} &\min_{x} \ f_n(x) \\ \text{s.t.} \ \ &f_i(x) \leq \varepsilon_i, \ \ \forall i \neq n, \\ &x \in X, \end{aligned} \tag{3.17}$$

where ε_i is the maximum acceptable threshold of the i-th objective function $f_i(x)$ and

is decided by decision makers.

Therefore, based on the framework of ε-constraint approach, the second objective function Eq.(3.4) can be transformed into the following constraint.

$$\sum_{s\in S} Pr_s \Psi_s = \sum_{s\in S} Pr_s \max_{k\in K, p\in K\setminus\{k\}} \mid \varrho_{kp}^s - \overline{\varrho_{kp}^s} \mid \leq \varepsilon. \tag{3.18}$$

Combined with Eq.(3.1)–(3.2), constraint (3.18) can be rewritten as follows:

$$\sum_{s\in S} Pr_s \left\{ \max_{k\in K, p\in K\setminus\{k\}} \left[\frac{\sum_{t\in T}\sum_{k'\in K}\sum_{p'\in K\setminus\{k'\}} D_{k'p't}^s}{\sum_{t\in T}\sum_{k'\in K}\sum_{p'\in K\setminus\{k'\}} q_{k'p't}^s} \left| \frac{\sum_{t\in T} q_{kpt}^s}{\sum_{t\in T} D_{kpt}^s} - \frac{1}{|\mathscr{P}|} \frac{\sum_{t\in T}\sum_{k'\in K}\sum_{p'\in K\setminus\{k'\}} q_{k'p't}^s}{\sum_{t\in T}\sum_{k'\in K}\sum_{p'\in K\setminus\{k'\}} D_{k'p't}^s} \right| \right] \right\} \leq \varepsilon, \tag{3.19}$$

where $\mid \mathscr{P} \mid$ is the number of OD pairs, $\mid \mathscr{P} \mid = \mid K \mid \times (\mid K \mid -1)$.

Constraint (3.19) poses inherent computational complexities due to nonlinearity arising from variables in the denominator, absolute values, and maximisation operations. Additionally, this problem is NP-hard and nonconvex; there is no closed-form solution, and it cannot be solved in polynomial time. While striving for an exact optimal solution is always desirable, it remains a significant challenge given the current optimisation technologies. However, despite the difficulty of obtaining the exact value of the original problem, some literature focuses on obtaining approximation solutions (Yang et al., 2021a; Ben-Tal and Nemirovski, 2009; Wang et al., 2021c). The core thinking is to seek a conservation solution in a subset of the origin feasible set to ensure the approximation solution is safe. Similar solution logic has been applied by several studies (Yin et al., 2019, 2023a). Similarly, we opt for an approximate technique to handle the constraint (3.19) to make it computationally tractable, resulting in a conservative solution. A conservative approximate transformation of constraint (3.19) is introduced as follows:

$$\max_{k\in K, p\in K\setminus\{k\}} \left\{ \frac{\sum_{t\in T}\sum_{k'\in K}\sum_{p'\in K\setminus\{k'\}} D_{k'p't}^s}{\sum_{t\in T}\sum_{k'\in K}\sum_{p'\in K\setminus\{k'\}} q_{k'p't}^s} \left| \frac{\sum_{t\in T} q_{kpt}^s}{\sum_{t\in T} D_{kpt}^s} - \frac{1}{|\mathscr{P}|} \frac{\sum_{t\in T}\sum_{k'\in K}\sum_{p'\in K\setminus\{k'\}} q_{k'p't}^s}{\sum_{t\in T}\sum_{k'\in K}\sum_{p'\in K\setminus\{k'\}} D_{k'p't}^s} \right| \right\}$$
$$\leq \varepsilon \left(Pr_s |S|\right)^{-1}, \quad \forall s \in S, \tag{3.20}$$

where $|S|$ is the number of scenarios.

Constraint (3.20) serves as a safe approximation of constraint (3.19) because the feasible domain of constraint (3.20) is a subset of the feasible domain of the original model, resulting in a more conservative solution. Therefore, we can safely substitute constraint (3.19) with constraint (3.20) to make the mathematical model computationally tractable through the conservative approximation. Within the context of UAM systems, conservative solutions are particularly acceptable. It is essential to increase the level of public trust and facilitate incremental progress during the nascent and evolving stages of UAM development (Rimjha et al., 2021). Relative conservative strategies promote service reliability and enhance public acceptance of novel transportation modes. Therefore, the conservative approaches can serve as a pragmatic means of mitigating risks and ensuring a smooth transition toward broader UAM adoption.

However, we observed that constraint (3.20) is non-linear, which poses difficulty in solving. According to Zografos and Jiang (2019), the constraint (3.20) can be substituted by the following linear constraints.

$$\frac{\sum_{t\in T}\sum_{k'\in K}\sum_{p'\in K\backslash\{k'\}} D^s_{k'p't}}{\sum_{t\in T}\sum_{k'\in K}\sum_{p'\in K\backslash\{k'\}} q^s_{k'p't}} \left| \frac{\sum_{t\in T} q^s_{kpt}}{\sum_{t\in T} D^s_{kpt}} - \frac{1}{|\mathscr{P}|} \frac{\sum_{t\in T}\sum_{k'\in K}\sum_{p'\in K\backslash\{k'\}} q^s_{k'p't}}{\sum_{t\in T}\sum_{k'\in K}\sum_{p'\in K\backslash\{k'\}} D^s_{k'p't}} \right|$$

$$\leq \varepsilon \left(Pr_s|S|\right)^{-1}, \forall s \in S,\ \forall k \in K,\ \forall p \in K\backslash\{k\}, \tag{3.21}$$

Furthermore, following the logic of the linearisation technique proposed by Guo et al. (2022a), the constraint (3.21) can be substituted by the following linear constraints.

$$\frac{\sum_{t\in T} q^s_{kpt}}{\sum_{t\in T} D^s_{kpt}} - \frac{1}{|\mathscr{P}|} \frac{\sum_{t\in T}\sum_{k'\in K}\sum_{p'\in K\backslash\{k'\}} q^s_{k'p't}}{\sum_{t\in T}\sum_{k'\in K}\sum_{p'\in K\backslash\{k'\}} D^s_{k'p't}} \leq \varepsilon \frac{1}{Pr_s|S|} \frac{\sum_{t\in T}\sum_{k'\in K}\sum_{p'\in K\backslash\{k'\}} q^s_{k'p't}}{\sum_{t\in T}\sum_{k'\in K}\sum_{p'\in K\backslash\{k'\}} D^s_{k'p't}},$$

$$\forall s \in S,\ \forall k \in K,\ \forall p \in K\backslash\{k\}, \tag{3.22}$$

$$\frac{1}{|\mathscr{P}|}\frac{\sum_{t\in T}\sum_{k'\in K}\sum_{p'\in K\backslash\{k'\}} q^s_{k'p't}}{\sum_{t\in T}\sum_{k'\in K}\sum_{p'\in K\backslash\{k'\}} D^s_{k'p't}} - \frac{\sum_{t\in T} q^s_{kpt}}{\sum_{t\in T} D^s_{kpt}} \leq \varepsilon \frac{1}{Pr_s|S|}\frac{\sum_{t\in T}\sum_{k'\in K}\sum_{p'\in K\backslash\{k'\}} q^s_{k'p't}}{\sum_{t\in T}\sum_{k'\in K}\sum_{p'\in K\backslash\{k'\}} D^s_{k'p't}},$$

$$\forall s \in S,\ \forall k \in K,\ \forall p \in K\backslash\{k\}. \tag{3.23}$$

Therefore, the original bi-objective mathematical programming can be transformed into the following optimisation model [P1].

[P1] Eq.(3.3)

s.t. Constraints (3.5)–(3.16), (3.22)–(3.23).

3.2.5 Interval robust optimisation model

In this study, the demand uncertainty is considered, which exists in constraints (3.9), (3.22) and (3.23). To cope with the parameter uncertainties, the method proposed by (Sun et al., 2022) is adopted here. For the uncertainty of user demand, we assume that $\widetilde{D^s_{kpt}}$ is a bounded and symmetric random variable whose realisations fall in the interval $\left[\overline{D^s_{kpt}}, \overline{D^s_{kpt}} + \widehat{r^s_{kpt}}\right]$, where $\overline{D^s_{kpt}}$ is the nominal demand value and $\widehat{r^s_{kpt}}$ is the data variability. For simplicity, we introduce a parameter $\Gamma^s_{kpt} \in [0, 1]$ to control the actual deviation from the nominal demand value, which is called the budget of uncertainty.

Note that the value of the budget of uncertainty can be chosen according to the risk preference of decision makers. It can adapt the robustness of the model based on the conservatism level of the solutions. When the budget of uncertainty is equal to 0, the robust model will be transformed into a deterministic one. Furthermore, as another special case, when it is equal to 1, the case will correspond to the worst-case problem, which is the most conservative one.

Adopting the above method, constraints (3.9), (3.22) and (3.23) can be reformulated as follows:

$$q^s_{kpt} + w^s_{kpt} = \overline{D^s_{kpt}} + \widehat{r^s_{kpt}}\Gamma^s_{kpt},\quad \forall k \in K,\ \forall p \in K\backslash\{k\},\ \forall s \in S,\ \forall t \in T, \tag{3.24}$$

$$\frac{\sum_{t\in T} q^s_{kpt}}{\sum_{t\in T}(\overline{D^s_{kpt}}+\widehat{r^s_{kpt}}\Gamma^s_{kpt})}-\frac{1}{|\mathscr{P}|}\frac{\sum_{t\in T}\sum_{k'\in K}\sum_{p'\in K\backslash\{k'\}} q^s_{k'p't}}{\sum_{t\in T}\sum_{k'\in K}\sum_{p'\in K\backslash\{k'\}}(\overline{D^s_{k'p't}}+\widehat{r^s_{k'p't}}\Gamma^s_{k'p't})}$$

$$\leq \varepsilon\frac{1}{Pr_s|S|}\frac{\sum_{t\in T}\sum_{k'\in K}\sum_{p'\in K\backslash\{k'\}} q^s_{k'p't}}{\sum_{t\in T}\sum_{k'\in K}\sum_{p'\in K\backslash\{k'\}}(\overline{D^s_{k'p't}}+\widehat{r^s_{k'p't}}\Gamma^s_{k'p't})}, \forall s\in S,\ \forall k\in K,\ \forall p\in K\backslash\{k\}, \tag{3.25}$$

$$\frac{1}{|\mathscr{P}|}\frac{\sum_{t\in T}\sum_{k'\in K}\sum_{p'\in K\backslash\{k'\}} q^s_{k'p't}}{\sum_{t\in T}\sum_{k'\in K}\sum_{p'\in K\backslash\{k'\}}(\overline{D^s_{k'p't}}+\widehat{r^s_{k'p't}}\Gamma^s_{k'p't})}-\frac{\sum_{t\in T} q^s_{kpt}}{\sum_{t\in T}(\overline{D^s_{kpt}}+\widehat{r^s_{kpt}}\Gamma^s_{kpt})}$$

$$\leq \varepsilon\frac{1}{Pr_s|S|}\frac{\sum_{t\in T}\sum_{k'\in K}\sum_{p'\in K\backslash\{k'\}} q^s_{k'p't}}{\sum_{t\in T}\sum_{k'\in K}\sum_{p'\in K\backslash\{k'\}}(\overline{D^s_{k'p't}}+\widehat{r^s_{k'p't}}\Gamma^s_{k'p't})}, \forall s\in S,\ \forall k\in K,\ \forall p\in K\backslash\{k\}. \tag{3.26}$$

Based on the above analysis, the interval robust optimisation model can be established as the following model [P2].

[P2] Eq.(3.3)

s.t. Constraints (3.5)–(3.8), (3.10)–(3.16), (3.24)–(3.26).

3.2.6 Scenario-based robust optimisation model

In this subsection, we adopt the scenario-based robust optimisation framework proposed by Mulvey et al. (1995) to this problem and incorporate the interval robust optimisation model into the scenario-based robust optimisation framework to enhance the performance of the solutions obtained from the interval robust optimisation model, referring to the literature by Sun et al. (2022). This framework considers two types of robustness: solution robustness and model robustness. Solution robustness refers to the stability of expected objectives when the scenarios change. Model robustness, on the other hand, ensures that the solution remains highly feasible across all scenarios. The solutions obtained from this approach are more robust and less sensitive to parameter uncertainties. The framework has some applications in the field of transportation

and logistics, such as the research byMirzapour Al-E-Hashem et al. (2011), Bakhtavar and Mahmoudi (2020), and Hu et al. (2023b).

In the scenario-based robust optimisation framework, the parameters τ and ω are introduced to represent the weight coefficients of solution robustness and model robustness, respectively. Hence, we can rewrite the interval robust optimisation model [P2] as follows:

$$\max \quad \sum_{s\in S} Pr_s \mathscr{H}_s - \tau \sum_{s\in S} Pr_S \left(\mathscr{H}_s - \sum_{s\in S} Pr_s \mathscr{H}_s \right)^2 - \omega \sum_{s\in S} Pr_s \sum_{t\in T} \sum_{k\in K} \sum_{p\in K\setminus\{k\}} w^s_{kpt} \tag{3.27}$$

$$\text{s.t.} \quad \mathscr{H}_s = \sum_{t\in T} \sum_{k\in K} \sum_{p\in K\setminus\{k\}} (R^{\mathrm{V}} - c^{\mathrm{Q}}) q^s_{kpt} - \sum_{t\in T} \sum_{k\in K} \sum_{p\in K\setminus\{k\}} c^{\mathrm{R}} r^s_{kpt}, \quad \forall s \in S, \tag{3.28}$$

$$\text{Constraints} (3.5) - (3.8), (3.10) - (3.16), (3.24) - (3.26),$$

where the first part means the expected value, the second part accounts for the risk penalty associated with value variance across all scenarios, and the third term represents the penalty for model infeasibility, which is expressed by the penalty cost of unmet demand.

In the objective function Eq. (3.27), the inclusion of quadratic terms introduces significant computational challenges to this model. Following Yu and Li (2000) and Leung et al. (2007), the objective function Eq. (3.27) can be replaced by the following equation.

$$\max \quad \sum_{s\in S} Pr_s \mathscr{H}_s - \tau \sum_{s\in S} Pr_S \left| \mathscr{H}_s - \sum_{s\in S} Pr_s \mathscr{H}_s \right| - \omega \sum_{s\in S} Pr_s \sum_{t\in T} \sum_{k\in K} \sum_{p\in K\setminus\{k\}} w^s_{kpt} \tag{3.29}$$

In Eq.(3.29), we observe the presence of a nonlinear term, which contributes to the

complexity of the model. Therefore, a linearisation technique is used in this study. After introducing an auxiliary variable δ_s, Eq.(3.29) will be reformulated as follows:

$$\max \sum_{s\in S} Pr_s \mathscr{H}_s - \tau \sum_{s\in S} Pr_s \left(\mathscr{H}_s - \sum_{s\in S} Pr_s \mathscr{H}_s + 2\delta_s \right) - \omega \sum_{s\in S} Pr_s \sum_{t\in T} \sum_{k\in K} \sum_{p\in K\setminus\{k\}} w^s_{kpt} \tag{3.30}$$

$$\text{s.t.} \quad \mathscr{H}_s - \sum_{s\in S} Pr_s \mathscr{H}_s + 2\delta_s \geq 0, \quad \forall s \in S. \tag{3.31}$$

Finally, the scenario-based robust optimisation model can be established as a model [P3].

[P3] Eq.(3.30)

s.t. Constraints (3.5)–(3.8), (3.10)–(3.16), (3.24)–(3.26), (3.28), (3.31).

3.3 Numerical Experiments

This section conducts a series of numerical experiments to validate the proposed model. Subsection 3.3.1 conducts the experiments through a small-scale example to test the model performance. Following this, in subsection 3.3.2, a large-scale case study is introduced to validate the effectiveness of the proposed model, and we conduct a series of sensitive analyses on specific key parameters. Finally, we propose several significant policy recommendations to support the UAM service providers in making decisions in subsection 3.3.3. All the numerical experiments are carried out using the Gurobi 10.0.0 commercial solver on a personal computer with an AMD Ryzen 9 7950X 16-Core Processor running at 4.50 GHz and 128.0 GB RAM, operating under Windows 10 (64-bit).

3.3.1 A small-scale example

In the first part of numerical experiments, we assess the proposed scenario-based robust optimisation model using a randomly generated small-scale example. This specific example comprises five distinct zones labelled A through E, resulting in a total of 20 OD pairs.

In terms of parameter settings, the straight-line distances between the centres of these five zones are presented in Table 5.2. Following Boyacı et al. (2021), the conversion coefficient for Euclidean distance to road distance typically falls within the range of approximately 1.2 to 1.4. Therefore, we set the flying distance between the two zones as 1.3 times the straight-line distance between their centres, referring to the ground transportation network. Additionally, this experiment incorporates five time periods, each spanning 30 min. Concerning parameters related to the investment in the vertiports and vertistops, the opening cost of parking stands at vertiports is set at 6000, while for vertistops, it is 2000. The fixed investment budget is set at 0.7 million. Regarding the UAM service, the unit price for UAM service demand is set as 800, accompanied by a unit in-service operational cost of 200, a unit repositioning cost of 250, and a penalty cost of 400 attributed to each unit unsatisfied demand (Tiketi, 2025). Due to the absence of historical data on UAM system operations, we simulate the demand for each OD pair during each time period, ranging from 4 to 6 across different scenarios. Furthermore, we introduce the parameter associated with the charging issue. Each parking stand at vertiports can provide a charging capacity of 300 kWh (Li et al., 2023), and the electricity consumption rate is set at 31 kWh per hundred kilometres[1]. Finally, we set the low-altitude airspace management capacity to 50.

[1]Data from Wallstreetcn: https://wallstreetcn.com/articles/3706419

Table 3.2: Distances between the origins and destinations (km).

	A	B	C	D	E
A	0	5	26	131	126
B	5	0	20	128	123
C	26	20	0	111	106
D	131	128	111	0	10
E	126	123	106	10	0

3.3.1.1 Computational results

To obtain the Pareto set of the small-scale example, we set different values of ε in this part. The parameter setting of ε needs to be carefully considered. If the value is set too high, the constraints regarding equity would lack the bound. Conversely, if the value is set too low, the solution might become unreasonable. That is, the total profit would be negative. In this study, we first solve the model without incorporating the equity constraints and the equity metric is obtained to set as the initial value of ε. Subsequently, we can acquire the updated ε value by decreasing it with a predetermined step size until no reasonable solution can be obtained. Figure 3.1 illustrates the Pareto front of the small-scale example. Note that a smaller equity value corresponds to a higher equity level. From Figure 3.1, we observe that decreasing the equity metric results in a reduction in total profit. This computational result indicates a trade-off between the two optimisation objectives. Consequently, decision makers can potentially compromise a portion of the profit to attain a specific equity level. Additionally, decision makers can flexibly select the equity level based on preferences and real-world circumstances.

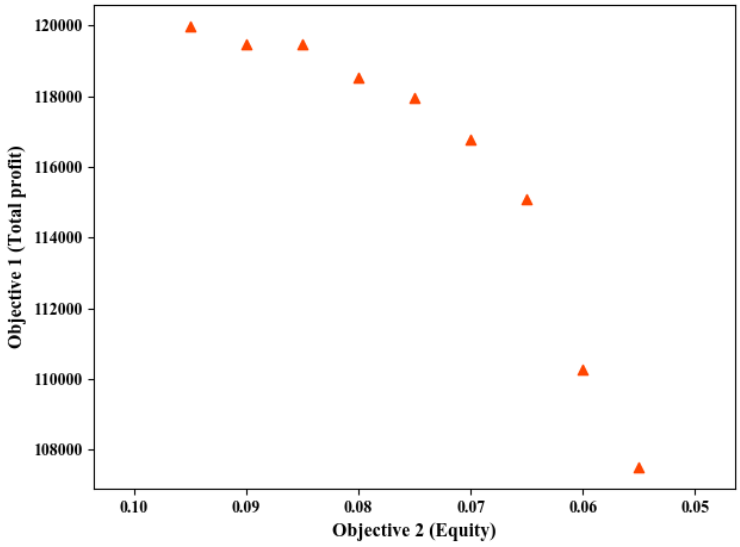

Figure 3.1: The Pareto front of the small-scale example (The smaller the equity value, the higher the equity level).

3.3.1.2 Model comparison and evaluation

In this part, we make a performance comparison between the proposed interval robust optimisation model [P2] and the scenario-based robust optimisation model that incorporates the interval robust optimisation model [P3] to evaluate the solution robustness of the model [P3]. It is noted that when the weight coefficient of solution robustness τ is equal to 0, the model [P3] will become equivalent to model [P2].

In this experiment, the budget of uncertainty and the data variability are both set to 0.1. We compare and analyse the computational results of expected operational profit $\mathscr{F}$ (Penalty costs are deducted), variance of operational profit $\mathscr{D}$, and variance of eVTOL fleet sizing $\mathscr{L}$ derived from two models, which are calculated based on the following Eq.(3.32) to Eq.(3.35). The main experimental results with $\tau = 0.5$ and $\varepsilon = 0.065$ are presented in Table 3.3. From Table 3.3, it can be found that the expected operational profit of model [P3] is only 0.18 % less than that of model [P2], with a 20.39 % reduction in the variance of operational profit compared to model [P2]. Furthermore,

we can find that the variance of the eVTOL fleet size derived from model [P3] is also smaller than that of model [P2]. It can be proved that the solution from model [P3] can enhance the stability and resilience of the decision-making process. These computational results highlight that the proposed scenario-based robust optimisation model exhibits significantly greater stability across all scenarios, even with inevitable economic trade-offs.

$$\mathscr{F} = \sum_{s \in S} Pr_s \mathscr{H}_s \tag{3.32}$$

$$\mathscr{D} = \sum_{s \in S} Pr_s \left(\mathscr{H}_s - \sum_{s \in S} Pr_s \delta_s \right) \tag{3.33}$$

$$\mathscr{A} = \sum_{s \in S} Pr_s \max_t \Omega_{ts} \tag{3.34}$$

$$\mathscr{L} = \sqrt{\sum_{s \in S} Pr_s \left(\max_t \Omega_{ts} - \mathscr{A} \right)^2} \tag{3.35}$$

Figure 3.2 illustrates the operational profit values for each scenario. It is evident that the solution derived from the proposed model [P3] demonstrates reduced sensitivity to different scenarios. This affirms the robust nature of our model [P3] across various situations. Given the significance of solution robustness to policymakers, our proposed model proves highly effective for operating UAM systems and mitigating the impact of user demand uncertainty.

3.3.2 A large-scale case study

In this subsection, we thoroughly examine the proposed optimisation model through a practical case study based on a megalopolis in southern China.

Table 3.3: Model comparison results.

Model	Expected operational profit	Variance of operational profit	Variance of eVTOL fleet size
[P2]	198,880	672	38
[P3]	198,510	535	12

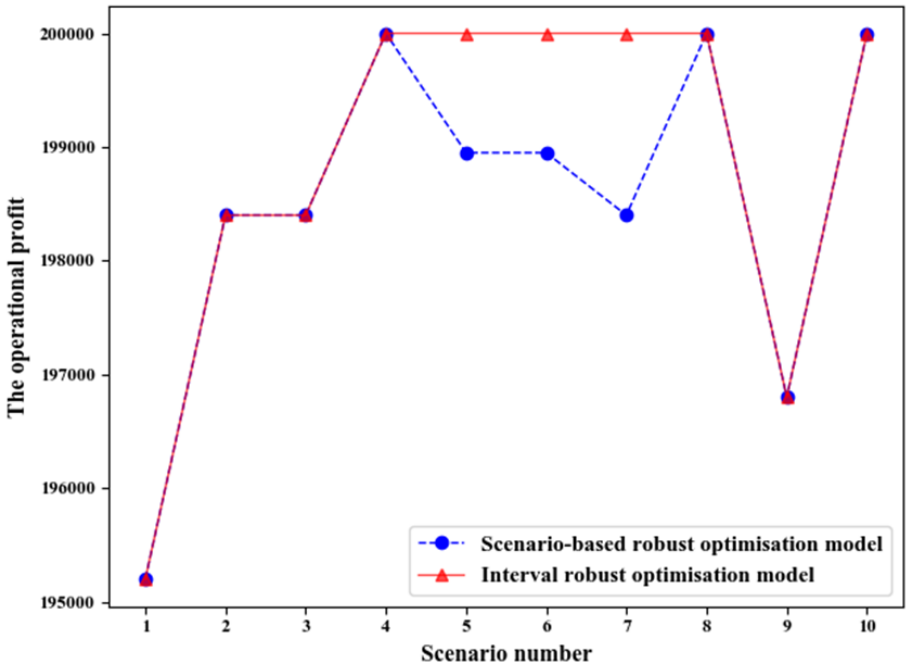

Figure 3.2: The operational profit for each scenario.

3.3.2.1 Case background and data settings

This study focuses on strategic and operational planning for the UAM system in eight core cities within the Guangdong-Hong Kong-Macao Greater Bay Area (GBA) of China. These eight cities include Hong Kong, Guangzhou, Shenzhen, Zhuhai, Macao, Dongguan, Foshan, and Zhongshan. This region is located in southern China and is highly developed, characterised by a thriving economy and substantial potential. According to the official statistics, daily travel between mainland cities has achieved 6 million between the mainland China cities of GBA, highlighting the growing need for contemporary transportation solutions. Notably, there is a significant proportion of high-income individuals in this region. This combination of urban prosperity and higher income levels points to a strong demand for new transportation modes, especially the UAM system. In fact, helicopter services are already operational between Shenzhen

and Hong Kong, Hong Kong and Macao, as well as Guangzhou and Shenzhen in this region. This existing infrastructure provides a solid foundation for the development of the UAM system in the coming years. Therefore, this region is selected as the case study to address the imminent need to establish an effective and convenient UAM system and mitigate ground traffic congestion in the future.

We divide the study area into 24 zones roughly according to the administrative divisions and economic development levels. The geographic region and zone division are depicted in Figure 3.3, with the centroids of the zones marked. In our case study, there are 552 different pairs of origins and destinations. The UAM system operation hours are designated from 7:00 a.m. to 21:00 p.m., divided into 28 intervals, each lasting 30 minutes. To stimulate the UAM demand, we randomly generate the daily market size of each time period for each origin-destination pair across three scenarios due to a lack of historical data. Specifically, we categorise these zones into two groups based on Gross Domestic Product (GDP) per capita: relatively high-income zones and relatively low-income zones. Subsequently, we generate demand for each time period between two relatively high-income zones ranging from 2 to 6, demand for each time period between relatively high-income zones and relatively low-income zones ranging from 2 to 4, and demand for each time period between two relatively low-income zones ranging from 1 to 3. The limits of the number of parking stands at vertiports and vertistops are randomly generated according to the land area and economic development level. Regarding the other parameters utilised in this study, the investment budget is set at 8 million, and the low-altitude airspace management capacity is set at 1,500. The remaining parameters align with those used in the experiment of the small-scale example discussed in the previous subsection.

3.3.2.2 Computational result analysis

To further analyse the relationship between the two optimisation objectives, a range

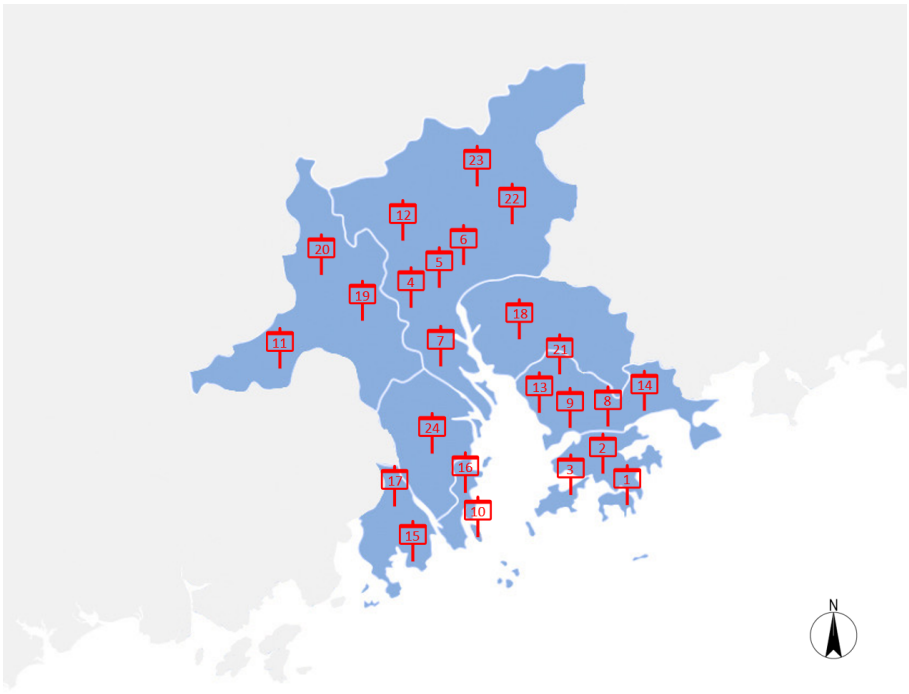

Figure 3.3: Geographic region and zone division of the case study.

of ε values (equity levels) are employed to solve the bi-objective optimisation model. Figure 3.4 shows the Pareto front of the large-scale case study. As anticipated, the two objectives conflict with each other, making it impossible to achieve an optimal solution that satisfies both simultaneously. In detail, the total profit decreases as the equity level becomes higher. This implies a less stringent equity requirement, leading to a higher profit. Furthermore, we can observe a significant decrease when the equity level drops below 0.2.

Additionally, we analyse the demand satisfaction rate of the UAM system and the number of repositioning eVTOLs when the equity metric is set as different values. The computational results are shown in Figure 3.5. From Figure 3.5, it is evident that the demand satisfaction rate of the UAM system slightly decreases when the equity metric ranges from 1.0 to 0.2. There is also a significant drop when the equity metric is smaller than 0.2. Furthermore, in terms of the number of repositioning eVTOLs, it

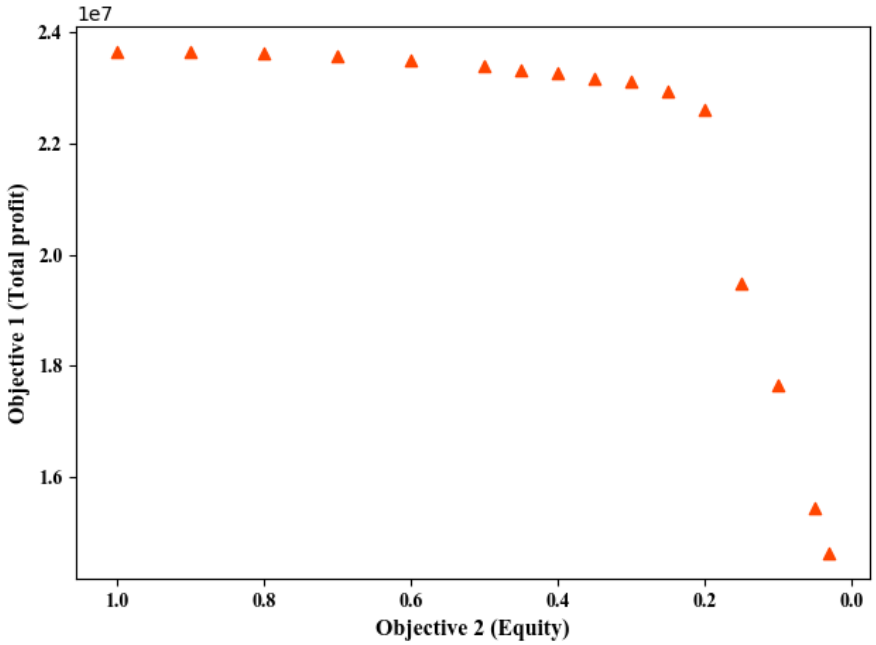

Figure 3.4: The Pareto front of the large-scale case study (The smaller the equity value, the higher the equity level).

is observable that the count exhibits a sharp rise when the equity metric ranges from 1.0 to 0.2. However, the number of repositioning eVTOLs has a significant decrease when the equity metric is smaller than 0.2. These results show that when the equity requirement is not too stringent, the system can strategically deploy a more significant number of repositioning eVTOLs to maintain the demand satisfaction rate to be nearly stable. However, when the equity requirement achieves a certain degree of strictness, the potential to maintain demand satisfaction by deploying more repositioning eVTOLs diminishes. Instead, the equity requirement can only be met by cancelling a substantial number of travel orders, leading to a low demand satisfaction rate of the UAM system. Therefore, when the equity requirement is not excessively stringent, the demand satisfaction rate of the UAM system can be kept at a nearly stable condition by increasing the number of repositioning eVTOLs. Meanwhile, an excessive pursuit of the equity requirement may lead to the risk of a significant decrease in profits, which

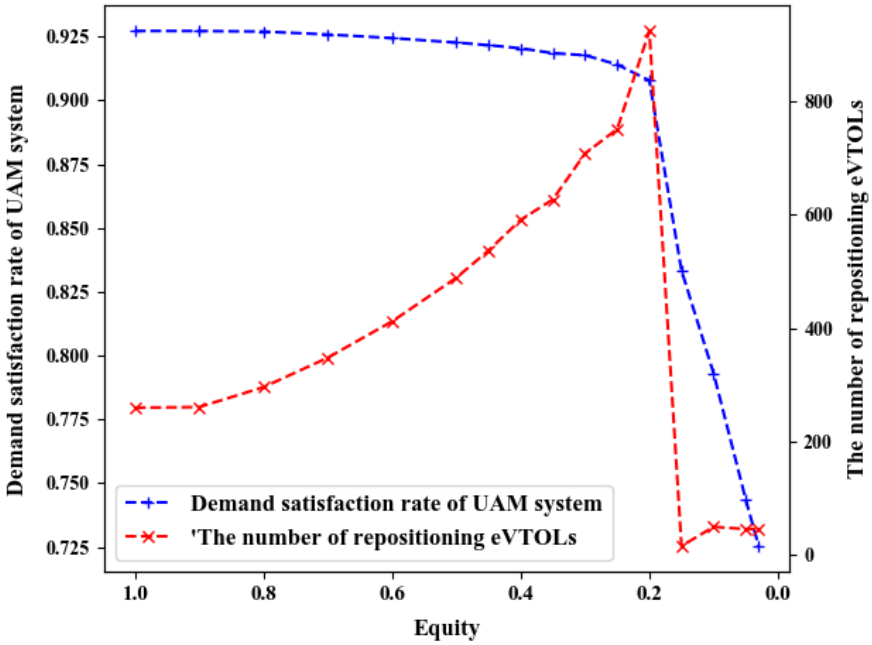

Figure 3.5: The demand satisfaction rate and the number of repositioning eVTOLs under different equity levels.

will cause the loss of passengers and low passenger satisfaction levels. Therefore, this insight underscores the necessity for policymakers to strike an equilibrium between financial performance and equity objectives. It prompts meticulous selection of the equity requirement and fosters a holistic decision making approach that strikes a trade-off between profit and equity.

3.3.2.3 The effect of uncertainty

The role of the uncertain parameters is to modulate the robustness of the proposed model concerning the level of conservatism in the process of decision-making. A series of experiments are conducted in this part to explore the impact of uncertain parameters. In this experiment, the budget of uncertainty and data variability are respectively varied from 0.3 to 0.9 in increments of 0.2. The computational results for different parameter combinations when the equity metric is 0.6 are shown in Figure 3.6. As we

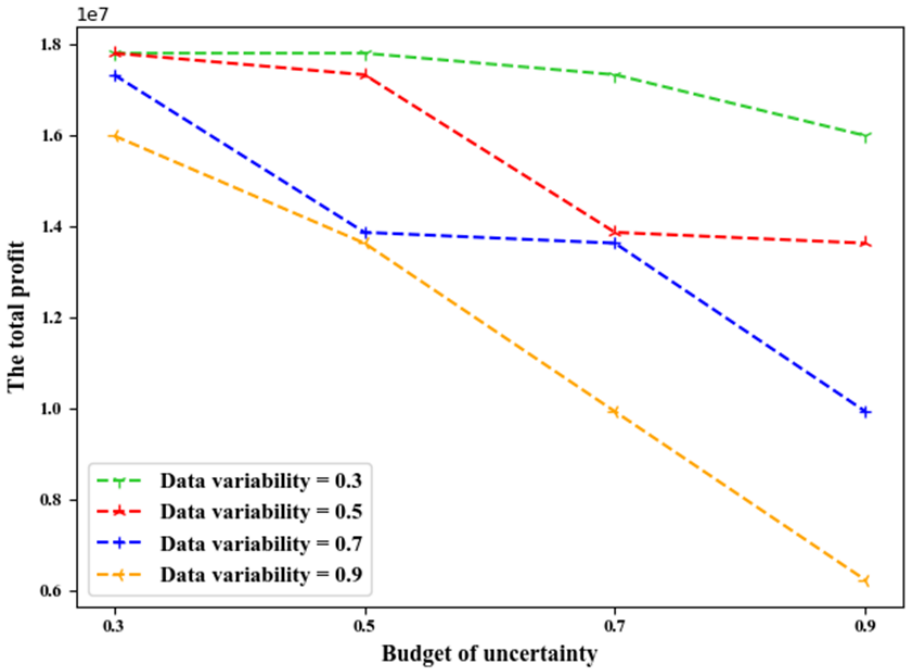

Figure 3.6: The experimental outcomes for different combinations of budget of uncertainty and data variability.

can see from Figure 3.6, when the budget of uncertainty remains fixed, the total profit decreases with the reduction of the data variability. Moreover, the total profit also decreases as the uncertainty budget becomes smaller while maintaining a fixed value for data variability. The optimal value derived from the model that does not account for uncertainty is 23,480,300, surpassing the objective values obtained from the instances that take uncertainty into consideration. Additionally, when the parameter combination is set to its maximum value, the objective function attains its least favourable value, which corresponds to the most conservation attitude of policymakers. Furthermore, this trend is likely due to the demand exceeding the service capacity, resulting in numerous unsatisfied orders. Hence, policymakers must adapt the service level and operational strategies, or accurately predict user demand to mitigate the risk caused by demand uncertainty to enhance company profits.

3.3.2.4 The effect of demand level

This experiment aims to explore the impact of demand levels on strategic planning and service operations of UAM systems. We categorise daily demand levels into three categories: low, medium, and high. With a fixed value of ε at 0.6, the principal experimental outcomes of the operational level are presented in Table 3.4. From Table 3.4, it is evident that as the demand level increases, the total profit and the number of repositioning eVTOLs all increase. The results are because the increased demand fosters more frequent repositioning of eVTOLs, thereby enhancing resource utilisation and optimising mobility service, ultimately contributing to profit augmentation. Additionally, it is noteworthy that the demand satisfaction rate exhibits a slight decrease when the demand level becomes higher. This decline can be attributed to additional constraints, including low-altitude airspace management capacity, investment budget, and equity considerations, which limit the capacity of the UAM system.

Furthermore, we calculate the number of eVTOL parking stands at both vertiports and vertistops to explore the impact of demand level on the strategic planning of UAM systems. The computational outcomes are presented in Table 3.5. From Table 3.5, it is evident that the number of eVTOL parking stands equipped with charging facilities at vertiports escalates in tandem with the augmentation of demand levels. As mentioned before, vertiports are equipped with charging facilities for eVTOLs. This phenomenon can be attributed to the escalating number of both repositioning and in-service eVTOLs necessitating electricity charging as the demand level becomes higher. Furthermore, in the scenario of a medium demand level, we find that the total number of eVTOL parking stands at both vertiports and vertistops is the largest across three demand levels. This occurrence is primarily attributed to an intricate trade-off relationship regarding the allocation of parking facilities between vertiports and vertistops imposed by the investment budget constraint. For the high demand level, the extensive opening of parking stands at vertiports is driven by the imperative of maximising

Table 3.4: he computational results of operational service level with different demand levels.

Demand level	Average demand	Total profit	Demand satisfaction rate	Quantity of repositioning eVTOLs
High	45,003	24,098,300	0.942359	1238
Medium	36,388	21,600,550	0.995273	241
Low	30,337	18,013,950	0.995319	185

demand fulfilment to ensure adequate provisions for electricity charging requirements. Therefore, the opening of a more significant number of parking stands at vertistops is hindered. This complex deliberation is driven by the strategic prioritisation of resource distribution, balancing the imperative of catering to both charging-equipped and demand-driven parking stands at vertiports while also accommodating demand-driven parking stands at vertistops. The spatial distribution of the opening scale of eVTOL parking stands of high, medium, and low demand level are depicted in Figure 3.7, 3.8, and 3.9, respectively. It becomes evident that regions marked by high demand or advanced economic development exhibit a correspondingly denser concentration of parking facilities in alignment with real-world demand trends. Besides, we calculate the eVTOL fleet size of different demand levels. As anticipated, it is evident that the fleet size is directly proportional to the demand level.

3.3.2.5 The effect of low-altitude airspace management capacity

Low-altitude airspace management will be crucial for the future of the UAM systems (Dai et al., 2021), which will have a significance on the operation efficiency of UAM systems. Due to the technology bottleneck of air traffic control or adverse weather conditions such as wind, rain, fog, and storms, the management capacity of low-altitude urban airspace (Alvarez et al., 2021) is limited. Therefore, we investigate the effect of the low-altitude airspace management capacity on the service operations of the UAM system in this part.

In this experiment, we set the equity metric ε as 0.3. The computational results of the total profit under different low-altitude airspace management capacities are presented in Table 6. From Table 3.6, we can find that the total profits rise with an increase in low-altitude airspace management capacity until they nearly stabilise. This is because the increasing low-altitude airspace management capacity allows for a greater number of orders to be fulfilled. However, additional constraints such as charg-

Table 3.5: The computational results of strategic planning level with different demand levels.

Demand level	The total number of eVTOL parking stands at vertiports and vertistops	The number of eVTOL parking stands with charging facilities at vertiports	eVTOL Fleet sizing
High	1880	1056	1656
Medium	1920	594	1567
Low	1852	585	1388

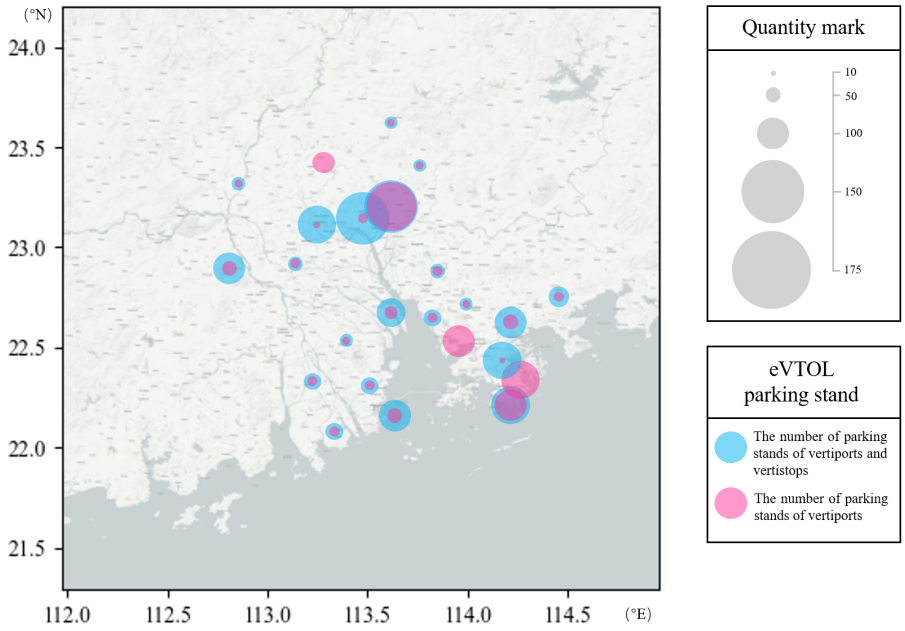

Figure 3.7: The spatial distribution of the opening scale of eVTOL parking stands at vertiports and vertistops (High demand level).

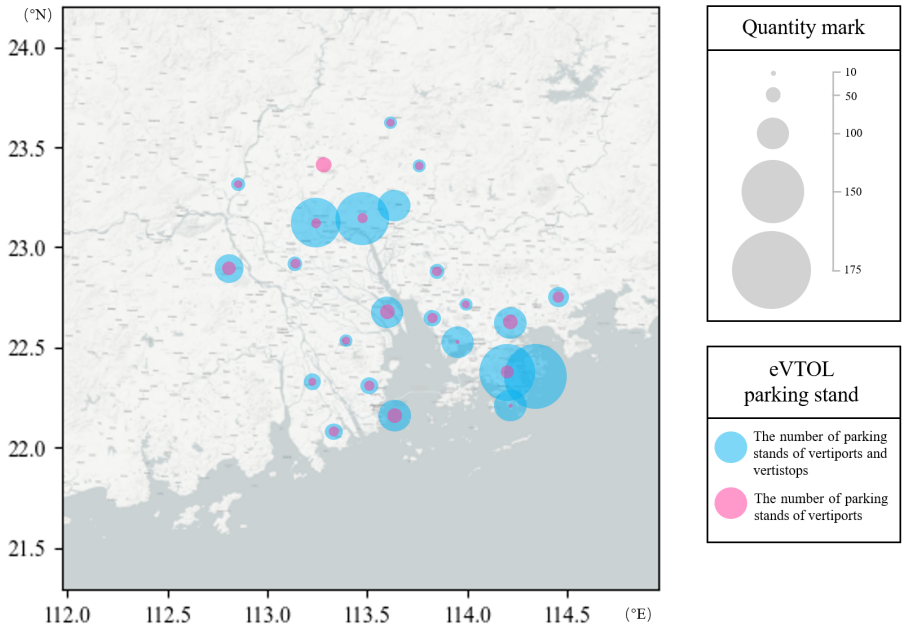

Figure 3.8: The spatial distribution of the opening scale of eVTOL parking stands at vertiports and vertistops (Medium demand level).

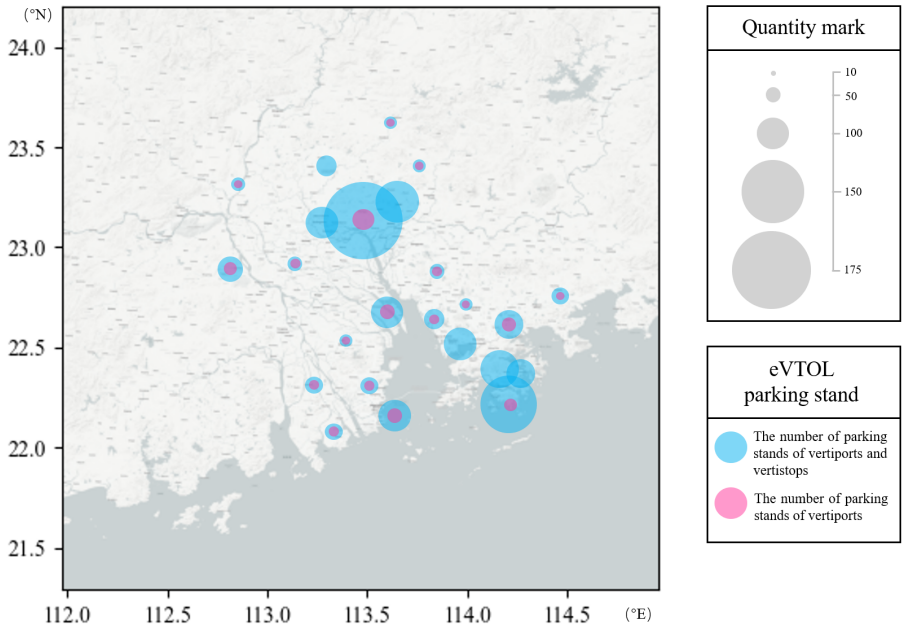

Figure 3.9: The spatial distribution of the opening scale of eVTOL parking stands at vertiports and vertistops (Low demand level).

ing capacity or vertiport/vertistop capacity force the total profit to remain stable after a profound increase. Furthermore, we also analyse the demand satisfaction rate of the UAM system and the number of repositioning eVTOLs under different low-altitude airspace management capacities in this experiment. The experimental results are presented in Figure 3.10. It is evident that the low-altitude airspace management capacity significantly affects both the demand satisfaction rate and the number of repositioning eVTOLs. As the low-altitude airspace management capacity increases, both the demand satisfaction rate of the UAM system and the number of repositioning eVTOLs rise. Specifically, when the low-altitude airspace management capacity increases from 1,400 to 1,800, the demand satisfaction rate experiences an 8.2 % growth, while the count of repositioning eVTOLs jumps from 0 to 1,867. From the computational results, we can conclude that a notable surplus of eVTOLs can be strategically repositioned to accommodate the prevailing demand, thereby fostering elevated satisfaction rates in scenarios characterised by ample airspace management capacity. Conversely, under circumstances marked by constrained airspace management capacity, the predominant allocation of eVTOLs is directed towards the fulfilment of user demand, consequently restricting the available airspace for the purpose of eVTOL repositioning.

The computational outcomes underscore a closed correlation between the low-altitude airspace management capacity and the service efficacy of the UAM system. Hence, it is imperative for policymakers to contemplate the augmentation of air traffic control services, encompassing both heightened service levels and advanced technologies. Furthermore, the prudent implementation of effective scheduling strategies emerges as a pivotal necessity, serving as an effective measure to counterbalance the potential deleterious impacts arising from the limited low-altitude airspace management capacity. This recommendation provides valuable guidance to UAM service providers in judicious interventions that harmonise the interplay between airspace utilisation, operational efficiency, and customer satisfaction within the UAM landscape.

Table 3.6: Computational results of the total profit under different low-altitude airspace management capacities.

Airspace management capacity	Total profit	Airspace management capacity	Total profit
1,400	21,198,800	1,550	23,629,550
1,450	22,227,550	1,600	23,887,550
1,480	22,896,550	1,700	23,941,050
1,500	23,116,550	1,800	23,941,050

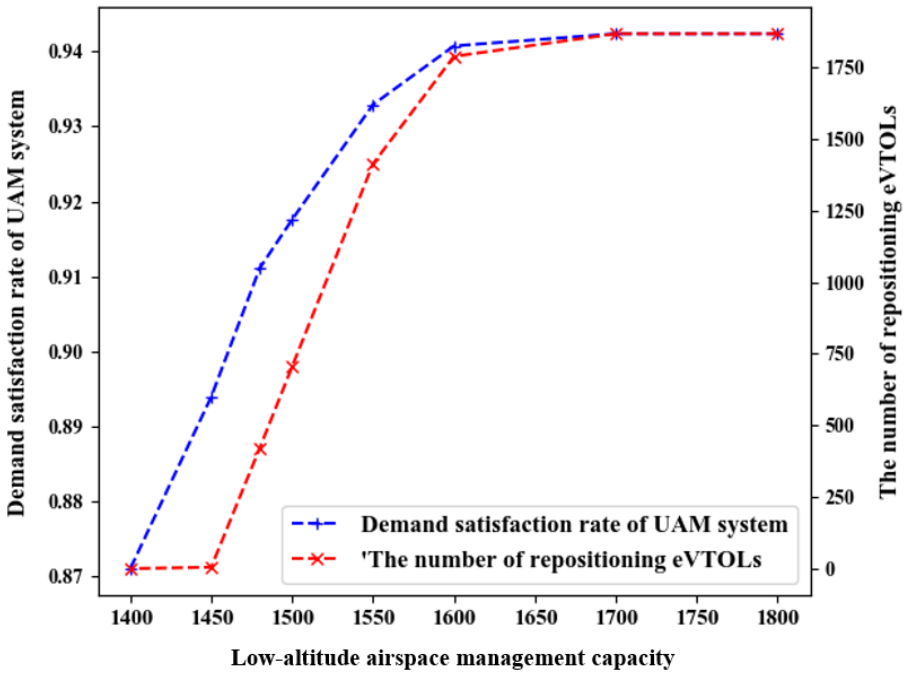

Figure 3.10: The demand satisfaction rate and the number of repositioning eVTOLs under different low-altitude airspace management capacities.

3.3.3 Policy recommendations

The above numerical results provide several significant policy recommendations for the UAM service providers. The detailed policy recommendations are as follows:

Firstly, it can be demonstrated that the solution derived from the scenario-based robust optimisation model contributes to the stability and resilience of the decision-making. From a managerial standpoint, despite entailing some degree of profit sacrifice, the scenario-based robust optimisation model markedly enhances stability across all scenarios. UAM service providers can adopt the scenario-based robust optimisation approach into their decision-making processes to fortify system resilience against the impacts of uncertain factors.

Secondly, there is a conflicting scenario in terms of benefits between the objectives of profit and spatial equity. UAM service providers are required to make a trade-off, potentially compromising a portion of their profit to attain a specific level of equity. When the equity requirement is not too stringent, the satisfied demand can remain nearly stable due to the increased number of repositioning eVTOLs. However, when the equity requirement is too rigorous and exceeds a threshold value, the profits witness a substantial decline. This outcome arises as the UAM system cannot guarantee spatial equity solely through eVTOL repositioning and may eventually necessitate cancelling a significant number of orders in the case of too stringent equity requirements. Therefore, policymakers should appropriately consider the equity requirement, which can contribute to the enhancement of social welfare. Nonetheless, it is noteworthy to mention that a reckless pursuit of spatial equity can paradoxically yield adverse effects.

Thirdly, we will give policy recommendations in terms of the determination of the equity requirement. During the initial phases of UAM implementation, strategically opting for a moderately lenient equity requirement can be advantageous. This approach not only fosters profit generation but also lays a resilient foundation for sustained de-

velopment in subsequent stages. As the UAM system becomes mature, managerial attention should pivot towards prioritising service levels and enhancing social welfare. Hence, in this advanced developmental phase, introducing a carefully stringent equity requirement becomes pivotal. This adjustment can facilitate the long-term development of the UAM system. Nevertheless, it is crucial to avoid an excessively stringent equity requirement, as this could result in a significant number of cancellation travel orders, negatively impacting the overall system development. Moreover, as the UAM system matures, the market will become more competitive. Larger UAM companies may opt for a more stringent equity requirement to focus more on social welfare enhancement, while smaller companies may strategically embrace a more lenient equity requirement to navigate the competitive landscape.

Fourthly, in regions characterised by economic prosperity or high demand, policymakers are advised to strategically invest in augmenting parking capacity at vertiports and vertistops to efficiently meet the heightened demand in these areas. However, it is crucial to tackle the challenge of potential ground transportation congestion near these vertiports or vertistops. The significant challenge arises during the first-mile travels (from origins to departure vertiports/vertistops) and last-mile travels (from arrival vertiports/vertistops to destinations), which will exacerbate the ground traffic congestion in the vicinity of vertistops and vertiports in the densely populated cities. One efficient solution involves coordinating ground public transportation services to facilitate passenger access to the vertiports or vertistops, thereby mitigating the impact of congestion in the vicinity of vertiports or vertistops. Furthermore, the UAM operating companies can provide ride-sharing services for both first-mile and last-mile travels in cities grappling with high levels of traffic congestion.

Lastly, the low-altitude airspace management capacity has a significant effect on the service efficacy of the UAM system. The computational results show that the total profits rise with an increase in low-altitude airspace management capacity until

they nearly stabilise. Furthermore, a large number of eVTOLs can be repositioned to enhance the demand satisfaction rate when the low-altitude airspace management capacity is ample. Therefore, it is essential for governments or policymakers to consider improving the efficiency of air traffic control services through adopting advanced technologies or other methods. Furthermore, policymakers can implement high-efficiency scheduling strategies to mitigate any potential adverse impacts that could arise from the limited low-altitude airspace management capacity.

3.4 Concluding Remarks of Chapter 3

This study primarily focuses on resolving an integrated optimisation problem encompassing the strategic planning and operational service aspects of a UAM system. Demand uncertainty and spatial equity consideration are incorporated in this study. This problem involves making joint decisions on various aspects, including the determination of parking stand numbers at vertiports and vertistops, eVTOL fleet size, and eVTOL fleet allocation and operations. To address this problem, we introduce a novel spatial equity metric and formulate a bi-objective optimisation model designed to strike a balance between service profitability and spatial equity. Furthermore, we transform the mathematical model into a tractable single-objective one based on ε-constraint approach and linearisation technique. To address the challenge arising from the uncertain demand, a scenario-based robust optimisation framework that integrates the interval robust method is proposed in this study. Finally, the performance of the proposed model is verified through a small-scale example, and the validity of the proposed model is further verified using a large-scale case study. Numerical results illustrate that solutions derived from the scenario-based robust optimisation model demonstrate notably enhanced stability across all scenarios, showcasing greater resilience against the influences of uncertain factors. Additionally, there is a contradictable relationship between

the objectives of profitability and spatial equity. Finally, a set of sensitivity analyses are conducted on various parameters, and several valuable policy recommendations are proposed to support the decision-making processes of UAM service providers.

Chapter 4

A Multistage Stochastic Programming Approach for Drone-Supported Last-Mile Humanitarian Logistics System Planning

Drone-supported last-mile humanitarian logistics systems play a crucial role in efficiently delivering essential relief items during disasters. In contrast to conventional truck-based transportation methods, drones provide a versatile and rapid transportation alternative. They are capable of navigating challenging terrain and bypassing damaged infrastructure. However, establishing an effective drone-supported last-mile humanitarian logistics system faces various challenges. This study introduces a novel approach to address these challenges by proposing a DLHLSP problem. The DLHLSP problem involves decision-making for both pre-disaster and post-disaster phases, taking into account the unique characteristics of drone-based delivery operations and uncertain

demands. In the pre-disaster phase, decisions include determining drone-supported relief facility locations, drone deployment strategies, and drone visit schedules to disaster sites. Post-disaster decisions focus on inventory management, relief item procurement, and drone-based delivery operations. To capture the demand realisation sequentially in a chaotic disaster environment, we establish a multistage stochastic programming model incorporating nonanticipativity constraints to make decisions at each stage without knowledge of the demand information in future time periods. Next, we employ the Benders decomposition algorithm to obtain exact solutions. Furthermore, we perform numerical experiments to verify the exact algorithm using randomly generated numerical instances. The results show that the algorithm significantly outperforms the Gurobi solver and could solve the problem on a practical scale. Finally, the study validates the proposed model based on a case study of the Lushan earthquake in China and provides several managerial implications and insights. Overall, this research contributes to the field of humanitarian logistics by offering a comprehensive framework for the planning of drone-supported last-mile humanitarian logistics systems.

4.1 Introduction

The significance of drone-supported last-mile humanitarian logistics cannot be overstated, as it enables swift and efficient delivery of critical aid to hard-to-access disaster-affected areas. Addressing demand uncertainty is crucial in logistics system planning.

In the current literature, there is widespread utilisation of a two-stage stochastic programming framework with discrete probability distributions to tackle demand uncertainty in the realm of humanitarian logistics planning (Wang and Nie, 2022; Shu et al., 2023). However, in the framework of two-stage stochastic programming, all information about uncertainty spanning the entire planning horizon is revealed after the first-stage decisions have been made. This framework cannot accurately reflect

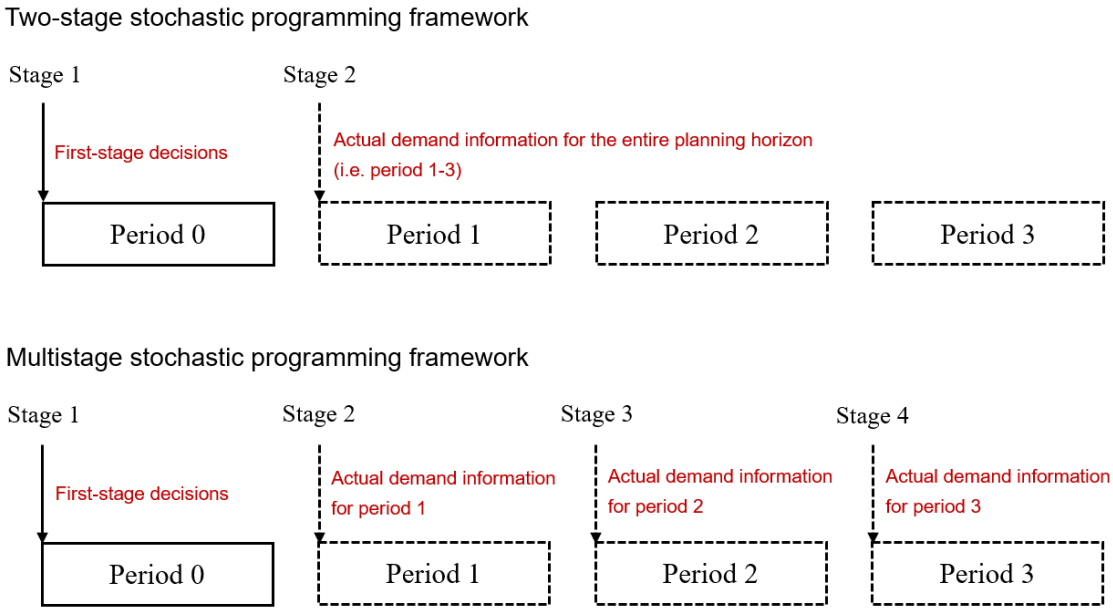

Figure 4.1: Illustration of frameworks of two-stage stochastic programming and multistage stochastic programming.

the uncertain environment in chaotic disaster scenarios. In reality, relief organisers only have access to the exact demand information for the current time period, along with the probability distribution of demand for the periods immediately following the moment of decisions. However, the demand information for all future time periods remains unknown. Therefore, we use the multistage stochastic programming framework to more accurately capture the uncertainty in demand. Specifically, for the multistage stochastic programming framework, demand information for each stage becomes available only after decisions have been made for the preceding stage. Figure 4.1 provides a visual representation of these two frameworks.

Overall, this study presents a multistage stochastic programming approach to address the Drone-Supported Last-Mile Humanitarian Logistics System Planning (DLHLSP) problem under demand uncertainty. Specifically, in the first stage, we consider the decisions spanning from drone-supported relief facility location, drone deployment, and drone visit schedule. Specifically, the drone visit schedule coordinates transportation

tasks for the individual drones to provide delivery service for their assigned disaster sites. It is critical to establish this schedule beforehand to effectively ensure workforce readiness (Adulyasak et al., 2015). Subsequent stages involve decisions in the post-disaster phase regarding inventory management, relief item procurement, and drone-based delivery. To conclude, we summarise the key contributions of the study as follows:

Firstly, we focus on a practical DLHLSP problem that considers the unique characteristics of drone-based delivery operations, including battery constraints and payload limitations. This problem integrates pre-disaster determinations encompassing drone-supported relief facility location, drone deployment, and drone visit schedule to disaster sites while also considering post-disaster decisions such as inventory management, relief item procurement, and drone-based delivery operation. To the best of our knowledge, our study is the first to integrate these determinations in this field.

Secondly, we propose a multistage stochastic programming model that incorporates nonanticipativity constraints to make decisions at each stage without knowledge of the demand information in future time periods. In other words, the demand information for a particular stage becomes known only after decisions have been made for the preceding stage, which can more precisely reflect the uncertain environments in this problem.

Thirdly, since the problem is NP-hard, we employ the Benders decomposition algorithm to obtain exact solutions for the multistage stochastic programming model. To evaluate the performance of this exact algorithm, we conduct numerical experiments across different computational scales. The results from these experiments demonstrate that the Benders decomposition algorithm has been shown to solve the problem efficiently, particularly for large-scale practical instances where the commercial solver exhibits poor computational performance.

Finally, we present a case study based on the Lushan earthquake in China and

conduct a series of sensitive analyses to validate the proposed mathematical model. Furthermore, we evaluate the value of the nonanticipativity constraints to demonstrate the superior performance of the proposed multistage stochastic programming model. Several managerial insights and implications are provided.

The remainder of this study is organised as follows. Section 4.2 describes the research problem and investigates a multistage stochastic programming model incorporating the nonanticipativity constraints. Section 4.3 provides the detailed process of solving the multistage stochastic programming model based on the Benders decomposition algorithm. Section 4.4 conducts numerical experiments to validate the exact algorithm and multistage stochastic programming model. Moreover, valuable managerial implications and insights are proposed. Finally, Section 4.5 provides conclusions and future research directions.

4.2 Problem Description and Mathematical Formulation

4.2.1 Problem description

With the development of intelligent unmanned autonomous system technologies, the utilisation of drones has gained significant popularity. This trend reflects the rising significance and acceptance of drones within the humanitarian sector. Drones offer a variety of capabilities, including swift delivery of crucial supplies such as pharmaceuticals, blood, and vaccines to remote or hard-to-reach areas, thereby significantly bolstering the efficiency of relief operations. Therefore, the establishment of the drone-supported last-mile humanitarian logistics system assumes paramount importance in providing essential logistical aid and services.

Here, we provide an overview of the DLHLSP problem, followed by the estab-

lishment of a multistage stochastic programming model in the subsequent subsection. To adapt to the framework of multistage stochastic programming, we segment the planning horizon into distinct time periods, each representing a stage. We use set $T = \{1, 2, ..., |T|\}$ to denote the set of time periods and $t \in T$ specifies one time period.

First, we present the notations in the first stage. Here, we concentrate on decisions concerning the locations of drone-supported relief facilities, deployment strategies for drones, and drone visit schedules. Let K denote the set of candidate drone-supported relief facilities and I denote the set of disaster sites. We define the binary variable x_{kt} that equals 1 if candidate location k is selected as a drone-supported relief facility in the time period t, and is 0 otherwise. The unit cost for opening a relief facility is denoted as c^{OP}. Next, we denote the set of drones as D and $d \in D$. We define the binary variable y_{dkt} that equals 1 if drone d is deployed to relief facility k in time period t, and is 0 otherwise. As previously mentioned, the drone visit schedule is determined here to facilitate a prompt response. Therefore, We let binary variable z_{idkt} equal to 1 if disaster site i is visited by drone d deployed to relief facility k in time period t, and is 0 otherwise.

Here, we designate the round trip from a certain relief facility to the disaster site and back as a *drone trip*. Considering the battery capacity requirements of drones, we introduce a non-negative parameter B^{MAX} to denote the maximum flying range of drones. Following previous studies such as Chauhan et al. (2019) and Zhu et al. (2022), we allow drones to conduct multiple drone trips until the battery capacity is depleted. We define a non-negative parameter denoted as c_{ki}^{TRS}, representing the unit flying cost from relief facility k to disaster site i. This study focuses on one type of relief item, as it can be assumed that the item can be delivered in bundled form (Elçi and Noyan, 2018).

Furthermore, we introduce the notations in the subsequent stages (corresponding to the post-disaster phase). Here, we determine decisions regarding drone-based delivery,

inventory management, and relief item procurement. We let Ω express the set of scenarios and $\omega \in \Omega$. The occurrence probability of scenario ω is denoted by p_ω. We let D_{it}^{ω} represent the random demand for disaster site i in time period t under scenario ω. Regarding the drone-based delivery decision, a continuous variable q_{idkt}^{ω} is introduced to denote the quantity of items transported to disaster site i by drone d deployed to relief facility k in time period t under scenario ω. Another important characteristic of drone delivery operations is that drones typically have payload weight limitations. Therefore, we let L^{MAX} denote the maximum payload limit. Additionally, we introduce a continuous variable m_{it}^{ω} to denote the quantity of unsatisfied demand of disaster site i in time period t under scenario ω. We define a non-negative parameter, denoted as c^{UN}, which represents the penalty cost incurred for each unit of unsatisfied demand. For decisions of inventory management, we let continuous variable v_{kt}^{ω} represent the inventory quantity at relief facility k at the end of time period t under scenario ω. The inventory capacity for relief facilities is denoted by Q^{MAX}. The unit inventory cost is represented by c^{INV}. Furthermore, we introduce a continuous variable u_{kt}^{ω} to represent the procurement decisions. This variable represents the procurement quantity for relief facility k in time period t under scenario ω. The unit procurement cost is represented by c^{PR} and there is a budget for procuring relief items denoted by H^{MAX}. The notations are summarised in Table 4.1.

Table 4.1: Notations for DLHLSP

Notation	Explanation
Sets	
I	The set of disaster sites, $i \in I$.
K	The set of candidate drone-supported relief facilities, $k \in K$.
D	The set of drones, $d \in D$.
T	The set of time periods, $t \in T$.
Ω	The set of scenarios, $\omega \in \Omega$.
Parameters	
c^{OP}	The unit cost for opening a drone-supported relief facility.
c^{TRS}_{ki}	The unit flying cost from facility k to disaster site i.
c^{INV}	The unit inventory cost.
c^{PR}	The unit cost for procuring relief items.
c^{UN}	The penalty cost for per unit unsatisfied demand.
B^{MAX}	The maximum flying range of drones.
L^{MAX}	The maximum payload limit of drones.
Q^{MAX}	The inventory capacity for relief facilities.
H^{MAX}	The maximum budget for procuring the relief items.
p_ω	The probability of the scenario ω.
D^ω_{it}	The demand of the disaster site i in time period t under scenario ω.
Variables	
x_{kt}	Equals 1 if candidate location k is selected as drone-supported relief facility in time period t; otherwise equals to 0.
y_{dkt}	Equals to 1 if drone d is deployed to facility k in time period t; otherwise equals 0.
z_{idkt}	Equals to 1 if disaster site i is served by drone d deployed to the facility k in time period t; otherwise equals to 0.
q^ω_{idkt}	Quantity of relief items delivered to disaster site i by drone d that is deployed to facility k in time period t under scenario ω.
m^ω_{it}	Quantity of unsatisfied demand of disaster site i in time period t under scenario ω.
v^ω_{kt}	Inventory quantity at facility k at the end of time period t under scenario ω.
u^ω_{kt}	Procurement quantity for facility k in time period t under scenario ω.
$\widetilde{q}^{\mathcal{N}^\omega_t}_{idkt}$	The variable q^ω_{idkt} associated with the scenario node $\mathcal{N}^\omega_t$.
$\widetilde{m}^{\mathcal{N}^\omega_t}_{it}$	The variable tm^ω_{it} associated with the scenario node $\mathcal{N}^\omega_t$.
$\widetilde{v}^{\mathcal{N}^\omega_t}_{kt}$	The variable tv^ω_{kt} associated with the scenario node $\mathcal{N}^\omega_t$.
$\widetilde{u}^{\mathcal{N}^\omega_t}_{kt}$	The variable tu^ω_{kt} associated with the scenario node $\mathcal{N}^\omega_t$.

4.2.2 Multistage stochastic programming with nonanticipativity constraints

In the context of multistage stochastic programming, decision-makers are required to make decisions at each stage without knowledge of future periods. This indicates that the uncertainty for each time period becomes realised only after decisions have been made for preceding time periods. Therefore, nonanticipativity constraints must be introduced in multistage problems (Adulyasak et al., 2015; Wu et al., 2023). These constraints ensure that decisions made at each stage depend only on the information available up to that stage and not on the knowledge that will be revealed in future stages. Meanwhile, the nonanticipativity constraints can also ensure the consistency of decisions between scenarios (Adulyasak et al., 2015).

In multistage problems, a scenario tree is an intuitive representation to depict the scenario construction process over the entire planning horizon. In the context of a scenario tree, the parent nodes represent the states of uncertainty that are revealed up to a certain point in time, while the child nodes represent different realisations or outcomes of uncertainty at later stages. Next, we present an illustrative example to explain the construction process of the nonanticipativity constraints in detail. Figure 4.2 illustrates a scenario tree with 4 time periods (from time period 0 to time period 3) and 12 scenarios. Time period 0 serves as an artificial period where first-stage decisions are made. Time periods 1-3 correspond to subsequent stages where decisions are determined after the corresponding actual information of uncertain parameters becomes known. Specifically, in time period 1, three scenarios representing uncertain demand information are known, denoted by nodes 1–3. In time period 2, 5 distinct realisations become known, denoted by nodes 4–8. The branching process continues until the final time period, which is time period 3. Each unique path from the root to a leaf node in the last period corresponds to a scenario, resulting in 12 scenarios in total. Therefore,

in a multistage stochastic programming model, a scenario represents a path from the root node to a leaf node.

Furthermore, to ensure that decisions in a specific period do not rely on future information, we introduce the nonanticipativity constraints for time periods 1 to 3. Here, we let notation $w_{t,s}$ denote the generic decision variable that is determined in time period t in scenario s. The nonanticipativity constraints of the illustrative example are formulated as follows:

$$w_{1,1} = w_{1,2} = w_{1,3} = w_{1,4}; w_{1,5} = w_{1,6} = w_{1,7} = w_{1,8} = w_{1,9}; w_{1,10} = w_{1,11} = w_{1,12};$$

$$w_{2,1} = w_{2,2}; w_{2,3} = w_{2,4}; w_{2,5} = w_{2,6} = w_{2,7}; w_{2,8} = w_{2,9}; w_{2,10} = w_{2,11} = w_{2,12}.$$

In other words, the nonanticipativity constraints ensure that, for any given decision point in the planning horizon, the decisions made are the same across all scenarios that share the same parent node because these decisions are made before the uncertainty is fully realised (i.e. before the child nodes diverge). This prevents the model from "cheating" by making decisions that depend on future information that is not available at the time of the decision.

In chaotic disaster scenarios, demand information for a particular stage becomes available only after decisions for the preceding stages have been made, which more accurately reflects real-world practices. Therefore, we employ a multistage stochastic programming approach to model our research problem.

4.2.3 Mathematical formulation

This subsection provides the multistage stochastic programming model considering the uncertainty of the demands of disaster sites as follows:

$$\min \sum_{t \in T} \left(\sum_{k \in K} c^{\mathrm{OP}} x_{kt} + \sum_{i \in I} \sum_{d \in D} \sum_{k \in K} c^{\mathrm{TRS}}_{ki} z_{idkt} \right)$$

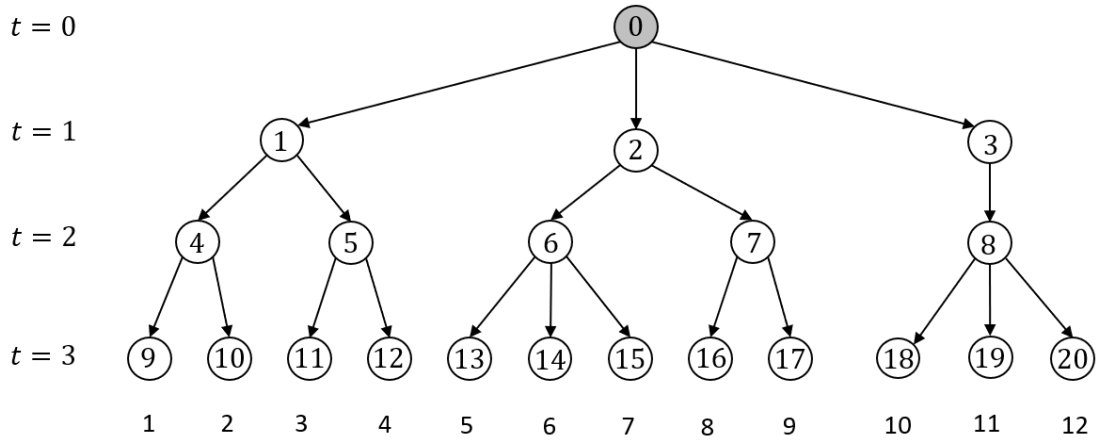

Figure 4.2: Illustrative example of a scenario tree and nonanticipativity constraints.

$$+\sum_{\omega\in\Omega} p_\omega \sum_{t\in T}\left(\sum_{k\in K} c^{\mathrm{INV}} v^\omega_{kt} + \sum_{k\in K} c^{\mathrm{PR}} u^\omega_{kt} + \sum_{i\in I} c^{\mathrm{UN}} m^\omega_{it}\right) \tag{4.1}$$

$$\text{s.t.} \quad \sum_{k\in K} x_{kt} \geq 1, \quad \forall t \in T, \tag{4.2}$$

$$y_{dkt} \leq x_{kt}, \quad \forall d \in D,\ \forall k \in K,\ \forall t \in T. \tag{4.3}$$

$$\sum_{k\in K} y_{dkt} \leq 1, \quad \forall d{\in}D,\ \forall t{\in}T, \tag{4.4}$$

$$z_{idkt} \leq y_{dkt}, \quad \forall k{\in}K,\ \forall i{\in}I, \forall d{\in}D,\ \forall t{\in}T, \tag{4.5}$$

$$\sum_{i\in I} d_{ki} z_{idkt} \leq B^{\mathrm{MAX}} y_{dkt}, \quad \forall k{\in}K,\ \forall d{\in}D,\ \forall t{\in}T, \tag{4.6}$$

$$\sum_{k\in K}\sum_{d\in D} z_{idkt} \geq 1, \quad \forall i{\in}I,\ \forall t{\in}T, \tag{4.7}$$

$$q^\omega_{idkt} \leq L^{\mathrm{MAX}} z_{idkt}, \quad \forall k{\in}K,\ \forall i{\in}I,\ \forall d{\in}D,\ \forall t{\in}T,\ \forall \omega{\in}\Omega, \tag{4.8}$$

$$v^{\omega}_{k,t-1} + u^{\omega}_{kt} = v^{\omega}_{kt} + \sum_{i\in I}\sum_{d\in D} q^{\omega}_{idkt}, \quad \forall k\in K,\ \forall t\in T,\ \forall \omega\in\Omega, \tag{4.9}$$

$$\sum_{k\in K}\sum_{d\in D} q^{\omega}_{idkt} + m^{\omega}_{it} \geq D^{\omega}_{it}, \quad \forall i\in I,\ \forall t\in T,\ \forall \omega\in\Omega, \tag{4.10}$$

$$v^{\omega}_{kt} \leq Q^{\mathrm{MAX}} x_{kt}, \quad \forall k\in T,\ \forall t\in T,\ \forall \omega\in\Omega, \tag{4.11}$$

$$c^{\mathrm{PR}} \sum_{t\in T}\sum_{k\in K} u^{\omega}_{kt} \leq H^{\mathrm{MAX}},\ \forall \omega\in\Omega, \tag{4.12}$$

$$q^{\omega}_{idkt} = \widetilde{q}^{\mathcal{N}^{\omega}_t}_{idkt}, \quad \forall k\in K,\ \forall i\in I,\ \forall d\in D,\ \forall t\in T,\ \forall \omega\in\Omega, \tag{4.13}$$

$$m^{\omega}_{it} = \widetilde{m}^{\mathcal{N}^{\omega}_t}_{it}, \quad \forall i\in I,\ \forall t\in T,\ \forall \omega\in\Omega, \tag{4.14}$$

$$v^{\omega}_{kt} = \widetilde{v}^{\mathcal{N}^{\omega}_t}_{kt}, \quad \forall k\in T,\ \forall t\in T,\ \forall \omega\in\Omega, \tag{4.15}$$

$$u^{\omega}_{kt} = \widetilde{u}^{\mathcal{N}^{\omega}_t}_{kt}, \quad \forall k\in T,\ \forall t\in T,\ \forall \omega\in\Omega, \tag{4.16}$$

$$x_{kt}\in\{0,1\}, \quad \forall k\in K,\ \forall t\in T, \tag{4.17}$$

$$y_{dkt}\in\{0,1\}, \quad \forall d\in D,\ \forall k\in K,\ \forall t\in T, \tag{4.18}$$

$$z_{idkt}\in\{0,1\}, \quad \forall k\in K,\ \forall i\in I, \forall d\in D,\ \forall t\in T, \tag{4.19}$$

$$q^{\omega}_{idkt},\ \widetilde{q}^{\mathcal{N}^{\omega}_t}_{idkt} \geq 0, \quad \forall k\in K,\ \forall i\in I,\ \forall d\in D,\ \forall t\in T,\ \forall \omega\in\Omega, \tag{4.20}$$

$$m^{\omega}_{it},\ \widetilde{m}^{\mathcal{N}^{\omega}_t}_{it} \geq 0, \quad \forall i\in I,\ \forall t\in T,\ \forall \omega\in\Omega, \tag{4.21}$$

$$v^{\omega}_{kt},\ \widetilde{v}^{\mathcal{N}^{\omega}_t}_{kt},\ u^{\omega}_{kt},\ \widetilde{u}^{\mathcal{N}^{\omega}_t}_{kt} \quad \forall k\in T,\ \forall t\in T,\ \forall \omega\in\Omega. \tag{4.22}$$

The objective function (4.1) minimises the total cost during the entire planning hori-

zon. Specifically, the first term represents the total first-stage costs, which include the costs associated with opening drone-supported relief facilities and drone flying. The second term focuses on minimising the total expected inventory costs, procurement costs, and penalty costs for unsatisfied demand. Constraints (4.2) mean that for any time period, at least one drone-supported relief facility is open. Constraints (4.3) guarantee the drones cannot be deployed to an unselected relief facility. Constraints (4.4) ensure drones cannot be assigned to more than one open drone-supported relief facility during a time period. Constraints (4.5) state that drones cannot provide delivery service if it is not deployed. Constraints (4.6) impose the battery range constraints on drones. Constraints (4.7) enforce that the disaster site cannot be served less than once during one time period to avoid significant shortages. Constraints (4.8) restrict that the delivered relief items cannot surpass the maximum payload limit. Constraints (4.9) enforce the inventory flow balance of the facilities. Constraints (4.10) ensure that the sum of delivered items and unsatisfied demands cannot be less than the demand of the disaster site for each time period. The inventory capacity of relief facilities is restricted by Constraints (4.11). Constraints (4.12) require that the cost of procuring relief items cannot exceed the maximum budget. Constraints (4.13)-(4.16) are the nonanticipativity constraints. Constraints (4.17)-(4.22) define the domains of decision variables.

4.3 Benders Decomposition

Benders decomposition is an exact algorithm proposed by Benders (1962), and it proves to be effective in addressing the multistage stochastic programming problem (Adulyasak et al., 2015; Wu et al., 2023). This approach involves decomposing the original problem into a master problem and a subproblem. The master problem is a relaxed version of the original problem that incorporates the integer variables. The

subproblem is a linear program that fixes the values of integer variables in the master problem. Leveraging linear programming duality theory, the subproblem is dualised, and its variables are projected out. Additionally, an artificial variable is introduced into the master problem, representing a lower bound for the subproblem. At each iteration, the solutions of the master problem are first obtained, and the dual subproblem is solved with the fixed integer variables in the master problem. Subsequently, the Benders optimality cuts or feasibility cuts can be generated according to the solutions of the dual subproblem and are added to the master problem. Specifically, if the subproblem is feasible and bounded, an optimality cut is added to the master problem, while if it is infeasible, a feasibility cut is added. The iterative process continues until either an optimal solution is derived for the original problem or an early stopping criterion is satisfied. Details of the Benders decomposition algorithm for the DLHLSP problem are presented next.

4.3.1 Subproblem

Let $\overline{\mathbf{x}}$, $\overline{\mathbf{y}}$, $\overline{\mathbf{z}}$ denote the solution vector of the first stage variables x_{kt}, y_{dkt}, and z_{idkt}, respectively. The decisions in the subsequent stages are solely dependent on $\overline{\mathbf{x}}$ and $\overline{\mathbf{z}}$, being independent of $\overline{\mathbf{y}}$. We denote the expected cost function as $\Theta(\overline{\mathbf{x}}, \overline{\mathbf{z}})$, obtained by $\Theta(\overline{\mathbf{x}}, \overline{\mathbf{z}}) = \sum_{\omega \in \Omega} p_\omega \Theta_\omega(\overline{\mathbf{x}}, \overline{\mathbf{z}})$, where $\Theta_\omega(\overline{\mathbf{x}}, \overline{\mathbf{z}})$ represents the total cost (excluding the first-stage cost) of scenario ω. Therefore, we define the primal subproblem [PSP] for a given scenario ω as follows:

$$\Theta_\omega(\overline{\mathbf{x}}, \overline{\mathbf{z}}) = \min \quad \sum_{t \in T} \left(\sum_{k \in K} c^{\mathrm{INV}} v_{kt}^{\omega} + \sum_{k \in K} c^{\mathrm{PR}} u_{kt}^{\omega} + \sum_{i \in I} c^{\mathrm{UN}} m_{it}^{\omega} \right) \tag{4.23}$$

$$\text{s.t.} \qquad q_{idkt}^{\omega} \leq L^{\mathrm{MAX}} \overline{z_{idkt}}, \quad \forall k \in K,\ \forall i \in I,\ \forall d \in D,\ \forall t \in T, \tag{4.24}$$

$$v^{\omega}_{k,t-1} + u^{\omega}_{kt} = v^{\omega}_{kt} + \sum_{i\in I}\sum_{d\in D} q^{\omega}_{idkt}, \quad \forall k\in K,\ \forall t\in T, \tag{4.25}$$

$$\sum_{k\in K}\sum_{d\in D} q^{\omega}_{idkt} + m^{\omega}_{it} \geq D^{\omega}_{it}, \quad \forall i\in I,\ \forall t\in T, \tag{4.26}$$

$$v^{\omega}_{kt} \leq Q^{\mathrm{MAX}}\overline{x_{kt}}, \quad \forall k\in T,\ \forall t\in T, \tag{4.27}$$

$$c^{\mathrm{PR}}\sum_{t\in T}\sum_{k\in K} u^{\omega}_{kt} \leq H^{\mathrm{MAX}}, \tag{4.28}$$

$$q^{\omega}_{idkt} = \widetilde{q}^{\mathcal{N}^{\omega}_t}_{idkt}, \quad \forall k\in K,\ \forall i\in I,\ \forall d\in D,\ \forall t\in T, \tag{4.29}$$

$$m^{\omega}_{it} = \widetilde{m}^{\mathcal{N}^{\omega}_t}_{it}, \quad \forall i\in I,\ \forall t\in T, \tag{4.30}$$

$$v^{\omega}_{kt} = \widetilde{v}^{\mathcal{N}^{\omega}_t}_{kt}, \quad \forall k\in T,\ \forall t\in T, \tag{4.31}$$

$$u^{\omega}_{kt} = \widetilde{u}^{\mathcal{N}^{\omega}_t}_{kt}, \quad \forall k\in T,\ \forall t\in T, \tag{4.32}$$

and constraints (4.20)–(4.22).

To generate the Benders cuts, we formulate the dual of the primal subproblem for each scenario $\omega \in \Omega$, denoted as [DSP]. To overcome the difficulty in deriving the dual caused by nonanticipativity constraints, we initially derive the dual formulation of the primal subproblem without incorporating nonanticipativity constraints, i.e., the constraints (4.29)–(4.32).

We let $\boldsymbol{\alpha} = (\alpha^{\omega}_{idkt} \leq 0 \ \mid \ \forall i \in I,\ \forall d \in D,\ \forall k \in K,\ \forall t \in T,\ \forall \omega \in \Omega)$, $\boldsymbol{\beta} = (\beta^{\omega}_{kt} \ \mid \ \forall k \in K,\ \forall t \in T,\ \forall \omega \in \Omega)$, $\boldsymbol{\gamma} = (\gamma^{\omega}_{it} \leq 0 \ \mid \ \forall i \in I,\ \forall t \in T,\ \forall \omega \in \Omega)$, $\boldsymbol{\delta} = (\delta^{\omega}_{kt} \leq 0 \ \mid \ \forall k \in K,\ \forall t \in T,\ \forall \omega \in \Omega)$ and $\boldsymbol{\kappa} = (\kappa^{\omega} \leq 0 \ \mid \ \forall \omega \in \Omega)$ denote the vectors of dual variables associated with constraints (4.24)–(4.28), respectively. Additionally, we let $\beta_{|T|+1,\omega} = 0$. The dual of the primal subproblem for scenario

ω of the stochastic programming model without nonanticipativity constraints can be formulated as follows:

$$\max \sum_{i\in I}\sum_{d\in D}\sum_{k\in K}\sum_{t\in T} L^{\mathrm{MAX}}\overline{z_{idkt}}\alpha^{\omega}_{idkt} - \sum_{i\in I}\sum_{t\in T} D^{\omega}_{it}\gamma^{\omega}_{it} + \sum_{k\in K}\sum_{t\in T} Q^{\mathrm{MAX}}\overline{x_{kt}}\delta^{\omega}_{kt} + H^{\mathrm{MAX}}\kappa^{\omega} \tag{4.33}$$

$$\text{s.t.} \quad \alpha^{\omega}_{idkt} - \beta^{\omega}_{kt} - \gamma^{\omega}_{it} \le 0, \qquad \forall k\in K,\ \forall i\in I,\ \forall d\in D,\ \forall t\in T, \tag{4.34}$$

$$-\gamma^{\omega}_{it} \le c^{\mathrm{UN}}, \qquad \forall i\in I,\ \forall t\in T, \tag{4.35}$$

$$\beta^{\omega}_{kt} + c^{\mathrm{PR}}\kappa^{\omega} \le c^{\mathrm{PR}}, \qquad \forall k\in K,\ \forall t\in T, \tag{4.36}$$

$$-\beta^{\omega}_{kt} + \beta^{\omega}_{k,t+1} + \delta^{\omega}_{kt} \le c^{\mathrm{INV}}, \qquad \forall k\in K,\ \forall t\in T, \tag{4.37}$$

$$\alpha^{\omega}_{idkt} \le 0, \qquad \forall k\in K,\ \forall i\in I,\ \forall d\in D,\ \forall t\in T, \tag{4.38}$$

$$\gamma^{\omega}_{it} \le 0, \qquad \forall i\in I,\ \forall t\in T, \tag{4.39}$$

$$\delta^{\omega}_{kt} \le 0, \qquad \forall k\in K,\ \forall t\in T, \tag{4.40}$$

$$\beta^{\omega}_{kt} \in \mathbb{R}, \qquad \forall k\in K,\ \forall t\in T, \tag{4.41}$$

$$\kappa^{\omega} \le 0. \tag{4.42}$$

Based on the above dual formulation, we proceed to derive the dual formulation for the primal subproblem in the multistage stochastic programming model. In a scenario tree, the set of nodes at time period t is denoted as $\mathcal{F}^t$. Additionally, we denote the set of scenarios associated with node n as $\mathcal{H}(n)$. To further explain the notations, we

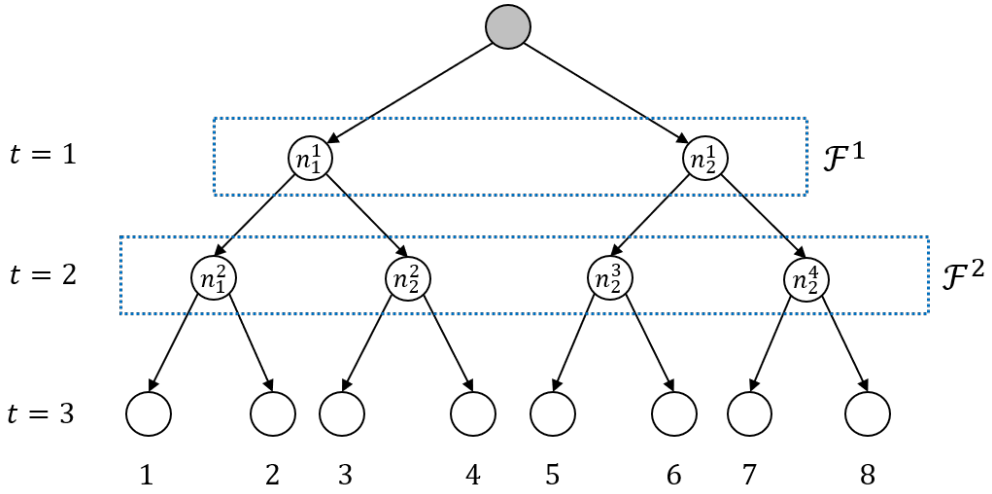

Figure 4.3: Illustrative example of the scenario tree.

provide an illustrative example using the scenario tree depicted in Figure 4.3. In the scenario tree, there are three time periods and eight scenarios. $\mathcal{F}^1$ consists of two nodes (n_1^1 and n_2^1), while $\mathcal{F}^2$ consists of four nodes (n_1^2, n_2^2, n_2^3, and n_2^4). For node n_1^1, scenarios 1 to 4 are all associated with it. Therefore, we have $\mathcal{H}(n_1^1) = \{1, 2, 3, 4\}$. Similarly, for node n_1^2, scenarios 1 and 2 are associated with it, so we have $\mathcal{H}(n_1^2) = \{1, 2\}$.

We let $\boldsymbol{\xi}^{\mathrm{q}} = (\xi^{\mathrm{q}}_{idkt\omega} \mid \forall i \in I,\ \forall d \in D,\ \forall k \in K,\ \forall t \in T,\ \forall \omega \in \Omega)$, $\boldsymbol{\xi}^{\mathrm{m}} = (\xi^{\mathrm{m}}_{it\omega} \mid \forall i \in I,\ \forall t \in T,\ \forall \omega \in \Omega)$, $\boldsymbol{\xi}^{\mathrm{u}} = (\xi^{\mathrm{u}}_{kt\omega} \mid \forall k \in K,\ \forall t \in T,\ \forall \omega \in \Omega)$, and $\boldsymbol{\xi}^{\mathrm{v}} = (\xi^{\mathrm{v}}_{kt\omega} \mid \forall k \in K,\ \forall t \in T,\ \forall \omega \in \Omega)$ represent the vectors of dual variables associated with constraints (4.29)–(4.32). Simultaneously, we also let $\xi^{\mathrm{q}}_{idk,|T|,\omega} = 0$, $\xi^{\mathrm{m}}_{i,|T|\omega} = 0$, $\xi^{\mathrm{u}}_{k,|T|\omega} = 0$, and $\xi^{\mathrm{v}}_{k,|T|\omega} = 0$. Subsequently, the dual formulation of the primal subproblem for scenario ω of the multistage stochastic programming model [DSP] can be derived as follows:

$$\max \sum_{i\in I}\sum_{d\in D}\sum_{k\in K}\sum_{t\in T} L^{\mathrm{MAX}}\overline{z_{idkt}}\alpha^{\omega}_{idkt} - \sum_{i\in I}\sum_{t\in T} D^{\omega}_{it}\gamma^{\omega}_{it} + \sum_{k\in K}\sum_{t\in T} Q^{\mathrm{MAX}}\overline{x_{kt}}\delta^{\omega}_{kt} + H^{\mathrm{MAX}}\kappa^{\omega} \tag{4.43}$$

$$\text{s.t.} \quad \alpha^{\omega}_{idkt} - \beta^{\omega}_{kt} - \gamma^{\omega}_{it} + \xi^{\mathrm{q}}_{idkt\omega} \leq 0, \qquad \forall k{\in}K,\ \forall i{\in}I,\ \forall d{\in}D,\ \forall t{\in}T, \tag{4.44}$$

$$-\gamma^{\omega}_{it} + \xi^{\mathrm{m}}_{it\omega} \leq c^{\mathrm{UN}}, \qquad \forall i{\in}I,\ \forall t{\in}T, \tag{4.45}$$

$$\beta^{\omega}_{kt} + c^{\mathrm{PR}}\kappa^{\omega} + \xi^{\mathrm{u}}_{kt\omega} \leq c^{\mathrm{PR}}, \qquad \forall k{\in}K,\ \forall t{\in}T, \tag{4.46}$$

$$-\beta^{\omega}_{kt} + \beta^{\omega}_{k,t+1} + \delta^{\omega}_{kt} + \xi^{\mathrm{v}}_{kt\omega} \leq c^{\mathrm{INV}}, \qquad \forall k{\in}K,\ \forall t{\in}T, \tag{4.47}$$

$$-\sum_{\omega\in\mathcal{H}(n)} \xi^{\mathrm{q}}_{idkt\omega} \leq 0, \qquad \forall k{\in}K,\ \forall i{\in}I,\ \forall d{\in}D,\ \forall t{\in}T\backslash|T|, \forall n{\in}\mathcal{F}^t, \tag{4.48}$$

$$-\sum_{\omega\in\mathcal{H}(n)} \xi^{\mathrm{m}}_{it\omega} \leq 0, \qquad \forall i{\in}I,\ \forall t{\in}T\backslash|T|, \forall n{\in}\mathcal{F}^t, \tag{4.49}$$

$$-\sum_{\omega\in\mathcal{H}(n)} \xi^{\mathrm{u}}_{kt\omega} \leq 0, \qquad \forall i{\in}I,\ \forall t{\in}T\backslash|T|, \forall n{\in}\mathcal{F}^t, \tag{4.50}$$

$$-\sum_{\omega\in\mathcal{H}(n)} \xi^{\mathrm{v}}_{kt\omega} \leq 0, \qquad \forall i{\in}I,\ \forall t{\in}T\backslash|T|, \forall n{\in}\mathcal{F}^t, \tag{4.51}$$

$$\alpha^{\omega}_{idkt} \leq 0, \qquad \forall k{\in}K,\ \forall i{\in}I,\ \forall d{\in}D,\ \forall t{\in}T, \tag{4.52}$$

$$\gamma^{\omega}_{it} \leq 0, \qquad \forall i{\in}I,\ \forall t{\in}T, \tag{4.53}$$

$$\delta^{\omega}_{kt} \leq 0, \qquad \forall k{\in}K,\ \forall t{\in}T, \tag{4.54}$$

$$\beta^{\omega}_{kt} \in \mathbb{R}, \qquad \forall k{\in}K,\ \forall t{\in}T, \tag{4.55}$$

$$\kappa^{\omega} \leq 0, \tag{4.56}$$

$$\xi^{\mathrm{q}}_{idkt\omega}, \xi^{\mathrm{m}}_{it\omega}, \xi^{\mathrm{u}}_{kt\omega}, \xi^{\mathrm{v}}_{kt\omega} \in \mathbb{R}, \qquad \forall k{\in}K,\ \forall i{\in}I,\ \forall d{\in}D,\ \forall t{\in}T. \tag{4.57}$$

4.3.2 Master problem

We let Δ_ω denote the polyhedron defined by constraints (4.44)–(4.57). Here we define the set Δ=$\bigcup_{\omega\in\Omega}\Delta_\omega$ and let Ξ_Δ represent the set of extreme points of Δ. Considering the variables m^ω_{it}, the [PSP] is always feasible as it allows for unsatisfied demand. Additionally, the cost parameters c^{INV}, c^{PR}, and c^{UN} are all finite, ensuring that any feasible solution of the [PSP] is bounded. Consequently, the dual formulation of [PSP] is both feasible and bounded. Hence, we can introduce the following optimality Benders cut to the master problem.

$$\eta \geq \sum_{\omega\in\Omega} p_\omega \Big(\sum_{i\in I}\sum_{d\in D}\sum_{k\in K}\sum_{t\in T} L^{\text{MAX}}\alpha^\omega_{idkt} z_{idkt} - \sum_{i\in I}\sum_{t\in T} D^\omega_{it}\gamma^\omega_{it} + \sum_{k\in K}\sum_{t\in T} Q^{\text{MAX}}\delta^\omega_{kt}x_{kt} + H^{\text{MAX}}\kappa^\omega\Big), \tag{4.58}$$

where η is an auxiliary variable, representing the underestimation variable for the expected cost of the primal subproblem [PSP]. Let $\chi_\omega(\boldsymbol{\gamma},\boldsymbol{\kappa}) = -\sum_{i\in I}\sum_{t\in T} D^\omega_{it}\gamma^\omega_{it} + H^{\text{MAX}}\kappa^\omega$. Then, the Benders master problem can be written as follows:

$$\min \quad \sum_{t\in T}\left(\sum_{k\in K} c^{\text{OP}}x_{kt} + \sum_{i\in I}\sum_{d\in D}\sum_{k\in K} c^{\text{TRS}}_{ki} z_{idkt}\right) + \eta \tag{4.59}$$

s.t. Constraints (4.2)–(4.7).

$$\eta \geq \sum_{\omega\in\Omega} p_\omega \Big(\sum_{i\in I}\sum_{d\in D}\sum_{k\in K}\sum_{t\in T} L^{\text{MAX}}\alpha^\omega_{idkt} z_{idkt} + \sum_{k\in K}\sum_{t\in T} Q^{\text{MAX}}\delta^\omega_{kt}x_{kt} + \chi_\omega(\boldsymbol{\gamma},\boldsymbol{\kappa})\Big),$$

$$\forall(\boldsymbol{\alpha},\boldsymbol{\beta},\boldsymbol{\gamma},\boldsymbol{\delta},\boldsymbol{\kappa},\boldsymbol{\xi}^{\text{q}},\boldsymbol{\xi}^{\text{m}},\boldsymbol{\xi}^{\text{u}},\boldsymbol{\xi}^{\text{v}}) \in \Xi_\Delta. \tag{4.60}$$

4.3.3 Implementation of Benders decomposition

We employ the Benders decomposition algorithm to tackle the problem. This exact algorithm operates on the principle that once decisions regarding facility location,

drone deployment, and drone visit schedules are made in the first stage and fixed, the resulting subproblems become linear programs solvable in polynomial time. Consequently, the master problem becomes an integer program, providing a lower bound for the problem, while the dual subproblems become linear programs, offering an upper bound. The detailed implementation of the Benders decomposition algorithm for the proposed model is outlined as Algorithm 1.

Algorithm 1 Benders decomposition

1: Initialisation: Set the lower bound LB to $-\infty$ and upper bound UB to $+\infty$.
2: Solve master problem [MP]: Obtain the optimal objective value as the updated LB and the initial solution $\widehat{\mathcal{I}}$.
3: **repeat**
4: Solve the dual formulation of the primal subproblem [DSP] with $\widehat{\mathcal{I}}$ to update the UB and obtain the incumbent solution.
5: Add the Benders optimality cut (4.58) to the cut pool of [MP].
6: Solve the [MP] with the new cut pool. If the [MP] is infeasible, stop; otherwise, update LB and $\mathcal{I}$ with the current optimal solution.
7: **until** UB $-$ LB $< \varepsilon$, where ε is the specified tolerance.
8: **return** Optimal solutions and UB.

4.4 Numerical Experiments

In this section, we utilise randomly generated numerical instances with different computational scales to evaluate the performance of the Benders decomposition algorithm. We then take the Lushan earthquake in Sichuan, China, as a case study to assess the proposed multistage stochastic programming model based on a series of experiments. The algorithms are coded in Python using the Gurobi 10.0.0 solver. The experiments were conducted on a personal computer running Windows 10 (64-bit), which has a 16-Core Processor and 128.0GB RAM.

4.4.1 Evaluation of algorithm performance

We test the Bender decomposition algorithm on randomly generated numerical instances. These instances have diverse computational scales, characterised by varying numbers of disaster sites, candidate drone-supported relief facilities, drone fleet sizes, time periods, nodes generated from a parent node in the scenario tree for each time period, and total scenarios. We denote ($|I|$, $|K|$, $|D|$, $|T|$, $|\Omega_t|$, $|\Omega|$) as a numerical instance with $|I|$ disaster sites, $|K|$ candidate drone-supported relief facilities, $|D|$ drones, $|T|$ time periods, $|\Omega_t|$ nodes generated from a parent node in the scenario tree for each time period, and $|\Omega|$ total scenarios. We generate $|I|$ nodes as the disaster sites in a 10 $\times$ 10 square, where we randomly choose $|K|$ nodes as candidate drone-supported relief facilities. We conduct a series of experiments to evaluate the algorithm, comprising 10 sets of small-scale numerical instances (each with 10–20 disaster sites and 64–256 scenarios), 10 sets of medium-scale numerical instances (each with 20–30 disaster sites and 256–729 scenarios), and 10 sets of large-scale numerical instances (each with 30–50 disaster sites and 343–1,000 scenarios).

Regarding the cost parameters, we define the unit cost for opening a drone-supported relief facility as 500 (Zhu et al., 2022). Following the literature from Shehadeh and Tucker (2022), unit inventory cost and procurement cost of relief items are set at 140 and 560, respectively. Additionally, the transportation cost per distance is fixed at 20 (Yang et al., 2023). Moreover, the penalty cost for each unit of unsatisfied demand is set at ten times the unit inventory cost (Noyan, 2012a). Concerning the drone parameters, we set the maximum flying range and maximum payload weight limit as 25 and 20, respectively (Wang and Sheu, 2019; Figliozzi, 2017). Additionally, we set the procurement budget at 150,000 and define the facility capacity as 500 (Chern et al., 2010). Initially, we solve the model using the Gurobi solver and subsequently apply the Benders decomposition algorithm. The computational time limit is set at 3,600 seconds,

considering the requirement for a swift response within a humanitarian context. We evaluate the algorithm performance based on computational time and objective values. The algorithm performances for 30 sets of numerical instances across small-scale, medium-scale, and large-scale scenarios are reported in Table 4.2–4.4.

For the small-scale numerical instances, We can find that S1–S6 instances can all find the optimal solutions based on the Gurobi solver and Benders decomposition algorithm from Table 4.2. The optimal solutions obtained from these two methods are the same. Hence, the accuracy of the proposed Benders decomposition algorithm is verified. Additionally, for instances S7–S10, Gurobi cannot find the optimal solution within a limited time; however, the Benders decomposition algorithm can find the optimal solution quickly. In summary, our Benders decomposition algorithm demonstrates significantly improved efficiency over Gurobi, with an average computational time of 50.83 seconds compared to 1,692.36 seconds. This remarkable time reduction, nearly 30 times faster, underscores the superior effectiveness of our algorithm in small-scale numerical instances. For the medium-scale numerical instances, we can find that Gurobi cannot find optimal solutions within the limited computational time from Table 4.3. The average gap is 1.44%. However, the Benders decomposition algorithm can find optimal solutions quickly, with an average computational time of 589.52 seconds. This showcases the superior performance of our algorithm compared to Gurobi when handling medium-scale numerical instances. For the large-scale numerical instances, it can be observed that Gurobi fails to find optimal solutions with an average gap of 60.48% for all the instances from Table 4.4. Even in certain numerical instances, the feasible upper bound within the limited computational time cannot be found. In contrast, our proposed decomposition algorithm consistently obtains optimal solutions with an average computational time of 2,063.58 seconds. This demonstrates the superior performance of our algorithm over Gurobi in large-scale numerical instances.

Subsequently, we present the convergence curve of the Benders decomposition for

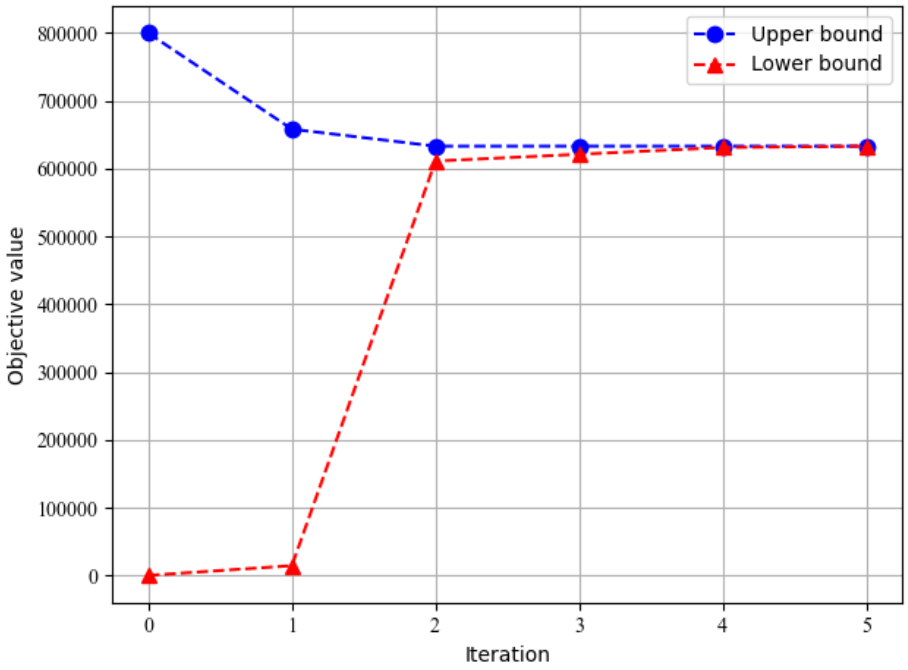

Figure 4.4: The convergence curve of the Benders decomposition algorithm.

instance L6. As shown in Figure 4.4, the algorithm converges to the target optimality gap in a limited number of iterations, further demonstrating the efficiency of the Benders decomposition algorithm.

Overall, the Benders decomposition algorithm demonstrates superior performance compared to the Gurobi solver across various instances with different computational scales. It is capable of finding optimal solutions within an hour and can be efficiently applied to solve the model, thereby enhancing response efficiency in disaster scenarios by quickly obtaining decisions.

4.4.2 Case study

We further conduct numerical experiments to validate the proposed model in a real-world application.

Table 4.2: Algorithm performance on small-scale numerical instances

Case ID	$\|I\|$	$\|K\|$	$\|D\|$	$\|T\|$	$\|\Omega_t\|$	$\|\Omega\|$	Gurobi			Benders Decomposition		
							Obj	Time (s)	Gap	Obj	Time (s)	Gap
S1	10	5	7	3	4	64	85,502.07	9.19	0	85,502.07	3.43	0
S2	10	5	7	3	5	125	86,335.00	25.3	0	86,335.00	7.09	0
S3	10	5	7	3	6	216	87,370.36	216.75	0	87,370.36	12.83	0
S4	15	7	10	3	4	64	127,761.51	147.27	0	127,761.51	11.49	0
S5	15	7	10	3	5	125	129,062.60	671.82	0	129,062.60	23.50	0
S6	15	7	10	3	6	216	130,322.02	1,453.22	0	130,322.02	39.95	0
S7	20	10	15	3	4	64	192,526.16	3,600	0.79%	192,526.16	33.88	0
S8	20	10	15	3	5	125	196,976.92	3,600	1.18%	196,874.91	67.14	0
S9	20	10	15	3	6	216	201,242.14	3,600	1.54%	201,242.14	118.73	0
S10	20	10	15	4	4	256	361,092.81	3,600	0.70%	360,926.55	190.24	0
							Avg	1,692.36	0.42%	**Avg**	50.83	0

Table 4.3: Algorithm performance on medium-scale numerical instances

Case ID	$\|I\|$	$\|K\|$	$\|D\|$	$\|T\|$	$\|\Omega_t\|$	$\|\Omega\|$	Gurobi			Benders Decomposition		
							Obj	Time (s)	Gap	Obj	Time (s)	Gap
M1	20	10	15	3	7	343	203,751.79	3,600	1.55%	203,623.49	199.74	0
M2	20	10	15	3	8	512	206,124.19	3,600	2.02%	205,344.91	290.67	0
M3	20	10	15	3	9	729	209,956.33	3,600	2.77%	207,543.34	437.55	0
M4	25	12	17	3	7	343	311,507.09	3,600	1.39%	311,164.30	337.44	0
M5	25	12	17	3	8	512	313,309.25	3,600	1.39%	312,954.53	543.72	0
M6	25	12	17	3	9	729	316,312.82	3,600	1.57%	315,359.91	802.30	0
M7	25	12	17	4	5	625	516,761.94	3,600	0.81%	515,658.96	902.25	0
M8	30	15	20	4	4	256	654,005.98	3,600	0.42%	653,699.90	675.38	0
M9	30	15	20	3	7	343	419,400.88	3,600	0.96%	418,103.59	665.78	0
M10	30	15	20	3	8	512	422,504.69	3,600	1.56%	420,871.21	1,040.31	0
							Avg	3,600	1.44%	**Avg**	589.52	0

Table 4.4: Algorithm performance on large-scale numerical instances

Case ID	$\|I\|$	$\|K\|$	$\|D\|$	$\|T\|$	$\|\Omega_t\|$	$\|\Omega\|$	Gurobi			Benders Decomposition		
							Obj	Time (s)	Gap	Obj	Time (s)	Gap
L1	30	15	20	3	9	729	425,748.50	3,600	1.70%	423,433.27	1,610.72	0
L2	30	15	20	3	10	1000	-	3,600	100%	425,799.19	2,325.33	0
L3	30	15	20	4	5	625	668,211.02	3,600	1.36%	663,614.66	1,693.83	0
L4	35	17	20	3	8	512	530,829.64	3,600	1.09%	528,812.27	1,402.32	0
L5	35	17	20	3	9	729	-	3,600	100%	531,827.45	2,117.61	0
L6	40	20	20	3	7	343	634,199.88	3,600	0.65%	633,259.42	1,248.98	0
L7	40	20	20	3	8	512	-	3,600	100%	636,528.32	2,010.91	0
L8	40	20	20	3	9	729	-	3,600	100%	639,925.41	2,810.19	0
L9	45	22	20	3	8	512	-	3,600	100%	743,607.29	2,591.81	0
L10	50	25	30	3	7	343	-	3,600	100%	845,970.90	2,824.08	0
							Avg	3,600	60.48%	**Avg**	2,063.58	0

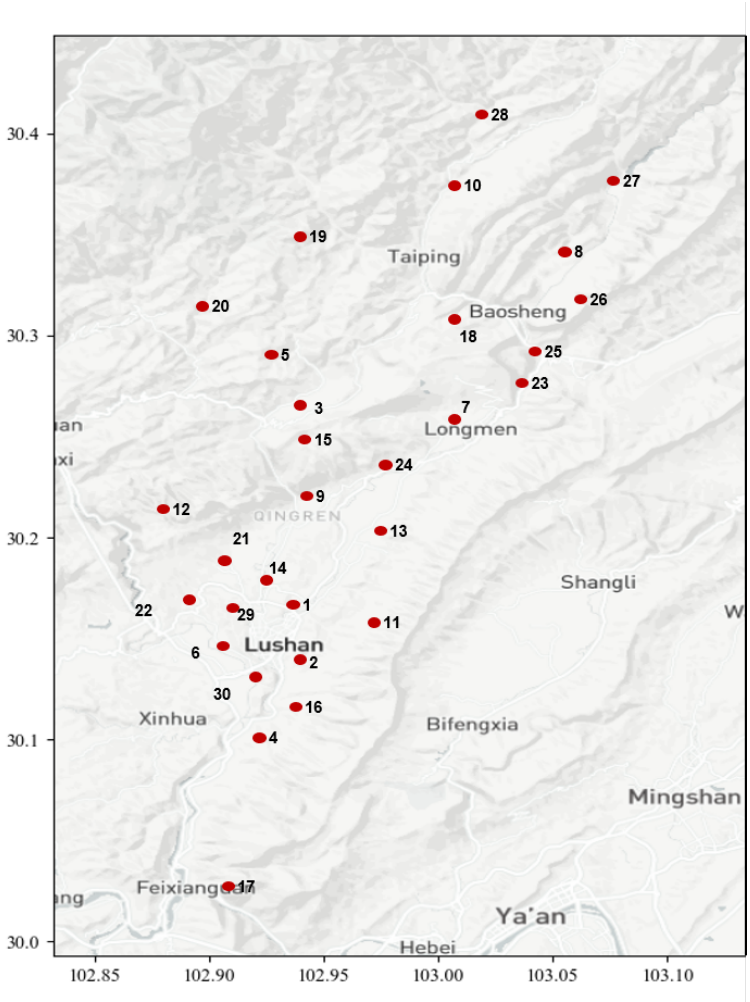

Figure 4.5: Case network.

4.4.2.1 Case background

The aftermath of the devastating 7.0 magnitude earthquake that struck Lushan County on April 20, 2013 was profound. Until 6:00 on April 23, 2013, reports indicated 193 casualties and 12,211 injuries, affecting a staggering 1.99 million individuals. In the wake of the disaster, rescue and transport operations faced significant hindrances as rolling rocks obstructed paths, impeding efforts to reach affected areas. Despite the immediate responses from local authorities, some challenges persisted in terms of the humanitarian logistics system.

The Lushan earthquake relief case highlights the critical need for integrating drones into last-mile humanitarian logistics to facilitate the swift delivery of emergency aid. By harnessing drone technology, obstacles such as impassable roads due to debris can be effectively mitigated. This ensures a more efficient and effective delivery of aid to affected regions, mitigating the negative impact of unpredictable environments of disaster-stricken areas and complicated terrain.

In this study, we adopt a computational scale equivalent to the M9 numerical instance mentioned earlier. There are 15 candidate drone-supported relief facilities (1–15) and 30 disaster sites (1–30). The case study network is shown in Figure 4.5. We define the entire planning horizon as 6 hours in total (Chauhan et al., 2019). Within this time duration, we divide the planning horizon into three equal time periods, each spanning 2 hours. For each of these time periods, a scenario tree generates seven nodes from a parent node, resulting in a total of 343 scenarios. If not explicitly stated, the parameters remain consistent with those utilised in the previous numerical experiments for algorithm validation. Following this, we will conduct a series of experiments to validate the proposed multistage stochastic programming model based on the case study.

4.4.2.2 Impact of opening cost of drone-supported relief facilities

In this section, we explore the impact of the opening cost of relief facilities. The parameter varies between 200 and 500, incrementing in steps of 100.

Figure 4.6 depicts the computational results of network topology under different opening costs of drone-supported relief facilities. In Figure 4.6, (a), (b), (c), and (d) are the network topology when the opening cost is 500, 400, 300, and 200, respectively. We find that the cost has a significant impact on the network structure. Additionally, we analyse the facility locations and transportation costs under varying opening costs, as displayed in Table 4.5. We observe that the facility location decisions remain consistent across different time periods. Notably, a negative correlation is observed between the opening cost and the number of open facilities, suggesting that higher opening costs deter the deployment of relief facilities. Additionally, the results indicate a decreasing trend in transportation costs with the increase in the number of open facilities. This trend can be attributed to the more significant number of opened drone-supported relief facilities, enabling broader coverage within the disaster zone. By expanding the coverage area, drones are able to access various locations more efficiently, thereby reducing the overall distance required to reach affected areas and facilitating swifter response and assistance delivery to those in need. Additionally, Table 4.5 also depicts that the total cost decreases with the increasing number of relief facilities, underscoring the holistic benefits of expanding the network of support infrastructure.

Therefore, relief organisers need to carefully consider cost factors when formulating opening strategies. This may involve exploring methods to reduce costs, such as negotiating with constructors or adopting more economical strategies. Additionally, opening more facilities can reduce transportation and overall costs. Expanding the network of support infrastructure demonstrates comprehensive cost-effectiveness, improving overall response to disasters and resource allocation efficiency. This enables organisations to deliver assistance more swiftly to areas in need, improving response

times and effectiveness and ultimately fostering public trust and recognition.

4.4.2.3 Impact of drone fleet size

In disaster scenarios, the size of the drone fleet is crucial in determining the effectiveness and efficiency of response efforts. However, the availability of resources in such situations is often limited, leading to uncertainty about the extent to which the drone fleet can be mobilised for relief purposes.

Therefore, we investigate the relationship between drone fleet size, total costs, and total flying distance in this experiment. We vary the drone fleet size from 7 to 11 in increments of 1. The computational results under different drone fleet sizes are reported in Table 4.6. From Table 4.6, we observe that the size of the drone fleet influences the location of facilities. The location decisions remain consistent during different time periods in this experiment. Furthermore, it is evident that increasing the drone fleet size leads to a reduction in total costs due to the presence of potential economies of scale. However, while this cost reduction is evident, it is accompanied by an increase in the total flying distance. In this study, we consider the drone flying speed as a constant, and then the response time is proportional to the total flying distance (Jin et al., 2024b). Therefore, this increase may lead to longer response times overall, although there is a slight decrease observed when the drone fleet size reaches 11. Note that the total delivery time is a critical criterion to evaluate the egalitarian objective in the context of humanitarian logistics (Tofighi et al., 2016). Finally, different drone fleet sizes will lead to different topologies of the aerial relief transportation network. Therefore, the total flying distance is distinct.

The findings highlight the importance of carefully determining the size of the drone fleet for disaster relief operations and consideration of the egalitarian objective when planning the system. Relief organisers should consider the trade-offs between total costs and response times when deciding on the drone fleet size. While larger fleets may

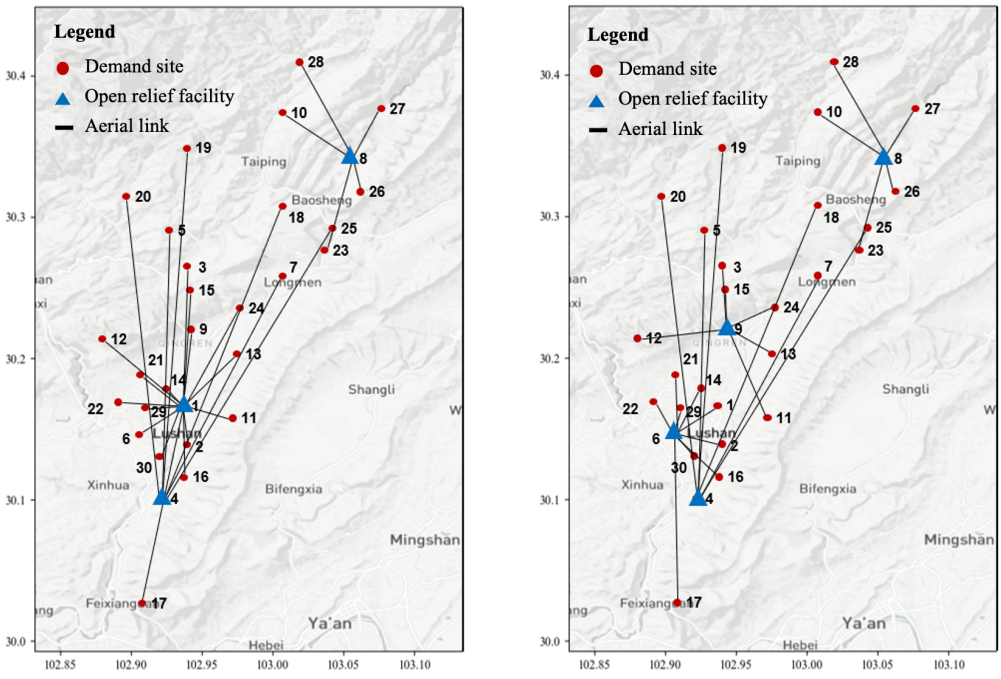

(a) Network topology when $c^{\mathrm{OP}} = 500$

(b) Network topology when $c^{\mathrm{OP}} = 400$

(c) Network topology when $c^{\mathrm{OP}} = 300$

(d) Network topology when $c^{\mathrm{OP}} = 200$

Figure 4.6: The network topologies under different opening costs of drone-supported relief facilities.

Table 4.5: Computational results under different opening costs of drone-supported relief facilities.

Unit opening cost	Drone-supported relief facility location	Total cost	Total transportation cost
200	4,6,7,8,9	373,574	4,884
300	4,6,8,9	374,822	5,532
400	4,6,8,9	376,022	5,532
500	1,4,8	377,006	6,816

result in lower costs due to the presence of potential economies of scale, the system may also lead to longer response times due to increased flying distances. Therefore, given the dynamic nature of disaster scenarios, relief organisers can remain adaptable and flexible in their approach to drone fleet size. For instance, during the early stages, prioritising response time over cost can be imperative. This strategy ensures swift and efficient delivery of relief items to affected areas, thereby minimising the impact of the disaster on vulnerable populations.

4.4.2.4 Impact of maximum flying range of drones

The maximum flight range of drones is a pivotal factor in determining the efficacy and efficiency of emergency response and rescue missions. However, this range is uncertain due to various factors, such as weather conditions (Kim et al., 2019). Consequently, conducting a sensitivity analysis on the maximum flying range in disaster scenarios becomes crucial.

In this experiment, we discuss the impact of this parameter on the model solution. We vary this parameter from 11 to 15, with an incremental step of 1. The computational results are illustrated in Figure 4.7. The computational results are reported in Figure 4.7. From Figure 4.7, it is evident that as the maximum flying distance of drones increases, the total cost decreases. However, the total flying distance demonstrates a noticeable upward trend as the flying range increases. Therefore, it is necessary to balance cost and response efficiency. Additionally, our analysis extends to examining the network topologies under various settings of maximum flying range. Figure 4.8(a) and Figure 4.8(b) depict the network topologies when the maximum flying ranges of drones are 12 and 14, respectively. The location decisions remain consistent during different time periods. From Figure 4.8, it becomes evident that the network topologies exhibit notable differences corresponding to different values of the maximum flying range of drones. These variations in network configurations underscore the impact of drone

Table 4.6: Computational results under different drone fleet sizes.

Drone fleet size	Total cost	Drone-supported relief facility location	Total flying distance
7	380,654	2,4,6,7,8,9,10	223.2
8	378,338	4,6,7,8,15	257.4
9	377,270	4,6,8,15	279
10	377,024	1,4,8	341.7
11	377,006	1,4,8	340.8

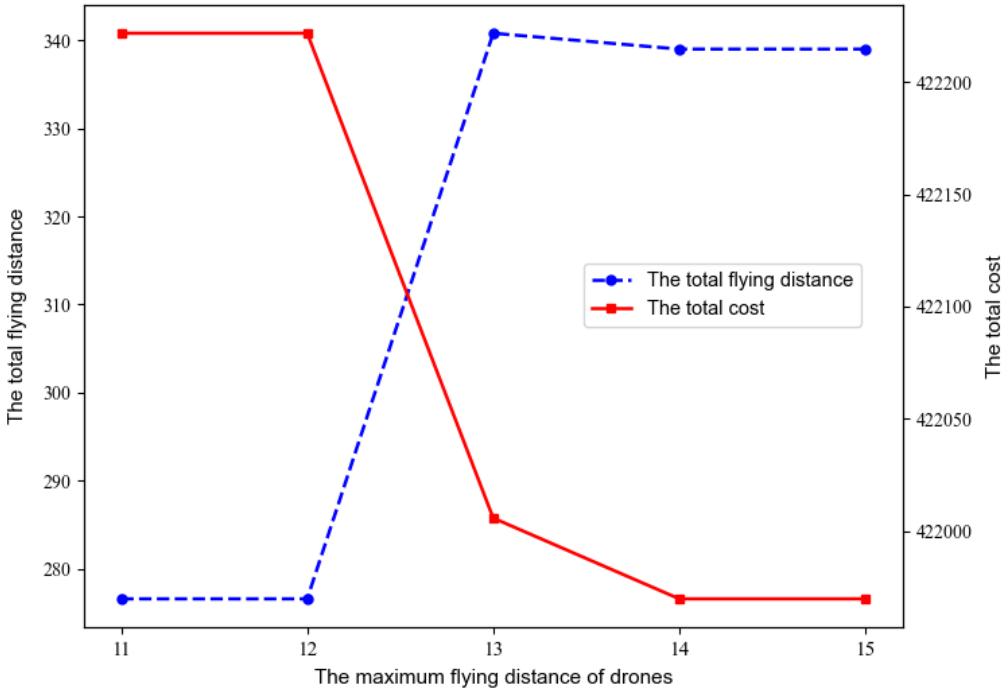

Figure 4.7: The impacts of the maximum flying range on the total cost and total flying distance.

battery duration on shaping the overall structure of the network.

Hence, it is imperative for decision-makers to meticulously evaluate the flying range when deploying drones for relief operations. By careful assessment, relief organisers can significantly enhance operational efficiency and reduce overall costs. Moreover, it is essential to maintain continuous monitoring of drone battery performance and adapt network structures and operational strategies accordingly. This proactive approach ensures optimal performance of disaster relief efforts.

4.4.2.5 Impact of payload weight limit of drones

Finally, we investigate the impact of varying the payload weight limit of drones on

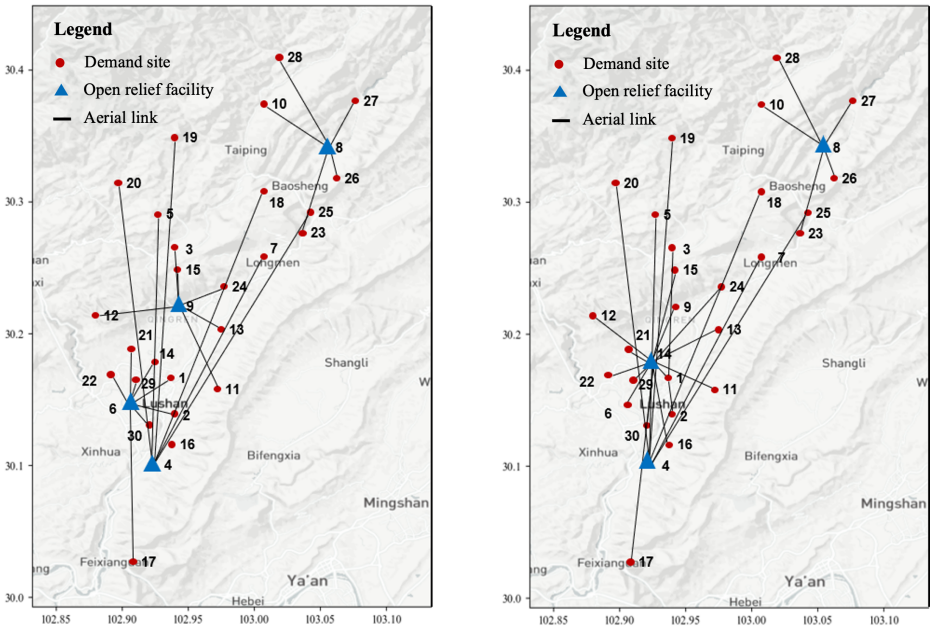

(a) Network topology when B^{MAX} =12

(b) Network topology when B^{MAX} =14

Figure 4.8: The network topologies under different maximum flying ranges of drones.

both the penalty cost of unsatisfied demand and the procurement cost. The payload weight limit ranges from 5 to 15 in increments of 2.5. In this experiment, we generate random demand ranging from 1 to 30. The inventory capacity is set as 1000, and the procurement budget is set as 5,000,000. The computational results depicted in Figure 4.9 reveal a noteworthy trend: as the payload limit increases, there is a marked decrease in unsatisfied demand alongside a corresponding increase in the procurement quantity. As the payload weight limit increases, the transportation capacity grows accordingly, reducing unsatisfied demand and enabling the procurement of more relief items within the budget.

From a managerial perspective, relief organisations can enhance their ability to meet demand effectively by investing in drones with higher payload capacities. Furthermore, while larger payload capacities increase procurement costs, more relief items can be transported. The unsatisfied demand decreases, potentially optimising resource

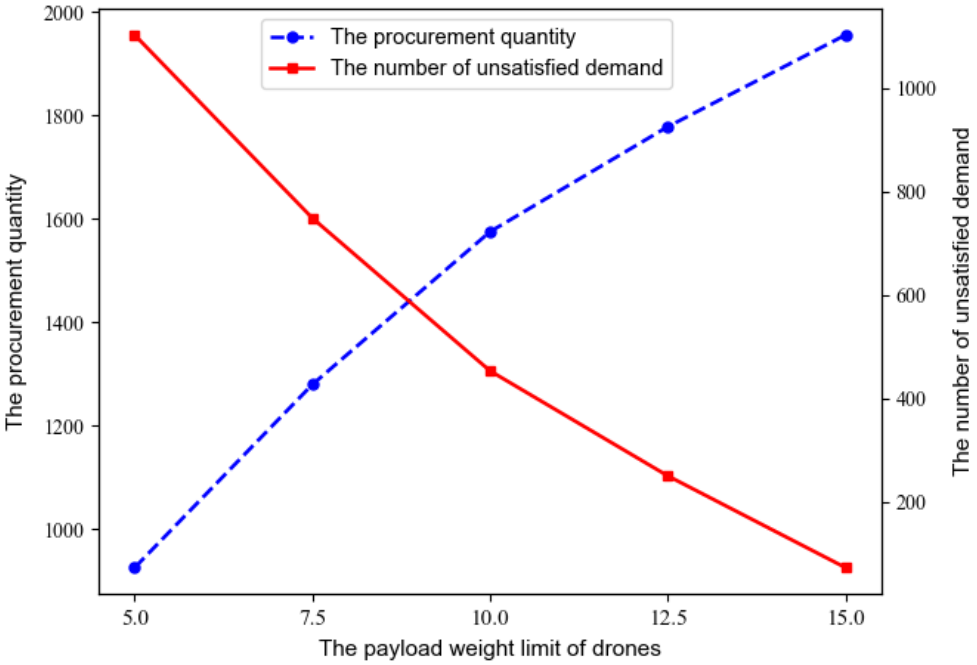

Figure 4.9: The impacts of drone payload weight limit on the procurement quantity and the number of unsatisfied demand.

utilisation and enhancing overall relief performance.

4.4.2.6 Value of incorporating nonanticipativity constraints

In this subsection, we assess the value of incorporating nonanticipativity constraints through comparison analysis. For simplicity, we let the multistage stochastic optimisation model incorporating nonanticipativity constraints call [M1] and let the model without incorporating constraints call [M2]. The optimal value of model [M1] is represented as Z. As mentioned before, the multistage model can make decisions without relying on the knowledge of demand information in future stages. In model [M2], the decision maker already knows which scenario will occur. Therefore, complete knowledge of demand in all future periods is available.

In practice, decisions regarding the recourse problem cannot be implemented because decision-makers do not have access to the complete actual information of the uncertainty. In this study, we employ a new approach for calculating the actual objective value of model [M2] proposed by Wu et al. (2023) to compare with the multistage stochastic programming model [M1]. We first determine the first-stage decisions for model [M2], which are denoted by the solution set $\mathbf{\Psi}$. Then, the decisions are made in a greedy manner after observing the actual demand in each period. Specifically, for each scenario $\omega \in \Omega$, at the beginning of each time period $t \in T$, we can make decisions regarding distribution, inventory, and procurement for the previous time periods $1, \ldots, t-1$, denoted by the solution set $\mathbf{\Theta}_\omega$. Additionally, once the actual demand for the current period is observed, we assume that future demand is zero. To this end, we optimise the model [M2] for each scenario $\omega \in \Omega$, using the decisions $\mathbf{\Psi}$ and $\mathbf{\Theta}_\omega$ from model [M2] and setting future demand is zero. This allows us to determine the optimal value $\widehat{Z}(\omega, |T|)$ for time period $|T|$ under scenario ω. Finally, the actual objective value of the model [M2] without incorporating nonanticipativity constraints can be calculated by $\widehat{Z} = \frac{1}{\Omega} \sum_{\omega \in \Omega} \widehat{Z}(\omega, |T|)$.

The difference between Z and $\widehat{Z}$ can assess the value of incorporating the nonanticipativity constraints. Then, we compare the two models when adopting the different number of time periods. As shown in Figure 4.10, the incorporation of the nonanticipativity constraints can lead to a 2.24% and 6.05% reduction in the total cost when $|T| = 2$ and $|T| = 3$. This indicates that decision makers can achieve cost-efficient outcomes using the multistage stochastic programming model. In disaster relief scenarios, it helps avoid the higher costs that may arise from "cheating" —making decisions based on future information that is not available at the current decision stage. Therefore, the proposed multistage stochastic programming model is effective in managing uncertainties while safeguarding the well-being of the affected population in disaster situations.

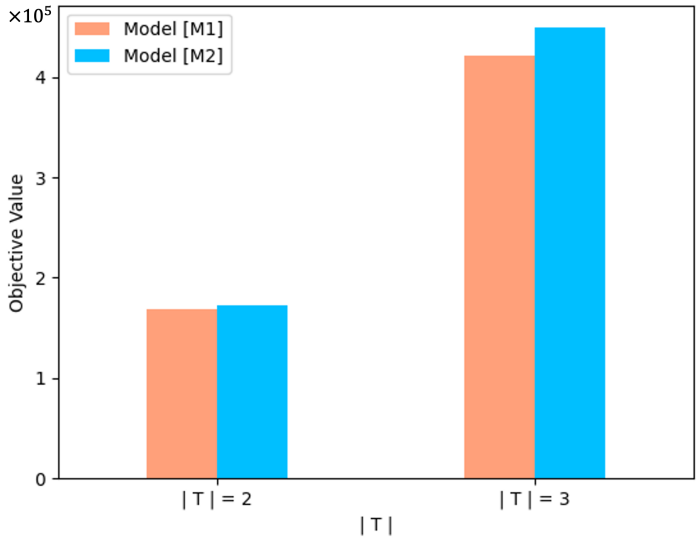

Figure 4.10: Comparison of model [M1] and [M2].

4.4.3 Managerial implications and insights

This subsection extracts key managerial insights, which are summarised as follows:

(1) Firstly, the proposed multistage stochastic programming model and the Benders decomposition algorithm are designed for uncertain disaster scenarios where demand information for each stage becomes available only after decisions have been made for the preceding stage. This approach more accurately reflects our problem and aligns with real-world practices. Simultaneously, our proposed model and algorithm enable relief organisers to improve operational efficiency in an uncertain disaster environment.

(2) Secondly, it is crucial for relief organisers to meticulously consider the opening cost when strategically deploying drone-supported relief facilities. This may entail exploring methods to reduce opening costs, such as engaging in negotiations with contractors or adopting more cost-effective approaches. Moreover, lower opening costs will lead to the expansion of opening facilities, which can lead to reductions in both transportation and overall costs. This expansion can promote cost efficiency and accelerate

delivery to affected regions, thereby enhancing both the efficiency and effectiveness of the response.

(3) Thirdly, we provide managerial insights on managing drone fleets. Decision-makers need to carefully assess the appropriate size of the drone fleet. While larger fleets may lead to cost savings, they could also result in longer response times. Hence, striking a balance between cost and operational efficiency is crucial. Moreover, given the dynamic nature of disaster scenarios, relief organisers should maintain flexibility in determining drone fleet size based on the characteristics of different time periods during the entire planning horizon. Furthermore, the maximum flying range of drones impacts network topologies significantly. Monitoring drone battery performance continuously and adjusting network structures and operational strategies is essential to optimise overall costs and response time. Finally, humanitarian organisers could consider deploying large drones to enhance operational efficiency.

4.5 Concluding Remarks of Chapter 4

In conclusion, this study proposes a DLHLSP problem to address the challenges of establishing an effective drone-supported last-mile humanitarian logistics system. The DLHLSP problem provides a comprehensive decision making framework that encompasses both the pre-disaster and post-disaster phases. The pre-disaster phase determines drone-supported relief facility locations, drone deployment, and drone visit schedules. In the post-disaster phase, we concentrate on inventory management, relief item procurement, and drone-based delivery operations, which are crucial for timely and efficient relief item distribution. To capture the demand uncertainty, a multistage stochastic programming model with nonanticipativity constraints is proposed. This approach can allow decisions to be made without the requirements for revealing precise knowledge of future demands. It better reflects our research problem and is in

line with real-world practices. Then, we apply the Benders decomposition algorithm to obtain the exact solutions of the multistage stochastic programming model. The experimental results demonstrate that the Benders decomposition algorithm significantly outperforms the Gurobi solver in terms of the computational time and gap between the upper bound and lower bound in numerical instances with different scales. Furthermore, this study conducts experiments to validate the approach and provides some valuable managerial insights.

Chapter 5

A Risk-Averse Distributionally Robust Optimisation Approach for Drone-Supported Relief Facility Location Problem

Drone-supported last-mile humanitarian logistics applications play a crucial role in the rapid and efficient delivery of essential relief items, such as medicine, blood, and vaccines, during disaster and emergency situations. In this chapter, we explore a novel DSRFLP that aims to establish an effective drone-supported last-mile humanitarian logistics system. The problem involves making joint decisions for both pre-disaster and post-disaster phases while considering the characteristics of drone-based delivery operations and uncertain demands. In the pre-disaster phase, we make the decisions regarding the locations of drone-supported relief facilities, inventory prepositioning of relief items, assignment of drones to the opened facilities, and allocation of drones to disaster demand sites. In the post-disaster phase, we make decisions related to delivery quantities. To address the challenge of incomplete demand distribution information in

chaotic disaster environments, we establish a DRO model to handle the demand uncertainty. This model adopts worst-case mean Conditional Value-at-Risk as the risk measurement, reflecting the risk-averse attitude of humanitarian organisers. In this study, three ambiguity sets (box, ellipsoidal, and polyhedral) are considered to describe the ambiguity distributions of demands. To overcome the computational challenge, we reformulate the DRO model under three ambiguity sets into two mixed-integer linear programming models and one second-order cone programming model, which can be efficiently solved by off-the-shelf solvers. Furthermore, we validate our proposed DRO model through a small-scale example and a large-scale case study based on the Lushan earthquake in China. The computational outcomes underscore the superior performance of the proposed DRO model. The model can mitigate the impact arising from incomplete probability distributions. We propose managerial implications and insights to support the decision-making of humanitarian organisations based on experimental results. Finally, we propose two extended models to incorporate multiple relief items and equity constraints in priority settings and conduct numerical experiments to adapt to various real-world disaster scenarios.

5.1 Introduction

When planning a drone-supported last-mile logistics system, uncertainty is an important characteristic that cannot be ignored, with demand uncertainty standing out as a critical factor in humanitarian logistics. The importance of managing demand uncertainty is underscored by the fact that a severe supply shortage could lead to ineffective rescue efforts and an increase in casualties (Bozorgi-Amiri et al., 2012; Zhong et al., 2020). The demand information from the disaster demand sites significantly influences decisions regarding the locations of drone-supported relief facilities. However, acquiring complete demand information is challenging due to the complexities of precisely

evaluating disaster situations in affected regions. To address this challenge, a DRO approach is proposed for the DSRFLP to capture the ambiguous demand information of the disaster demand sites. Furthermore, in chaotic disaster relief systems, decision makers are often risk-averse rather than adopting a risk-neutral stance (Wang et al., 023a). Conventional risk-neutral models may produce suboptimal results when applied to specific instances of random data, potentially leading to undesirable outcomes (Elçi and Noyan, 2018). Therefore, it becomes imperative to account for the risk-averse attitudes of decision makers and employ an appropriate risk measurement to mitigate risks in drone-supported last-mile humanitarian logistics. Conditional Value-at-Risk (CVaR) stands out as a widely utilised risk measurement. However, it primarily concentrates on the mean loss above a specified confidence level, neglecting the portion below the confidence level (Guan et al., 2024). To address this limitation, scholars propose to introduce a weight parameter to integrate the expectation with CVaR, named mean-CVaR (MCVaR) (Wang et al., 2021b; Guan et al., 2022). Moreover, traditional CVaR is commonly applied based on the assumption of a known probability distribution for uncertain parameters, but it often lacks robustness (Wang et al., 023a). To cope with this challenge, the worst-case CVaR (WCVaR) has gained increasing attention (Zhu and Fukushima, 2009). Hence, we establish a risk-averse DRO model incorporating the worst-case MCVaR (WMCVaR) as the risk measurement to solve the DSRFLP in this study. Currently, there is some literature that integrates the DRO approach and risk preference measures (Chang et al., 2017; Wang et al., 2021b). In essence, this combination enables the DRO model to tackle challenges associated with incomplete probability distributions of random parameters and hedge against uncertainty to avoid high-risk solutions (Feng et al., 2023).

More specifically, we address the DSRFLP under the uncertainty of disaster site demand within a two-stage decision framework. In the first stage, we determine the pre-disaster decisions, including the locations of drone-supported relief facilities, inven-

tory prepositioning of relief items, drone assignment to the opened facilities, and drone allocation to disaster demand sites. This aligns with real-world practices, where certain higher-level decisions, such as those related to location planning and inventory, must be pre-determined and kept fixed to prevent significant disruptions in the pre-disaster phase. Moreover, in disaster-stricken environments, it is crucial to determine the drone visit schedule in the pre-disaster phase because humanitarian organisers need to communicate in advance to the managers of both disaster sites and low-altitude air traffic to ensure adequate preparation of the necessary workforce and equipment. Moreover, determining the drone visit schedule in advance is crucial for the planning of drone aerial paths, especially considering the complexities of geological and meteorological environments. This proactive approach ensures rapid and effective relief support in the post-disaster phase. Therefore, in this study, the decision regarding drone allocations to disaster demand sites is considered in the first stage, involving the coordination of transportation tasks for each drone to access its designated disaster demand sites. Importantly, this decision can be conducted independently of the demand realisations in the pre-disaster phase. Existing literature has addressed the decisions associated with vehicle visits in the first stage in the field of transportation and logistics planning (Adulyasak et al., 2015; Tricoire et al., 2012). Particularly in disaster relief scenarios, the advance determinations regarding drone visits assume more paramount significance due to the imperative of ensuring a prompt and efficient response. After the demand information becomes known, subsequent decisions regarding the delivery quantity can be made in the post-disaster phase.

Additionally, we propose two extended models to adapt to different real-world disaster scenarios, building upon the mathematical model of DSRFLP. One model aims to consider multiple relief items, encompassing diverse emergency needs such as medical kits, blood, and vaccines. This approach ensures that a diverse range of urgent needs can be met promptly and efficiently. The other model extension incorporates an

equity constraint in priority setting. We prioritise relief resource allocation according to the urgent degree and incorporate equity constraints to ensure a fair distribution of resources among affected populations. This approach promotes the efficiency and efficacy of drone-supported last-mile humanitarian logistics but also reflects principles of social justice and enhances social welfare.

To sum up, the main contributions of this research are summarised as follows:

(1) We concentrate on a practical DSRFLP that incorporates joint decisions during pre-disaster and post-disaster phases, including drone-supported relief facility location, inventory prepositioning of relief items, drone assignment to the opened facilities, drone allocation to disaster demand sites, and delivery quantity decisions. To encompass the specific features of drone-based delivery operations, we incorporate considerations of battery capacity requirements and payload weight limitations into this problem. Additionally, we consider the uncertainty of the demands of disaster demand sites. This study is the first attempt to integrate these decisions within the field of drone-supported last-mile humanitarian logistics management.

(2) Considering the difficulty of acquiring the complete demand information in disaster scenarios, we propose a two-stage DRO model for DSRFLP to capture the ambiguous distribution information of uncertain demand. Additionally, WMCVaR risk measurement is adopted in this DRO model to reflect the decision maker's risk-averse attitude. This is the first study to adopt the risk-averse DRO approach to make hybrid decisions under partial probability distribution regarding uncertain demands in the field of drone-supported last-mile humanitarian logistics.

(3) Three ambiguity sets (box, ellipsoidal, and polyhedral) are designed to depict the partial probability distributions of the demand. Furthermore, we reformulate the DRO model under three ambiguity sets into the corresponding equivalent computationally tractable formulations. Additionally, we conduct a series of experiments using a small-scale example and a large-scale case study based on the Lushan Earthquake

to verify the effectiveness of the DRO model under three ambiguity sets. The results of the numerical experiments demonstrate that the DRO model exhibits better performance than the stochastic programming model, which presents a compelling motivation for relief organisers to embrace the DRO approach. Finally, we provide several valuable managerial implications and insights, serving as a valuable reference for the decision-making processes of humanitarian organisers.

(4) We propose two extended problems of DSRFLP to consider multiple relief items and equity constraint in priority setting. For these problems, we first present the two-stage stochastic programming models and then establish the corresponding DRO models under box, ellipsoidal, and polyhedral ambiguity sets to address the demand uncertainty. Moreover, we perform numerical experiments to validate the performance of the proposed extended model, thereby providing valuable insights for optimising disaster relief efforts and adapting to various real-world disaster scenarios.

The remainder of this study is organised as follows. In Section 5.2, we investigate a risk-averse two-stage stochastic programming and introduce a DRO model within three ambiguity sets (box, ellipsoidal, and polyhedral). Moreover, we transform the DRO model, considering different ambiguity sets, into an equivalent computationally tractable formulation suitable for resolution with a commercial solver. Section 5.3 details various numerical experiments conducted to validate the efficacy of the DRO model and presents several managerial insights. In Section 5.4, we introduce two extended models aimed at incorporating multiple relief items and equity constraint in priority setting, establishing upon the foundation of the DSRFLP. Additionally, we conduct numerical experiments to evaluate the performance of the proposed extended models. Finally, Section 5.5 provides conclusions and outlines potential avenues for future research.

5.2 Problem Description and Mathematical Formulations

5.2.1 Problem description

In contemporary disaster relief scenarios, there has been a notable surge in the utilisation of drones. This escalating trend underscores the growing prominence and adoption of drone technology in the humanitarian sector. The diverse capabilities of drones, encompassing efficient delivery of essential supplies (medicine, blood, vaccines, etc.) to remote or inaccessible areas, significantly contribute to enhancing the overall effectiveness and responsiveness of disaster relief efforts. In drone-supported last-mile humanitarian logistics, the drone-supported relief facilities play a pivotal role in furnishing essential logistical support and services. However, the number of open drone-supported relief facilities might be limited because of geographical and practical factors. Therefore, in this study, we focus on a practical DSRFLP aimed at optimising the planning of the drone-supported last-mile humanitarian logistics system.

We present a comprehensive overview of the DSRFLP and subsequently propose a two-stage stochastic programming model. For this problem, our modelling framework incorporates decision-making in both the pre-disaster and post-disaster phases. First, we outline the sets, decision variables, and parameters in the first stage (pre-disaster). During the pre-disaster phase, our focus spans the determination of optimal locations for drone-supported relief facilities, inventory prepositioning of relief items, drone assignment to the opened facilities, and drone allocation to disaster demand sites. In this problem, the drone-supported relief facility functions both as a warehouse for storing relief items and as a distribution hub where a limited number of drones can pick up items destined for the disaster demand sites and change the battery. We let K and L denote the set of candidate drone-supported relief facilities and the set of capacity

levels of the open drone-supported relief facilities, respectively. For each $k \in K$ and $l \in L$, we introduce the binary variable x_{kl} that equals 1 if a drone-supported relief facility is open at location k with a designated capacity level l, and is 0 otherwise. The unit opening cost for a drone-supported relief facility with the capacity level l is represented as a non-negative parameter c_l^{OPEN}. Let D denote the set of available drones, and each available drone $d \in D$ can be assigned to an opened drone-supported relief facility to transport the relief items to the disaster demand sites. For each $d \in D$ and $k \in K$, we define binary variable y_{dk} that equals 1 if the drone d is assigned to the open drone-supported relief facility k, and is 0 otherwise. As mentioned earlier, our approach involves determining the allocation of drones to disaster demand sites during the pre-disaster phase, ensuring a swift response in the post-disaster phase. Here, we let I represent the set of disaster demand sites. Hence, for each $i \in I$, $d \in D$, and $k \in K$, we define z_{idk} that equals 1 if disaster demand site i is visited by drone d assigned to the drone-supported relief facility k, and is 0 otherwise. In this study, each assigned drone launches from the drone-supported relief facility while carrying a parcel, travelling to the disaster demand site, delivering the relief items, and returning to the drone-supported relief facility. This entire transportation process is termed a *drone trip*. For drone operation research, battery capacity is a key element that needs to be considered compared to the traditional truck-based delivery operations (Kim et al., 2019; Hong et al., 2018; Chen et al., 2021). Therefore, we introduce the maximum flying range B^{MAX} resulting from the limited battery capacity to meet the requirements of battery capacity of drone-based delivery operations. Drones are permitted to make multiple trips if their battery capacity allows, as in prior studies (Zhu et al., 2022; Chauhan et al., 2019). Figure 5.1 shows an illustrative example of a drone-supported last-mile humanitarian logistics system. In this system, there are two open drone-supported relief facilities F1–F2 and 12 disaster demand sites S1–S12. Six drones are assigned to provide relief delivery services for the disaster sites. We

note that drones can make several one-to-one drone trips (open drone-supported relief facility to disaster demand site and back) until the battery is depleted. For instance, drone 1 completes three drone trips to serve disaster demand sites S1, S2, and S6, while drone 2 makes two drone trips to serve disaster demand sites S4 and S5. Once the drone visit schedules are established, the subsequent step involves planning and managing the aerial paths in the pre-disaster phase. This process could incur drone aerial path management costs, which might be associated with path planning and the deployment of manpower or equipment to manage low-altitude airspace. Therefore, we define a non-negative parameter c_{ki}^{MANA} as drone aerial path management cost from the drone-supported relief facility k to the disaster demand site i. Additionally, in our consideration, we focus on a singular type of relief supply, where critical items (such as blood, medical kits, and pharmaceuticals) can be provided in the bundled form (Elçi and Noyan, 2018). For each $k \in K$, we define the non-negative continuous decision variable v_k as the inventory prepositioning quantity of relief items in the drone-supported relief facility k. The open drone-supported relief facility has a capacity level l and corresponding limited inventory capacity of relief items represented by W_l and drone capacity denoted by Q_l. The unit inventory prepositioning cost for relief items is represented as a non-negative parameter c^{INV}.

Furthermore, we illustrate the sets, decision variables, and parameters in the second stage (post-disaster). Transitioning to the post-disaster phase, our model encompasses the critical decision-making process related to the delivery quantity of relief items to the disaster demand sites. We let Ξ represent the set of scenarios and $\xi \in \Xi$. Regarding the uncertain parameter, we let D_i^{ξ} indicate the demand of relief item for the disaster demand site i under scenario ξ. For each $i \in I$, $k \in K$, and $\xi \in \Xi$, we introduce the non-negative continuous decision variable w_{ik}^{ξ}, representing the number of relief items delivered to disaster demand site i from drone-supported relief facility k under scenario ξ. In drone-supported transportation, the payload weight limit is an important issue

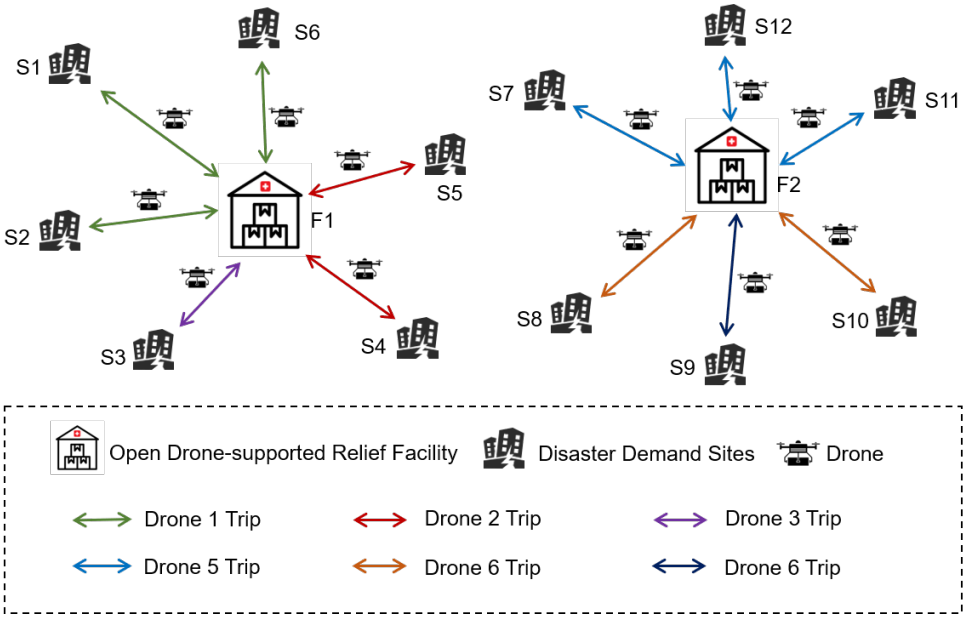

Figure 5.1: An illustrative example of a drone-supported last-mile humanitarian logistics system.

that needs to be considered (Golabi and Nejad, 2022). In this study, we consider the determination of the delivered quantity of individual drones. For each $i \in I$, $d \in D$, $k \in K$, and $\xi \in \Xi$, we let the non-negative continuous decision variable q_{idk}^{ξ} represent the number of relief items delivered to disaster demand site i by the drone d that is assigned to drone-supported relief facility k under scenario ξ. Note that another special characteristic of drone delivery operations that needs to be considered is that drones may only deliver a small number of items per trip due to payload weight limitations, in contrast to traditional truck-based delivery operations (Chen et al., 2021). Therefore, we denote the maximum payload weight limit of drones as L^{MAX} to constrain the quantity of relief items transported by drones per drone trip. The delivery cost for unit demand from the drone-supported relief facility k to the disaster demand site i is represented by the non-negative parameter c_{ki}^{DELI}. Finally, for each $i \in I$ and $\xi \in \Xi$, the non-negative continuous decision variable u_i^{ξ} is introduced, which means the quantity of unsatisfied demand of disaster demand site i for the relief items under scenario ξ.

And for each $k \in K$ and $\xi \in \Xi$, we let the non-negative continuous decision variable r_k^ξ express the quantity of unused inventory of the relief items at the drone-supported relief facility k under scenario ξ. The penalty cost for per unit unsatisfied demand of relief items and unused relief items are represented by the non-negative parameters c^{UNS} and c^{UNU}, respectively. We summarise the notation in Table 5.1.

Table 5.1: Notations of DSRFLP

Notation	Definition
Sets	
I	The set of disaster demand sites, $i \in I$.
K	The set of candidate drone-supported relief facilities, $k \in K$.
L	The set of capacity levels of drone-supported relief facilities, $l \in L$.
D	The set of available drones, $d \in D$.
Ξ	The set of scenarios, $\xi \in \Xi$.
Parameters	
c_l^{OPEN}	The unit opening cost for a drone-supported relief facility with capacity level l.
c_{ki}^{MANA}	The drone aerial path management cost from the drone-supported relief facility k to the disaster demand site i.
c^{INV}	The unit inventory prepositioning cost for relief items.
c_{ki}^{DELI}	The delivery cost for unit demand from the drone-supported relief facility k to the disaster demand site i.
c^{UNS}	The penalty cost for per unit unsatisfied demand of relief items.
c^{UNU}	The penalty cost for per unit unused relief items.
Q_l	The capacity of drones for the drone-supported relief facility with capacity level l.
W_l	The inventory capacity of relief items for the drone-supported relief facility with capacity level l.
B^{MAX}	The maximum flying range of drones due to the limited battery capacity.
L^{MAX}	The maximum payload weight limit of drones.
D_i^{ξ}	The demand of relief item for the disaster demand site i under scenario ξ.
Variables	
First-stage variables	
x_{kl}	Binary variable, if the candidate location k is chosen as drone-supported relief facility with capacity level l, it equals 1; otherwise, it equals 0.
y_{dk}	Binary variable, if the drone d is assigned to the drone-supported relief facility k, it equals 1; otherwise, it equals 0.
z_{idk}	Binary variable, if the disaster demand site i is visited by drone d assigned to the drone-supported relief facility k, it equals 1; otherwise, it equals 0.
v_k	Continuous variable, the inventory prepositioning quantity of relief items in the drone-supported relief facility k.
Second-stage variables	
w_{ik}^{ξ}	Continuous variable, the number of relief items delivered to disaster demand site i from drone-supported relief facility k under scenario ξ.
q_{idk}^{ξ}	Continuous variable, the number of relief items delivered to disaster demand site i by the drone d that is assigned to drone-supported relief facility k under scenario ξ.
u_i^{ξ}	Continuous variable, the quantity of unsatisfied demand of disaster demand site i for the relief items under scenario ξ.
r_k^{ξ}	Continuous variable, the quantity of unused inventory of the relief items at the drone-supported relief facility k under scenario ξ.

5.2.2 Risk-averse two-stage stochastic programming

In this subsection, the risk-averse two-stage stochastic programming model for the DSRFLP is presented, which relies on the perfect distribution information of the random demand.

We first introduce the risk-neutral two-stage stochastic programming model. In the first stage, we focus on the pre-disaster decisions regarding the drone-supported relief facility locations, inventory prepositioning of relief items, drone assignment to the opened facilities, and drone allocation to disaster demand sites. Our primary objective is to minimise the total cost, which encompasses the opening cost of drone-supported relief facilities, the inventory prepositioning cost of relief items, and the drone aerial path management cost. The objective function can be formulated as follows:

$$\min \sum_{k\in K}\sum_{l\in L} c_l^{\mathrm{OPEN}} x_{kl} + \sum_{k\in K} c^{\mathrm{INV}} v_k + \sum_{i\in I}\sum_{d\in D}\sum_{k\in K} c_{ki}^{\mathrm{MANA}} z_{idk} \tag{5.1}$$

The constraints in the first stage are expressed as follows:

$$\sum_{l\in L} x_{kl} \leq 1, \quad \forall k\in K, \tag{5.2}$$

$$y_{dk} \leq \sum_{l\in L} x_{kl}, \quad \forall d\in D,\ \forall k\in K, \tag{5.3}$$

$$\sum_{k\in K} y_{dk} \leq 1, \quad \forall d\in D, \tag{5.4}$$

$$\sum_{d\in D} y_{dk} \leq \sum_{l\in L} Q_l x_{kl}, \quad \forall k\in K, \tag{5.5}$$

$$v_k \leq \sum_{l\in L} W_l x_{kl}, \quad \forall k\in K, \tag{5.6}$$

$$z_{idk} \leq y_{dk}, \quad \forall k \in K,\ \forall i \in I, \forall d \in D, \tag{5.7}$$

$$\sum_{k \in K} \sum_{d \in D} z_{idk} \geq 1, \quad \forall i \in I, \tag{5.8}$$

$$\sum_{i \in I} d_{ki} z_{idk} \leq B^{\mathrm{MAX}} y_{dk}, \quad \forall k \in K,\ \forall d \in D, \tag{5.9}$$

$$x_{kl} \in \{0, 1\}, \quad \forall k \in K,\ \forall l \in L, \tag{5.10}$$

$$y_{dk} \in \{0, 1\}, \quad \forall d \in D,\ \forall k \in K, \tag{5.11}$$

$$z_{idk} \in \{0, 1\}, \quad \forall k \in K,\ \forall i \in I, \forall d \in D, \tag{5.12}$$

$$v_k \geq 0, \quad \forall k \in K. \tag{5.13}$$

Constraints (5.2) ensure that at most one capacity level can be chosen for each candidate drone-supported relief facility. Constraints (5.3) forbid drones to be assigned to a candidate drone-supported relief facility that is not open. Constraints (5.4) force each drone can only be assigned to an open drone-supported relief facility once at most. Constraints (5.5) guarantee the number of assigned drones cannot exceed the capacity of drones for each open drone-supported relief facility. Constraints (5.6) impose an inventory capacity limit on the quantity of inventory prepositioning for relief items at each open drone-supported relief facility. Constraints (5.7) state that no relief delivery service can be provided if a drone is not assigned to one certain drone-supported relief facility. Constraints (5.8) require each disaster demand site to be visited by drones at least once to prevent a severe shortage of relief items. Constraints (5.9) enforce battery range constraints on each drone d assigned to drone-supported relief facility k. Finally, constraints (5.10)-(5.13) define the domains of first stage variables.

In the second stage, we consider the post-disaster delivery quantity decisions in

response to different disaster scenarios, which are made after the demand information becomes known. The objective of the second stage is to minimise the delivery cost as well as the penalty cost of unsatisfied demand and unused relief items. Given a set of the first stage decisions $\{\mathbf{x}, \mathbf{y}, \mathbf{z}, \mathbf{v}\}$ and the random input data vector $\mathbf{\Theta}(\xi)$, the recourse problem, defined as $Q(\mathbf{x}, \mathbf{y}, \mathbf{z}, \mathbf{v}, \mathbf{\Theta}(\xi))$ can be expressed as follows:

$$Q(\mathbf{x}, \mathbf{y}, \mathbf{z}, \mathbf{v}, \mathbf{\Theta}(\xi)) = \min \sum_{i \in I} \sum_{d \in D} \sum_{k \in K} c_{ki}^{\mathrm{DELI}} q_{idk}^{\xi} + \sum_{i \in I} c^{\mathrm{UNS}} u_i^{\xi} + \sum_{k \in K} c^{\mathrm{UNU}} r_k^{\xi} \tag{5.14}$$

$$\text{s.t.} \quad \sum_{k \in K} w_{ik}^{\xi} + u_i^{\xi} = D_i^{\xi}, \quad \forall i \in I, \tag{5.15}$$

$$\sum_{i \in I} w_{ik}^{\xi} + r_k^{\xi} = v_k, \quad \forall k \in K, \tag{5.16}$$

$$w_{ik}^{\xi} - \sum_{d \in D} q_{idk}^{\xi} = 0, \quad \forall k \in K, \ \forall i \in I, \tag{5.17}$$

$$q_{idk}^{\xi} \leq L^{\mathrm{MAX}} z_{idk}, \quad \forall k \in K, \ \forall i \in I, \ \forall d \in D, \tag{5.18}$$

$$w_{ik}^{\xi} \geq 0, \quad \forall k \in K, \ \forall i \in I, \tag{5.19}$$

$$q_{idk}^{\xi} \geq 0, \quad \forall k \in K, \ \forall i \in I, \ \forall d \in D, \tag{5.20}$$

$$u_i^{\xi} \geq 0, \quad \forall i \in I, \tag{5.21}$$

$$r_k^{\xi} \geq 0, \quad \forall k \in K. \tag{5.22}$$

Formula (5.14) is the objective function of the second stage under scenario ξ associated with the transportation of the relief items to the disaster sites as well as the penalties of unsatisfied demand and unused inventory. Constraints (5.15) give a bal-

anced formulation; that is, the number of delivered relief items plus the quantity of unsatisfied demand is equivalent to the corresponding demand for each disaster demand site. Constraints (5.16) mean the number of relief items delivered from the relief facility plus unused inventory equals the corresponding inventory prepositioning quantity. Constraints (5.17) indicate the relationship between the two variables. The number of delivered relief items for individual drones can be calculated based on this equation. Constraints (5.18) require the number of relief items delivered by the drone cannot exceed the maximum payload weight limit. Ultimately, constraints (5.19)-(5.22) specify the domains of second stage variables.

Hence, the risk-neutral two-stage stochastic programming model for the DSRFLP is given as follows:

$$\min_{\boldsymbol{x},\boldsymbol{y},\boldsymbol{z},\boldsymbol{v},\boldsymbol{\Psi}} \left\{ \sum_{k\in K}\sum_{l\in L} c_l^{\mathrm{OPEN}} x_{kl} + \sum_{k\in K} c^{\mathrm{INV}} v_k + \sum_{i\in I}\sum_{d\in D}\sum_{k\in K} c_{ki}^{\mathrm{MANA}} z_{idk} + \mathbb{E}[Q(\mathbf{x},\mathbf{y},\mathbf{z},\mathbf{v},\boldsymbol{\Theta}(\xi))] \right\} \tag{5.23}$$

$$\text{s.t.} \quad \text{Constraints (5.2)–(5.13), Constraints (5.15)–(5.22),}$$

where Ψ denotes the vector composed by the variables of the second stage, i.e., $\Psi = \{\boldsymbol{w}, \boldsymbol{q}, \boldsymbol{u}, \boldsymbol{r}\}$.

Due to the infrequency of catastrophic events, it is necessary to incorporate the risk consideration in the humanitarian logistics (Wang et al., 023b). While the expected value criterion is widely used in stochastic optimization, its effectiveness in disaster relief settings can be limited due to the infrequent and high-impact nature of disasters. The expected value focuses on average performance across many realizations, which may not be representative when disasters are rare but severe. To address this, we adopt a mean-CVaR (MCVaR) approach, where the expected value ensures cost-effectiveness under typical scenarios, and the CVaR component explicitly manages the risk of extreme outcomes. By integrating both criteria, our model provides a balanced

solution that is efficient in general cases and resilient to worst-case scenarios. This is particularly important in humanitarian logistics, where the consequences of inadequate response in rare but severe disasters can be catastrophic (Noyan, 2012b). Subsequently, we elaborate on the risk-averse two-stage stochastic programming model for the DSR-FLP. Some definitions are introduced before the establishment of the model.

Definition 5.1. The Conditional Value-at-Risk (CVaR) for the random variable Z at a confidence level $\alpha \in [0, 1)$ is defined (Rockafellar and Uryasev, 2002) as

$$\text{CVaR}_\alpha(Z) := \inf_{\eta \in \mathbb{R}} \left\{ \eta + \frac{1}{1-\alpha} \mathbb{E}[(Z-\eta)_+] \right\}, \tag{5.24}$$

where $(a)_+ := \max\{a, 0\}$ for $a \in \mathbb{R}$, and $\mathbb{E}$ is the expected value operator. η represents the value of the maximum loss suffered by the function $Q(\mathbf{x}, \mathbf{y}, \mathbf{z}, \mathbf{v}, \boldsymbol{\Theta}(\xi))$ when the confidence level is α.

Definition 5.2. The MCVaR for the random variable Z at a confidence level $\alpha \in [0, 1)$ and a weight parameter $\lambda \in [0, 1]$ is defined (Luan et al., 2022) as

$$\text{MCVaR}(Z) := (1-\lambda)\mathbb{E}(Z) + \lambda \text{CVaR}_\alpha(Z). \tag{5.25}$$

Remark 5.1. Note that the relative significance of the risk term will increase when weight parameter λ increases and so would lead to more risk-averse decisions.

Remark 5.2. Suppose that Z is a discrete random variable with realisations Z^ξ and corresponding probabilities p^ξ for scenario $\xi \in \Xi$, the expression (5.25) can be represented as the following linear program for finite probability spaces by introducing the auxiliary variable s^ξ (Mahmutoğulları et al., 2018).

$$\text{MCVaR}(Z) = \min (1-\lambda) \sum_{\xi \in \Xi} p^\xi Z^\xi + \lambda(\eta + \frac{1}{1-\alpha} \sum_{\xi \in \Xi} p^\xi s^\xi) \tag{5.26}$$

$$\text{s.t.} \quad s^{\xi} \geq Z^{\xi} - \eta, \quad \forall \xi \in \Xi, \tag{5.27}$$

$$s^{\xi} \geq 0, \quad \forall \xi \in \Xi. \tag{5.28}$$

We observe that the MCVaR risk measure incorporates information about the expected value and CVaR of a random variable. As the values of α or λ increase, decision makers tend to become more risk-averse.

Leveraging these definitions, we propose the risk-averse two-stage stochastic programming model [SP-DSRFLP] as follows:

[SP-DSRFLP]

$$\begin{aligned} \min_{\boldsymbol{x},\boldsymbol{y},\boldsymbol{z},\boldsymbol{v},\boldsymbol{\Psi},\eta} & \sum_{k\in K}\sum_{l\in L} c_l^{\text{OPEN}} x_{kl} + \sum_{k\in K} c^{\text{INV}} v_k + \sum_{i\in I}\sum_{d\in D}\sum_{k\in K} c_{ki}^{\text{MANA}} z_{idk} \\ & + (1-\lambda)\sum_{\xi\in\Xi} p^{\xi} Q(\mathbf{x},\mathbf{y},\mathbf{z},\mathbf{v},\boldsymbol{\Theta}(\xi)) + \lambda(\eta + \frac{1}{1-\alpha}\sum_{\xi\in\Xi} p^{\xi} s^{\xi}) \end{aligned} \tag{5.29}$$

$$\text{s.t.} \quad s^{\xi} \geq Q(\mathbf{x},\mathbf{y},\mathbf{z},\mathbf{v},\boldsymbol{\Theta}(\xi)) - \eta, \quad \forall \xi \in \Xi, \tag{5.30}$$

$$s^{\xi} \geq 0, \quad \forall \xi \in \Xi. \tag{5.31}$$

5.2.3 Distributionally robust optimisation model

In reality, it is challenging to obtain the actual probability distribution of the demand due to complex environmental factors in disaster areas. Hence, we assume the demand distribution information $\mathbf{p}$ is incomplete and belongs to the ambiguity set $\mathcal{P}$. Therefore, the DRO model [DRO-DSRFLP] based on WMCVaR can be formally established as follows:

[DRO-DSRFLP]

$$\begin{aligned} \min_{\boldsymbol{x},\boldsymbol{y},\boldsymbol{z},\boldsymbol{v},\boldsymbol{\Psi}} & \sum_{k\in K}\sum_{l\in L} c_l^{\text{OPEN}} x_{kl} + \sum_{k\in K} c^{\text{INV}} v_k + \sum_{i\in I}\sum_{d\in D}\sum_{k\in K} c_{ki}^{\text{MANA}} z_{idk} \\ & + \text{WMCVaR}_{\alpha}(Q(\mathbf{x},\mathbf{y},\mathbf{z},\mathbf{v},\boldsymbol{\Theta}(\xi))) \end{aligned} \tag{5.32}$$

s.t. Constraints (5.2)–(5.13), Constraints (5.15)–(5.22),

where $\mathrm{WMCVaR}_\alpha(Q(\mathbf{x},\mathbf{y},\mathbf{z},\mathbf{v},\boldsymbol{\Theta}(\xi))) = \sup_{\mathbf{p}\in\mathcal{P}} \mathrm{MCVaR}_\alpha(Q(\mathbf{x},\mathbf{y},\mathbf{z},\mathbf{v},\boldsymbol{\Theta}(\xi)))$ expresses worst-case MCVaR of the second stage cost under ambiguity set $\mathcal{P}$. In this formula, $\sup_{\mathbf{p}\in\mathcal{P}}(\cdot)$ denote the worst-case scenario, i.e., min-max robust criterion. The objective (5.32) minimises the total cost of the first stage cost, the expected cost of the second stage, and the MCVaR of the worst distribution from the ambiguity set $\mathcal{P}$. Based on the definition of the MCVaR (Definition 5.2), we have $\sup_{\mathbf{p}\in\mathcal{P}} \mathrm{MCVaR}_\alpha(Q(\mathbf{x},\mathbf{y},\mathbf{z},\mathbf{v},\boldsymbol{\Theta}(\xi))) = (1-\lambda)\sup_{\mathbf{p}\in\mathcal{P}} \mathbb{E}(Q(\mathbf{x},\mathbf{y},\mathbf{z},\mathbf{v},\boldsymbol{\Theta}(\xi))) + \lambda\mathrm{WCVaR}_\alpha(Q(\mathbf{x},\mathbf{y},\mathbf{z},\mathbf{v},\boldsymbol{\Theta}(\xi)))$. Note that we let $\mathrm{WCVaR}_\alpha(Q(\mathbf{x},\mathbf{y},\mathbf{z},\mathbf{v},\boldsymbol{\Theta}(\xi)))$ denote the worst-case CVaR. Therefore, the above model can be transformed into as follows:

$$\begin{aligned}\min_{\boldsymbol{x},\boldsymbol{y},\boldsymbol{z},\boldsymbol{v},\boldsymbol{\Psi}} & \sum_{k\in K}\sum_{l\in L} c_l^{\mathrm{OPEN}} x_{kl} + \sum_{k\in K} c^{\mathrm{INV}} v_k + \sum_{i\in I}\sum_{d\in D}\sum_{k\in K} c_{ki}^{\mathrm{MANA}} z_{idk} \\ & + (1-\lambda)\sup_{\mathbf{p}\in\mathcal{P}} \mathbb{E}(Q(\mathbf{x},\mathbf{y},\mathbf{z},\mathbf{v},\boldsymbol{\Theta}(\xi))) + \lambda\mathrm{WCVaR}_\alpha(Q(\mathbf{x},\mathbf{y},\mathbf{z},\mathbf{v},\boldsymbol{\Theta}(\xi)))\end{aligned} \tag{5.33}$$

s.t. Constraints (5.2)–(5.13), Constraints (5.15)–(5.22).

Assuming the uncertain parameter follows a discrete distribution, we can transform the model (5.33) as follows:

$$\begin{aligned}\min_{\boldsymbol{x},\boldsymbol{y},\boldsymbol{z},\boldsymbol{v},\boldsymbol{\Psi}} & \sum_{k\in K}\sum_{l\in L} c_l^{\mathrm{OPEN}} x_{kl} + \sum_{k\in K} c^{\mathrm{INV}} v_k + \sum_{i\in I}\sum_{d\in D}\sum_{k\in K} c_{ki}^{\mathrm{MANA}} z_{idk} \\ & + (1-\lambda)\max_{\mathbf{p}\in\mathcal{P}} Q(\mathbf{x},\mathbf{y},\mathbf{z},\mathbf{v},\boldsymbol{\Theta}(\xi))^\intercal \mathbf{p} + \lambda\mathrm{WCVaR}_\alpha(Q(\mathbf{x},\mathbf{y},\mathbf{z},\mathbf{v},\boldsymbol{\Theta}(\xi)))\end{aligned} \tag{5.34}$$

s.t. Constraints (5.2)–(5.13), Constraints (5.15)–(5.22),

where $\mathbf{p}\in\mathcal{P}$ has finite support set Ξ, and $\mathbf{p} = \left\{p^1, p^2, \cdots, p^{|\Xi|}\right\}^\intercal$, in which $p^\xi > 0$ is the

probability of the scenario $\xi \in \Xi$ and $\sum_{\xi \in \Xi} p^{\xi} = 1$.

This DRO model is an intractable semi-infinite programming model and lacks the amenability to leverage established optimisation techniques and commercial solvers for solving (Ling et al., 2017). Consequently, the need arises to transform the model [DRO-DSRFLP] into an equivalent computationally tractable formulation.

5.2.3.1 Ambiguity sets

Generally speaking, there are two principles that can be followed when choosing the ambiguity set. Firstly, the ambiguity set needs to harness the existing information pertaining to the distribution of uncertain parameters, i.e., a collection of historical data, which can be deemed as data samples extracted from the true distribution. Secondly, the ambiguity set needs to facilitate computationally tractable formulations (Guan et al., 2024). Based on the above principles, in this study, we address the partial information on the demand probability distribution of the disaster demand sites by constructing three ambiguity sets: box, ellipsoidal, and polyhedral. In the context of drone-supported last-mile humanitarian logistics planning, it is reasonable to consider these three ambiguity sets. Relief organisers commonly estimate the nominal demand distribution according to historical demand data. Moreover, to address the inexact distribution resulting from incomplete data, refinement can be achieved by introducing a disturbance term to improve accuracy. These three ambiguity sets have found applications in engineering and management fields, particularly, and have also been employed in addressing specific relief planning problems (Zhu and Fukushima, 2009; Guan et al., 2024; Qiu et al., 2014; Wang et al., 023a, 2021b). We define the box, ellipsoidal, and polyhedral ambiguity sets as the following definitions.

Definition 5.3. A box ambiguity set $\mathcal{P}^{\text{Box}}$, to which the distribution probability $\mathbf{p}$,

can be defined as

$$\mathcal{P}^{\text{Box}} = \left\{ \mathbf{p} \mid \mathbf{p} = \mathbf{p^0} + \boldsymbol{\epsilon}, \mathbf{e}^{\text{T}}\boldsymbol{\epsilon} = 0, \|\boldsymbol{\epsilon}\|_\infty \leq \omega \right\}, \tag{5.35}$$

where $\mathbf{e}$ is the unit column vector; $\mathbf{p^0}$ represents the nominal probability distribution vector of the uncertain demand, which means the most likely probability distribution; $\boldsymbol{\epsilon}$ is the perturbation vector, $\boldsymbol{\epsilon} = \left\{\epsilon_1, \epsilon_2, \cdots, \epsilon_{|\Xi|}\right\}^{\intercal}$; ω expresses the allowable bias limit of the perturbation vector $\boldsymbol{\epsilon}$, which can be adjusted and $\omega \in [0, 1]$. Note that $\mathbf{e}^{\text{T}}\boldsymbol{\epsilon} = 0$ is necessary to ensure that the vector $\mathbf{p}$ can satisfy the basic requirements of the probability distribution.

Definition 5.4. An ellipsoidal ambiguity set $\mathcal{P}^{\text{Ellipsoidal}}$, to which the distribution probability $\mathbf{p}$, can be defined as

$$\mathcal{P}^{\text{Ellipsoidal}} = \left\{ \mathbf{p} \mid \mathbf{p} = \mathbf{p^0} + \boldsymbol{A}_1\boldsymbol{\epsilon}, \mathbf{e}^{\intercal}\boldsymbol{A}_1\boldsymbol{\epsilon} = 0, \mathbf{p^0} + \boldsymbol{A}_1\boldsymbol{\epsilon} \geq 0, \|\boldsymbol{\epsilon}\|_2 \leq 1 \right\}, \tag{5.36}$$

where $\boldsymbol{A}_1$ is the known scaling matrix of the elliposidal. $\boldsymbol{\epsilon}$ expresses the uncertain parameter vector. The conditions $\mathbf{e}^{\intercal}\boldsymbol{A}_1\boldsymbol{\epsilon} = 0$ and $\mathbf{p^0} + \boldsymbol{A}_1\boldsymbol{\epsilon} \geq 0$ can ensure the satisfaction of the probability distribution requirements.

Definition 5.5. A polyhedral ambiguity set $\mathcal{P}^{\text{Polyhedral}}$, to which the distribution probability $\mathbf{p}$, can be defined as

$$\mathcal{P}^{\text{Polyhedral}} = \left\{ \mathbf{p} \mid \mathbf{p} = \mathbf{p^0} + \boldsymbol{A}_2\boldsymbol{\epsilon}, \mathbf{e}^{\intercal}\boldsymbol{A}_2\boldsymbol{\epsilon} = 0, \mathbf{p^0} + \boldsymbol{A}_2\boldsymbol{\epsilon} \geq 0, \|\boldsymbol{\epsilon}\|_1 \leq 1 \right\}, \tag{5.37}$$

where $\boldsymbol{A}_2$ is the known scaling matrix of the polyhedral. $\boldsymbol{\epsilon}$ expresses the uncertain parameter vector. The conditions $\mathbf{e}^{\intercal}\boldsymbol{A}_2\boldsymbol{\epsilon} = 0$ and $\mathbf{p^0} + \boldsymbol{A}_2\boldsymbol{\epsilon} \geq 0$ can ensure the satisfaction of the probability distribution requirements.

5.2.3.2 Model equivalent reformulations

The DRO models mentioned above are computationally intractable. Therefore, we reformulate the proposed DRO model [DRO-DSRFLP] under three ambiguity sets into the equivalent reformulations that can be solved computationally.

THEOREM 5.1. If the probability distribution vector $\mathbf{p}$ belongs to the box ambiguity set $\mathcal{P}^{\text{Box}}$, the model [DRO-DSRFLP] can be equivalently reformulated into the following mixed-integer linear programming model.

$$
\begin{aligned}
\min_{\boldsymbol{x},\boldsymbol{y},\boldsymbol{z},\boldsymbol{v},\boldsymbol{\Psi},\tau,\boldsymbol{\varsigma},\boldsymbol{\varrho},\widehat{\tau},\widehat{\boldsymbol{\varsigma}},\widehat{\boldsymbol{\varrho}},\mathbf{s},\eta} \quad & \sum_{k\in K}\sum_{l\in L} c_l^{\text{OPEN}} x_{kl} + \sum_{k\in K} c^{\text{INV}} v_k + \sum_{i\in I}\sum_{d\in D}\sum_{k\in K} c_{ki}^{\text{MANA}} z_{idk} + \lambda\eta \\
& + (1-\lambda)\left[Q(\mathbf{x},\mathbf{y},\mathbf{z},\mathbf{v},\boldsymbol{\Theta}(\xi))^{\intercal}\mathbf{p^0} + \boldsymbol{\Omega}^{\intercal}\boldsymbol{\varsigma} + \boldsymbol{\Omega}^{\intercal}\boldsymbol{\varrho}\right] \\
& + \frac{\lambda}{1-\alpha}[(\mathbf{p^0})^{\intercal}\mathbf{s} + \boldsymbol{\Omega}^{\intercal}\widehat{\boldsymbol{\varsigma}} + \boldsymbol{\Omega}^{\intercal}\widehat{\boldsymbol{\varrho}}] \\
\text{s.t.} \quad & \mathbf{e}\tau + \boldsymbol{\varsigma} - \boldsymbol{\varrho} = Q(\mathbf{x},\mathbf{y},\mathbf{z},\mathbf{v},\boldsymbol{\Theta}(\xi)), \\
& \mathbf{e}\widehat{\tau} + \widehat{\boldsymbol{\varsigma}} - \widehat{\boldsymbol{\varrho}} = \mathbf{s}, \\
& \mathbf{s} \geq Q(\mathbf{x},\mathbf{y},\mathbf{z},\mathbf{v},\boldsymbol{\Theta}(\xi)) - \eta\mathbf{e}, \\
& \boldsymbol{\varsigma} \geq \mathbf{0}, \boldsymbol{\varrho} \geq \mathbf{0}, \widehat{\boldsymbol{\varsigma}} \geq \mathbf{0}, \widehat{\boldsymbol{\varrho}} \geq \mathbf{0}, \mathbf{s} \geq \mathbf{0}, \\
& \text{Constraints (5.2)} - \text{(5.13)}, \text{Constraints (5.15)} - \text{(5.22)},
\end{aligned}
\tag{5.38}
$$

where $(\tau, \boldsymbol{\varsigma}, \boldsymbol{\varrho}, \widehat{\tau}, \widehat{\boldsymbol{\varsigma}}, \widehat{\boldsymbol{\varrho}}) \in \mathbb{R} \times \mathbb{R}_+^{|\Xi|} \times \mathbb{R}_+^{|\Xi|} \times \mathbb{R} \times \mathbb{R}_+^{|\Xi|} \times \mathbb{R}_+^{|\Xi|}$ are dual variables.

Proof of Theorem 5.1. The proof of Theorem 5.1 is given in Appendix A. Note that Proposition 5.1 is necessary during the proof process of Theorem 5.1. Proposition 5.1 and the corresponding proof can be found in Appendix B and Appendix C.

THEOREM 5.2. If the probability distribution vector $\mathbf{p}$ belongs to the ellipsoidal ambiguity set $\mathcal{P}^{\text{Ellipsoidal}}$, the model [DRO-DSRFLP] can be equivalently reformulated into

the following second-order cone programming model.

$$
\begin{aligned}
\min_{\boldsymbol{x},\boldsymbol{y},\boldsymbol{z},\boldsymbol{v},\boldsymbol{\Psi},\boldsymbol{\vartheta},\theta,\zeta,\widehat{\boldsymbol{\vartheta}},\widehat{\theta},\widehat{\zeta},\mathbf{s},\eta} \quad & \sum_{k\in K}\sum_{l\in L} c_l^{\mathrm{OPEN}} x_{kl} + \sum_{k\in K} c^{\mathrm{INV}} v_k + \sum_{i\in I}\sum_{d\in D}\sum_{k\in K} c_{ki}^{\mathrm{MANA}} z_{idk} + \lambda\eta \\
& + (1-\lambda)\left[Q(\mathbf{x},\mathbf{y},\mathbf{z},\mathbf{v},\boldsymbol{\Theta}(\xi))^{\intercal}\mathbf{p^0} + (\boldsymbol{p^0})^{\intercal}\boldsymbol{\vartheta} + \zeta\right] \\
& + \frac{\lambda}{1-\alpha}[(\mathbf{p}^0)^{\intercal}\mathbf{s} + \left(\mathbf{p}^0\right)^{\intercal}\widehat{\boldsymbol{\vartheta}} + \widehat{\zeta}] \\
\text{s.t.} \quad & \|\boldsymbol{A}_1^{\intercal}\boldsymbol{\vartheta} + \boldsymbol{A}_1^{\intercal}Q(\mathbf{x},\mathbf{y},\mathbf{z},\mathbf{v},\boldsymbol{\Theta}(\xi)) - \theta\boldsymbol{A}_1^{\intercal}\mathbf{e}\|_2 \le \zeta, \\
& \|\boldsymbol{A}_1^{\intercal}\widehat{\boldsymbol{\vartheta}} + \boldsymbol{A}_1^{\intercal}\mathbf{s} - \widehat{\theta}\boldsymbol{A}_1^{\intercal}\mathbf{e}\|_2 \le \widehat{\zeta}, \\
& \mathbf{s} \ge Q(\mathbf{x},\mathbf{y},\mathbf{z},\mathbf{v},\boldsymbol{\Theta}(\xi)) - \eta\mathbf{e}, \\
& \boldsymbol{\vartheta} \ge \mathbf{0}, \quad \zeta \ge 0, \quad \widehat{\boldsymbol{\vartheta}} \ge \mathbf{0}, \quad \widehat{\zeta} \ge 0, \quad \mathbf{s} \ge 0, \\
& \text{Constraints } (5.2) - (5.13), \text{Constraints } (5.15) - (5.22),
\end{aligned}
\tag{5.39}
$$

where $\left(\boldsymbol{\vartheta}, \theta, \zeta, \widehat{\boldsymbol{\vartheta}}, \widehat{\theta}, \widehat{\zeta}\right) \in \mathbb{R}_+^{|\Xi|} \times \mathbb{R} \times \mathbb{R}_+ \times \mathbb{R}_+^{|\Xi|} \times \mathbb{R} \times \mathbb{R}_+$ are Lagrange multipliers.

Proof of Theorem 5.2. The proof of Theorem 5.2 is given in Appendix D.

THEOREM 5.3. If the probability distribution vector $\mathbf{p}$ belongs to the polyhedral ambiguity set $\mathcal{P}^{\mathrm{Polyhedral}}$, the model [DRO-DSRFLP] can be equivalently reformulated into the following mixed-integer linear programming model.

$$
\begin{aligned}
\min_{\boldsymbol{x},\boldsymbol{y},\boldsymbol{z},\boldsymbol{v},\boldsymbol{\Psi},\boldsymbol{\pi},\kappa,\varphi,\widehat{\boldsymbol{\pi}},\widehat{\kappa},\widehat{\varphi},\mathbf{s},\eta} \quad & \sum_{k\in K}\sum_{l\in L} c_l^{\mathrm{OPEN}} x_{kl} + \sum_{k\in K} c^{\mathrm{INV}} v_k + \sum_{i\in I}\sum_{d\in D}\sum_{k\in K} c_{ki}^{\mathrm{MANA}} z_{idk} + \lambda\eta \\
& + (1-\lambda)\left[Q(\mathbf{x},\mathbf{y},\mathbf{z},\mathbf{v},\boldsymbol{\Theta}(\xi))^{\intercal}\mathbf{p^0} + (\boldsymbol{p^0})^{\intercal}\boldsymbol{\pi} + \varphi\right] \\
& + \frac{\lambda}{1-\alpha}[(\mathbf{p}^0)^{\intercal}\mathbf{s} + \left(\mathbf{p}^0\right)^{\intercal}\widehat{\boldsymbol{\pi}} + \widehat{\varphi}] \\
\text{s.t.} \quad & \|\boldsymbol{A}_2^{\intercal}\boldsymbol{\pi} + \boldsymbol{A}_2^{\intercal}Q(\mathbf{x},\mathbf{y},\mathbf{z},\mathbf{v},\boldsymbol{\Theta}(\xi)) - \kappa\boldsymbol{A}_2^{\intercal}\mathbf{e}\|_\infty \leq \varphi, \\
& \|\boldsymbol{A}_2^{\intercal}\widehat{\boldsymbol{\pi}} + \boldsymbol{A}_2^{\intercal}\mathbf{s} - \widehat{\kappa}\boldsymbol{A}_2^{\intercal}\mathbf{e}\|_\infty \leq \widehat{\varphi}, \\
& \mathbf{s} \geq Q(\mathbf{x},\mathbf{y},\mathbf{z},\mathbf{v},\boldsymbol{\Theta}(\xi)) - \eta\mathbf{e}, \\
& \boldsymbol{\pi} \geq \mathbf{0}, \quad \varphi \geq 0, \quad \widehat{\boldsymbol{\pi}} \geq \mathbf{0}, \quad \widehat{\varphi} \geq 0, \quad \mathbf{s} \geq 0, \\
& \text{Constraints (5.2)} - \text{(5.13)}, \text{Constraints (5.15)} - \text{(5.22)},
\end{aligned}
\tag{5.40}
$$

where $(\boldsymbol{\pi}, \kappa, \varphi, \widehat{\boldsymbol{\pi}}, \widehat{\kappa}, \widehat{\varphi}) \in \mathbb{R}_+^{|\Xi|} \times \mathbb{R} \times \mathbb{R}_+ \times \mathbb{R}_+^{|\Xi|} \times \mathbb{R} \times \mathbb{R}_+$ are Lagrange multipliers.

Proof of Theorem 5.3. The proof of Theorem 5.3 is given in Appendix E.

5.3 Numerical Experiments

This section verifies the validity of the proposed model by conducting experiments on both a small-scale example and a large-scale case study. We utilise the Gurobi 10.0.0 commercial solver, executed on a personal computer equipped with an AMD Ryzen 9 7950X 16-Core Processor running at 4.50GHz and 128.0GB RAM, operating under Windows 10 (64-bit).

5.3.1 A small-scale example

5.3.1.1 Parameter settings

The proposed model specifically addresses DSRFLP to promote the relief operations of drone-supported last-mile humanitarian logistics, which generally have a much smaller service area compared to traditional trucks (Zhu et al., 2022). Therefore, publicly accessible datasets for the relief facility location problem are not appropriate for this specific research problem. To overcome this limitation, we randomly generate a small-case example specifically tailored to the characteristics of drone-supported relief operations to validate the performance of proposed models referring to the research conducted by Zhu et al. (2022).

This small-scale example involves 10 disaster demand sites S1–S10 and five candidate drone-supported relief facilities F1–F5. We consider three categories of drone-supported relief facilities with different capacity levels, i.e., small (S), medium (M), and large (L). Referring to the literature conducted by Zhu et al. (2022), the opening costs of small, medium, and large drone-supported relief facilities are set as 200, 300, and 500, respectively. The inventory capacities of relief items for the facilities are 50, 80, and 120, respectively. Furthermore, the capacities of drones for the facilities are 10, 15, and 25, respectively. In terms of the parameter settings related to relief items, the unit inventory prepositioning cost c^{INV} is assumed to be 140 (Shehadeh and Tucker, 2022). The unit delivery cost for unit demand from the drone-supported relief facility k to the disaster demand site i is proportional to the Euclidean distance between two nodes, which can be expressed as $c_{ki}^{\mathrm{DELI}} = 5 \times d_{ki}$, where d_{ki} represents the euclidean distance between the drone-supported relief facility k and the disaster demand site i (Zhu et al., 2022). The Euclidean distances between the disaster demand sites and drone-supported relief facilities are reported in Table 5.2. The flying speed of drones is 80km/h. Additionally, we have a definition of shortage penalty coefficient ϵ to cal-

culate the unit penalty cost per unit unsatisfied demand c^{UNS}. It equals the shortage penalty coefficient times the unit inventory prepositioning cost, which can be expressed as $c^{\mathrm{UNS}} = \epsilon \times c^{\mathrm{INV}}$ (Noyan, 2012b). Regarding the penalty cost per unit unused relief items c^{UNS}, we supposed that it equals 1.2 times as expensive as the unit inventory prepositioning cost. As to the parameter settings related to drones, the drone aerial path management cost per unit flying time from the drone-supported relief facility to the disaster demand site is set as 2. According to the literature from Shavarani et al. (2018), the maximum flying range of drones is set as 15. Besides, the maximum payload weight limit of drones is 30.

For the uncertain demands, we consider 10 scenarios, assuming that the nominal probability distribution follows a discrete probability distribution. We let each scenario $\xi \in \Xi$ has the same nominal probability $1/|\Xi|$ (Guan et al., 2024). The uncertain demands are generated randomly between 20 and 40. Regarding the ambiguity sets, without the loss of generality, we assume the allowable bias limit of the perturbation vector of box ambiguity set ω can take value from the interval [0,1], and the scaling matrix in the ellipsoidal and polyhedral ambiguity set is respectively set as $\boldsymbol{A}_1 = a^{\mathrm{E}}\boldsymbol{I}$ and $\boldsymbol{A}_2 = a^{\mathrm{P}}\boldsymbol{I}$, where $\boldsymbol{I}$ is an identity matrix. The ambiguity scopes can be adjusted by changing the value settings of ω, a^{P}, and a^{E} (Qiu et al., 2014).

5.3.1.2 Computational results

In this part, we analyse the influence of the confidence level α and weight parameter λ on optimal solutions. In this numerical instance, we let $\omega = 0.01$, $a^{\mathrm{P}} = 0.001$, and $a^{\mathrm{E}} = 0.0005$. Table 5.3 to Table 5.5 depicts the computational results of the optimal solution of different risk preferences under the three ambiguity sets. As we can see from Table 5.3-Table 5.5, when confidence level α remains fixed, the optimal objective values under three ambiguity sets increase as weight parameter λ increases. Furthermore, for a fixed value of weight parameter λ, a larger α value will also result in a higher optimal

Table 5.2: Euclidean distances between the disaster demand sites and the candidate drone-supported relief facilities.

	F1	F2	F3	F4	F5	S1	S2	S3	S4	S5	S6	S7	S8	S9	S10
F1	0	3.87	2.08	1.47	2.96	3.27	2.27	5.93	2.16	2.39	4.6	3.69	2.94	6.84	3
F2	3.87	0	5.9	4.53	5.78	6.41	5.23	7.38	5.3	5.76	7.58	7.42	1.1	3.43	4.38
F3	2.08	5.9	0	2.53	2.22	2	1.81	6.66	2.6	1.24	4.33	1.63	4.9	8.93	3.52
F4	1.47	4.53	2.53	0	4.16	4.28	3.5	4.51	0.81	3.38	3.25	4.08	3.85	6.95	4.47
F5	2.96	5.78	2.22	4.16	0	0.75	0.69	8.61	4.54	0.98	6.52	2.53	4.68	9.15	1.9
S1	3.27	6.41	2	4.28	0.75	0	1.18	8.62	4.53	0.9	6.3	1.88	5.31	9.74	2.64
S2	2.27	5.23	1.81	3.5	0.69	1.18	0	7.98	3.92	0.73	6.01	2.58	4.14	8.57	1.79
S3	5.93	7.38	6.66	4.51	8.61	8.62	7.98	0	4.09	7.75	3.15	7.83	7.3	7.92	8.92
S4	2.16	5.3	2.6	0.81	4.54	4.53	3.92	4.09	0	3.66	2.46	3.98	4.65	7.58	5.09
S5	2.39	5.76	1.24	3.38	0.98	0.9	0.73	7.75	3.66	0	5.56	1.86	4.68	9.02	2.52
S6	4.6	7.58	4.33	3.25	6.52	6.3	6.01	3.15	2.46	5.56	0	5.08	7.05	9.34	7.42
S7	3.69	7.42	1.63	4.08	2.53	1.88	2.58	7.83	3.98	1.86	5.08	0	6.38	10.53	4.34
S8	2.94	1.1	4.9	3.85	4.68	5.31	4.14	7.3	4.65	4.68	7.05	6.38	0	4.51	3.32
S9	6.84	3.43	8.93	6.95	9.15	9.74	8.57	7.92	7.58	9.02	9.34	10.53	4.51	0	7.81
S10	3	4.38	3.52	4.47	1.9	2.64	1.79	8.92	5.09	2.52	7.42	4.34	3.32	7.81	0

Table 5.3: Computational results of optimal objective values under the box ambiguity set.

	$\lambda = 0.3$	$\lambda = 0.5$	$\lambda = 0.7$	$\lambda = 0.9$
$\alpha = 0.5$	54,478.56	54,943.49	55,395.16	55,823.35
$\alpha = 0.6$	54,735.38	55,314.23	55,885.25	56,456.27
$\alpha = 0.7$	54,986.24	55,802.68	56,609.78	57,416.87
$\alpha = 0.8$	55,422.82	56,361.12	57,183.15	57,987.26
$\alpha = 0.9$	55,490.69	56,396.71	57,288.49	58,180.26

Table 5.4: Computational results of optimal objective values under the ellipsoidal ambiguity set.

	$\lambda = 0.3$	$\lambda = 0.5$	$\lambda = 0.7$	$\lambda = 0.9$
$\alpha = 0.5$	54,304.89	54,811.81	55,310.27	55,777.60
$\alpha = 0.6$	54,527.94	55,196.70	55,795.83	56,405.12
$\alpha = 0.7$	54,749.20	55,651.08	56,508.53	57,360.68
$\alpha = 0.8$	55,197.26	56,221.97	57,095.56	57,956.78
$\alpha = 0.9$	55,325.60	56,266.30	57,211.97	58,155.66

solution. This can be attributed to the fact that α serves as an indicator of risk preferences. Specifically, when the α value approaches 1, the resulting solution is the most conservative one, indicating the most risk-averse attitude. Vice versa, when the α value approaches 0, the decision maker is risk-neutral. Therefore, higher values of confidence level α and weight parameter λ both correspond to a greater risk level, leading to more risk-averse policies. Decision makers should select the combination of these two coefficients flexibly based on their risk preferences.

Table 5.5: Computational results of optimal objective values under the polyhedral ambiguity set.

	$\lambda = 0.3$	$\lambda = 0.5$	$\lambda = 0.7$	$\lambda = 0.9$
$\alpha = 0.5$	54,318.23	54,829.00	55,330.84	55,802.42
$\alpha = 0.6$	54,546.04	55,192.12	55,799.60	56,407.07
$\alpha = 0.7$	54,777.44	55,678.00	56,534.97	57,391.94
$\alpha = 0.8$	55,211.56	56,231.12	57,102.04	57,954.47
$\alpha = 0.9$	55,321.98	56,277.93	57,217.22	58,156.51

Furthermore, we investigate how these risk parameter combinations affect the inventory decisions under the three ambiguity sets. In this numerical experiment, we set $\omega = 0.01$, $a^{\mathrm{P}} = 0.05$, and $a^{\mathrm{E}} = 0.0005$. Besides, we respectively fix the confidence level $\alpha = 0.7, 0.8, 0.9$ and vary the weight parameter λ from 0.1 to 0.9 in increments of 0.1. The computational results are shown in Figures 5.2 to 5.4. It is obvious that a larger weight parameter λ leads to a higher quantity of inventory prepositioning of relief items. However, the quantity of inventory prepositioning of relief items does not change monotonically as a function of confidence level α. This variation tendency is in accord with the computational results from Noyan (2012b). Therefore, the incorporation of the CVaR criterion within DRO models assumes a pivotal role, which contributes significantly to making diversifying inventory prepositioning decisions based on different risk preferences.

Figure 5.5 shows the computational results of the drone-supported last-mile humanitarian logistics system planning under the box ambiguity set with $\alpha = \lambda = 0.9$. More specifically, F1 to F4 are designated as open drone-supported relief facilities with medium capacity level, each equipped with one drone. The connections between facilities and disaster demand sites represent the drone visit schedule. For instance, at

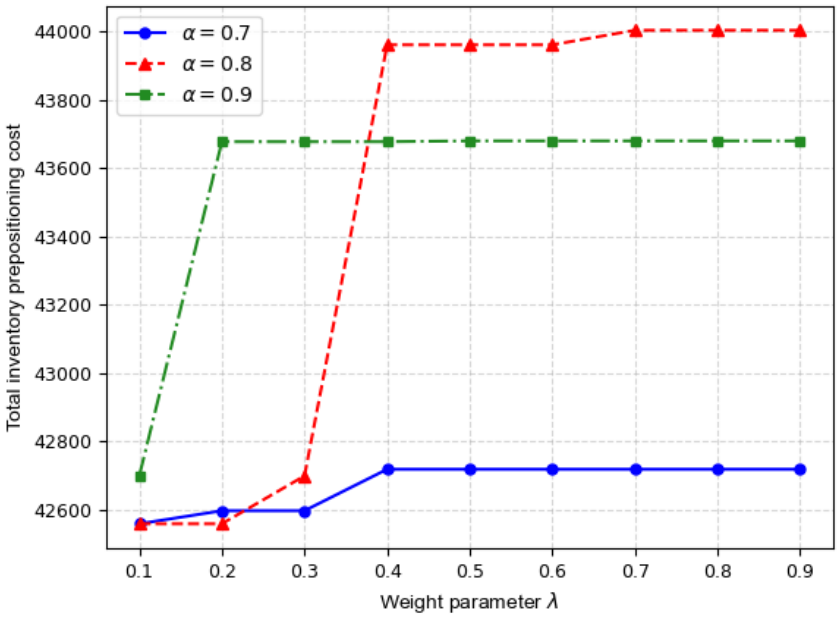

Figure 5.2: Total inventory prepositioning cost under the box ambiguity set.

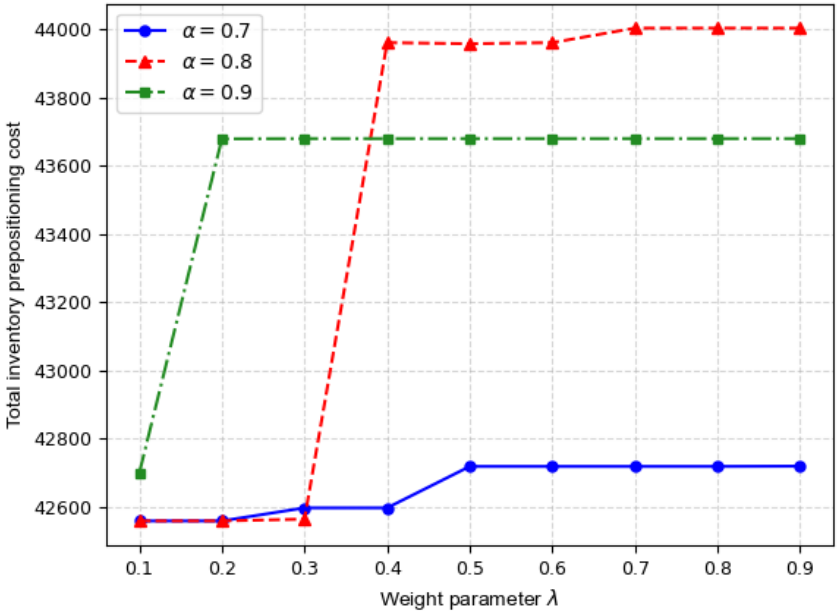

Figure 5.3: Total inventory prepositioning cost under the ellipsoidal ambiguity set.

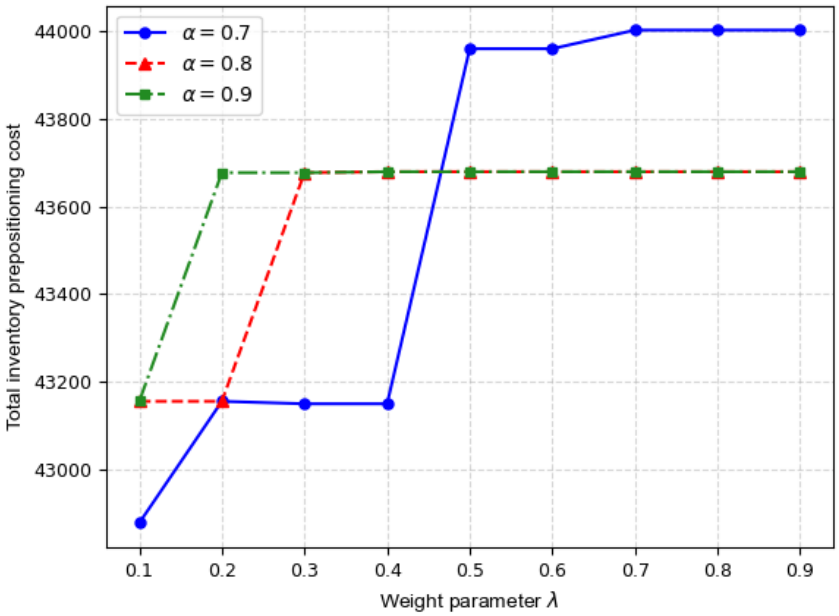

Figure 5.4: Total inventory prepositioning cost under the polyhedral ambiguity set.

the drone-supported relief facility F4, the drone is allocated to provide relief services to disaster demand sites S3, S4, S6, and S8. In essence, this implies four drone trips for the drone assigned to the F4 facility.

5.3.1.3 Analysis of solution quality

In this part, we assess the quality of the solution derived from the proposed model [DRO-DSRFLP] by conducting a series of numerical experiments. Firstly, we analyse the optimal values derived from models [DRO-DSRFLP] and [SP-DSRFLP]. In order to obtain the differences, the Price of Distributional Robustness (PDR) is introduced (Guan et al., 2024) as

$$PDR = \frac{(DRO)^* - (NSO)^*}{(NSO)^*}, \tag{5.41}$$

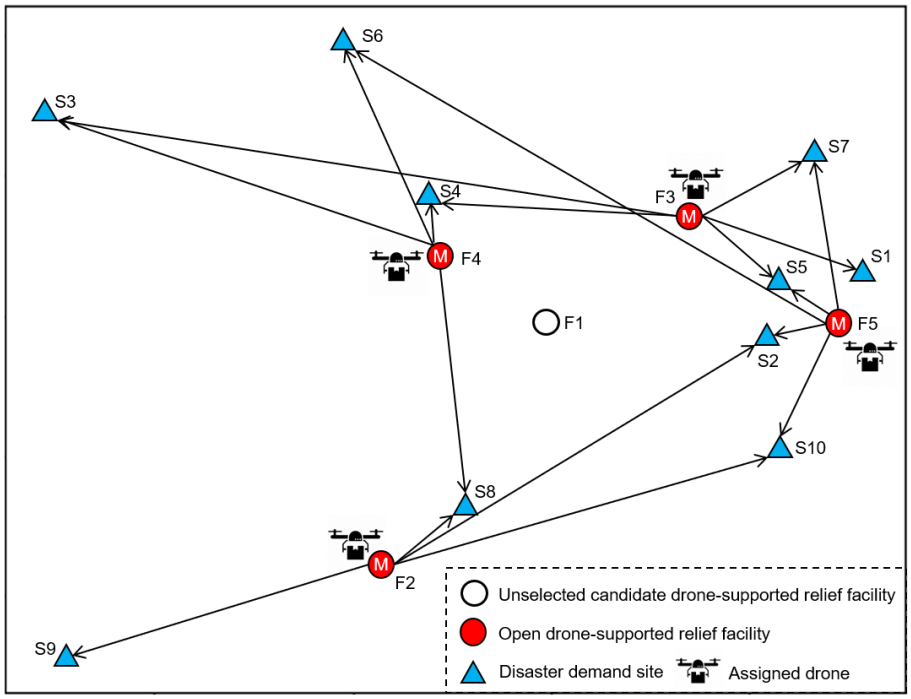

Figure 5.5: An illustrative example of drone-supported last-mile humanitarian logistics system planning.

where $(NSO)^*$ and $(DRO)^*$ denote the optimal solutions of the stochastic programming model [SP-DSRFLP] and DRO model [DRO-DSRFLP], respectively. Table 5.6 demonstrates the PDR values under $\alpha = \lambda = 0.9$ with the different adjustable ambiguity scopes. As is illustrated in Table 5.6, a larger ambiguity scope leads to a higher PDR value. The larger the scope of the ambiguity set, the more probability information is incorporated and considered, leading to a larger additional cost. As the adjustable ambiguity scope decreases, the ambiguity set converges toward a precise probability distribution, leading to the proposed DRO model [DRO-DSRFLP] degenerating into the stochastic programming model [SP-DSRFLP]. Moreover, the maximum PDR value remains below 0.8%. In essence, the proposed DRO model adeptly mitigates the uncertainty in probability distribution at a minimal cost and exhibits better resilience performance when faced with partial distribution information.

Table 5.6: Computational results of the PDR.

Box ambiguity set		Ellipsoidal ambiguity set		Polyhedral ambiguity set	
ω	PDR	a^{E}	PDR	a^{P}	PDR
0.001	0.0045%	0.00005	0.0002%	0.0005	0.0023%
0.01	0.0454%	0.0001	0.0018%	0.005	0.0227%
0.01	0.4539%	0.0005	0.0025%	0.05	0.227%
0.15	0.5565%	0.001	0.0054%	0.01	0.4539%
0.2	0.644%	0.01	0.0097%	0.5	0.8119%

Furthermore, we evaluate the solution quality derived from the proposed DRO model [DRO-DSRFLP] by conducting an out-of-sample simulation experiment. More specifically, the stochastic programming model [SP-DSRFLP] and DRO model [DRO-DSRFLP] are solved under the given in-sample data, and the optimal first stage solutions $\{\mathbf{x}, \mathbf{y}, \mathbf{z}, \mathbf{v}\}$ are derived respectively. Then we randomly generate 5,000 testing samples based on the distribution that we use for generating the in-sample data points. For the decision $\{\mathbf{x}, \mathbf{y}, \mathbf{z}, \mathbf{v}\}$ and each test sample, the second-stage recourse problem is

solved and the optimal total cost (including the costs incurred in the first stage and second stage) can be calculated. Finally, we obtain 5,000 random total costs of model [SP-DSRFLP] and [DRO-DSRFLP], and the solution quality can be evaluated.

Table 5.7 illustrates the various statistics of optimal total costs derived from model [DRO-DSRFLP] and [SP-DSRFLP] by conducting the out-of-sample experiments. As is shown in Table 5.7, the model [DRO-DSRFLP] under three ambiguity sets performs better than the [SP-DSRFLP] in terms of total costs on average and at all percentile in both cases. Overall, the findings indicate the proposed model [DRO-DSRFLP] is more adept at mitigating the potential risks caused by ambiguous or partial information about the uncertain parameter. This makes it a more attractive option for humanitarian organisers who are risk-averse. Hence, the better performance of the proposed model [DRO-DSRFLP] highlights the importance of considering the ambiguity of probability distributions related to uncertain parameters in the modelling process.

5.3.2 A large-scale case study

This subsection implements a case study to verify the proposed models. This study focuses on drone-supported last-mile humanitarian logistics planning in Lushan County, which is located in Sichuan Province, China.

5.3.2.1 Case background and data description

Lushan County, situated along the Longmenshan fault zone, experienced a seismic event of magnitude 7.0 on April 20, 2013, with a focal depth of approximately 13 km. Subsequent to the earthquake, the aftermath, reported as of 6:00 on April 23, 2013, resulted in 193 casualties, affecting 1.99 million individuals, including tourists. Additionally, 12,211 people were injured, and the total economic loss was estimated at around 85.17 billion. Following the earthquake, rapid responses from local authorities

Table 5.7: Statistics of out-of-sample optimal total costs derived from model [DRO-DSRFLP] and [SP-DSRFLP].

Model	Mean	25th percentile	75th percentile	95th percentile	Worst
[SP-DSRFLP]	52,622.96	50,519.98	55,159.818	60,536.56	82,869.29
[DRO-DSRFLP] (Box, $\omega = 0.001$)	52,606.14	50,460.12	55,075.23	59,993.73	82,215.01
[DRO-DSRFLP] (Box, $\omega = 0.01$)	52,526.74	50,472.81	55,106.99	60,034.07	79,436.48
[DRO-DSRFLP] (Ellipsoidal, a^{E}=0.0001)	52,434.78	50,393.77	54,883.17	59,665.18	81,456.58
[DRO-DSRFLP] (Ellipsoidal, a^{E}=0.001)	52,522.82	50,475.49	54,982.67	60,257.04	79,320.5
[DRO-DSRFLP] (Polyhedral, a^{P}=0.002)	52,548.61	50,435.30	55,056.18	60,346.68	81,775.27
[DRO-DSRFLP] (Polyhedral, a^{P}=0.02)	52,389.71	50,377.72	54,918.9	59,782.53	80,058.29

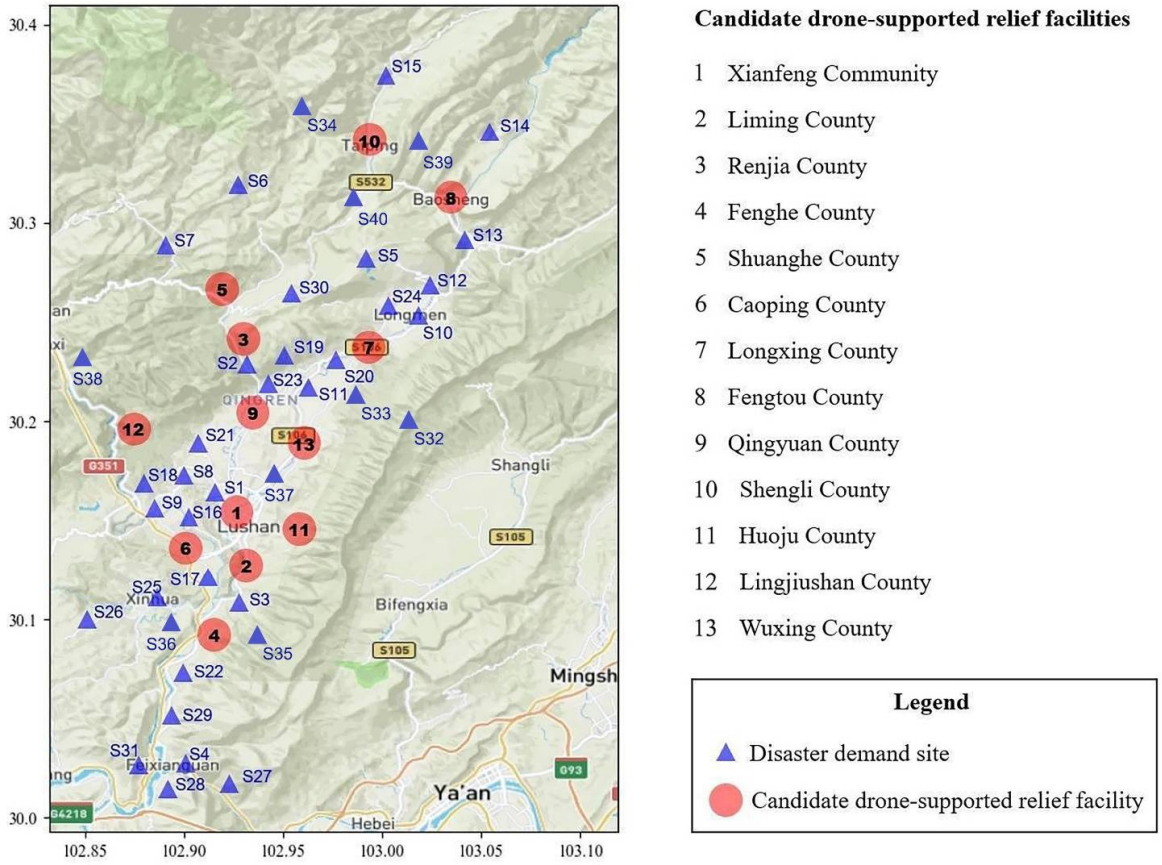

Figure 5.6: Case study network.

and charitable organisations addressed immediate needs. However, the rolling rocks impeded the path of rescue and transport vehicles, affecting the rescue operations. The Lushan earthquake relief case underscores the crucial importance of incorporating drones into the final stretch of humanitarian logistics, guaranteeing the prompt delivery of emergency relief items.

This case study was originated by Xu et al. (2016), which consists of 5 candidate sites for the distribution centres and 25 disaster points. In this study, we extend the case study with 13 candidate drone-supported relief facilities and 40 disaster sites S1–S40, as is shown in Figure 5.6. For comparative analysis, we investigate three case study

instances with varying problem sizes, i.e., small, medium, and large. For both three case studies, we consider 13 potential drone-supported relief facilities. In the small-size case study, there are 15 disaster demand sites, while there are 31 in the medium-size case study and 40 in the large-size case study. The problem sizes of different scale instances for the case study are reported in Table 5.8. Moreover, the demands of disaster sites lie within the range of [20,40], with undisclosed occurrence probabilities. We let the nominal probability of each scenario be equal to $1/|\Xi|$. Particularly, for the medium-size and large-size case studies, we designated the inventory capacities of drone-supported relief facilities with small, medium, and large capacity levels as 100, 150, and 250, with opening costs of 500, 550, and 650, respectively. This selection is made to ensure alignment with the requirements of large-scale disaster scenarios, aiming to prevent severe shortages caused by insufficient inventory. As for the other parameters in the medium-size and large-size case studies, the settings are the same as the small-scale example in the last subsection.

5.3.2.2 Computational results and analysis of small-size case study

In this part, we conducted experiments on a small-scale case study to validate the accuracy of our model. Firstly, we examine the influence of various combinations of confidence level α and weight parameter λ on the proposed model. The computational results under three ambiguity sets are reported in Tables 5.9 to 5.11. As can be observed from Tables 5.9 to 5.11, the objective value increases when the confidence level α and weight parameter λ become larger under three ambiguity sets. Additionally, the parameters have an influence on the facility locations and the inventory prepositioning. Table 5.12 lists the results of the inventory prepositioning quantity under three ambiguity sets when confidence level α and weight parameter λ take different values. From Table 5.12, it can be observed that a larger α or λ will cause a more conservative solution with more quantities of inventory prepositioning.

Table 5.8: Problem sizes of different scale instances for the case study.

	Small-size	Medium-size	Large-size
Disaster demand sites	15	31	40
Candidate drone-supported relief facilities	13	13	13
Drones	20	30	40
Scenarios	50	200	200
Variables (Box)	210,615	2,520,935	4,296,975
Constraints (Box)	210,794	2,520,970	4,297,159
Variables (Ellipsoidal)	210,617	2,520,937	4,296,977
Constraints (Ellipsoidal)	210,796	2,520,972	4,297,159
Variables (Polyhedral)	210,717	2,521,337	4,297,377
Constraints (Polyhedral)	210,796	2,521,370	4,297,559

Furthermore, we conduct extensive sensitive analysis with respect to some parameters to evaluate the impact on the model. Firstly, we explore the impacts of the shortage penalty coefficient on the penalty cost of unsatisfied demand and unused relief items. Figures 5.7 to 5.9 depict the computational results of the penalty costs when the shortage penalty coefficient takes different values. As is shown in Figures 5.7 to 5.9, it is evident that the penalty cost for unsatisfied demand decreases as the shortage penalty coefficient becomes smaller. Conversely, the penalty cost for unused inventory increases with the rise of the shortage penalty coefficient. The findings emphasise the importance of selecting an appropriate shortage penalty coefficient during the different stages of disaster relief. Careful consideration of this coefficient can decrease unsatisfied demand, contributing to more effective relief operations and greatly reducing casualties. Decision makers should conduct a thorough evaluation of the prevailing conditions and context to make informed decisions regarding the shortage penalty coef-

Table 5.9: Computational results of the small-size case study under the box ambiguity set

α	λ	Objective value	Location (Capacity level, Inventory quantity)	CPU time/s	Gap
0.5	0.5	80,641.27	1(S,50); 2(S,50); 4(M,68);5(S,37); 6(S,50); 7(S,50);8(M,73.5);9(S,50); 10(S,35)	214.83	-
	0.7	80,880.85	1(S,50); 2(S,50); 4(S,50);5(S,39); 6(S,50); 7(M,76.73);8(S,50);9(S,50); 10(S,49)	215.94	-
	0.9	81,097.02	1(S,50); 2(S,50); 4(S,50);5(S,40); 6(S,50); 7(M,76.1);8(S,50);9(S,50); 10(S,49)	245.61	-
0.7	0.5	81,322.14	1(S,50); 2(S,50); 4(M,73);5(S,37); 6(S,50); 7(S,50);8(M,71.54);9(S,50); 10(S,35)	205.49	-
	0.7	81,728.32	1(S,50); 2(S,50); 4(M,76.68);5(S,37); 6(S,50); 7(S,50);8(M,69);9(S,50); 10(S,35)	236.42	-
	0.9	82,127.71	1(S,50); 2(S,50); 4(M,77);5(S,38); 6(S,50); 7(S,50);8(M,69.3);9(S,50); 10(S,35)	210.36	-
0.9	0.5	82,019.01	1(S,50); 2(S,50); 4(S,50);5(S,41); 6(S,50); 7(S,50);8(M,71.69);9(S,37); 10(S,35); 13(S,34)	225.36	-
	0.7	82,657.30	1(S,48.12); 2(S,50); 4(M,68);5(S,35); 6(S,50); 7(S,50);8(M,70);9(S,37); 10(S,32); 13(S,29)	216.16	-
	0.9	83,267.32	1(S,50); 2(S,50); 4(M,74);5(S,31); 6(S,50); 7(S,50);8(S,50);9(S,40.5); 10(S,44.15); 13(S,30)	181.3	-

Table 5.10: Computational results of the small-size case study under the ellipsoidal ambiguity set

α	λ	Objective value	Location (Capacity level, Inventory quantity)	CPU time/s	Gap
0.5	0.5	80,289.43	1(S,48.72); 2(S,50); 4(S,50);5(S,40); 6(S,50); 7(M,73.27);8(S,50);9(S,50); 10(S,45)	7,200	0.39%
	0.7	80,607.03	1(S,50); 2(S,50); 4(M,68.56);5(S,37); 6(S,50); 7(S,70);8(M,73);9(S,50); 10(S,35)	7,200	0.11%
	0.9	81,074.80	1(S,50); 2(S,50); 4(M,77.33);5(S,40); 6(S,50); 7(S,50);8(S,50);9(S,50); 10(S,48)	7,200	0.13%
0.7	0.5	80,835.59	1(S,50); 2(S,50); 4(M,71.43);5(S,37); 6(S,50); 7(S,50);8(M,73);9(S,50); 10(S,35)	7,200	0.03%
	0.7	81,436.53	1(S,50); 2(S,50); 4(M,78);5(S,36.67); 6(S,50); 7(S,50);8(M,68);9(S,50); 10(S,35)	7,200	0.01%
	0.9	82,100.03	1(S,50); 2(S,50); 4(S,50);5(S,40); 6(S,50); 7(M,75);8(M,67);9(S,50); 10(S,37)	7,200	0.09%
0.9	0.5	81,572.43	1(S,50); 2(S,50); 4(S,50);5(S,40); 6(S,50); 7(M,74.16);8(M,69);9(S,50); 10(S,35)	7,200	0.03%
	0.7	82,418.59	1(S,48.11); 2(S,49.8); 4(S,50);5(S,41); 6(S,50); 7(S,50);8(M,71.07);9(S,37); 10(S,35); 13(S,36.82)	7,200	0.05%
	0.9	83,197.07	1(S,50); 2(S,50); 4(M,74);5(S,30); 6(S,50); 7(S,50);8(S,50);9(S,41.44); 10(S,45); 13(S,29.23)	7,200	0.03%

Table 5.11: Computational results of the small-size case study under the polyhedral ambiguity set

α	λ	Objective value	Location (Capacity level, Inventory quantity)	CPU time/s	Gap
0.5	0.5	80,171.50	1(S,50); 2(S,50); 4(M,68);5(S,37); 6(S,50); 7(S,50);8(M,73.5);9(S,50); 10(S,35)	202.11	-
	0.7	80,655.29	1(S,50); 2(S,50); 4(S,50);5(S,39); 6(S,50); 7(M,76.73);8(S,50);9(S,50); 10(S,49)	193.93	-
	0.9	81,102.39	1(S,50); 2(S,50); 4(S,50);5(S,40); 6(S,50); 7(M,76.1);8(S,50);9(S,50); 10(S,49)	182.27	-
0.7	0.5	80,913.03	1(S,50); 2(S,50); 4(M,73);5(S,37); 6(S,50); 7(S,50);8(M,71.54);9(S,50); 10(S,35)	225.88	-
	0.7	81,528.58	1(S,50); 2(S,50); 4(M,76.68);5(S,37); 6(S,50); 7(S,50);8(M,69);9(S,50); 10(S,35)	161.07	-
	0.9	82,102.27	1(S,50); 2(S,50); 4(M,77);5(S,38); 6(S,50); 7(S,50);8(M,69.3);9(S,50); 10(S,35)	163.18	-
0.9	0.5	81,615.63	1(S,50); 2(S,50); 4(S,50);5(S,41); 6(S,50); 7(S,50);8(M,71.69);9(S,37); 10(S,35); 13(S,34)	285.05	-
	0.7	82,425.90	1(S,48.12); 2(S,50); 4(M,68);5(S,35); 6(S,50); 7(S,50);8(M,70);9(S,37); 10(S,32); 13(S,29)	210.87	-
	0.9	83,209.17	1(S,50); 2(S,50); 4(M,74);5(S,31); 6(S,50); 7(S,50);8(S,50);9(S,40.5); 10(S,44.15); 13(S,30)	277.76	-

Table 5.12: Computational results the quantity of the inventory prepositioning under three ambiguity sets

α	λ	Total inventory (Box)	Total inventory (Ellipsoidal)	Total inventory (Polyhedral)
0.5	0.5	463.5	456.99	463.03
	0.7	464.73	463.56	463.48
	0.9	465.1	465.33	464.69
0.7	0.5	466.54	466.42	466
	0.7	467.68	467.67	467.32
	0.9	469.3	469	469.3
0.9	0.5	468.69	468.16	468.67
	0.7	469.12	468.72	468.75
	0.9	469.65	469.67	469.61

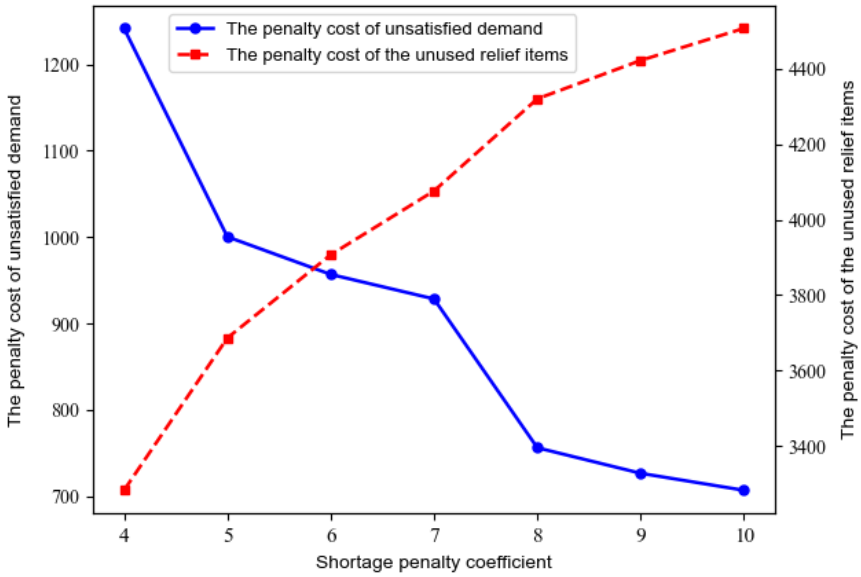

Figure 5.7: The impacts of the shortage penalty coefficients on unsatisfied demand and unused relief items under the box ambiguity set.

ficient. Moreover, recognising the varying conditions across different disaster districts, the shortage penalty coefficient can also be reasonably adjusted.

In addition, due to the unpredictable nature of meteorological factors and potential progress in battery technology, the maximum flying range of drones can be treated as a variable parameter. Therefore, numerical experiments are conducted to examine the influence caused by the parameter. In humanitarian logistics, an egalitarian policy is crucial and can be measured by the total delivery time to beneficiaries (Duran et al., 2011). To investigate the impact of the maximum flying range of drones on the total delivery time, we conducted a further sensitivity analysis, obtaining the total delivery time under different maximum flying ranges. The resulting variations in the total delivery time under three ambiguity sets are shown in Figure 5.10. It can be concluded from Figure 5.10 that the total delivery time exhibits significant fluctuation and peaks when the maximum flying range is set to 25. The fluctuation can be

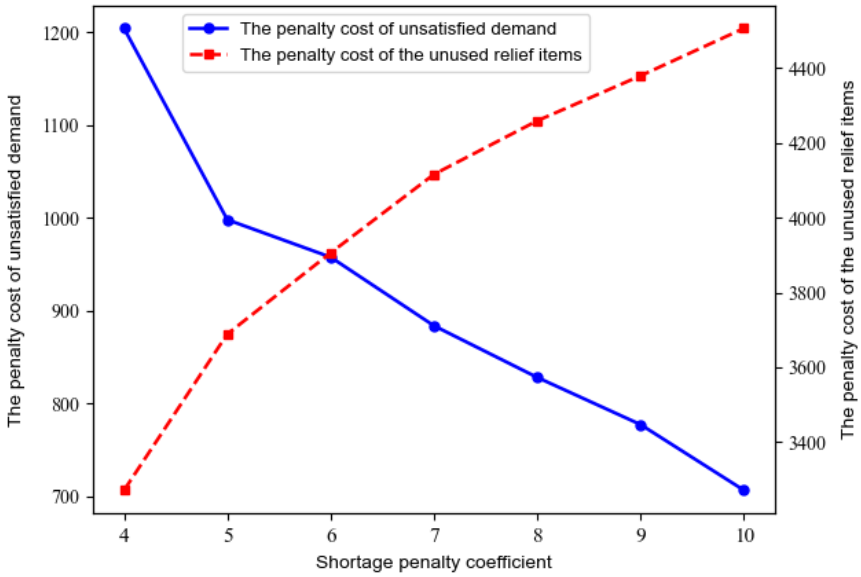

Figure 5.8: The impacts of the shortage penalty coefficients on unsatisfied demand and unused relief items under the ellipsoidal ambiguity set.

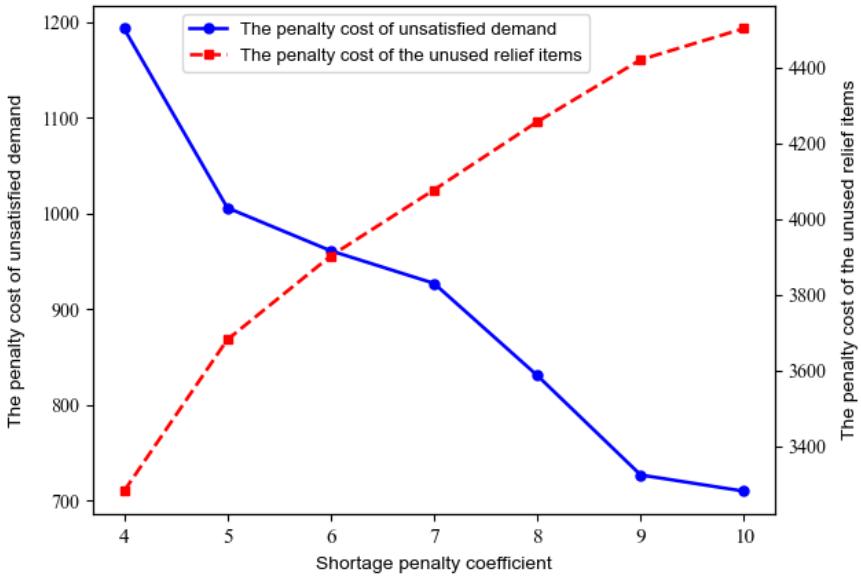

Figure 5.9: The impacts of the shortage penalty coefficients on unsatisfied demand and unused relief items under the polyhedral ambiguity set.

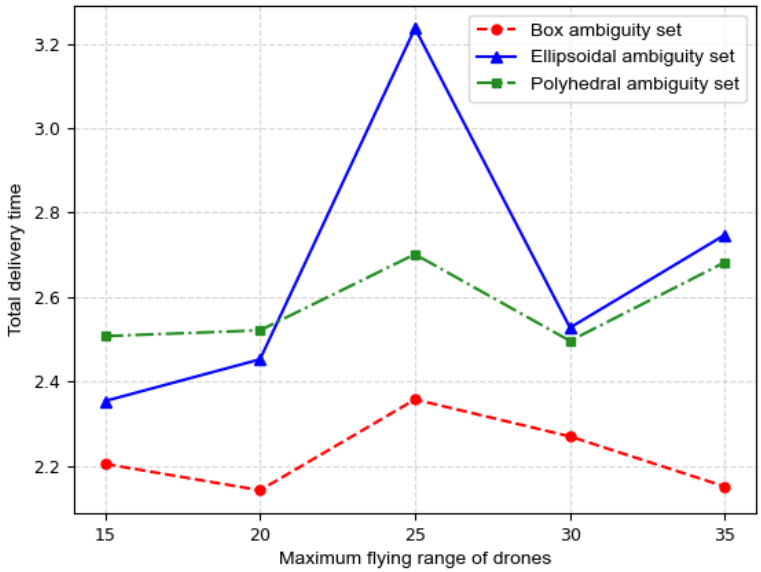

Figure 5.10: The impacts of different maximum flying distances of drones on the total delivery time.

attributed to the distinct configurations of last-mile humanitarian logistics networks resulting from variations in the maximum flying range of drones. Therefore, decision makers should carefully consider the maximum flying range as a crucial parameter when selecting drones for disaster relief operations, incorporating the egalitarian objective into drone-supported last-mile humanitarian logistics planning. Furthermore, tailoring drone specifications based on the specific requirements of the relief mission and the geographical characteristics of the affected areas is essential. Finally, it is also necessary to implement real-time monitoring systems for drone battery performance.

As a final sensitivity analysis, the maximum payload weight limit of drones is varied from 10 to 30 in increments of 5. The computational results of the total cost under three ambiguity sets are shown in Figure 5.11. From Figure 5.11, it can be found that a larger maximum payload weight limit of drones leads to a significant decrease in total cost. Increasing the maximum payload weight limit can lead to a more efficient

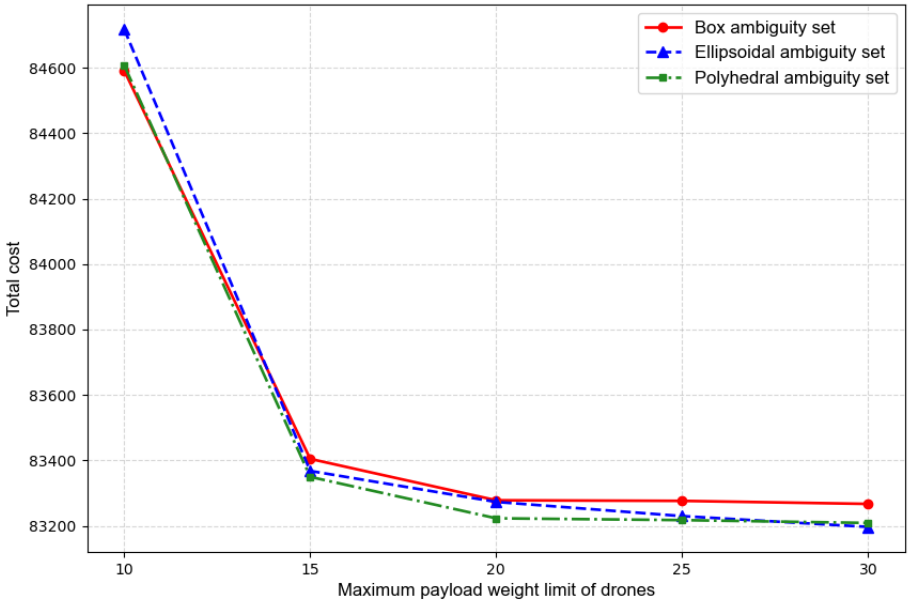

Figure 5.11: The impacts of different maximum payload weight limits of drones on the total cost.

use of drone resources and, subsequently, a reduction in the total cost of operations. Drones with larger payload capacities can facilitate the delivery of more relief supplies in a single trip, thereby enhancing the overall delivery capabilities. Therefore, from the managerial perspective, decision makers should explore opportunities to invest in drones with higher payload capacities to achieve cost savings in disaster relief missions, especially in situations requiring large-scale and rapid relief efforts.

5.3.2.3 Computational results of medium-size and large-size case studies

In this part, a series of numerical experiments are conducted on both medium-size and large-size case studies to further validate the effectiveness of the DRO model. We set the computational time limit to 3 hours. The computational results of the medium-size and large-size case studies for various combinations of the confidence level

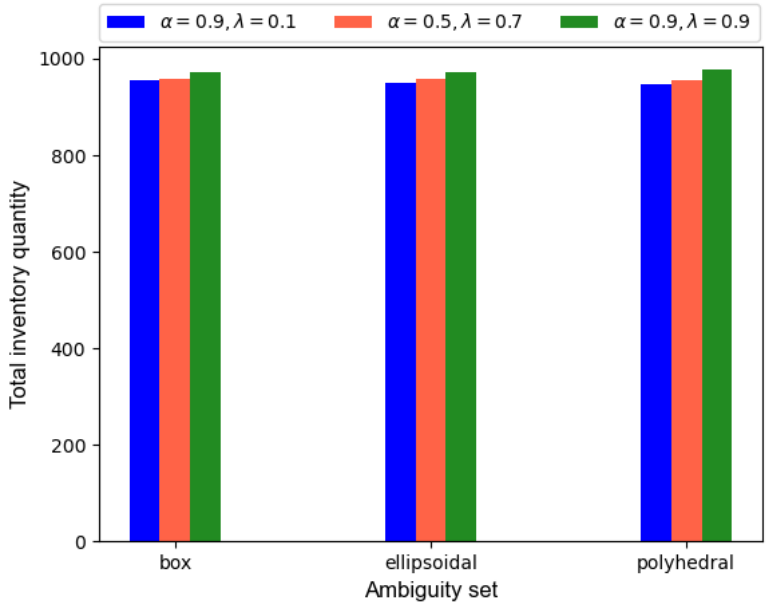

Figure 5.12: Total inventory quantity of the large-scale case study under the three ambiguity sets.

α and weight parameter λ under three ambiguity sets are presented in Table 5.13 and Table 5.14, respectively.

From Table 5.13, it can be observed that the computational gap obtained by Gurobi is below 5% for most case instances and below 6.5% for all case instances in the medium-size case study, indicating the acceptability of the solutions. Additionally, the inventory prepositioning quantities under three ambiguity sets of the medium-size case study are illustrated in Figure 5.12. From this figure, we observe that the risk parameter combinations significantly influence the total inventory quantity. Furthermore, it can be observed from Table 14 that the computational gap obtained by Gurobi is below 10% for all case instances, further demonstrating the computational feasibility of the proposed model. This indicates that the model's performance in terms of computational efficiency remains satisfactory across different problem sizes, enhancing its reliability and applicability in real-world decision-making processes.

Table 5.13: Computational results of the medium-size case study under three ambiguity sets

Ambiguity set	α	λ	Objective value	Location (Capacity level)	Gap
Box	0.5	0.7	177,976.72	1(S); 2(L); 3(S);4(M); 5(S); 6(M); 7(M); 10(S); 12(S); 13(S)	5.34%
	0.9	0.1	174,756.01	1(S); 2(L); 3(S); 4(S); 5(S); 6(L); 7(L); 8(S); 10(S); 12(S)	3.94%
	0.9	0.9	180,001.19	2(L); 4(S); 6(L); 7(M); 8(S); 11(L)	1.17%
Ellipsoidal	0.5	0.7	179,464.94	2(L); 6(L); 7(M); 10(S); 11(S)	6.24%
	0.9	0.1	172,888.30	2(L); 6(L); 7(M); 8(S); 10(S) ;11(S)	3.54%
	0.9	0.9	183,611.56	2(L); 4(M,); 6(L); 7(M); 8(S); 11(M)	3.54%
Polyhedral	0.5	0.7	173,993.75	2(L); 3(S); 4(S); 6(L); 7(L); 8(S); 9(S); 10(S); 12(S); 13(S)	2.46%
	0.9	0.1	178,559.80	2(L); 6(L); 7(L); 11(L)	6.13%
	0.9	0.9	179,874.83	2(L); 3(S); 4(S); 5(S); 6(L); 7(L); 8(S); 10(S); 12(S)	0.89%

Table 5.14: Computational results of the large-size case study under three ambiguity sets

Ambiguity set	α	λ	Objective value	Location (Capacity level)	Gap
Box	0.5	0.7	220,158.04	2(L); 6(L); 7(L); 10(L); 11(L)	3.28%
	0.9	0.1	219,598.15	2(L); 6(L); 7(M); 8(M); 10(M); 11(L)	3.65%
	0.9	0.9	225,426.93	1(S); 2(L); 3(S); 4(S); 5(S); 6(L); 7(M); 8(S); 10(M); 12(M); 13(M)	0.86%
Ellipsoidal	0.5	0.7	223,367.03	2(L); 4(M); 5(S); 6(L); 7(M); 10(M); 11(L)	5.05%
	0.9	0.1	218,410.17	2(L); 6(L); 7(L); 10(L); 11(L)	3.66%
	0.9	0.9	237,566	2(L); 4(S); 6(L); 7(M); 8(S); 10(M); 11(L); 13(S)	6.15%
Polyhedral	0.5	0.7	225,707.98	2(L); 6(L); 7(L); 10(L); 11(L)	5.13%
	0.9	0.1	215,817.87	2(L); 4(S); 6(L); 7(M); 8(S); 10(M); 11(L)	1.85%
	0.9	0.9	244,675.91	1(S); 2(L); 4(S); 5(S); 6(L); 7(L); 8(S); 10(L); 12(L); 13(S)	8.54%

5.3.3 Managerial implications and insights

The above numerical experiments can provide several significant managerial implications and insights for humanitarian organisers. The following summary highlights our key findings.

(1) Firstly, our study focuses on drone-supported last-mile humanitarian operations in data-scarce disaster scenarios. Computational results demonstrate the better performance of the proposed DRO model in handling uncertain demand with ambiguous distribution. Despite additional costs, the DRO model mitigates the unrealistic assumption of decision makers having complete distribution knowledge, effectively addressing distributional ambiguity in uncertain demand. In terms of managerial insights, humanitarian organisers can strategically employ the DRO model to mitigate the influence of ambiguous demand information in decision-making during unexpected disasters.

(2) The different risk parameter combinations impact the optimal objective and decision outcomes. Larger values for the risk parameters indicate a higher degree of risk aversion by the decision makers. Consequently, humanitarian organisers should judiciously select these parameters based on risk preferences and prevailing disaster circumstances.

(3) Decision makers should select an appropriate shortage penalty coefficient at different stages of disaster relief. Underestimating the coefficient could result in excess unsatisfied demand, leading to substantial disaster losses, while overestimation may yield unnecessary unused inventory. A deliberate consideration of this coefficient can minimise unsatisfied demand and achieve effective inventory management, which helps enhance the efficacy of relief operations and significantly reduce casualties. Humanitarian organisers ought to thoroughly assess prevailing conditions and context to make well-informed decisions about the shortage penalty coefficient, with the flexibility to

adjust it based on varying conditions across different disaster districts.

(4) Finally, regarding drone fleet management, drones with larger payload capacities enable the delivery of more relief supplies in a single trip, thereby improving overall delivery capabilities. Increasing the maximum payload weight limit enhances the efficient use of drone resources, leading to a reduction in overall operational costs. Consequently, decision makers should consider investing in drones with higher payload capacities to realise cost savings, especially in situations requiring large-scale and swift relief efforts. Additionally, the maximum flying range of drones has a significant influence on the egalitarian objective indicated by total delivery time. Therefore, tailoring drone specifications to align with the unique demands of relief missions and the geographical characteristics of the operational area becomes imperative for effective and efficient drone deployment. Furthermore, it is crucial to implement real-time monitoring systems for drone battery performance to ensure the reliable operation of drones throughout their missions.

5.4 Model Extensions

We now explore extensions of the fundamental model aimed at considering multiple relief items and incorporating equity constraints.

5.4.1 Model considering multiple relief items

In the realm of drone-supported disaster relief operations, the consideration of multiple relief items is paramount(Yang et al., 2021b). Disasters give rise to a diverse range of needs, spanning from medical kits and blood to vaccines and sanitation provisions. Each relief item is pivotal in meeting the varied requirements of affected populations and expediting their recovery process. Therefore, incorporating multiple relief items into our model is essential to tailor logistical strategies more effectively to meet the

diverse needs of disaster-stricken areas, ultimately enhancing the efficiency and effectiveness of drone-supported last-mile humanitarian logistics operations.

5.4.1.1 Problem description

In this extended model, we consider multiple relief items to meet the diverse needs within the disaster-affected areas.

We let B denote the set of relief items and $b \in B$. Now, we introduce the new decision variables and parameters in this extended model. In the first stage, for each $k \in K$, $b \in B$, we define a non-negative continuous decision variable v_{kb} as the inventory prepositioning quantity of relief item b in the drone-supported relief facility k. The unit inventory prepositioning cost for relief item b is denoted by a non-negative parameter c_b^{INV}. Additionally, the open drone-supported relief facility with capacity level l has limited inventory capacity, denoted by W_l. In the second stage, we let D_{ib}^{ξ} denote the random demand of relief item b or the disaster demand site i under scenario ξ. For each $i \in I$, $k \in K$, $b \in B$, and $\xi \in \Xi$, we let the non-negative continuous variable w_{ikb}^{ξ} express the number of relief items b delivered to disaster demand site i from drone-supported relief facility k under scenario ξ. We remark that the drone can carry multiple relief items to the assigned disaster demand area and return to the drone-supported relief facility for each drone trip. The unit weight of relief item b is represented by a non-negative parameter a_b. For each $i \in I$, $k \in K$, $d \in D$, $b \in B$, and $\xi \in \Xi$, we represent the number of relief items b delivered to disaster demand site i by the drone d that is assigned to drone-supported relief facility k under scenario ξ as the non-negative continuous variable q_{idkb}^{ξ}. The delivery cost for unit relief item b from the drone-supported relief facility k to the disaster demand site i is represented by the non-negative parameter c_{kib}^{DELI}. Finally, for each $i \in I$, $b \in B$, and $\xi \in \Xi$, we let the non-negative continuous variable u_{ib}^{ξ} express the quantity of unsatisfied demand of disaster demand site i for the relief item b under scenario ξ. And for each $k \in K$,

$b \in B$, and $\xi \in \Xi$, the non-negative continuous variable r_{kb}^{ξ} introduced, which means the quantity of unused inventory of the relief item b at the drone-supported relief facility k under scenario ξ. The penalty cost for per unit unsatisfied demand of relief item b and unused relief item b are represented by the non-negative parameters c_b^{UNS} and c_b^{UNU}, respectively.

5.4.1.2 Mathematical programming formulation

Using the additional notation to the basic DSRFLP, the extended risk-averse stochastic model considering multiple relief items is as follows:

$$\begin{aligned}\min \quad & \sum_{k\in K}\sum_{l\in L} c_l^{\mathrm{OPEN}} x_{kl} + \sum_{k\in K}\sum_{b\in B} c_b^{\mathrm{INV}} v_{kb} + \sum_{i\in I}\sum_{d\in D}\sum_{k\in K} c_{ki}^{\mathrm{MANA}} z_{idk} \\ & + (1-\lambda)\mathbb{E}[U_1(\mathbf{x},\mathbf{y},\mathbf{z},\mathbf{v},\boldsymbol{\Theta}(\xi))] + \lambda \mathrm{CVaR}[U_1(\mathbf{x},\mathbf{y},\mathbf{z},\mathbf{v},\boldsymbol{\Theta}(\xi))] \end{aligned} \tag{5.42}$$

$$\text{s.t.} \quad \sum_{b\in B} v_{kb} \le \sum_{l\in L} W_l x_{kl}, \quad \forall k\in K, \tag{5.43}$$

$$v_{kb} \ge 0, \quad \forall k\in K,\ \forall b\in B, \tag{5.44}$$

Constraints $(5.2)-(5.5), (5.7)-(5.12)$,

$$\begin{aligned}\text{where} \quad & U_1(\mathbf{x},\mathbf{y},\mathbf{z},\mathbf{v},\boldsymbol{\Theta}(\xi)) \\ =& \min \sum_{i\in I}\sum_{d\in D}\sum_{k\in K}\sum_{b\in B} c_{kib}^{\mathrm{DELI}} q_{idkb}^{\xi} + \sum_{i\in I}\sum_{b\in B} c_b^{\mathrm{UNS}} u_{ib}^{\xi} + \sum_{k\in K}\sum_{b\in B} c_b^{\mathrm{UNU}} r_{kb}^{\xi} \end{aligned} \tag{5.45}$$

$$\text{s.t.} \quad \sum_{k\in K} w_{ikb}^{\xi} + u_{ib}^{\xi} = D_{ib}^{\xi}, \quad \forall i\in I,\ \forall b\in B, \tag{5.46}$$

$$\sum_{i\in I} w_{ikb}^{\xi} + r_{kb}^{\xi} = v_{kb}, \quad \forall k\in K,\ \forall b\in B, \tag{5.47}$$

$$w_{ikb}^{\xi} - \sum_{d \in D} q_{idkb}^{\xi} = 0, \quad \forall k \in K,\ \forall i \in I,\ \forall b \in B, \tag{5.48}$$

$$\sum_{b \in B} a_b q_{idkb}^{\xi} \leq L^{\mathrm{MAX}} z_{idk}, \quad \forall k \in K,\ \forall i \in I,\ \forall d \in D, \tag{5.49}$$

$$w_{ikb}^{\xi} \geq 0, \quad \forall k \in K,\ \forall i \in I,\ \forall b \in B, \tag{5.50}$$

$$q_{idkb}^{\xi} \geq 0, \quad \forall k \in K,\ \forall i \in I,\ \forall d \in D,\ \forall b \in B, \tag{5.51}$$

$$u_{ib}^{\xi} \geq 0, \quad \forall i \in I,\ \forall b \in B, \tag{5.52}$$

$$r_{kb}^{\xi} \geq 0, \quad \forall k \in K.\ \forall b \in B. \tag{5.53}$$

The objective function (5.42) minimises the cost of the first-stage decisions and the expected cost of the second-stage decisions. Constraints (5.43) enforce the inventory restrictions on relief items. Formula (5.45) defines the new recourse problem considering multiple relief items. Constraints (5.46) and (5.47) impose the flow balance of multiple relief items at the disaster area and drone-supported relief facility. Constraints (5.48) determine the individual delivery quantity of each drone. Constraints (5.49) require the total number of multiple relief items delivered by the drone not to exceed the maximum payload weight limit. Constraints (5.44) and (5.50)-(5.53) specify the domains of variables.

Similar to the proof logic of Theorem 5.1–5.3, we can derive the corresponding tractable DRO models of the extended model under box, ellipsoidal, and polyhedral ambiguity sets. In Appendix F, we provide the specific DRO model formulations.

5.4.1.3 Computational experiments

We utilise instances from the aforementioned case study with $|I| = 30$, $|J| = 13$, $|D| = 20$, and $|\Xi| = 50$ to validate the extended model. Specifically, we examine three

types of relief items: blood, vaccines, and medical kits. The inventory capacities of drone-supported relief facilities with small, medium, and large capacity levels are as follows: 80, 120, and 160. The unit weight of blood, vaccines, and medical kits is 1, 1.2, and 1.5, respectively. Additionally, regarding the parameters related to costs, the holding costs of blood, vaccines, and medical kits are 140, 120, and 100. The unit transportation cost per unit distance for medical kits, vaccines, and blood is 4, 4, and 5. The other parameter settings remain consistent with the above case study. In this experiment, we simulate varying demand levels (high and low) to represent distinct stages of disaster relief. High demand for relief items corresponds to the early stages, while low demand for relief items corresponds to the later stages. We determine the demand range for each relief item across various demand level scenarios as follows: 20 to 40 for the high demand level and 5 to 15 for the low demand level.

The computational results for different demand levels under three ambiguity sets are presented in Figures 5.13 to 5.15. It is evident from these figures that demand levels exert a significant influence on inventory decisions regarding multiple relief items. For instance, in scenarios with high demand levels, nearly all candidate drone-supported relief facilities are operational, and the chosen capacity levels are the largest, resulting in large inventory quantities. Therefore, it is crucial to consider demand variability when making inventory decisions for multiple relief items in drone-supported last-mile humanitarian logistics systems.

Expanding on the managerial implications, these findings highlight the necessity for adaptive inventory management strategies that can accommodate varying demand levels in disaster scenarios. Implementing dynamic inventory policies that adjust facility operations and resource allocation based on real-time demand information can enhance the responsiveness and effectiveness of relief efforts. Additionally, prioritising the establishment of drone-supported relief facilities in areas with anticipated high demand can help ensure the timely and sufficient delivery of essential relief items to affected

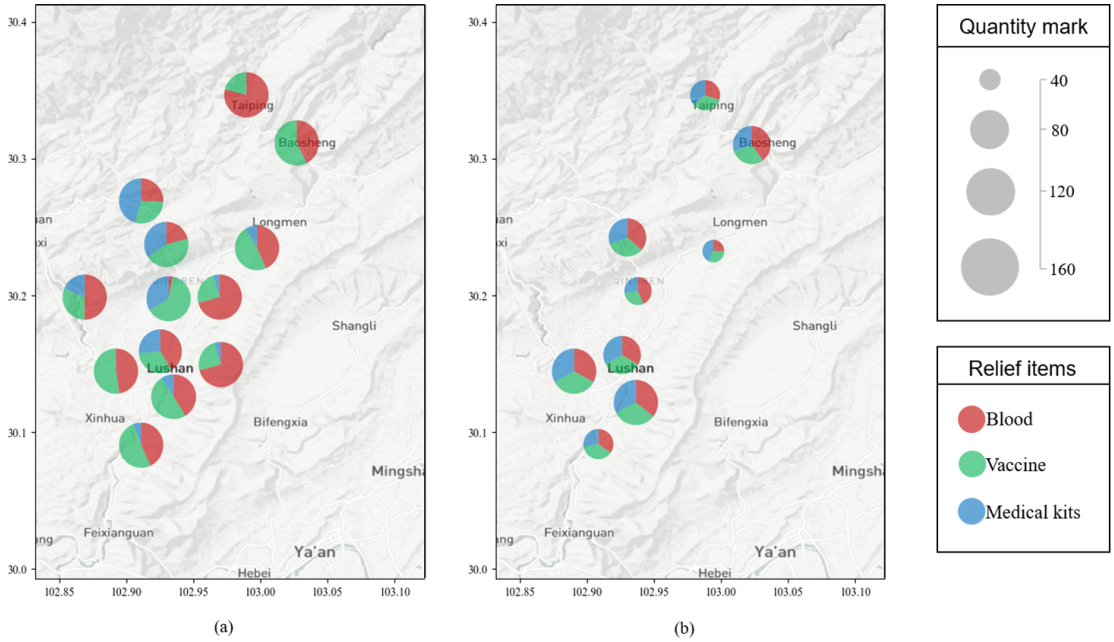

Figure 5.13: The inventory of multiple relief items under box ambiguity set – (a) High demand level; (b) Low demand level.

populations. By proactively addressing demand variability, humanitarian organisations can better allocate resources and mitigate the impact of disasters on vulnerable communities.

5.4.2 Model considering equity constraint in priority setting

In the realm of drone-supported disaster relief operations, it is crucial to recognise the varying impacts across different disaster-affected regions and the diverse requirements for different types of relief items (Cheng et al., 2021). Therefore, prioritising resource allocation is essential to address the most critical needs promptly, minimising loss and maximising effectiveness. Simultaneously, equity is a significant objective that needs to be considered in humanitarian operations (Farahani et al., 2020; Çankaya et al., 2019). Disparities resulting from unequal distribution of relief resources can exacerbate existing inequalities and impede humanitarian efforts, particularly in scenarios of severe

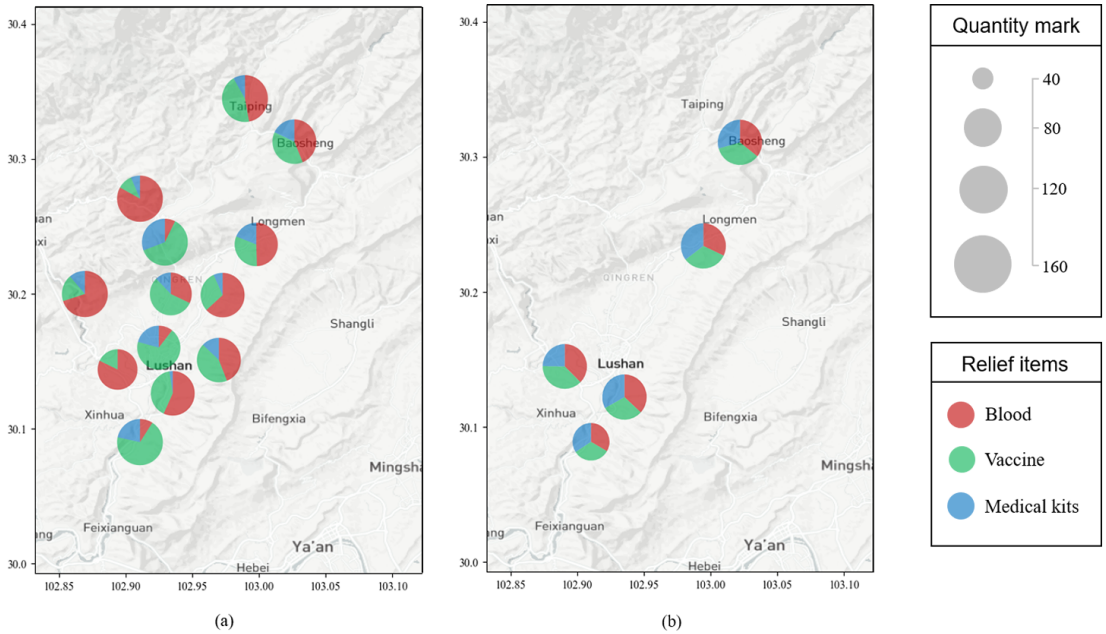

Figure 5.14: The inventory of multiple relief items under ellipsoidal ambiguity set – (a) High demand level; (b) Low demand level.

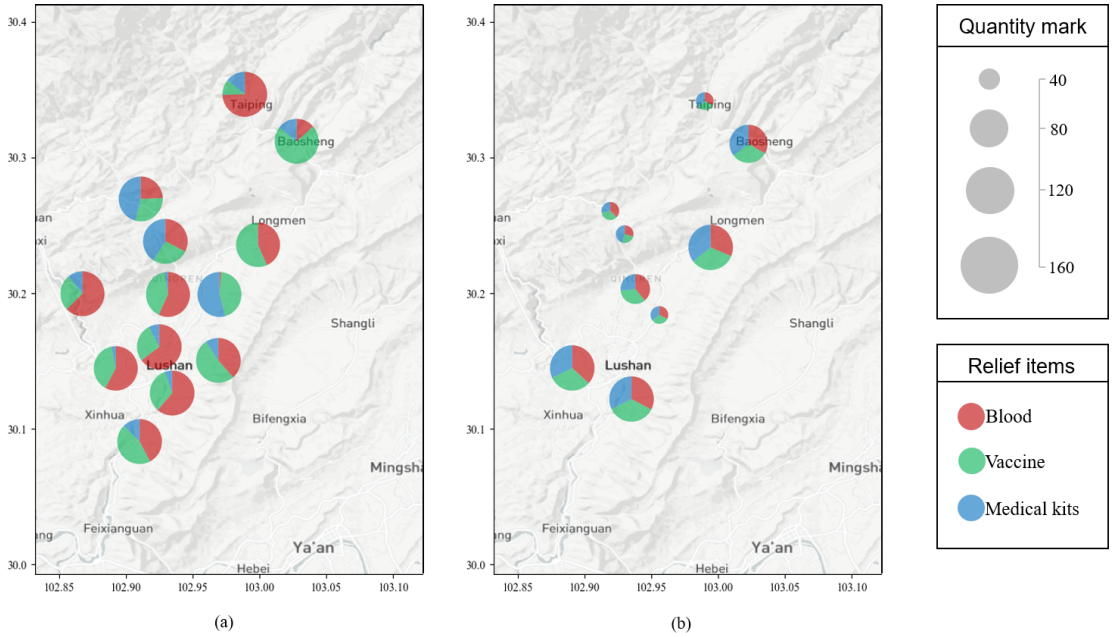

Figure 5.15: The inventory of multiple relief items under polyhedral ambiguity set – (a) High demand level; (b) Low demand level.

shortage of relief resources. By incorporating equity constraints into the model, a fair distribution of resources can be guaranteed, considering the specific needs and severity of each disaster-stricken area. This integration not only enhances the efficiency and efficacy of drone-supported last-mile humanitarian logistics but also promotes social justice and welfare. Therefore, we propose an extended model incorporating equity constraints in priority setting to consider priority and equity simultaneously, optimising resource utilisation and fostering social equity amidst crises.

5.4.2.1 Problem description

In this problem, we integrate the consideration of relief item priority to facilitate the equitable distribution of relief resources.

Specifically, we denote Φ_{ib} as the priority assigned to relief item b at disaster demand site i. This parameter is related to the severity degree of the disaster sites and the importance of the relief item type for each specific site. Note that the greater the priority assigned to a relief item at a disaster site, the higher the penalty cost for unsatisfied demand. Concurrently, we introduce an equity constraint in priority setting to consider the priority and equity simultaneously. We introduce an equity tolerance coefficient, denoted by the non-negative parameter Δ, to ensure a specific level of distributional equity. This coefficient guarantees that the difference in the ratio of unsatisfied demand between two disaster demand sites is within a certain degree. Accordingly, we propose a novel extended model considering equity constraint in priority setting to optimise the reasonable utilisation of relief resources and enhance social welfare simultaneously.

5.4.2.2 Mathematical programming formulation

Using the additional notation to the above-extended model considering multiple relief items, the extended risk-averse stochastic model considering equity constraint in

priority setting can be formulated as follows.

$$\begin{aligned}\min \quad & \sum_{k\in K}\sum_{l\in L} c_l^{\mathrm{OPEN}} x_{kl} + \sum_{k\in K}\sum_{b\in B} c_b^{\mathrm{INV}} v_{kb} + \sum_{i\in I}\sum_{d\in D}\sum_{k\in K} c_{ki}^{\mathrm{MANA}} z_{idk} \\ & + (1-\lambda)\mathbb{E}[U_2(\mathbf{x},\mathbf{y},\mathbf{z},\mathbf{v},\boldsymbol{\Theta}(\xi))] + \lambda \mathrm{CVaR}[U_2(\mathbf{x},\mathbf{y},\mathbf{z},\mathbf{v},\boldsymbol{\Theta}(\xi))] \end{aligned} \tag{5.54}$$

$$\text{s.t.} \quad \text{Constraints (5.2)} - \text{(5.5)}, \text{(5.7)} - \text{(5.12)}, \text{(5.43)} - \text{(5.44)},$$

$$\begin{aligned}\text{where} \quad & U_2(\mathbf{x},\mathbf{y},\mathbf{z},\mathbf{v},\boldsymbol{\Theta}(\xi)) \\ & = \min \sum_{i\in I}\sum_{d\in D}\sum_{k\in K}\sum_{b\in B} c_{kib}^{\mathrm{DELI}} q_{idkb}^{\xi} + \sum_{i\in I}\sum_{b\in B} c_b^{\mathrm{UNS}} \Phi_{ib} u_{ib}^{\xi} + \sum_{k\in K}\sum_{b\in B} c_b^{\mathrm{UNU}} r_{kb}^{\xi} \end{aligned} \tag{5.55}$$

$$\text{s.t.} \quad -\Delta \le \frac{\sum_{b\in B} u_{ib}^{\xi}}{\sum_{b\in B} D_{ib}^{\xi}} - \frac{\sum_{b\in B} u_{jb}^{\xi}}{\sum_{b\in B} D_{jb}^{\xi}} \le \Delta, \quad \forall i,j \in I,\ i \ne j,\ \forall \xi \in \Xi, \tag{5.56}$$

$$\text{Constraints (5.46)} - \text{(5.53)}.$$

The objective function (5.54) minimises the cost of the first stage decisions and the expected cost of the second stage decisions. Formula (5.55) defines the new recourse problem considering relief item priority. Constraints (5.56) enforce that the difference in the ratio of the quantity of unsatisfied demand to the total demand between any two disaster demand sites cannot exceed the equity tolerance coefficient, ensuring a certain degree of equity.

Similar to the proof logic of Theorem 5.1–5.3, we can derive the corresponding tractable DRO models of the extended model under box, ellipsoidal, and polyhedral ambiguity sets. In Appendix G, we provide the specific DRO model formulations.

5.4.2.3 Computational experiments

We evaluate the extended model using the same network scale and parameter set-

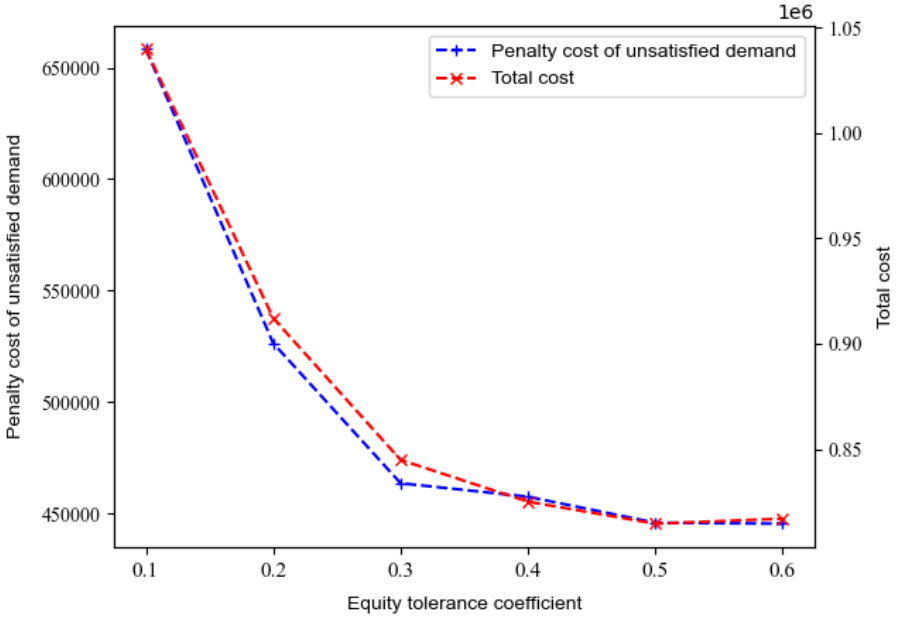

Figure 5.16: The impacts of equity tolerance coefficients on total cost and penalty cost of unsatisfied demand under box ambiguity set.

tings as those employed in the previous model extension. The priority of relief items is randomly generated within the range of 1 to 5. We randomly generate the demand for each relief item within the range of [20,40]. In this experiment, we conduct a sensitivity analysis of the parameter equity tolerance coefficient Δ. We vary Δ from 0.1 to 0.6 in increments of 0.1 and examine the total cost and penalty costs of unsatisfied demand under different values of equity tolerance coefficients. Note that the greater the equity tolerance coefficient, the less stringent the equity requirement. The computational results under three ambiguity sets are illustrated from Figure 5.16 to Figure 5.18.

Observing from Figure 5.16 to Figure 5.18, it is evident that both the total cost and the penalty cost of unsatisfied demand decrease with the increase in the equity tolerance coefficient. This implies that stricter equity requirements result in higher costs incurred and a greater occurrence of unsatisfied demand. Additionally, the decreased speed becomes lower as the equity tolerance coefficient increases. From the perspective

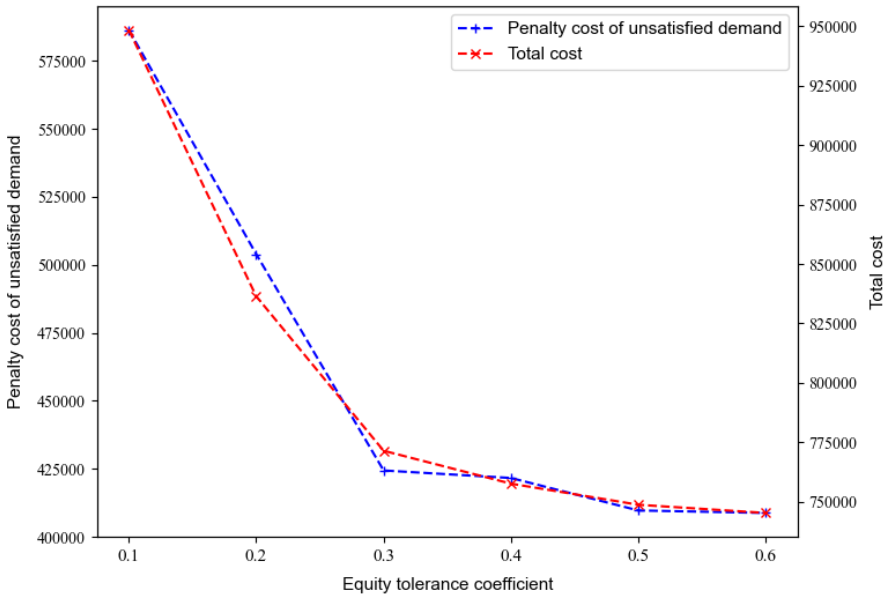

Figure 5.17: The impacts of equity tolerance coefficients on total cost and penalty cost of unsatisfied demand under ellipsoidal ambiguity set.

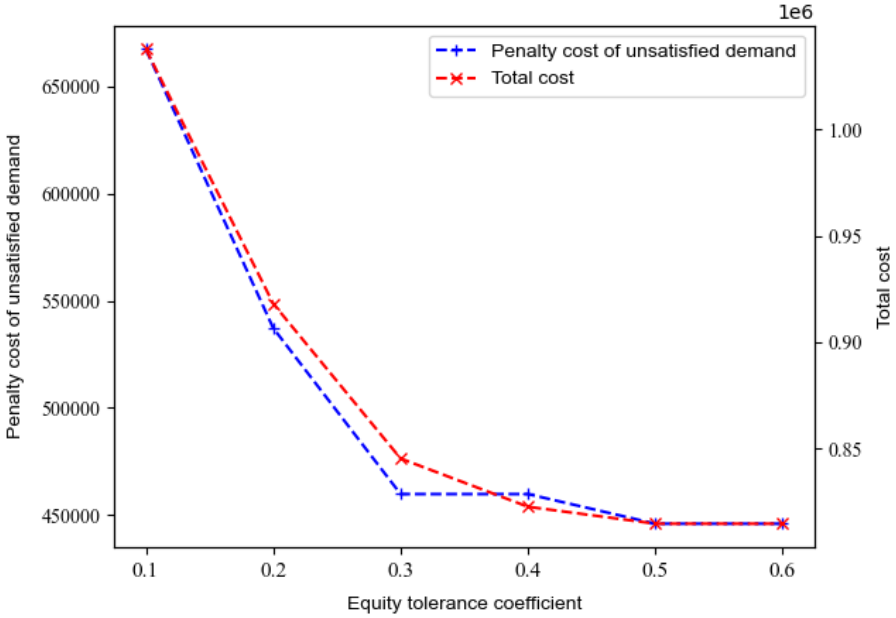

Figure 5.18: The impacts of equity tolerance coefficients on total cost and penalty cost of unsatisfied demand under polyhedral ambiguity set.

of disaster relief management, while equity considerations are important in decision-making processes, it is crucial for managers to consider equity requirements. Strict equity requirements may lead to higher unsatisfied demand, potentially compromising operational efficiency. Hence, it is essential to assess the trade-offs between equity and effectiveness when formulating strategies. In the initial stages of relief operations, the primary focus should be on ensuring the timely delivery of aid to affected areas, even if it means temporarily sacrificing some aspects of equity. This approach helps maximise the effectiveness of relief efforts and saves lives in critical situations. Finally, managers should continuously adjust the equity-related policies as needed. By staying flexible and responsive to changing conditions, organisations can better enhance overall disaster relief performance in the long run.

5.5 Concluding Remarks of Chapter 5

In this study, we focus on the DSRFLP to make joint decisions considering random demands in the pre-disaster and post-disaster phases to promote the efficient operations of drone-supported last-mile humanitarian logistics. During the pre-disaster phase, our considerations involve determining the drone-supported relief facility location, inventory prepositioning of relief items, drone assignment to the opened facilities, and drone allocation to disaster demand sites. In the post-disaster phase, we address the decisions related to post-disaster delivery quantities in response to various disaster scenarios, which are made after the demand information becomes known. Due to the difficulty of obtaining an accurate probability distribution of the uncertain demands in disaster scenarios, we establish a two-stage DRO model in which uncertain demands can follow uncertain distributions defined by a box, ellipsoidal, and polyhedral ambiguity set to optimise the joint decisions of pre-disaster and post-disaster phases. Additionally, WMCVaR risk measurement is adopted in this DRO model to reflect the risk-averse attitude of humanitarian organisers in chaotic disaster relief systems. To address the challenge of computational intractability, we equivalently reformulate the DRO model with three ambiguity sets into a computationally tractable one. Furthermore, the validity of the proposed DRO model is verified through a small-scale example and a large-scale case study. The numerical results of the small-scale example demonstrate that the proposed DRO model exhibits superior performance in hedging against the influence of incomplete information on uncertain demand. According to the experimental results, we put forth several managerial implications and insights to support the decision-making processes for humanitarian organisations. Finally, we propose two extended models to address multiple relief items and equity constraints in priority setting and perform numerical experiments, aiming to adapt to various real-world disaster scenarios.

Chapter 6

Summary and Future Research

6.1 Conclusions

In conclusion, we develop innovative models and solution methods to tackle these challenges within the context of strategic planning for the AAM system under uncertainty in scenarios of urban transportation and humanitarian logistics.

In the scenario of urban transportation, we focus on addressing an integrated optimisation problem that encompasses both the strategic planning and operational service aspects of UAM systems. This involves making joint decisions on several factors, such as determining the number of parking stands at vertiports and vertistops, the size of the eVTOL fleet, and the allocation and operation of the fleet. We introduce an innovative spatial equity metric and develop a bi-objective optimisation model aimed at balancing service profitability with spatial equity. To address the challenges posed by uncertain demand, we propose a scenario-based robust optimisation framework that incorporates the interval robust method.

For humanitarian logistics, we examine drone-supported last-mile humanitarian logistics planning under demand uncertainty considering two scenarios: one where the demand uncertainty is realised sequentially and the other one where the demand in-

formation is only partially available. In cases with sequential realisation of uncertain demand, we propose the DLHLSP problem and employ the multistage stochastic programming framework incorporating nonanticipativity constraints to model this problem. This problem involves determining drone-supported relief facility locations, drone deployment strategies, drone visit schedules, inventory management, relief item procurement, and delivery operations. This approach can make decisions at each stage without knowledge of the demand information in future time periods, which is more adaptive to disaster scenarios. By utilising the Benders decomposition algorithm, we obtain exact solutions in a quick computational time.

When historical data are lacking and distribution information is incomplete, we investigate a novel problem called DSRFLP. This problem determines the locations of drone-supported relief facilities, inventory prepositioning of relief items, drone assignment to the opened facilities, drone allocation to disaster demand sites, and drone-based transportation. To address the challenge of obtaining the accurate distribution of the uncertain demand, we explored a DRO framework to handle the uncertainty. Therefore, we propose a two-stage DRO model for DSRFLP to capture the ambiguous distribution information of the uncertain demand. Additionally, WMCVaR risk measurement is adopted in this DRO model to reflect the risk-averse attitude of decision makers. Additionally, three ambiguity sets (box, ellipsoidal, and polyhedral) are designed to depict the partial probability distributions of the demand. Furthermore, we reformulate the DRO model under three ambiguity sets into the corresponding equivalent computationally tractable formulations based on mathematical theories.

Finally, we validate our UAM system planning model and solution method through a case study of a megalopolis in southern China. We offer valuable policy recommendations to guide future decision-making processes and provide insights for UAM service providers, particularly in disaster scenarios. In the context of drone-supported last-mile humanitarian logistics system planning, the Lushan earthquake in China demonstrates

the practical applicability and effectiveness of our models and methods. We provide valuable managerial implications and insights for humanitarian organisations, supporting their decision-making processes in disaster scenarios.

Overall, this thesis significantly contributes to the advancement of strategic planning for AAM systems in both urban transportation and humanitarian logistics applications. By developing adaptable and efficient solutions, our objective is to enhance the decision-making capabilities of managers facing uncertainty in these fields. These contributions can support long-term strategic planning, ensuring that AAM systems can improve operational performance and resilience while providing high-quality services.

6.2 Future Research

Several future research directions are introduced as follows:

There are some limitations that can be extended in future research for the strategic planning of the UAM system. Firstly, it would be interesting to investigate the influence of other equity metrics, such as accessibility equity and income equity, on the strategic planning and service operations of the UAM systems. Secondly, other uncertain factors, such as battery consumption, can be considered in the research. Thirdly, ride-sharing and heterogeneous characteristics of different OD pairs, such as low-altitude airspace management capacities, could be incorporated into our mathematical model. Fourthly, exact computational techniques can be explored to solve larger-scale problems. Finally, it is worth developing a mathematical model to optimise the micro-level operations of UAM systems, such as the eVTOL scheduling and routing, considering different demand distributions and travel behaviour.

Additionally, there are also several promising avenues for future research that could further enhance the efficiency and adaptability of drone-supported relief operations. Firstly, future research could explore the integration of additional uncertain factors

into the current optimisation model. There are multiple uncertain factors that could significantly influence the humanitarian logistics system. Specifically, uncertainties related to energy consumption, travel time, policy changes, dynamic weather conditions, and fluctuating payload weights should be examined in more detail. Secondly, real-time algorithms can be developed to adapt drone paths to constantly changing conditions during disaster scenarios, such as new obstacles and damaged infrastructure. Additionally, it would be interesting to explore how multiple drones can work together in disaster scenarios to optimise coverage areas and avoid congestion, particularly when operating in high-risk or highly dynamic environments. Third, we can use the machine learning and predictive analytics approach to forecast drone battery degradation to improve operational efficiency and reliability. Finally, we could explore the use of a synchronised truck-drone delivery system to improve last-mile delivery in humanitarian logistics. Specifically, it is significant to develop models and algorithms for coordinating the movement of trucks and drones to optimise the efficiency and timeliness of deliveries, especially in congested or hard-to-reach areas.

Appendix A

Mathematical Proof of Theorem 5.1

Proof of Theorem 5.1. If the probability distribution of the discrete uncertain demand belongs to a box ambiguity set $\mathcal{P}^{\text{Box}}$ that is defined in Eq. (5.35), the expectation part of the model (5.34) can be reformulated as

$$\begin{aligned}
&\min_{\boldsymbol{x},\boldsymbol{y},\boldsymbol{z},\boldsymbol{v},\boldsymbol{\Psi}} \max_{\mathbf{p}\in\mathcal{P}^{\text{Box}}} Q(\mathbf{x},\mathbf{y},\mathbf{z},\mathbf{v},\boldsymbol{\Theta}(\xi))^{\intercal}\mathbf{p} \\
&= \min_{\boldsymbol{x},\boldsymbol{y},\boldsymbol{z},\boldsymbol{v},\boldsymbol{\Psi}} \left\{ Q(\mathbf{x},\mathbf{y},\mathbf{z},\mathbf{v},\boldsymbol{\Theta}(\xi))^{\intercal}\mathbf{p}^{\mathbf{0}} + \max_{\boldsymbol{\epsilon}} \left[Q(\mathbf{x},\mathbf{y},\mathbf{z},\mathbf{v},\boldsymbol{\Theta}(\xi))^{\intercal}\boldsymbol{\epsilon} \mid \mathbf{e}^{\mathrm{T}}\boldsymbol{\epsilon} = 0, \|\boldsymbol{\epsilon}\|_{\infty} \leq \omega \right] \right\}.
\end{aligned} \tag{A.1}$$

Based on the linear programming duality theory, the above model can be reformulated as

$$\min_{\boldsymbol{x},\boldsymbol{y},\boldsymbol{z},\boldsymbol{v},\boldsymbol{\Psi}} \left\{ Q(\mathbf{x},\mathbf{y},\mathbf{z},\mathbf{v},\boldsymbol{\Theta}(\xi))^{\intercal}\mathbf{p}^{\mathbf{0}} + \min_{\tau,\boldsymbol{\varsigma},\boldsymbol{\varrho}} \left[\boldsymbol{\Omega}^{\intercal}\boldsymbol{\varsigma} + \boldsymbol{\Omega}^{\intercal}\boldsymbol{\varrho} \,\middle|\, \begin{array}{c} \mathbf{e}\tau + \boldsymbol{\varsigma} - \boldsymbol{\varrho} = Q(\mathbf{x},\mathbf{y},\mathbf{z},\mathbf{v},\boldsymbol{\Theta}(\xi)), \\ \boldsymbol{\varsigma} \geq \mathbf{0}, \boldsymbol{\varrho} \geq \mathbf{0}. \end{array} \right] \right\}, \tag{A.2}$$

where $(\tau, \boldsymbol{\varsigma}, \boldsymbol{\varrho}) \in \mathbb{R} \times \mathbb{R}_{+}^{|\Xi|} \times \mathbb{R}_{+}^{|\Xi|}$ are the dual variables and $\boldsymbol{\Omega} = \omega\mathbf{e}$.

Recall that the WCVaR denotes the worst-case CVaR, and suppose that $\mathcal{P}^{\text{Box}}$ is a compact convex set. Then, the $\text{WCVaR}_{\alpha}(Q(\mathbf{x},\mathbf{y},\mathbf{z},\mathbf{v},\boldsymbol{\Theta}(\xi)))$ can be expressed as (Zhu

and Fukushima, 2009)

$$\begin{aligned}\mathrm{WCVaR}_\alpha(Q(\mathbf{x},\mathbf{y},\mathbf{z},\mathbf{v},\boldsymbol{\Theta}(\xi))) &= \max_{\mathbf{p}\in\mathcal{P}^{\mathrm{Box}}} \mathrm{CVaR}_\alpha(Q(\mathbf{x},\mathbf{y},\mathbf{z},\mathbf{v},\boldsymbol{\Theta}(\xi))) \\ &= \max_{\mathbf{p}\in\mathcal{P}^{\mathrm{Box}}} \min_{\eta} \eta + \frac{1}{1-\alpha}\sum_{\xi\in\Xi} p^\xi \left[Q(\mathbf{x},\mathbf{y},\mathbf{z},\mathbf{v},\boldsymbol{\Theta}(\xi)) - \eta\right]^+ \\ &= \min_{\eta} \max_{\mathbf{p}\in\mathcal{P}^{\mathrm{Box}}} \eta + \frac{1}{1-\alpha}\sum_{\xi\in\Xi} p^\xi \left[Q(\mathbf{x},\mathbf{y},\mathbf{z},\mathbf{v},\boldsymbol{\Theta}(\xi)) - \eta\right]^+ .\end{aligned} \tag{A.3}$$

We can exchange the order of the operators $\max_{\mathbf{p}\in\mathcal{P}^{\mathrm{Box}}}$ and $\min_\eta$ mainly because the formula $\eta + \frac{1}{1-\alpha}\sum_{\xi\in\Xi} p^\xi \left[Q(\mathbf{x},\mathbf{y},\mathbf{z},\mathbf{v},\boldsymbol{\Theta}(\xi)) - \eta\right]^+$ is convex in η (Rockafellar and Uryasev, 2002) and affine (concave) in $\mathbf{p}$.

Therefore, we can rewrite the WCVaR part in the problem (5.34) as

$$\begin{aligned}&\min_{\boldsymbol{x},\boldsymbol{y},\boldsymbol{z},\boldsymbol{v},\boldsymbol{\Psi}} \mathrm{WCVaR}_\alpha(Q(\mathbf{x},\mathbf{y},\mathbf{z},\mathbf{v},\boldsymbol{\Theta}(\xi))) \\ =&\min_{\boldsymbol{x},\boldsymbol{y},\boldsymbol{z},\boldsymbol{v},\boldsymbol{\Psi},\eta} \max_{\mathbf{p}\in\mathcal{P}^{\mathrm{Box}}} \eta + \frac{1}{1-\alpha}\sum_{\xi\in\Xi} p^\xi \left[Q(\mathbf{x},\mathbf{y},\mathbf{z},\mathbf{v},\boldsymbol{\Theta}(\xi)) - \eta\right]^+ .\end{aligned} \tag{A.4}$$

By introducing an auxiliary vector $\boldsymbol{s} = \left\{s_1, s_2, \cdots, s_{|\Xi|}\right\}^\intercal$, we can equivalently rewrite Eq. (A.4) as the following problem:

$$\min_{\boldsymbol{x},\boldsymbol{y},\boldsymbol{z},\boldsymbol{v},\boldsymbol{\Psi},\mathbf{s},\eta} \max_{\mathbf{p}\in\mathcal{P}^{\mathrm{Box}}} \eta + \frac{1}{1-\alpha}\mathbf{p}^\intercal\mathbf{s} \tag{A.5}$$

$$\text{s.t.} \quad \mathbf{s} \geq Q(\mathbf{x},\mathbf{y},\mathbf{z},\mathbf{v},\boldsymbol{\Theta}(\xi)) - \eta\mathbf{e}, \tag{A.6}$$

$$\mathbf{s} \geq \mathbf{0}. \tag{A.7}$$

Hence, the equivalent formulation of the above problem can be expressed as the

following minimisation problem.

$$\begin{aligned} &\min_{\boldsymbol{x},\boldsymbol{y},\boldsymbol{z},\boldsymbol{v},\boldsymbol{\Psi},\mathbf{s},\Lambda,\eta} \Lambda \\ &\text{s.t.} \quad \Lambda \geq \max_{\mathbf{p}\in\mathcal{P}^{\text{Box}}} \eta + \frac{1}{1-\alpha}\mathbf{p}^{\intercal}\mathbf{s}, \\ &\qquad\qquad \text{Constraints (A.6)–(A.7).} \end{aligned} \tag{A.8}$$

In light of the max operation present in the first constraints of problem (A.8), it becomes imperative to transform this problem into a tractable one. Recall that the distribution probability $\mathbf{p}$ belongs to the box ambiguity set $\mathcal{P}^{\text{Box}}$ expressed in Eq.(5.35), we have

$$\eta + \frac{1}{1-\alpha}\mathbf{p}^{\intercal}\mathbf{s} = \eta + \frac{1}{1-\alpha}(\mathbf{p^0})^{\intercal}\mathbf{s} + \frac{1}{1-\alpha}\boldsymbol{\epsilon}^{\intercal}\mathbf{s}. \tag{A.9}$$

Therefore, the right-side hand of the first constraints of problem (A.8) can be formulated as

$$\max_{\mathbf{p}\in\mathcal{P}^{\text{Box}}} \eta + \frac{1}{1-\alpha}\mathbf{p}^{\intercal}\mathbf{s} = \eta + \frac{1}{1-\alpha}(\mathbf{p^0})^{\intercal}\mathbf{s} + \frac{\Upsilon^*(\mathbf{s})}{1-\alpha}, \tag{A.10}$$

where $\Upsilon^*(\mathbf{s})$ denotes the optimal value of the following linear program.

$$\max_{\boldsymbol{\epsilon}} \left\{ \boldsymbol{\epsilon}^{\intercal}\mathbf{s} \mid \mathbf{e}^{\mathrm{T}}\boldsymbol{\epsilon} = 0, \|\boldsymbol{\epsilon}\|_{\infty} \leq \omega \right\}. \tag{A.11}$$

Based on the duality theory, the dual program of Eq.(A.11) is as follows:

$$\Upsilon^*(\mathbf{s}) = \min_{\widehat{\tau},\widehat{\boldsymbol{\varsigma}},\widehat{\boldsymbol{\varrho}}} \left\{ \boldsymbol{\Omega}^{\intercal}\widehat{\boldsymbol{\varsigma}} + \boldsymbol{\Omega}^{\intercal}\widehat{\boldsymbol{\varrho}} \;\middle|\; \begin{array}{ll} \mathbf{e}\widehat{\tau} + \widehat{\boldsymbol{\varsigma}} - \widehat{\boldsymbol{\varrho}} = \mathbf{s}, \\ \widehat{\boldsymbol{\varsigma}} \geq \mathbf{0}, \quad \widehat{\boldsymbol{\varrho}} \geq \mathbf{0}. \end{array} \right\}. \tag{A.12}$$

Hence, we have the following minimisation problem.

$$
\begin{aligned}
\min_{\boldsymbol{x},\boldsymbol{y},\boldsymbol{z},\boldsymbol{v},\boldsymbol{\Psi},\mathbf{s},\Lambda,\widehat{\boldsymbol{\varsigma}},\widehat{\boldsymbol{\varrho}},\widehat{\tau},\eta} \quad & \Lambda \\
\text{s.t.} \quad & \Lambda \geq \eta + \frac{1}{1-\alpha}(\mathbf{p^0})^{\intercal}\mathbf{s} + \frac{1}{1-\alpha}\left(\boldsymbol{\Omega}^{\intercal}\widehat{\boldsymbol{\varsigma}} + \boldsymbol{\Omega}^{\intercal}\widehat{\boldsymbol{\varrho}}\right), \\
& \mathbf{e}\widehat{\tau} + \widehat{\boldsymbol{\varsigma}} - \widehat{\boldsymbol{\varrho}} = \mathbf{s}, \\
& \mathbf{s} \geq Q(\mathbf{x},\mathbf{y},\mathbf{z},\mathbf{v},\boldsymbol{\Theta}(\xi)) - \eta\mathbf{e}, \\
& \widehat{\boldsymbol{\varsigma}} \geq \mathbf{0}, \quad \widehat{\boldsymbol{\varrho}} \geq \mathbf{0}, \quad \mathbf{s} \geq \mathbf{0}.
\end{aligned}
\tag{A.13}
$$

Note that solving Problem (A.8) is equivalent to addressing Problem (A.13). Proposition 1, proposed in Appendix B, demonstrates the equivalence between these two problems.

Therefore, we can express the formula $\min_{\boldsymbol{x},\boldsymbol{y},\boldsymbol{z},\boldsymbol{v},\boldsymbol{\Psi}} \mathrm{WMCVaR}_{\alpha}(Q(\mathbf{x},\mathbf{y},\mathbf{z},\mathbf{v},\boldsymbol{\Theta}(\xi)))$ in the problem (5.32) as

$$
\begin{aligned}
&\min_{\boldsymbol{x},\boldsymbol{y},\boldsymbol{z},\boldsymbol{v},\boldsymbol{\Psi}} \mathrm{WMCVaR}_{\alpha}(Q(\mathbf{x},\mathbf{y},\mathbf{z},\mathbf{v},\boldsymbol{\Theta}(\xi))) \\
&= \min_{\boldsymbol{x},\boldsymbol{y},\boldsymbol{z},\boldsymbol{v},\boldsymbol{\Psi}} (1-\lambda) \sup_{\mathbf{p}\in\mathcal{P}^{\mathrm{Box}}} \mathbb{E}(Q(\mathbf{x},\mathbf{y},\mathbf{z},\mathbf{v},\boldsymbol{\Theta}(\xi))) + \lambda \mathrm{WCVaR}_{\alpha}(Q(\mathbf{x},\mathbf{y},\mathbf{z},\mathbf{v},\boldsymbol{\Theta}(\xi))) \\
&= \min_{\boldsymbol{x},\boldsymbol{y},\boldsymbol{z},\boldsymbol{v},\boldsymbol{\Psi}} \left\{ \begin{array}{l|c}
\min\limits_{\tau,\boldsymbol{\varsigma},\boldsymbol{\varrho}} (1-\lambda)[Q(\mathbf{x},\mathbf{y},\mathbf{z},\mathbf{v},\boldsymbol{\Theta}(\xi))^{\intercal}\mathbf{p^0} + \boldsymbol{\Omega}^{\intercal}\boldsymbol{\varsigma} + \boldsymbol{\Omega}^{\intercal}\boldsymbol{\varrho}] & \begin{array}{c} \mathbf{e}\tau + \boldsymbol{\varsigma} - \boldsymbol{\varrho} = Q(\mathbf{x},\mathbf{y},\mathbf{z},\mathbf{v},\boldsymbol{\Theta}(\xi)), \\ \boldsymbol{\varsigma} \geq \mathbf{0}, \boldsymbol{\varrho} \geq \mathbf{0}. \end{array} \\
+\lambda \min\limits_{\widehat{\tau},\widehat{\boldsymbol{\varsigma}},\widehat{\boldsymbol{\varrho}},\mathbf{s},\eta} \left\{ \eta + \frac{1}{1-\alpha}(\mathbf{p^0})^{\intercal}\mathbf{s} + \frac{1}{1-\alpha}\left(\boldsymbol{\Omega}^{\intercal}\widehat{\boldsymbol{\varsigma}} + \boldsymbol{\Omega}^{\intercal}\widehat{\boldsymbol{\varrho}}\right) \right| & \begin{array}{c} \mathbf{e}\widehat{\tau} + \widehat{\boldsymbol{\varsigma}} - \widehat{\boldsymbol{\varrho}} = \mathbf{s}, \\ \mathbf{s} \geq Q(\mathbf{x},\mathbf{y},\mathbf{z},\mathbf{v},\boldsymbol{\Theta}(\xi)) - \eta\mathbf{e}, \\ \widehat{\boldsymbol{\varsigma}} \geq \mathbf{0}, \quad \widehat{\boldsymbol{\varrho}} \geq \mathbf{0}, \quad \mathbf{s} \geq \mathbf{0}. \end{array} \right\}
\end{array} \right\}.
\end{aligned}
\tag{A.14}
$$

Finally, the proposed DRO model [DRP-DSRFLP] under the box ambiguity set

$\mathcal{P}^{\text{Box}}$ can be equivalently reformulated as follows:

$$
\begin{aligned}
\min_{\boldsymbol{x},\boldsymbol{y},\boldsymbol{z},\boldsymbol{v},\boldsymbol{\Psi},\tau,\boldsymbol{\varsigma},\boldsymbol{\varrho},\widehat{\tau},\widehat{\boldsymbol{\varsigma}},\widehat{\boldsymbol{\varrho}},\mathbf{s},\eta} \quad & \sum_{k\in K}\sum_{l\in L} c_l^{\text{OPEN}} x_{kl} + \sum_{k\in K} c^{\text{INV}} v_k + \sum_{i\in I}\sum_{d\in D}\sum_{k\in K} c_{ki}^{\text{MANA}} z_{idk} + \lambda\eta \\
& + (1-\lambda)\left[Q(\mathbf{x},\mathbf{y},\mathbf{z},\mathbf{v},\boldsymbol{\Theta}(\xi))^{\intercal}\mathbf{p^0} + \boldsymbol{\Omega}^{\intercal}\boldsymbol{\varsigma} + \boldsymbol{\Omega}^{\intercal}\boldsymbol{\varrho}\right] \\
& + \frac{\lambda}{1-\alpha}[(\mathbf{p^0})^{\intercal}\mathbf{s} + \boldsymbol{\Omega}^{\intercal}\widehat{\boldsymbol{\varsigma}} + \boldsymbol{\Omega}^{\intercal}\widehat{\boldsymbol{\varrho}}] \\
\text{s.t.} \quad & \mathbf{e}\tau + \boldsymbol{\varsigma} - \boldsymbol{\varrho} = Q(\mathbf{x},\mathbf{y},\mathbf{z},\mathbf{v},\boldsymbol{\Theta}(\xi)), \\
& \mathbf{e}\widehat{\tau} + \widehat{\boldsymbol{\varsigma}} - \widehat{\boldsymbol{\varrho}} = \mathbf{s}, \\
& \mathbf{s} \geq Q(\mathbf{x},\mathbf{y},\mathbf{z},\mathbf{v},\boldsymbol{\Theta}(\xi)) - \eta\mathbf{e}, \\
& \boldsymbol{\varsigma} \geq \mathbf{0}, \boldsymbol{\varrho} \geq \mathbf{0}, \widehat{\boldsymbol{\varsigma}} \geq \mathbf{0}, \widehat{\boldsymbol{\varrho}} \geq \mathbf{0}, \mathbf{s} \geq \mathbf{0}, \\
& \text{Constraints}(5.2) - (5.13), \text{Constraints}(5.15) - (5.22),
\end{aligned}
\tag{A.15}
$$

where $(\tau, \boldsymbol{\varsigma}, \boldsymbol{\varrho}, \widehat{\tau}, \widehat{\boldsymbol{\varsigma}}, \widehat{\boldsymbol{\varrho}}) \in \mathbb{R} \times \mathbb{R}_+^{|\Xi|} \times \mathbb{R}_+^{|\Xi|} \times \mathbb{R} \times \mathbb{R}_+^{|\Xi|} \times \mathbb{R}_+^{|\Xi|}$ are dual variables.

The proof of Theorem 5.1 is complete. □

Appendix B

Proposition 5.1

PROPOSITION 5.1. If $(\boldsymbol{x}^*, \boldsymbol{y}^*, \boldsymbol{z}^*, \boldsymbol{v}^*, \boldsymbol{\Psi}^*, \mathbf{s}^*, \Lambda^*, \widehat{\boldsymbol{\varsigma}}^*, \widehat{\boldsymbol{\varrho}}^*, \widehat{\tau}^*, \eta^*)$ solves problem (A.13), then $(\boldsymbol{x}^*, \boldsymbol{y}^*, \boldsymbol{z}^*, \boldsymbol{v}^*, \boldsymbol{\Psi}^*, \mathbf{s}^*, \Lambda^*, \eta^*)$ solves problem (A.8); Conversely, if $\left(\tilde{\boldsymbol{x}}^*, \tilde{\boldsymbol{y}}^*, \tilde{\boldsymbol{z}}^*, \tilde{\boldsymbol{v}}^*, \tilde{\boldsymbol{\Psi}}^*, \tilde{\mathbf{s}}^*, \tilde{\Lambda}^*, \tilde{\eta}^*\right)$ solves problem (A.8), then $\left(\widetilde{\boldsymbol{x}}^*, \widetilde{\boldsymbol{y}}^*, \widetilde{\boldsymbol{z}}^*, \widetilde{\boldsymbol{v}}^*, \widetilde{\boldsymbol{\Psi}}^*, \widetilde{\mathbf{s}}^*, \widetilde{\Lambda}^*, \widetilde{\boldsymbol{\varsigma}}^*, \widetilde{\boldsymbol{\varrho}}^*, \widetilde{\tau}^*, \widetilde{\eta}^*\right)$ solves problem (A.13), where $\left(\widetilde{\boldsymbol{\varsigma}}^*, \widetilde{\boldsymbol{\varrho}}^*, \widetilde{\tau}^*\right)$ is the optimal solution of (A.12).

Appendix C

Mathematical Proof of Proposition 5.1

We let $(\boldsymbol{x}^*, \boldsymbol{y}^*, \boldsymbol{z}^*, \boldsymbol{v}^*, \boldsymbol{\Psi}^*, \mathbf{s}^*, \Lambda^*, \widehat{\boldsymbol{\varsigma}}^*, \widehat{\boldsymbol{\varrho}}^*, \widehat{\tau}^*, \eta^*)$ solves problem (A.13). Based on the Lagrange weak duality theorem, we have

$$\Upsilon^*(\mathbf{s}^*) \leq \boldsymbol{\Omega}^\intercal \widehat{\boldsymbol{\varsigma}}^* + \boldsymbol{\Omega}^\intercal \widehat{\boldsymbol{\varrho}}^*. \tag{C.1}$$

Hence, we have

$$\begin{aligned} \max_{\mathbf{p} \in \mathcal{P}^{\text{Box}}} \eta^* + \frac{1}{1-\alpha} \mathbf{p}^\intercal \mathbf{s}^* &= \eta^* + \frac{1}{1-\alpha} (\mathbf{p}^{\mathbf{0}})^\intercal \mathbf{s}^* + \frac{\Upsilon^*(\mathbf{s}^*)}{1-\alpha} \\ &\leq \eta^* + \frac{1}{1-\alpha} (\mathbf{p}^{\mathbf{0}})^\intercal \mathbf{s}^* + \frac{1}{1-\alpha} (\boldsymbol{\Omega}^\intercal \widehat{\boldsymbol{\varsigma}}^* + \boldsymbol{\Omega}^\intercal \widehat{\boldsymbol{\varrho}}^*). \\ &\leq \Lambda^*. \end{aligned} \tag{C.2}$$

Together with constraints (A.6) and (A.7), we can conclude that $(\boldsymbol{x}^*, \boldsymbol{y}^*, \boldsymbol{z}^*, \boldsymbol{v}^*, \boldsymbol{\Psi}^*, \mathbf{s}^*, \Lambda^*, \eta^*)$ is a feasible solution to problem (A.8).

Now we assume that $(\boldsymbol{x}^*, \boldsymbol{y}^*, \boldsymbol{z}^*, \boldsymbol{v}^*, \boldsymbol{\Psi}^*, \mathbf{s}^*, \Lambda^*, \eta^*)$ is not an optimal solution to

problem (A.8). There exists an optimal solution $\left(\underline{\boldsymbol{x}}^*, \underline{\boldsymbol{y}}^*, \underline{\boldsymbol{z}}^*, \underline{\boldsymbol{v}}^*, \underline{\boldsymbol{\Psi}}^*, \underline{\mathbf{s}}^*, \underline{\Lambda}^*, \underline{\eta}^*\right)$ to problem (A.8) such that

$$\underline{\Lambda}^* < \Lambda^*. \tag{C.3}$$

We let $\left(\widehat{\underline{\boldsymbol{\varsigma}}}^*, \widehat{\underline{\boldsymbol{\varrho}}}^*, \widehat{\underline{\tau}}^*\right)$ be an optimal solution to problem (A.11), Based on the strong duality theorem, we have

$$\begin{aligned} & \underline{\eta}^* + \frac{1}{1-\alpha}(\mathbf{p^0})^\intercal \underline{\mathbf{s}}^* + \frac{1}{1-\alpha}(\boldsymbol{\Omega}^\intercal \widehat{\underline{\boldsymbol{\varsigma}}}^* + \boldsymbol{\Omega}^\intercal \widehat{\underline{\boldsymbol{\varrho}}}^*) \\ = \; & \underline{\eta}^* + \frac{1}{1-\alpha}(\mathbf{p^0})^\intercal \underline{\mathbf{s}}^* + \frac{\Upsilon^*(\underline{\mathbf{s}}^*)}{1-\alpha} \\ = \; & \max_{\mathbf{p}\in\mathcal{P}^{\text{Box}}} \underline{\eta}^* + \frac{1}{1-\alpha}\mathbf{p}^\intercal \underline{\mathbf{s}}^* \leq \; \underline{\Lambda}^*. \end{aligned} \tag{C.4}$$

Together with constraints (A.6), (A.7), and the constraints in (A.12), we can find that $\left(\underline{\boldsymbol{x}}^*, \underline{\boldsymbol{y}}^*, \underline{\boldsymbol{z}}^*, \underline{\boldsymbol{v}}^*, \underline{\boldsymbol{\Psi}}^*, \underline{\mathbf{s}}^*, \underline{\Lambda}^*, \widehat{\underline{\boldsymbol{\varsigma}}}^*, \widehat{\underline{\boldsymbol{\varrho}}}^*, \widehat{\underline{\tau}}^*, \underline{\eta}^*\right)$ is feasible to problem (A.13), which contradicts the assumptions that $(\boldsymbol{x}^*, \boldsymbol{y}^*, \boldsymbol{z}^*, \boldsymbol{v}^*, \boldsymbol{\Psi}^*, \mathbf{s}^*, \Lambda^*, \widehat{\boldsymbol{\varsigma}}^*, \widehat{\boldsymbol{\varrho}}^*, \widehat{\tau}^*, \eta^*)$ is an optimal solution to problem (A.13) because $\underline{\Lambda}^* < \Lambda^*$.

Conversely, we let $\left(\widetilde{\boldsymbol{x}}^*, \widetilde{\boldsymbol{y}}^*, \widetilde{\boldsymbol{z}}^*, \widetilde{\boldsymbol{v}}^*, \widetilde{\boldsymbol{\Psi}}^*, \widetilde{\mathbf{s}}^*, \widetilde{\Lambda}^*, \widetilde{\eta}^*\right)$ be a solution to (A.8) and let $\left(\widetilde{\widehat{\boldsymbol{\varsigma}}}^*, \widetilde{\widehat{\boldsymbol{\varrho}}}^*, \widetilde{\widehat{\tau}}^*\right)$ represent the optimal solution of (A.12). It is obvious to find that the vector $\left(\widetilde{\boldsymbol{x}}^*, \widetilde{\boldsymbol{y}}^*, \widetilde{\boldsymbol{z}}^*, \widetilde{\boldsymbol{v}}^*, \widetilde{\boldsymbol{\Psi}}^*, \widetilde{\mathbf{s}}^*, \widetilde{\Lambda}^*, \widetilde{\widehat{\boldsymbol{\varsigma}}}^*, \widetilde{\widehat{\boldsymbol{\varrho}}}^*, \widetilde{\widehat{\tau}}^*, \widetilde{\eta}^*\right)$ must be a solution to problem (A.13). Similarly, we make an assumption that if $\left(\widetilde{\boldsymbol{x}}^*, \widetilde{\boldsymbol{y}}^*, \widetilde{\boldsymbol{z}}^*, \widetilde{\boldsymbol{v}}^*, \widetilde{\boldsymbol{\Psi}}^*, \widetilde{\mathbf{s}}^*, \widetilde{\Lambda}^*, \widetilde{\widehat{\boldsymbol{\varsigma}}}^*, \widetilde{\widehat{\boldsymbol{\varrho}}}^*, \widetilde{\widehat{\tau}}^*, \widetilde{\eta}^*\right)$ is not the optimal solution of problem (A.13), i.e., the existence of a solution in our research $\left(\underline{\boldsymbol{x}}^*, \underline{\boldsymbol{y}}^*, \underline{\boldsymbol{z}}^*, \underline{\boldsymbol{v}}^*, \underline{\boldsymbol{\Psi}}^*, \underline{\mathbf{s}}^*, \underline{\Lambda}^*, \widehat{\underline{\boldsymbol{\varsigma}}}^*, \widehat{\underline{\boldsymbol{\varrho}}}^*, \widehat{\underline{\tau}}^*, \underline{\eta}^*\right)$ such that $\underline{\Lambda}^* < \widetilde{\Lambda}^*$. Following the logic of the first part of this proof, we can find that $\left(\underline{\boldsymbol{x}}^*, \underline{\boldsymbol{y}}^*, \underline{\boldsymbol{z}}^*, \underline{\boldsymbol{v}}^*, \underline{\boldsymbol{\Psi}}^*, \underline{\mathbf{s}}^*, \underline{\Lambda}^*, \underline{\eta}^*\right)$ is an optimal solution of problem (A.8) This contradicts to the assumption that $\left(\widetilde{\boldsymbol{x}}^*, \widetilde{\boldsymbol{y}}^*, \widetilde{\boldsymbol{z}}^*, \widetilde{\boldsymbol{v}}^*, \widetilde{\boldsymbol{\Psi}}^*, \widetilde{\mathbf{s}}^*, \widetilde{\Lambda}^*, \widetilde{\eta}^*\right)$ solves problem (A.8) because $\underline{\Lambda}^* < \widetilde{\Lambda}^*$.

The proof of Proposition 5.1 is complete. □

Appendix D

Mathematical Proof of Theorem 5.2

Proof of Theorem 5.2. If the probability distribution of the discrete uncertain demand belongs to an ellipsoidal ambiguity set $\mathcal{P}^{\text{Ellipsoidal}}$ that is defined in Eq.(5.36), the expectation part of the model (5.34) can be reformulated as

$$\begin{aligned}
&\min_{\boldsymbol{x},\boldsymbol{y},\boldsymbol{z},\boldsymbol{v},\boldsymbol{\Psi}} \max_{\mathbf{p}\in\mathcal{P}^{\text{Ellipsoidal}}} Q(\mathbf{x},\mathbf{y},\mathbf{z},\mathbf{v},\boldsymbol{\Theta}(\xi))^{\intercal}\mathbf{p} \\
&= \min_{\boldsymbol{x},\boldsymbol{y},\boldsymbol{z},\boldsymbol{v},\boldsymbol{\Psi}} \left\{Q(\mathbf{x},\mathbf{y},\mathbf{z},\mathbf{v},\boldsymbol{\Theta}(\xi))^{\intercal}\mathbf{p^0}\right\} \\
&+ \min_{\boldsymbol{x},\boldsymbol{y},\boldsymbol{z},\boldsymbol{v},\boldsymbol{\Psi}} \left\{\max_{\boldsymbol{\epsilon}} \left[Q(\mathbf{x},\mathbf{y},\mathbf{z},\mathbf{v},\boldsymbol{\Theta}(\xi))^{\intercal}\boldsymbol{A}_1\boldsymbol{\epsilon} \mid \mathbf{e}^{\intercal}\boldsymbol{A}_1\boldsymbol{\epsilon} = 0, \mathbf{p^0} + \boldsymbol{A}_1\boldsymbol{\epsilon} \geq 0, \|\boldsymbol{\epsilon}\|_2 \leq 1\right]\right\}.
\end{aligned} \tag{D.1}$$

Now we consider the inner maximisation problem of Eq.(D.1).

$$\max_{\boldsymbol{\epsilon}} \left[Q(\mathbf{x},\mathbf{y},\mathbf{z},\mathbf{v},\boldsymbol{\Theta}(\xi))^{\intercal}\boldsymbol{A}_1\boldsymbol{\epsilon} \mid \mathbf{e}^{\intercal}\boldsymbol{A}_1\boldsymbol{\epsilon} = 0, \mathbf{p^0} + \boldsymbol{A}_1\boldsymbol{\epsilon} \geq 0, \|\boldsymbol{\epsilon}\|_2 \leq 1\right]. \tag{D.2}$$

The above maximisation problem is equivalent to the following minimisation problem.

$$\min_{\boldsymbol{\epsilon}} \left[-Q(\mathbf{x},\mathbf{y},\mathbf{z},\mathbf{v},\boldsymbol{\Theta}(\xi))^{\intercal}\boldsymbol{A}_1\boldsymbol{\epsilon} \mid \mathbf{e}^{\intercal}\boldsymbol{A}_1\boldsymbol{\epsilon} = 0, \mathbf{p^0} + \boldsymbol{A}_1\boldsymbol{\epsilon} \geq 0, \|\boldsymbol{\epsilon}\|_2 \leq 1\right]. \tag{D.3}$$

The Lagrange function of the above optimisation problem (D.3) is as follows:

$$\mathcal{L}\big(\boldsymbol{\vartheta}, \theta, \zeta; \boldsymbol{\epsilon}\big) = -Q(\mathbf{x}, \mathbf{y}, \mathbf{z}, \mathbf{v}, \boldsymbol{\Theta}(\xi))^{\intercal} \boldsymbol{A}_1 \boldsymbol{\epsilon} + \boldsymbol{\vartheta}^{\intercal}(-\mathbf{p^0} - \mathbf{e}^{\intercal}\boldsymbol{A}_1)\boldsymbol{\epsilon} + \theta(\mathbf{e}^{\intercal}\boldsymbol{A}_1\boldsymbol{\epsilon}) + \zeta(\|\boldsymbol{\epsilon}\|_2 - 1), \tag{D.4}$$

where $\big(\boldsymbol{\vartheta}, \theta, \zeta\big) \in \mathbb{R}^{|\Xi|} \times \mathbb{R} \times \mathbb{R}$ are the Lagrange multipliers.

Then the Lagrange dual function can be formulated as

$$\begin{aligned}
\mathcal{D}\big(\boldsymbol{\vartheta}, \theta, \zeta\big) &= \min_{\boldsymbol{\epsilon}} \mathcal{L}\big(\boldsymbol{\vartheta}, \theta, \zeta; \boldsymbol{\epsilon}\big) \\
&= -(\boldsymbol{p^0})^{\intercal}\boldsymbol{\vartheta} - \zeta - \max_{\boldsymbol{\epsilon}} \left\{ \left[\boldsymbol{A}_1^{\intercal}\boldsymbol{\vartheta} + \boldsymbol{A}_1^{\intercal} Q(\mathbf{x}, \mathbf{y}, \mathbf{z}, \mathbf{v}, \boldsymbol{\Theta}(\xi)) - \theta \boldsymbol{A}_1^{\intercal}\mathbf{e}\right] \boldsymbol{\epsilon} - \zeta\|\boldsymbol{\epsilon}\|_2 \right\} \\
&= -(\boldsymbol{p^0})^{\intercal}\boldsymbol{\vartheta} - \zeta - \mathcal{R}^* \left[\boldsymbol{A}_1^{\intercal}\boldsymbol{\vartheta} + \boldsymbol{A}_1^{\intercal} Q(\mathbf{x}, \mathbf{y}, \mathbf{z}, \mathbf{v}, \boldsymbol{\Theta}(\xi)) - \theta \boldsymbol{A}_1^{\intercal}\mathbf{e}\right],
\end{aligned} \tag{D.5}$$

where

$$\mathcal{R}^*(\cdot) = \begin{cases} 0 & \|\cdot\|_2 \leq \zeta \\ \infty & \text{otherwise} \end{cases} \tag{D.6}$$

is the conjugate function of $\mathcal{R} = \zeta\|\boldsymbol{\epsilon}\|_2$ (Boyd and Vandenberghe, 2004). For any $\zeta \geq 0$ and $\boldsymbol{\vartheta} \geq \mathbf{0}$, the Lagrange dual function can yield lower bounds. Hence, we have the following equivalent problem of Eq.(D.3).

$$\max_{\boldsymbol{\vartheta}, \theta, \zeta} \mathcal{D}\big(\boldsymbol{\vartheta}, \theta, \zeta\big) = \max_{\boldsymbol{\vartheta}, \theta, \zeta} \left\{ -(\boldsymbol{p^0})^{\intercal}\boldsymbol{\vartheta} - \zeta \,\middle|\, \begin{array}{c} \|\boldsymbol{A}_1^{\intercal}\boldsymbol{\vartheta} + \boldsymbol{A}_1^{\intercal} Q(\mathbf{x}, \mathbf{y}, \mathbf{z}, \mathbf{v}, \boldsymbol{\Theta}(\xi)) - \theta \boldsymbol{A}_1^{\intercal}\mathbf{e}\|_2 \leq \zeta \\ \boldsymbol{\vartheta} \geq \mathbf{0}, \quad \zeta \geq 0. \end{array} \right\}. \tag{D.7}$$

Hence, we have the equivalent minimisation problem as follows:

$$\min_{\boldsymbol{\vartheta}, \theta, \zeta} \left\{ (\boldsymbol{p^0})^{\intercal}\boldsymbol{\vartheta} + \zeta \,\middle|\, \begin{array}{c} \|\boldsymbol{A}_1^{\intercal}\boldsymbol{\vartheta} + \boldsymbol{A}_1^{\intercal} Q(\mathbf{x}, \mathbf{y}, \mathbf{z}, \mathbf{v}, \boldsymbol{\Theta}(\xi)) - \theta \boldsymbol{A}_1^{\intercal}\mathbf{e}\|_2 \leq \zeta \\ \boldsymbol{\vartheta} \geq \mathbf{0}, \quad \zeta \geq 0. \end{array} \right\}. \tag{D.8}$$

Therefore, we have

$$\begin{aligned}
&\min_{\boldsymbol{x},\boldsymbol{y},\boldsymbol{z},\boldsymbol{v},\boldsymbol{\Psi},\boldsymbol{\vartheta},\theta,\zeta} \max_{\mathbf{p}\in\mathcal{P}^{\text{Ellipsoidal}}} Q(\mathbf{x},\mathbf{y},\mathbf{z},\mathbf{v},\boldsymbol{\Theta}(\xi))^{\intercal}\mathbf{p} \\
&= \min_{\boldsymbol{x},\boldsymbol{y},\boldsymbol{z},\boldsymbol{v},\boldsymbol{\Psi},\boldsymbol{\vartheta},\theta,\zeta} \left\{ Q(\mathbf{x},\mathbf{y},\mathbf{z},\mathbf{v},\boldsymbol{\Theta}(\xi))^{\intercal}\mathbf{p}^{\mathbf{0}} \right. \\
&\quad \left. +(\boldsymbol{p}^{\mathbf{0}})^{\intercal}\boldsymbol{\vartheta}+\zeta \middle| \begin{array}{c} \|\boldsymbol{A}_1^{\intercal}\boldsymbol{\vartheta}+\boldsymbol{A}_1^{\intercal}Q(\mathbf{x},\mathbf{y},\mathbf{z},\mathbf{v},\boldsymbol{\Theta}(\xi))-\theta\boldsymbol{A}_1^{\intercal}\mathbf{e}\|_2 \le \zeta \\ \boldsymbol{\vartheta}\ge\mathbf{0}, \quad \zeta\ge 0. \end{array} \right\}.
\end{aligned} \tag{D.9}$$

Following the logic of the proof of Theorem 5.1, we can derive the equivalent problem of the $\min_{\boldsymbol{x},\boldsymbol{y},\boldsymbol{z},\boldsymbol{v},\boldsymbol{\Psi}} \text{WCVaR}_{\alpha}(Q(\mathbf{x},\mathbf{y},\mathbf{z},\mathbf{v},\boldsymbol{\Theta}(\xi)))$ as follows:

$$\begin{aligned}
&\min_{\boldsymbol{x},\boldsymbol{y},\boldsymbol{z},\boldsymbol{v},\boldsymbol{\Psi},\mathbf{s},\Lambda,\eta} \Lambda \\
&\text{s.t.} \quad \Lambda \ge \max_{\mathbf{p}\in\mathcal{P}^{\text{Ellipsoidal}}} \eta+\frac{1}{1-\alpha}\mathbf{p}^{\intercal}\mathbf{s}, \\
&\qquad\qquad \text{Constraints (A.6)–(A.7).}
\end{aligned} \tag{D.10}$$

Recall that the distribution probability $\mathbf{p}$ belongs to the ellipsoidal ambiguity set $\mathcal{P}^{\text{Ellipsoidal}}$ expressed in Eq.(5.36), the right-side hand of the first constraints in problem (D.10) can be expressed as

$$\max_{\mathbf{p}\in\mathcal{P}^{\text{Ellipsoidal}}} \eta+\frac{1}{1-\alpha}\mathbf{p}^{\intercal}\mathbf{s} = \eta+\frac{1}{1-\alpha}(\mathbf{p}^{\mathbf{0}})^{\intercal}\mathbf{s}+\frac{\Upsilon^{*}(\mathbf{s})}{1-\alpha}, \tag{D.11}$$

where $\Upsilon^{*}(\mathbf{s})$ denotes the optimal value of the following second-order cone programming.

$$\max_{\boldsymbol{\epsilon}} \left\{ \boldsymbol{s}^{\intercal}\boldsymbol{A}_1\boldsymbol{\epsilon} \mid \mathbf{e}^{\intercal}\boldsymbol{A}_1\boldsymbol{\epsilon}=0, -\mathbf{p}^{\mathbf{0}}-\boldsymbol{A}_1\boldsymbol{\epsilon}\le 0, \|\boldsymbol{\epsilon}\|_2-1\le 0 \right\}. \tag{D.12}$$

Similar to the methodology used to reformulate the expectation part, we have

$$\Upsilon^{*}(\mathbf{s}) = \min_{\widehat{\boldsymbol{\vartheta}},\widehat{\theta},\widehat{\zeta}} \left\{ (\mathbf{p}^{\mathbf{0}})^{\intercal}\widehat{\boldsymbol{\vartheta}}+\widehat{\zeta} \middle| \begin{array}{c} \|\boldsymbol{A}_1^{\intercal}\widehat{\boldsymbol{\vartheta}}+\boldsymbol{A}_1^{\intercal}\mathbf{s}-\widehat{\theta}\boldsymbol{A}_1^{\intercal}\mathbf{e}\|_2 \le \widehat{\zeta} \\ \mathbf{s}\ge Q(\mathbf{x},\mathbf{y},\mathbf{z},\mathbf{v},\boldsymbol{\Theta}(\xi))-\mathbf{e}\eta \\ \widehat{\boldsymbol{\vartheta}}\ge\mathbf{0}, \quad \widehat{\zeta}\ge 0, \quad \mathbf{s}\ge 0. \end{array} \right\}. \tag{D.13}$$

Hence, we have the following minimisation problem.

$$\begin{aligned}\min_{\boldsymbol{x},\boldsymbol{y},\boldsymbol{z},\boldsymbol{v},\boldsymbol{\Psi},\mathbf{s},\Lambda,\widehat{\boldsymbol{\vartheta}},\widehat{\zeta},\widehat{\theta},\eta} \quad & \Lambda \\ \text{s.t.} \quad & \Lambda \geq \eta + \frac{1}{1-\alpha}(\mathbf{p}^0)^\intercal \mathbf{s} + \frac{1}{1-\alpha}\left[(\mathbf{p}^{\mathbf{0}})^\intercal \widehat{\boldsymbol{\vartheta}} + \widehat{\zeta}\right], \\ & \|\boldsymbol{A}_1^\intercal \widehat{\boldsymbol{\vartheta}} + \boldsymbol{A}_1^\intercal \mathbf{s} - \widehat{\theta}\boldsymbol{A}_1^\intercal \mathbf{e}\|_2 \leq \widehat{\zeta}, \\ & \mathbf{s} \geq Q(\mathbf{x},\mathbf{y},\mathbf{z},\mathbf{v},\boldsymbol{\Theta}(\xi)) - \mathbf{e}\eta, \\ & \widehat{\boldsymbol{\vartheta}} \geq \mathbf{0}, \quad \widehat{\zeta} \geq 0, \quad \mathbf{s} \geq 0.\end{aligned} \tag{D.14}$$

Following the logic of Proposition 5.1, we can prove the problem (D.10) is equivalent to problem (D.14).

Therefore, we can express the formula $\min_{\boldsymbol{x},\boldsymbol{y},\boldsymbol{z},\boldsymbol{v},\boldsymbol{\Psi}} \mathrm{WMCVaR}_\alpha(Q(\mathbf{x},\mathbf{y},\mathbf{z},\mathbf{v},\boldsymbol{\Theta}(\xi)))$ in the problem (5.32) as

$$\begin{aligned}&\min_{\boldsymbol{x},\boldsymbol{y},\boldsymbol{z},\boldsymbol{v},\boldsymbol{\Psi}} \mathrm{WMCVaR}_\alpha(Q(\mathbf{x},\mathbf{y},\mathbf{z},\mathbf{v},\boldsymbol{\Theta}(\xi))) \\ =& \min_{\boldsymbol{x},\boldsymbol{y},\boldsymbol{z},\boldsymbol{v},\boldsymbol{\Psi}} (1-\lambda) \sup_{\mathbf{p}\in\mathcal{P}^{\text{Ellipsoidal}}} \mathbb{E}(Q(\mathbf{x},\mathbf{y},\mathbf{z},\mathbf{v},\boldsymbol{\Theta}(\xi))) + \lambda \mathrm{WCVaR}_\alpha(Q(\mathbf{x},\mathbf{y},\mathbf{z},\mathbf{v},\boldsymbol{\Theta}(\xi))) \\ =& \min_{\boldsymbol{x},\boldsymbol{y},\boldsymbol{z},\boldsymbol{v},\boldsymbol{\Psi}} \left\{ \begin{array}{l} \min_{\boldsymbol{\vartheta},\theta,\zeta} (1-\lambda)[Q(\mathbf{x},\mathbf{y},\mathbf{z},\mathbf{v},\boldsymbol{\Theta}(\xi))^\intercal \mathbf{p}^{\mathbf{0}} + (\boldsymbol{p}^{\mathbf{0}})^\intercal \boldsymbol{\vartheta} + \zeta] \left| \begin{array}{c} \|\boldsymbol{A}_1^\intercal \boldsymbol{\vartheta} + \boldsymbol{A}_1^\intercal Q(\mathbf{x},\mathbf{y},\mathbf{z},\mathbf{v},\boldsymbol{\Theta}(\xi)) - \theta \boldsymbol{A}_1^\intercal \mathbf{e}\|_2 \\ \leq \zeta, \quad \boldsymbol{\vartheta} \geq \mathbf{0}, \quad \zeta \geq 0. \end{array} \right. \\ \quad +\lambda \min_{\widehat{\boldsymbol{\vartheta}},\widehat{\theta},\widehat{\zeta},\mathbf{s},\eta} \left\{ \eta + \frac{1}{1-\alpha}(\mathbf{p}^{\mathbf{0}})^\intercal \mathbf{s} + \frac{1}{1-\alpha}[(\mathbf{p}^0)^\intercal \widehat{\boldsymbol{\vartheta}} + \widehat{\zeta}] \left| \begin{array}{c} \|\boldsymbol{A}_1^\intercal \widehat{\boldsymbol{\vartheta}} + \boldsymbol{A}_1^\intercal \mathbf{s} - \widehat{\theta}\boldsymbol{A}_1^\intercal \mathbf{e}\|_2 \leq \widehat{\zeta}, \\ \mathbf{s} \geq Q(\mathbf{x},\mathbf{y},\mathbf{z},\mathbf{v},\boldsymbol{\Theta}(\xi)) - \mathbf{e}\eta, \\ \widehat{\boldsymbol{\vartheta}} \geq \mathbf{0}, \quad \widehat{\zeta} \geq 0, \quad \mathbf{s} \geq 0. \end{array} \right. \right\} \end{array} \right\}. \end{aligned} \tag{D.15}$$

Finally, the proposed DRO model [DRP-DSRFLP] under the ellipsoidal ambiguity

set $\mathcal{P}^{\text{Ellipsoidal}}$ can be equivalently reformulated as follows:

$$
\begin{aligned}
\min_{\boldsymbol{x},\boldsymbol{y},\boldsymbol{z},\boldsymbol{v},\boldsymbol{\Psi},\boldsymbol{\vartheta},\theta,\zeta,\widehat{\boldsymbol{\vartheta}},\widehat{\theta},\widehat{\zeta},\mathbf{s},\eta} \quad & \sum_{k\in K}\sum_{l\in L} c_l^{\text{OPEN}} x_{kl} + \sum_{k\in K} c^{\text{INV}} v_k + \sum_{i\in I}\sum_{d\in D}\sum_{k\in K} c_{ki}^{\text{MANA}} z_{idk} + \lambda\eta \\
& + (1-\lambda)\left[Q(\mathbf{x},\mathbf{y},\mathbf{z},\mathbf{v},\boldsymbol{\Theta}(\xi))^{\intercal}\mathbf{p^0} + (\boldsymbol{p^0})^{\intercal}\boldsymbol{\vartheta} + \zeta\right] \\
& + \frac{\lambda}{1-\alpha}[(\mathbf{p}^0)^{\intercal}\mathbf{s} + \left(\mathbf{p}^0\right)^{\intercal}\widehat{\boldsymbol{\vartheta}} + \widehat{\zeta}] \\
\text{s.t.} \quad & \|\boldsymbol{A}_1^{\intercal}\boldsymbol{\vartheta} + \boldsymbol{A}_1^{\intercal}Q(\mathbf{x},\mathbf{y},\mathbf{z},\mathbf{v},\boldsymbol{\Theta}(\xi)) - \theta\boldsymbol{A}_1^{\intercal}\mathbf{e}\|_2 \leq \zeta, \\
& \|\boldsymbol{A}_1^{\intercal}\widehat{\boldsymbol{\vartheta}} + \boldsymbol{A}_1^{\intercal}\mathbf{s} - \widehat{\theta}\boldsymbol{A}_1^{\intercal}\mathbf{e}\|_2 \leq \widehat{\zeta}, \\
& \mathbf{s} \geq Q(\mathbf{x},\mathbf{y},\mathbf{z},\mathbf{v},\boldsymbol{\Theta}(\xi)) - \eta\mathbf{e}, \\
& \boldsymbol{\vartheta} \geq \mathbf{0}, \quad \zeta \geq 0, \quad \widehat{\boldsymbol{\vartheta}} \geq \mathbf{0}, \quad \widehat{\zeta} \geq 0, \quad \mathbf{s} \geq 0, \\
& \text{Constraints (5.2)} - \text{(5.13)}, \text{Constraints (5.15)} - \text{(5.22)},
\end{aligned}
\tag{D.16}
$$

where $\left(\boldsymbol{\vartheta},\theta,\zeta,\widehat{\boldsymbol{\vartheta}},\widehat{\theta},\widehat{\zeta}\right) \in \mathbb{R}_+^{|\Xi|}\times\mathbb{R}\times\mathbb{R}_+\times\mathbb{R}_+^{|\Xi|}\times\mathbb{R}\times\mathbb{R}_+$ are Lagrange multipliers.

The proof of Theorem 5.2 is complete. □

Appendix E

Mathematical Proof of Theorem 5.3

Proof of Theorem 5.3. If the probability distribution of the discrete uncertain demand belongs to a polyhedral ambiguity set $\mathcal{P}^{\text{Polyhedral}}$ that is defined in Eq.(5.37), the expectation part of the model (5.34) can be reformulated as

$$\begin{aligned}
&\min_{\boldsymbol{x},\boldsymbol{y},\boldsymbol{z},\boldsymbol{v},\boldsymbol{\Psi}} \max_{\mathbf{p}\in\mathcal{P}^{\text{Polyhedral}}} Q(\mathbf{x},\mathbf{y},\mathbf{z},\mathbf{v},\boldsymbol{\Theta}(\xi))^{\intercal}\mathbf{p} \\
&= \min_{\boldsymbol{x},\boldsymbol{y},\boldsymbol{z},\boldsymbol{v},\boldsymbol{\Psi}} \left\{Q(\mathbf{x},\mathbf{y},\mathbf{z},\mathbf{v},\boldsymbol{\Theta}(\xi))^{\intercal}\mathbf{p^0}\right\} \\
&+ \min_{\boldsymbol{x},\boldsymbol{y},\boldsymbol{z},\boldsymbol{v},\boldsymbol{\Psi}} \left\{\max_{\boldsymbol{\epsilon}} \left[Q(\mathbf{x},\mathbf{y},\mathbf{z},\mathbf{v},\boldsymbol{\Theta}(\xi))^{\intercal}\boldsymbol{A}_2\boldsymbol{\epsilon} \mid \mathbf{e}^{\intercal}\boldsymbol{A}_2\boldsymbol{\epsilon}=0, \mathbf{p^0}+\boldsymbol{A}_2\boldsymbol{\epsilon}\geq 0, \|\boldsymbol{\epsilon}\|_1\leq 1\right]\right\}.
\end{aligned} \tag{E.1}$$

The Lagrange function of the inner maximisation problem can be expressed as follows:

$$\mathcal{L}\big(\boldsymbol{\pi},\kappa,\varphi;\boldsymbol{\epsilon}\big) = -Q(\mathbf{x},\mathbf{y},\mathbf{z},\mathbf{v},\boldsymbol{\Theta}(\xi))^{\intercal}\boldsymbol{A}_2\boldsymbol{\epsilon} + \boldsymbol{\pi}^{\intercal}(-\mathbf{p^0}-\mathbf{e}^{\intercal}\boldsymbol{A}_2)\boldsymbol{\epsilon} + \kappa(\mathbf{e}^{\intercal}\boldsymbol{A}_2\boldsymbol{\epsilon}) + \varphi(\|\boldsymbol{\epsilon}\|_1 - 1), \tag{E.2}$$

where $\big(\boldsymbol{\pi},\kappa,\varphi\big) \in \mathbb{R}^{|\Xi|}\times\mathbb{R}\times\mathbb{R}$ are the Lagrange multipliers.

Then the Lagrange dual function can be formulated as

$$\begin{aligned}\mathcal{D}\left(\boldsymbol{\pi}, \kappa, \varphi; \boldsymbol{\epsilon}\right) &= \min_{\boldsymbol{\epsilon}} \mathcal{L}\left(\boldsymbol{\pi}, \kappa, \varphi; \boldsymbol{\epsilon}\right) \\ &= -(\boldsymbol{p^0})^\intercal \boldsymbol{\pi} - \varphi - \max_{\boldsymbol{\epsilon}} \left\{ \left[\boldsymbol{A}_2^\intercal \boldsymbol{\pi} + \boldsymbol{A}_2^\intercal Q(\mathbf{x}, \mathbf{y}, \mathbf{z}, \mathbf{v}, \boldsymbol{\Theta}(\xi)) - \kappa \boldsymbol{A}_2^\intercal \mathbf{e}\right] \boldsymbol{\epsilon} - \varphi \|\boldsymbol{\epsilon}\|_1 \right\} \\ &= -(\boldsymbol{p^0})^\intercal \boldsymbol{\pi} - \varphi - \mathcal{R}^* \left[\boldsymbol{A}_2^\intercal \boldsymbol{\pi} + \boldsymbol{A}_2^\intercal Q(\mathbf{x}, \mathbf{y}, \mathbf{z}, \mathbf{v}, \boldsymbol{\Theta}(\xi)) - \kappa \boldsymbol{A}_2^\intercal \mathbf{e}\right], \end{aligned} \tag{E.3}$$

where

$$\mathcal{R}^*(\cdot) = \begin{cases} 0 & \|\cdot\|_\infty \leq \varphi \\ \infty & \text{otherwise} \end{cases} \tag{E.4}$$

is the conjugate function of $\mathcal{R} = \varphi\|\boldsymbol{\epsilon}\|_1$ (Boyd and Vandenberghe, 2004). For any $\varphi \geq 0$ and $\boldsymbol{\pi} \geq \mathbf{0}$, the Lagrange dual function can yield lower bounds. Referring the logic of the proof of Theorem 5.2, we have the equivalent problem of the expectation part as follows:

$$\begin{aligned} &\min_{\boldsymbol{x},\boldsymbol{y},\boldsymbol{z},\boldsymbol{v},\boldsymbol{\Psi}} \max_{\mathbf{p}\in\mathcal{P}^{\text{Polyehedral}}} Q(\mathbf{x}, \mathbf{y}, \mathbf{z}, \mathbf{v}, \boldsymbol{\Theta}(\xi))^\intercal \mathbf{p} \\ &= \min_{\boldsymbol{x},\boldsymbol{y},\boldsymbol{z},\boldsymbol{v},\boldsymbol{\Psi},\boldsymbol{\pi},\kappa,\varphi} \left\{ Q(\mathbf{x}, \mathbf{y}, \mathbf{z}, \mathbf{v}, \boldsymbol{\Theta}(\xi))^\intercal \mathbf{p^0} + (\boldsymbol{p^0})^\intercal \boldsymbol{\pi} + \varphi \;\middle|\; \begin{array}{c} \|\boldsymbol{A}_2^\intercal \boldsymbol{\pi} + \boldsymbol{A}_2^\intercal Q(\mathbf{x}, \mathbf{y}, \mathbf{z}, \mathbf{v}, \boldsymbol{\Theta}(\xi)) - \kappa \boldsymbol{A}_2^\intercal \mathbf{e}\|_\infty \leq \varphi \\ \boldsymbol{\pi} \geq \mathbf{0}, \quad \varphi \geq 0. \end{array} \right\}. \end{aligned} \tag{E.5}$$

Similar to the logic of the Theorem 5.1, we can derive the equivalent problem of the $\min_{\boldsymbol{x},\boldsymbol{y},\boldsymbol{z},\boldsymbol{v},\boldsymbol{\Psi}} \text{WCVaR}_\alpha(Q(\mathbf{x}, \mathbf{y}, \mathbf{z}, \mathbf{v}, \boldsymbol{\Theta}(\xi)))$ as follows:

$$\begin{aligned} &\min_{\boldsymbol{x},\boldsymbol{y},\boldsymbol{z},\boldsymbol{v},\boldsymbol{\Psi},\mathbf{s},\Lambda,\eta} \Lambda \\ &\text{s.t.} \quad \Lambda \geq \max_{\mathbf{p}\in\mathcal{P}^{\text{Polyhedral}}} \eta + \frac{1}{1-\alpha}\mathbf{p}^\intercal \mathbf{s}, \\ &\qquad\qquad \text{Constraints (A.6)–(A.7).} \end{aligned} \tag{E.6}$$

Based on the logic of the proof of Theorem 5.2, we have the following equivalent minimisation problem.

$$
\begin{aligned}
\min_{\boldsymbol{x},\boldsymbol{y},\boldsymbol{z},\boldsymbol{v},\boldsymbol{\Psi},\mathbf{s},\Lambda,\widehat{\boldsymbol{\pi}},\widehat{\varphi},\widehat{\kappa},\eta} \quad & \Lambda \\
\text{s.t.} \quad & \Lambda \geq \eta + \frac{1}{1-\alpha}(\mathbf{p}^0)^{\intercal}\mathbf{s} + \frac{1}{1-\alpha}\left[(\mathbf{p}^{\mathbf{0}})^{\intercal}\widehat{\boldsymbol{\pi}} + \widehat{\varphi}\right], \\
& \|\boldsymbol{A}_2^{\intercal}\widehat{\boldsymbol{\pi}} + \boldsymbol{A}_2^{\intercal}\mathbf{s} - \widehat{\kappa}\boldsymbol{A}_2^{\intercal}\mathbf{e}\|_{\infty} \leq \widehat{\varphi}, \\
& \mathbf{s} \geq Q(\mathbf{x},\mathbf{y},\mathbf{z},\mathbf{v},\boldsymbol{\Theta}(\xi)) - \mathbf{e}\eta, \\
& \widehat{\boldsymbol{\pi}} \geq \mathbf{0}, \quad \widehat{\varphi} \geq 0, \quad \mathbf{s} \geq 0.
\end{aligned}
\tag{E.7}
$$

Following the logic of Proposition 5.1, we can prove the problem (E.7) is equivalent to problem (E.6).

Therefore, we can express the formula $\min_{\boldsymbol{x},\boldsymbol{y},\boldsymbol{z},\boldsymbol{v},\boldsymbol{\Psi}} \mathrm{WMCVaR}_{\alpha}(Q(\mathbf{x},\mathbf{y},\mathbf{z},\mathbf{v},\boldsymbol{\Theta}(\xi)))$ in the problem (5.32) as

$$
\begin{aligned}
& \min_{\boldsymbol{x},\boldsymbol{y},\boldsymbol{z},\boldsymbol{v},\boldsymbol{\Psi}} \mathrm{WMCVaR}_{\alpha}(Q(\mathbf{x},\mathbf{y},\mathbf{z},\mathbf{v},\boldsymbol{\Theta}(\xi))) \\
= & \min_{\boldsymbol{x},\boldsymbol{y},\boldsymbol{z},\boldsymbol{v},\boldsymbol{\Psi}} (1-\lambda) \sup_{\mathbf{p}\in\mathcal{P}^{\mathrm{Polyhedral}}} \mathbb{E}(Q(\mathbf{x},\mathbf{y},\mathbf{z},\mathbf{v},\boldsymbol{\Theta}(\xi))) + \lambda \mathrm{WCVaR}_{\alpha}(Q(\mathbf{x},\mathbf{y},\mathbf{z},\mathbf{v},\boldsymbol{\Theta}(\xi))) \\
= & \min_{\boldsymbol{x},\boldsymbol{y},\boldsymbol{z},\boldsymbol{v},\boldsymbol{\Psi}} \left\{ \begin{array}{l} \min\limits_{\boldsymbol{\pi},\kappa,\varphi} (1-\lambda)[Q(\mathbf{x},\mathbf{y},\mathbf{z},\mathbf{v},\boldsymbol{\Theta}(\xi))^{\intercal}\mathbf{p}^{\mathbf{0}} + (\boldsymbol{p}^{\mathbf{0}})^{\intercal}\boldsymbol{\pi} + \varphi] \left| \begin{array}{l} \|\boldsymbol{A}_2^{\intercal}\boldsymbol{\pi} + \boldsymbol{A}_2^{\intercal}Q(\mathbf{x},\mathbf{y},\mathbf{z},\mathbf{v},\boldsymbol{\Theta}(\xi)) - \kappa\boldsymbol{A}_2^{\intercal}\mathbf{e}\|_{\infty} \\ \leq \varphi, \quad \boldsymbol{\pi} \geq \mathbf{0}, \quad \varphi \geq 0. \end{array} \right. \\ \quad +\lambda \min\limits_{\widehat{\boldsymbol{\pi}},\widehat{\kappa},\widehat{\varphi},\mathbf{s},\eta} \left\{ \eta + \frac{1}{1-\alpha}(\mathbf{p}^{\mathbf{0}})^{\intercal}\mathbf{s} + \frac{1}{1-\alpha}[(\mathbf{p}^{\mathbf{0}})^{\intercal}\widehat{\boldsymbol{\pi}} + \widehat{\varphi}] \left| \begin{array}{c} \|\boldsymbol{A}_2^{\intercal}\widehat{\boldsymbol{\pi}} + \boldsymbol{A}_2^{\intercal}\mathbf{s} - \widehat{\kappa}\boldsymbol{A}_2^{\intercal}\mathbf{e}\|_{\infty} \leq \widehat{\varphi}, \\ \mathbf{s} \geq Q(\mathbf{x},\mathbf{y},\mathbf{z},\mathbf{v},\boldsymbol{\Theta}(\xi)) - \mathbf{e}\eta, \\ \widehat{\boldsymbol{\pi}} \geq \mathbf{0}, \quad \widehat{\varphi} \geq 0, \quad \mathbf{s} \geq 0. \end{array} \right. \right\} \end{array} \right\}.
\end{aligned}
\tag{E.8}
$$

Finally, the proposed DRO model [DRP-DSRFLP] under the polyhedral ambiguity

set $\mathcal{P}^{\text{Polyhedral}}$ can be equivalently reformulated as follows:

$$
\begin{aligned}
\min_{\boldsymbol{x},\boldsymbol{y},\boldsymbol{z},\boldsymbol{v},\boldsymbol{\Psi},\boldsymbol{\pi},\kappa,\varphi,\widehat{\boldsymbol{\pi}},\widehat{\kappa},\widehat{\varphi},\mathbf{s},\eta} \quad & \sum_{k\in K}\sum_{l\in L} c_l^{\text{OPEN}} x_{kl} + \sum_{k\in K} c^{\text{INV}} v_k + \sum_{i\in I}\sum_{d\in D}\sum_{k\in K} c_{ki}^{\text{MANA}} z_{idk} + \lambda\eta \\
& + (1-\lambda)\left[Q(\mathbf{x},\mathbf{y},\mathbf{z},\mathbf{v},\boldsymbol{\Theta}(\xi))^{\intercal}\mathbf{p^0} + (\boldsymbol{p^0})^{\intercal}\boldsymbol{\pi} + \varphi\right] \\
& + \frac{\lambda}{1-\alpha}[(\mathbf{p}^0)^{\intercal}\mathbf{s} + \left(\mathbf{p}^0\right)^{\intercal}\widehat{\boldsymbol{\pi}} + \widehat{\varphi}] \\
\text{s.t.} \quad & \|\boldsymbol{A}_2^{\intercal}\boldsymbol{\pi} + \boldsymbol{A}_2^{\intercal}Q(\mathbf{x},\mathbf{y},\mathbf{z},\mathbf{v},\boldsymbol{\Theta}(\xi)) - \kappa\boldsymbol{A}_2^{\intercal}\mathbf{e}\|_\infty \le \varphi, \\
& \|\boldsymbol{A}_2^{\intercal}\widehat{\boldsymbol{\pi}} + \boldsymbol{A}_2^{\intercal}\mathbf{s} - \widehat{\kappa}\boldsymbol{A}_2^{\intercal}\mathbf{e}\|_\infty \le \widehat{\varphi}, \\
& \mathbf{s} \ge Q(\mathbf{x},\mathbf{y},\mathbf{z},\mathbf{v},\boldsymbol{\Theta}(\xi)) - \eta\mathbf{e}, \\
& \boldsymbol{\pi} \ge \mathbf{0}, \quad \varphi \ge 0, \quad \widehat{\boldsymbol{\pi}} \ge \mathbf{0}, \quad \widehat{\varphi} \ge 0, \quad \mathbf{s} \ge 0, \\
& \text{Constraints (5.2)} - \text{(5.13)}, \text{Constraints (5.15)} - \text{(5.22)},
\end{aligned}
\tag{E.9}
$$

where $(\boldsymbol{\pi}, \kappa, \varphi, \widehat{\boldsymbol{\pi}}, \widehat{\kappa}, \widehat{\varphi}) \in \mathbb{R}_+^{|\Xi|} \times \mathbb{R} \times \mathbb{R}_+ \times \mathbb{R}_+^{|\Xi|} \times \mathbb{R} \times \mathbb{R}_+$ are Lagrange multipliers.

The proof of Theorem 5.3 is complete. □

Appendix F

DRO Formulations of Model Extension Considering Multiple Relief Items

The DRO formulation under the box ambiguity set is as follows:

$$
\begin{aligned}
\min_{\boldsymbol{x},\boldsymbol{y},\boldsymbol{z},\boldsymbol{v},\boldsymbol{\Psi},\tau,\boldsymbol{\varsigma},\boldsymbol{\varrho},\widehat{\tau},\widehat{\boldsymbol{\varsigma}},\widehat{\boldsymbol{\varrho}},\mathbf{s},\eta} \quad & \sum_{k\in K}\sum_{l\in L} c_l^{\mathrm{OPEN}} x_{kl} + \sum_{k\in K}\sum_{b\in B} c_b^{\mathrm{INV}} v_{kb} + \sum_{i\in I}\sum_{d\in D}\sum_{k\in K} c_{ki}^{\mathrm{MANA}} z_{idk} + \lambda\eta \\
& + (1-\lambda)\left[U_1(\mathbf{x},\mathbf{y},\mathbf{z},\mathbf{v},\boldsymbol{\Theta}(\xi))^{\intercal}\mathbf{p^0} + \boldsymbol{\Omega}^{\intercal}\boldsymbol{\varsigma} + \boldsymbol{\Omega}^{\intercal}\boldsymbol{\varrho}\right] \\
& + \frac{\lambda}{1-\alpha}[(\mathbf{p^0})^{\intercal}\mathbf{s} + \boldsymbol{\Omega}^{\intercal}\widehat{\boldsymbol{\varsigma}} + \boldsymbol{\Omega}^{\intercal}\widehat{\boldsymbol{\varrho}}] \\
\text{s.t.} \quad & \mathbf{e}\tau + \boldsymbol{\varsigma} - \boldsymbol{\varrho} = U_1(\mathbf{x},\mathbf{y},\mathbf{z},\mathbf{v},\boldsymbol{\Theta}(\xi)), \\
& \mathbf{e}\widehat{\tau} + \widehat{\boldsymbol{\varsigma}} - \widehat{\boldsymbol{\varrho}} = \mathbf{s}, \\
& \mathbf{s} \geq U_1(\mathbf{x},\mathbf{y},\mathbf{z},\mathbf{v},\boldsymbol{\Theta}(\xi)) - \eta\mathbf{e}, \\
& \boldsymbol{\varsigma} \geq \mathbf{0}, \boldsymbol{\varrho} \geq \mathbf{0}, \widehat{\boldsymbol{\varsigma}} \geq \mathbf{0}, \widehat{\boldsymbol{\varrho}} \geq \mathbf{0}, \mathbf{s} \geq \mathbf{0}, \\
& \text{Constraints (5.2)} - \text{(5.5)}, \text{(5.7)} - \text{(5.12)}, \\
& \text{(5.43)} - \text{(5.44) and (5.46)} - \text{(5.53)},
\end{aligned}
\tag{F.1}
$$

where $(\tau, \boldsymbol{\varsigma}, \boldsymbol{\varrho}, \widehat{\tau}, \widehat{\boldsymbol{\varsigma}}, \widehat{\boldsymbol{\varrho}}) \in \mathbb{R} \times \mathbb{R}_+^{|\Xi|} \times \mathbb{R}_+^{|\Xi|} \times \mathbb{R} \times \mathbb{R}_+^{|\Xi|} \times \mathbb{R}_+^{|\Xi|}$ are dual variables.

The DRO formulation under the ellipsoidal ambiguity set is as follows:

$$
\begin{aligned}
\min_{\boldsymbol{x},\boldsymbol{y},\boldsymbol{z},\boldsymbol{v},\boldsymbol{\Psi},\boldsymbol{\vartheta},\theta,\zeta,\widehat{\boldsymbol{\vartheta}},\widehat{\theta},\widehat{\zeta},\mathbf{s},\eta} \quad & \sum_{k\in K}\sum_{l\in L} c_l^{\mathrm{OPEN}} x_{kl} + \sum_{k\in K}\sum_{b\in B} c_b^{\mathrm{INV}} v_{kb} + \sum_{i\in I}\sum_{d\in D}\sum_{k\in K} c_{ki}^{\mathrm{MANA}} z_{idk} + \lambda\eta \\
& + (1-\lambda)\left[U_1(\mathbf{x},\mathbf{y},\mathbf{z},\mathbf{v},\boldsymbol{\Theta}(\xi))^\intercal \mathbf{p^0} + (\boldsymbol{p^0})^\intercal \boldsymbol{\vartheta} + \zeta\right] \\
& + \frac{\lambda}{1-\alpha}[(\mathbf{p}^0)^\intercal \mathbf{s} + \left(\mathbf{p}^0\right)^\intercal \widehat{\boldsymbol{\vartheta}} + \widehat{\zeta}] \\
\text{s.t.} \quad & \|\boldsymbol{A}_1^\intercal \boldsymbol{\vartheta} + \boldsymbol{A}_1^\intercal U_1(\mathbf{x},\mathbf{y},\mathbf{z},\mathbf{v},\boldsymbol{\Theta}(\xi)) - \theta \boldsymbol{A}_1^\intercal \mathbf{e}\|_2 \le \zeta, \\
& \|\boldsymbol{A}_1^\intercal \widehat{\boldsymbol{\vartheta}} + \boldsymbol{A}_1^\intercal \mathbf{s} - \widehat{\theta} \boldsymbol{A}_1^\intercal \mathbf{e}\|_2 \le \widehat{\zeta}, \\
& \mathbf{s} \ge U_1(\mathbf{x},\mathbf{y},\mathbf{z},\mathbf{v},\boldsymbol{\Theta}(\xi)) - \eta \mathbf{e}, \\
& \boldsymbol{\vartheta} \ge \mathbf{0}, \quad \zeta \ge 0, \quad \widehat{\boldsymbol{\vartheta}} \ge \mathbf{0}, \quad \widehat{\zeta} \ge 0, \quad \mathbf{s} \ge 0, \\
& \text{Constraints (5.2)} - \text{(5.5)}, \text{(5.7)} - \text{(5.12)}, \\
& \text{(5.43)} - \text{(5.44) and (5.46)} - \text{(5.53)},
\end{aligned}
\tag{F.2}
$$

where $\left(\boldsymbol{\vartheta}, \theta, \zeta, \widehat{\boldsymbol{\vartheta}}, \widehat{\theta}, \widehat{\zeta}\right) \in \mathbb{R}_+^{|\Xi|} \times \mathbb{R} \times \mathbb{R}_+ \times \mathbb{R}_+^{|\Xi|} \times \mathbb{R} \times \mathbb{R}_+$ are Lagrange multipliers.

The DRO formulation under the polyhedral ambiguity set is as follows:

$$
\begin{aligned}
\min_{\boldsymbol{x},\boldsymbol{y},\boldsymbol{z},\boldsymbol{v},\boldsymbol{\Psi},\boldsymbol{\pi},\kappa,\varphi,\widehat{\boldsymbol{\pi}},\widehat{\kappa},\widehat{\varphi},\mathbf{s},\eta} \quad & \sum_{k\in K}\sum_{l\in L} c_l^{\mathrm{OPEN}} x_{kl} + \sum_{k\in K}\sum_{b\in B} c_b^{\mathrm{INV}} v_{kb} + \sum_{i\in I}\sum_{d\in D}\sum_{k\in K} c_{ki}^{\mathrm{MANA}} z_{idk} + \lambda\eta \\
& + (1-\lambda)\left[U_1(\mathbf{x},\mathbf{y},\mathbf{z},\mathbf{v},\boldsymbol{\Theta}(\xi))^{\intercal}\mathbf{p^0} + (\boldsymbol{p^0})^{\intercal}\boldsymbol{\pi} + \varphi\right] \\
& + \frac{\lambda}{1-\alpha}[(\mathbf{p}^0)^{\intercal}\mathbf{s} + \left(\mathbf{p}^0\right)^{\intercal}\widehat{\boldsymbol{\pi}} + \widehat{\varphi}] \\
\text{s.t.} \quad & \|\boldsymbol{A}_2^{\intercal}\boldsymbol{\pi} + \boldsymbol{A}_2^{\intercal}U_1(\mathbf{x},\mathbf{y},\mathbf{z},\mathbf{v},\boldsymbol{\Theta}(\xi)) - \kappa\boldsymbol{A}_2^{\intercal}\mathbf{e}\|_\infty \le \varphi, \\
& \|\boldsymbol{A}_2^{\intercal}\widehat{\boldsymbol{\pi}} + \boldsymbol{A}_2^{\intercal}\mathbf{s} - \widehat{\kappa}\boldsymbol{A}_2^{\intercal}\mathbf{e}\|_\infty \le \widehat{\varphi}, \\
& \mathbf{s} \ge U_1(\mathbf{x},\mathbf{y},\mathbf{z},\mathbf{v},\boldsymbol{\Theta}(\xi)) - \eta\mathbf{e}, \\
& \boldsymbol{\pi} \ge \mathbf{0}, \quad \varphi \ge 0, \quad \widehat{\boldsymbol{\pi}} \ge \mathbf{0}, \quad \widehat{\varphi} \ge 0, \quad \mathbf{s} \ge 0, \\
& \text{Constraints (5.2)} - \text{(5.5)}, \text{(5.7)} - \text{(5.12)}, \\
& \text{(5.43)} - \text{(5.44) and (5.46)} - \text{(5.53)},
\end{aligned}
\tag{F.3}
$$

where $(\boldsymbol{\pi}, \kappa, \varphi, \widehat{\boldsymbol{\pi}}, \widehat{\kappa}, \widehat{\varphi}) \in \mathbb{R}_+^{|\Xi|} \times \mathbb{R} \times \mathbb{R}_+ \times \mathbb{R}_+^{|\Xi|} \times \mathbb{R} \times \mathbb{R}_+$ are Lagrange multipliers.

Appendix G

DRO Formulations of Model Extension Considering Equity Constraint in Priority Setting

The DRO formulation under the box ambiguity set is as follows:

$$
\begin{aligned}
\min_{\boldsymbol{x},\boldsymbol{y},\boldsymbol{z},\boldsymbol{v},\boldsymbol{\Psi},\tau,\boldsymbol{\varsigma},\boldsymbol{\varrho},\widehat{\tau},\widehat{\boldsymbol{\varsigma}},\widehat{\boldsymbol{\varrho}},\mathbf{s},\eta} \quad & \sum_{k\in K}\sum_{l\in L} c_l^{\text{OPEN}} x_{kl} + \sum_{k\in K}\sum_{b\in B} c_b^{\text{INV}} v_{kb} + \sum_{i\in I}\sum_{d\in D}\sum_{k\in K} c_{ki}^{\text{MANA}} z_{idk} + \lambda\eta \\
& + (1-\lambda)\left[U_2(\mathbf{x},\mathbf{y},\mathbf{z},\mathbf{v},\boldsymbol{\Theta}(\xi))^{\intercal}\mathbf{p^0} + \boldsymbol{\Omega}^{\intercal}\boldsymbol{\varsigma} + \boldsymbol{\Omega}^{\intercal}\boldsymbol{\varrho}\right] \\
& + \frac{\lambda}{1-\alpha}[(\mathbf{p^0})^{\intercal}\mathbf{s} + \boldsymbol{\Omega}^{\intercal}\widehat{\boldsymbol{\varsigma}} + \boldsymbol{\Omega}^{\intercal}\widehat{\boldsymbol{\varrho}}] \\
\text{s.t.} \quad & \mathbf{e}\tau + \boldsymbol{\varsigma} - \boldsymbol{\varrho} = U_2(\mathbf{x},\mathbf{y},\mathbf{z},\mathbf{v},\boldsymbol{\Theta}(\xi)), \\
& \mathbf{e}\widehat{\tau} + \widehat{\boldsymbol{\varsigma}} - \widehat{\boldsymbol{\varrho}} = \mathbf{s}, \\
& \mathbf{s} \geq U_2(\mathbf{x},\mathbf{y},\mathbf{z},\mathbf{v},\boldsymbol{\Theta}(\xi)) - \eta\mathbf{e}, \\
& \boldsymbol{\varsigma} \geq \mathbf{0}, \boldsymbol{\varrho} \geq \mathbf{0}, \widehat{\boldsymbol{\varsigma}} \geq \mathbf{0}, \widehat{\boldsymbol{\varrho}} \geq \mathbf{0}, \mathbf{s} \geq \mathbf{0}, \\
& \text{Constraints (5.2)} - \text{(5.5)}, \text{(5.7)} - \text{(5.12)}, \\
& \text{(5.43)} - \text{(5.44)}, \text{(5.46)} - \text{(5.53)} \text{ and (5.56)},
\end{aligned}
\tag{G.1}
$$

where $(\tau, \boldsymbol{\varsigma}, \boldsymbol{\varrho}, \widehat{\tau}, \widehat{\boldsymbol{\varsigma}}, \widehat{\boldsymbol{\varrho}}) \in \mathbb{R} \times \mathbb{R}_+^{|\Xi|} \times \mathbb{R}_+^{|\Xi|} \times \mathbb{R} \times \mathbb{R}_+^{|\Xi|} \times \mathbb{R}_+^{|\Xi|}$ are dual variables.

The DRO formulation under the ellipsoidal ambiguity set is as follows:

$$
\begin{aligned}
\min_{\boldsymbol{x},\boldsymbol{y},\boldsymbol{z},\boldsymbol{v},\boldsymbol{\Psi},\boldsymbol{\vartheta},\theta,\zeta,\widehat{\boldsymbol{\vartheta}},\widehat{\theta},\widehat{\zeta},\mathbf{s},\eta} \quad & \sum_{k\in K}\sum_{l\in L} c_l^{\mathrm{OPEN}} x_{kl} + \sum_{k\in K}\sum_{b\in B} c_b^{\mathrm{INV}} v_{kb} + \sum_{i\in I}\sum_{d\in D}\sum_{k\in K} c_{ki}^{\mathrm{MANA}} z_{idk} + \lambda\eta \\
& + (1-\lambda)\left[U_2(\mathbf{x},\mathbf{y},\mathbf{z},\mathbf{v},\boldsymbol{\Theta}(\xi))^\intercal \mathbf{p^0} + (\boldsymbol{p^0})^\intercal \boldsymbol{\vartheta} + \zeta\right] \\
& + \frac{\lambda}{1-\alpha}[(\mathbf{p}^0)^\intercal \mathbf{s} + \left(\mathbf{p}^0\right)^\intercal \widehat{\boldsymbol{\vartheta}} + \widehat{\zeta}] \\
\text{s.t.} \quad & \|\boldsymbol{A}_1^\intercal \boldsymbol{\vartheta} + \boldsymbol{A}_1^\intercal U_2(\mathbf{x},\mathbf{y},\mathbf{z},\mathbf{v},\boldsymbol{\Theta}(\xi)) - \theta \boldsymbol{A}_1^\intercal \mathbf{e}\|_2 \le \zeta, \\
& \|\boldsymbol{A}_1^\intercal \widehat{\boldsymbol{\vartheta}} + \boldsymbol{A}_1^\intercal \mathbf{s} - \widehat{\theta} \boldsymbol{A}_1^\intercal \mathbf{e}\|_2 \le \widehat{\zeta}, \\
& \mathbf{s} \ge U_2(\mathbf{x},\mathbf{y},\mathbf{z},\mathbf{v},\boldsymbol{\Theta}(\xi)) - \eta \mathbf{e}, \\
& \boldsymbol{\vartheta} \ge \mathbf{0}, \quad \zeta \ge 0, \quad \widehat{\boldsymbol{\vartheta}} \ge \mathbf{0}, \quad \widehat{\zeta} \ge 0, \quad \mathbf{s} \ge 0, \\
& \text{Constraints (5.2)} - \text{(5.5)}, \text{(5.7)} - \text{(5.12)}, \\
& \text{(5.43)} - \text{(5.44)}, \ \text{(5.46)} - \text{(5.53)} \text{ and (5.56)},
\end{aligned}
\tag{G.2}
$$

where $\left(\boldsymbol{\vartheta}, \theta, \zeta, \widehat{\boldsymbol{\vartheta}}, \widehat{\theta}, \widehat{\zeta}\right) \in \mathbb{R}_+^{|\Xi|} \times \mathbb{R} \times \mathbb{R}_+ \times \mathbb{R}_+^{|\Xi|} \times \mathbb{R} \times \mathbb{R}_+$ are Lagrange multipliers.

The DRO formulation under the polyhedral ambiguity set is as follows:

$$
\begin{aligned}
\min_{\boldsymbol{x},\boldsymbol{y},\boldsymbol{z},\boldsymbol{v},\boldsymbol{\Psi},\boldsymbol{\pi},\kappa,\varphi,\widehat{\boldsymbol{\pi}},\widehat{\kappa},\widehat{\varphi},\mathbf{s},\eta} \quad & \sum_{k\in K}\sum_{l\in L} c_l^{\mathrm{OPEN}} x_{kl} + \sum_{k\in K}\sum_{b\in B} c_b^{\mathrm{INV}} v_{kb} + \sum_{i\in I}\sum_{d\in D}\sum_{k\in K} c_{ki}^{\mathrm{MANA}} z_{idk} + \lambda\eta \\
& + (1-\lambda)\left[U_2(\mathbf{x},\mathbf{y},\mathbf{z},\mathbf{v},\boldsymbol{\Theta}(\xi))^{\intercal}\mathbf{p^0} + (\boldsymbol{p^0})^{\intercal}\boldsymbol{\pi} + \varphi\right] \\
& + \frac{\lambda}{1-\alpha}[(\mathbf{p}^0)^{\intercal}\mathbf{s} + \left(\mathbf{p}^0\right)^{\intercal}\widehat{\boldsymbol{\pi}} + \widehat{\varphi}] \\
\text{s.t.} \quad & \|\boldsymbol{A}_2^{\intercal}\boldsymbol{\pi} + \boldsymbol{A}_2^{\intercal}U_2(\mathbf{x},\mathbf{y},\mathbf{z},\mathbf{v},\boldsymbol{\Theta}(\xi)) - \kappa\boldsymbol{A}_2^{\intercal}\mathbf{e}\|_\infty \le \varphi, \\
& \|\boldsymbol{A}_2^{\intercal}\widehat{\boldsymbol{\pi}} + \boldsymbol{A}_2^{\intercal}\mathbf{s} - \widehat{\kappa}\boldsymbol{A}_2^{\intercal}\mathbf{e}\|_\infty \le \widehat{\varphi}, \\
& \mathbf{s} \ge U_2(\mathbf{x},\mathbf{y},\mathbf{z},\mathbf{v},\boldsymbol{\Theta}(\xi)) - \eta\mathbf{e}, \\
& \boldsymbol{\pi} \ge \mathbf{0}, \quad \varphi \ge 0, \quad \widehat{\boldsymbol{\pi}} \ge \mathbf{0}, \quad \widehat{\varphi} \ge 0, \quad \mathbf{s} \ge 0, \\
& \text{Constraints (5.2)} - \text{(5.5)}, \text{(5.7)} - \text{(5.12)}, \\
& \text{(5.43)} - \text{(5.44)}, \ \text{(5.46)} - \text{(5.53) and (5.56)},
\end{aligned}
\tag{G.3}
$$

where $(\boldsymbol{\pi}, \kappa, \varphi, \widehat{\boldsymbol{\pi}}, \widehat{\kappa}, \widehat{\varphi}) \in \mathbb{R}_+^{|\Xi|} \times \mathbb{R} \times \mathbb{R}_+ \times \mathbb{R}_+^{|\Xi|} \times \mathbb{R} \times \mathbb{R}_+$ are Lagrange multipliers.

References

Adulyasak, Y., Cordeau, J.-F., and Jans, R. (2015). Benders decomposition for production routing under demand uncertainty. *Operations Research*, 63(4):851–867. 67, 72, 76, 108

Ahmadi, M., Seifi, A., and Tootooni, B. (2015). A humanitarian logistics model for disaster relief operation considering network failure and standard relief time: A case study on san francisco district. *Transportation Research Part E: Logistics and Transportation Review*, 75:145–163. 12

Akbari, V., Shiri, D., and Salman, F. S. (2021). An online optimization approach to post-disaster road restoration. *Transportation Research Part B: Methodological*, 150:1–25. 2

Al Haddad, C., Chaniotakis, E., Straubinger, A., Plötner, K., and Antoniou, C. (2020). Factors affecting the adoption and use of urban air mobility. *Transportation Research Part A: Policy and Practice*, 132:696–712. 1

Ale-Ahmad, H. and Mahmassani, H. S. (2021). Capacitated location-allocation-routing problem with time windows for on-demand urban air taxi operation. *Transportation Research Record*, 2675(10):1092–1114. 9

Alem, D., Clark, A., and Moreno, A. (2016). Stochastic network models for logistics

planning in disaster relief. *European Journal of Operational Research*, 255(1):187–206. 12

Alvarez, L. E., Jones, J. C., Bryan, A., and Weinert, A. J. (2021). Demand and capacity modeling for advanced air mobility. In *AIAA Aviation 2021 Forum*, page 2381. 52

Avishan, F., Elyasi, M., Yanıkoğlu, İ., Ekici, A., and Özener, O. Ö. (2023). Humanitarian relief distribution problem: An adjustable robust optimization approach. *Transportation Science*. 14

Bakhtavar, E. and Mahmoudi, H. (2020). Development of a scenario-based robust model for the optimal truck-shovel allocation in open-pit mining. *Computers & Operations Research*, 115:104539. 37

Ben-Tal, A., Do Chung, B., Mandala, S. R., and Yao, T. (2011). Robust optimization for emergency logistics planning: Risk mitigation in humanitarian relief supply chains. *Transportation Research Part B: Methodological*, 45(8):1177–1189. 3

Ben-Tal, A. and Nemirovski, A. (2009). On safe tractable approximations of chance-constrained linear matrix inequalities. *Mathematics of Operations Research*, 34(1):1–25. 33

Benders, J. F. (1962). Partitioning procedures for solving mixed-variables programming problems. *Numerische Mathematik*, 4(1):238–252. 76

Bertsimas, D. and Sim, M. (2004). The price of robustness. *Operations Research*, 52(1):35–53. 14

Boyacı, B., Dang, T. H., and Letchford, A. N. (2021). Vehicle routing on road networks: How good is euclidean approximation? *Computers & Operations Research*, 129:105197. 39

Boyd, S. P. and Vandenberghe, L. (2004). *Convex optimization*. Cambridge University Press. 181, 186

Bozorgi-Amiri, A., Jabalameli, M. S., Alinaghian, M., and Heydari, M. (2012). A modified particle swarm optimization for disaster relief logistics under uncertain environment. *The International Journal of Advanced Manufacturing Technology*, 60:357–371. 106

Bravo, R. Z. B., Leiras, A., and Cyrino Oliveira, F. L. (2019). The use of uavs in humanitarian relief: An application of pomdp-based methodology for finding victims. *Production and Operations Management*, 28(2):421–440. 3

Brunelli, M., Ditta, C. C., and Postorino, M. N. (2023). New infrastructures for urban air mobility systems: A systematic review on vertiport location and capacity. *Journal of Air Transport Management*, 112:102460. 20

Caggiani, L., Colovic, A., and Ottomanelli, M. (2020). An equality-based model for bike-sharing stations location in bicycle-public transport multimodal mobility. *Transportation Research Part A: Policy and Practice*, 140:251–265. 10

Çankaya, E., Ekici, A., and Özener, O. Ö. (2019). Humanitarian relief supplies distribution: An application of inventory routing problem. *Annals of Operations Research*, 283:119–141. 160

Chang, Z., Song, S., Zhang, Y., Ding, J.-Y., Zhang, R., and Chiong, R. (2017). Distributionally robust single machine scheduling with risk aversion. *European Journal of Operational Research*, 256(1):261–274. 107

Chauhan, D., Unnikrishnan, A., and Figliozzi, M. (2019). Maximum coverage capacitated facility location problem with range constrained drones. *Transportation Research Part C: Emerging Technologies*, 99:1–18. 16, 69, 91, 112

Chen, B. Y., Wang, Y., Wang, D., and Lam, W. H. (2019). Understanding travel time uncertainty impacts on the equity of individual accessibility. *Transportation Research Part D: Transport and Environment*, 75:156–169. 22

Chen, H., Hu, Z., and Solak, S. (2021). Improved delivery policies for future drone-based delivery systems. *European Journal of Operational Research*, 294(3):1181–1201. 112, 114

Chen, L., Wandelt, S., Dai, W., and Sun, X. (2022). Scalable vertiport hub location selection for air taxi operations in a metropolitan region. *INFORMS Journal on Computing*, 34(2):834–856. 2, 8

Chen, Q., Fu, C., Zhu, N., Ma, S., and He, Q.-C. (2023). A target-based optimization model for bike-sharing systems: From the perspective of service efficiency and equity. *Transportation Research Part B: Methodological*, 167:235–260. 10, 22, 28

Chen, Y. and Liu, Y. (2023). Integrated optimization of planning and operations for shared autonomous electric vehicle systems. *Transportation Science*, 57(1):106–134. 3, 27

Cheng, J., Feng, X., and Bai, X. (2021). Modeling equitable and effective distribution problem in humanitarian relief logistics by robust goal programming. *Computers & Industrial Engineering*, 155:107183. 160

Chern, C.-C., Chen, Y.-L., and Kung, L.-C. (2010). A heuristic relief transportation planning algorithm for emergency supply chain management. *International Journal of Computer Mathematics*, 87(7):1638–1664. 84

Chin, C., Gopalakrishnan, K., Egorov, M., Evans, A., and Balakrishnan, H. (2021). Efficiency and fairness in unmanned air traffic flow management. *IEEE Transactions on Intelligent Transportation Systems*, 22(9):5939–5951. 11

Chin, C., Saravanan, A., Balakrishnan, H., and Andreeva-Mori, A. (2023). Strategic planning of aerial assets for disaster response: Enabling efficient and equitable access to drone-based search resources. In *15th USA/Europe Air Traffic Management Research and Development Seminar (ATM2023)*. 11

Chowdhury, S., Emelogu, A., Marufuzzaman, M., Nurre, S. G., and Bian, L. (2017). Drones for disaster response and relief operations: A continuous approximation model. *International Journal of Production Economics*, 188:167–184. 3

Clarke, D. (2022). Vertiport or vertistop? the answer may surprise you. https://aerocarjournal.com/vertiport-or-vertistop/. 21

Coppola, P., De Fabiis, F., and Silvestri, F. (2024). Urban air mobility (uam): Airport shuttles or city-taxis? *Transport Policy*, 150:24–34. 1

Crabtree, J. (2021). Drones delivering vaccines to help fight coronavirus. https://www.coverdrone.com/ca/drones-delivering-vaccines-to-help-fight-coronavirus/. 3

Dai, W., Pang, B., and Low, K. H. (2021). Conflict-free four-dimensional path planning for urban air mobility considering airspace occupancy. *Aerospace Science and Technology*, 119:107154. 52

Delage, E. and Ye, Y. (2010). Distributionally robust optimization under moment uncertainty with application to data-driven problems. *Operations Research*, 58(3):595–612. 14

Demir, E., Bektaş, T., and Laporte, G. (2014). The bi-objective pollution-routing problem. *European Journal of Operational Research*, 232(3):464–478. 32

Dukkanci, O., Koberstein, A., and Kara, B. Y. (2023). Drones for relief logistics

under uncertainty after an earthquake. *European Journal of Operational Research*, 310(1):117–132. 16

Duran, S., Gutierrez, M. A., and Keskinocak, P. (2011). Pre-positioning of emergency items for care international. *Interfaces*, 41(3):223–237. 147

Elçi, Ö. and Noyan, N. (2018). A chance-constrained two-stage stochastic programming model for humanitarian relief network design. *Transportation Research Part B: Methodological*, 108:55–83. 12, 69, 107, 113

Farahani, R. Z., Lotfi, M., Baghaian, A., Ruiz, R., and Rezapour, S. (2020). Mass casualty management in disaster scene: A systematic review of or&ms research in humanitarian operations. *European Journal of Operational Research*, 287(3):787–819. 3, 160

Feitelson, E. (2002). Introducing environmental equity dimensions into the sustainable transport discourse: issues and pitfalls. *Transportation Research Part D: Transport and Environment*, 7(2):99–118. 22

Feng, Y., Chen, Y., and Liu, Y. (2023). Optimising two-stage robust supplier selection and order allocation problem under risk-averse criterion. *International Journal of Production Research*, 61(19):6356–6380. 107

Figliozzi, M. A. (2017). Lifecycle modeling and assessment of unmanned aerial vehicles (drones) co2e emissions. *Transportation Research Part D: Transport and Environment*, 57:251–261. 84

Garrow, L. A., German, B. J., and Leonard, C. E. (2021). Urban air mobility: A comprehensive review and comparative analysis with autonomous and electric ground transportation for informing future research. *Transportation Research Part C: Emerging Technologies*, 132:103377. 4

Ghelichi, Z., Gentili, M., and Mirchandani, P. B. (2022). Drone logistics for uncertain demand of disaster-impacted populations. *Transportation Research Part C: Emerging Technologies*, 141:103735. 15, 16

Goh, J. and Sim, M. (2010). Distributionally robust optimization and its tractable approximations. *Operations Research*, 58(4-part-1):902–917. 14

Golabi, M. and Nejad, M. G. (2022). Intelligent and fuzzy uav transportation applications in aviation 4.0. *Intelligent and Fuzzy Techniques in Aviation 4.0: Theory and Applications*, pages 431–458. 114

Gong, Z., Zhang, F., Liu, W., and Graham, D. J. (2023). On the effects of airport capacity expansion under responsive airlines and elastic passenger demand. *Transportation Research Part B: Methodological*, 170:48–76. 4

Gonzalez, C. J. D. (2020). Rooftop-place suitability analysis for urban air mobility hubs: a gis and neural network approach. Master's thesis, Universidade NOVA de Lisboa (Portugal). 8

Gorissen, B. L., Yanıkoğlu, İ., and den Hertog, D. (2015). A practical guide to robust optimization. *Omega*, 53:124–137. 14

Gu, R., Liu, Y., and Poon, M. (2023). Dynamic truck–drone routing problem for scheduled deliveries and on-demand pickups with time-related constraints. *Transportation Research Part C: Emerging Technologies*, 151:104139. 4

Guan, Z., Mou, Y., and Sun, M. (2022). Hybrid robust and stochastic optimization for a capital-constrained fresh product supply chain integrating risk-aversion behavior and financial strategies. *Computers & Industrial Engineering*, 169:108224. 107

Guan, Z., Mou, Y., and Zhang, J. (2024). Incorporating risk aversion and time preference into omnichannel retail operations considering assortment and inventory op-

timization. *European Journal of Operational Research*, 314:579–596. 107, 124, 130, 135

Guo, Y., Hu, M., Zou, B., Hansen, M., Zhang, Y., and Xie, H. (2022a). Air traffic flow management integrating separation management and ground holding: An efficiency-equity bi-objective perspective. *Transportation Research Part B: Methodological*, 155:394–423. 10, 30, 34

Guo, Z., Hao, M., Liu, J., Yu, B., and Jiang, Y. (2022b). Joint routing and charging optimization for evtol aircraft recovery. *Aerospace Science and Technology*, 126:107595. 27

Haan, J., Garrow, L. A., Marzuoli, A., Roy, S., and Bierlaire, M. (2021). Are commuter air taxis coming to your city? a ranking of 40 cities in the united states. *Transportation Research Part C: Emerging Technologies*, 132:103392. 4

He, X., He, F., Li, L., Zhang, L., and Xiao, G. (2022). A route network planning method for urban air delivery. *Transportation Research Part E: Logistics and Transportation Review*, 166:102872. 10

Hong, I., Kuby, M., and Murray, A. T. (2018). A range-restricted recharging station coverage model for drone delivery service planning. *Transportation Research Part C: Emerging Technologies*, 90:198–212. 112

Hu, S., Han, C., Dong, Z. S., and Meng, L. (2019). A multi-stage stochastic programming model for relief distribution considering the state of road network. *Transportation Research Part B: Methodological*, 123:64–87. 12

Hu, S., Hu, Q., Tao, S., and Dong, Z. S. (2023a). A multi-stage stochastic programming approach for pre-positioning of relief supplies considering returns. *Socio-Economic Planning Sciences*, 88:101617. 13

Hu, S.-L., Han, C.-F., and Meng, L.-P. (2017). Stochastic optimization for joint decision making of inventory and procurement in humanitarian relief. *Computers & Industrial Engineering*, 111:39–49. 12

Hu, Y., Li, S., Wang, Y., Zhang, H., Wei, Y., and Yang, L. (2023b). Robust metro train scheduling integrated with skip-stop pattern and passenger flow control strategy under uncertain passenger demands. *Computers & Operations Research*, 151:106116. 37

Jin, Z., Ng, K. K., and Zhang, C. (2024a). Robust optimisation for vertiport location problem considering travel mode choice behaviour in urban air mobility systems. *Journal of the Air Transport Research Society*, 2:100006. 1

Jin, Z., Ng, K. K., Zhang, C., Liu, W., Zhang, F., and Xu, G. (2024b). A risk-averse distributionally robust optimisation approach for drone-supported relief facility location problem. *Transportation Research Part E: Logistics and Transportation Review*, 186:103538. 93

Johnson, W. and Silva, C. (2022). Nasa concept vehicles and the engineering of advanced air mobility aircraft. *The Aeronautical Journal*, 126(1295):59–91. 1

Kandavel, S. (2023). Drones from tamil nadu head to turkey for rescue efforts, medicine supply. https://www.thehindu.com/news/national/tamil-nadu/drones-from-tamil-nadu-head-to-turkey-for-rescue-operations/article66484987.ece. 3

Kim, D., Lee, K., and Moon, I. (2019). Stochastic facility location model for drones considering uncertain flight distance. *Annals of Operations Research*, 283:1283–1302. 16, 96, 112

Kleinbekman, I. C., Mitici, M. A., and Wei, P. (2018). evtol arrival sequencing and

scheduling for on-demand urban air mobility. In *2018 IEEE/AIAA 37th Digital Avionics Systems Conference (DASC)*, pages 1–7. IEEE. 10

Kovács, G. and Spens, K. (2009). Identifying challenges in humanitarian logistics. *International Journal of Physical Distribution & Logistics Management*, 39(6):506–528. 2

Lebcir, R. M. and Roy, P. (2023). Impact of coordination on post-earthquake last mile relief distribution operations in india. *International Journal of Emergency Management*, 18(3):293–316. 2

Leung, S. C., Tsang, S. O., Ng, W.-L., and Wu, Y. (2007). A robust optimization model for multi-site production planning problem in an uncertain environment. *European Journal of Operational Research*, 181(1):224–238. 37

Li, G., Luo, T., and Song, Y. (2022). Spatial equity analysis of urban public services for electric vehicle charging—implications of chinese cities. *Sustainable Cities and Society*, 76:103519. 22

Li, S., Egorov, M., and Kochenderfer, M. J. (2020). Analysis of fleet management and infrastructure constraints in on-demand urban air mobility operations. In *AIAA Aviation 2020 Forum*, page 2907. 9

Li, X., Peng, Y., Tian, Q., Feng, T., Wang, W., Cao, Z., and Song, X. (2023). A decomposition-based optimization method for integrated vehicle charging and operation scheduling in automated container terminals under fast charging technology. *Transportation Research Part E: Logistics and Transportation Review*, 180:103338. 39

Lim, E. and Hwang, H. (2019). The selection of vertiport location for on-demand mobility and its application to seoul metro area. *International Journal of Aeronautical and Space Sciences*, 20:260–272. 8

Ling, A., Sun, J., Xiu, N., and Yang, X. (2017). Robust two-stage stochastic linear optimization with risk aversion. *European Journal of Operational Research*, 256(1):215–229. 124

Lu, Y., Yang, C., and Yang, J. (2022). A multi-objective humanitarian pickup and delivery vehicle routing problem with drones. *Annals of Operations Research*, 319(1):291–353. 15

Luan, F., Zhang, W., and Liu, Y. (2022). Robust international portfolio optimization with worst-case mean-cvar. *European Journal of Operational Research*, 303(2):877–890. 121

Mahmutoğulları, A. İ., Çavuş, Ö., and Aktürk, M. S. (2018). Bounds on risk-averse mixed-integer multi-stage stochastic programming problems with mean-cvar. *European Journal of Operational Research*, 266(2):595–608. 121

Manopiniwes, W. and Irohara, T. (2017). Stochastic optimisation model for integrated decisions on relief supply chains: preparedness for disaster response. *International Journal of Production Research*, 55(4):979–996. 12

Mavrotas, G. (2009). Effective implementation of the ε-constraint method in multi-objective mathematical programming problems. *Applied Mathematics and Computation*, 213(2):455–465. 32

Meier, P. (2014). Humanitarian in the sky: drones for disaster response. *Virgin blog.* 3

Mirzapour Al-E-Hashem, S., Malekly, H., and Aryanezhad, M. B. (2011). A multi-objective robust optimization model for multi-product multi-site aggregate production planning in a supply chain under uncertainty. *International Journal of Production Economics*, 134(1):28–42. 37

Moreno, A., Alem, D., Ferreira, D., and Clark, A. (2018). An effective two-stage stochastic multi-trip location-transportation model with social concerns in relief supply chains. *European Journal of Operational Research*, 269(3):1050–1071. 11

Moshref-Javadi, M. and Winkenbach, M. (2021). Applications and research avenues for drone-based models in logistics: A classification and review. *Expert Systems with Applications*, 177:114854. 3

Mulvey, J. M., Vanderbei, R. J., and Zenios, S. A. (1995). Robust optimization of large-scale systems. *Operations Research*, 43(2):264–281. 36

Najy, W., Archetti, C., and Diabat, A. (2023). Collaborative truck-and-drone delivery for inventory-routing problems. *Transportation Research Part C: Emerging Technologies*, 146:103791. 15

Ni, W., Shu, J., and Song, M. (2018). Location and emergency inventory pre-positioning for disaster response operations: Min-max robust model and a case study of yushu earthquake. *Production and Operations Management*, 27(1):160–183. 14

Noyan, N. (2012a). Risk-averse two-stage stochastic programming with an application to disaster management. *Computers & Operations Research*, 39(3):541–559. 84

Noyan, N. (2012b). Two-stage stochastic programming involving cvar with an application to disaster management. *Computers & Operations Research*, 39(3):541–559. 121, 130, 133

Noyan, N., Rudolf, G., and Lejeune, M. (2022). Distributionally robust optimization under a decision-dependent ambiguity set with applications to machine scheduling and humanitarian logistics. *INFORMS Journal on Computing*, 34(2):729–751. 3

Oksuz, M. K. and Satoglu, S. I. (2020). A two-stage stochastic model for location

planning of temporary medical centers for disaster response. *International Journal of Disaster Risk Reduction*, 44:101426. 13

Paul, J. A. and Zhang, M. (2019). Supply location and transportation planning for hurricanes: A two-stage stochastic programming framework. *European Journal of Operational Research*, 274(1):108–125. 12

Preis, L. (2021). Quick sizing, throughput estimating and layout planning for vtol aerodromes–a methodology for vertiport design. In *AIAA Aviation 2021 Forum*, page 2372. 21

Purtell, C., Hong, S.-J., and Hiatt, B. (2024). Bibliometric analysis on advanced air mobility and drones. *Journal of Air Transport Management*, 116:102569. 2

Qiu, R., Shang, J., and Huang, X. (2014). Robust inventory decision under distribution uncertainty: A cvar-based optimization approach. *International Journal of Production Economics*, 153:13–23. 124, 130

Rabta, B., Wankmüller, C., and Reiner, G. (2018). A drone fleet model for last-mile distribution in disaster relief operations. *International Journal of Disaster Risk Reduction*, 28:107–112. 16

Rajendran, S. and Srinivas, S. (2020). Air taxi service for urban mobility: A critical review of recent developments, future challenges, and opportunities. *Transportation Research Part E: Logistics and Transportation Review*, 143:102090. 20, 21

Rath, S. and Chow, J. Y. (2022). Air taxi skyport location problem with single-allocation choice-constrained elastic demand for airport access. *Journal of Air Transport Management*, 105:102294. 9, 27

Rath, S., Gendreau, M., and Gutjahr, W. J. (2016). Bi-objective stochastic program-

ming models for determining depot locations in disaster relief operations. *International Transactions in Operational Research*, 23(6):997–1023. 12

Rimjha, M., Hotle, S., Trani, A., and Hinze, N. (2021). Commuter demand estimation and feasibility assessment for urban air mobility in northern california. *Transportation Research Part A: Policy and Practice*, 148:506–524. 9, 34

Rockafellar, R. T. and Uryasev, S. (2002). Conditional value-at-risk for general loss distributions. *Journal of Banking & Finance*, 26(7):1443–1471. 121, 173

Ruiz, M., Segui-Pons, J. M., and Mateu-LLadó, J. (2017). Improving bus service levels and social equity through bus frequency modelling. *Journal of Transport Geography*, 58:220–233. 10

Shao, J., Xu, Y., Sun, L., Kong, D., and Lu, H. (2022). Equity-oriented integrated optimization of train timetable and stop plans for suburban railways system. *Computers & Industrial Engineering*, 173:108721. 11

Shavarani, S. M., Nejad, M. G., Rismanchian, F., and Izbirak, G. (2018). Application of hierarchical facility location problem for optimization of a drone delivery system: A case study of amazon prime air in the city of san francisco. *The International Journal of Advanced Manufacturing Technology*, 95:3141–3153. 130

Shehadeh, K. S. and Tucker, E. L. (2022). Stochastic optimization models for location and inventory prepositioning of disaster relief supplies. *Transportation Research Part C: Emerging Technologies*, 144:103871. 15, 84, 129

Shin, H., Lee, T., and Lee, H.-R. (2022). Skyport location problem for urban air mobility system. *Computers & Operations Research*, 138:105611. 8

Shu, J., Song, M., Wang, B., Yang, J., and Zhu, S. (2023). Humanitarian relief network

design: Responsiveness maximization and a case study of typhoon rammasun. *IISE Transactions*, 55(3):301–313. 12, 65

Siddig, M. and Song, Y. (2021). A multistage stochastic programming model for hurricane relief logistics planning. In *Proceedings of the 2021 IISE Annual Conference*. 13

Song, K. and Yeo, H. (2021). Development of optimal scheduling strategy and approach control model of multicopter vtol aircraft for urban air mobility (uam) operation. *Transportation Research Part C: Emerging Technologies*, 128:103181. 10

Straubinger, A., Rothfeld, R., Shamiyeh, M., Büchter, K.-D., Kaiser, J., and Plötner, K. O. (2020). An overview of current research and developments in urban air mobility–setting the scene for uam introduction. *Journal of Air Transport Management*, 87:101852. 8

Sun, H., Li, J., Wang, T., and Xue, Y. (2022). A novel scenario-based robust bi-objective optimization model for humanitarian logistics network under risk of disruptions. *Transportation Research Part E: Logistics and Transportation Review*, 157:102578. 35, 36

Sun, H., Wang, Y., and Xue, Y. (2021). A bi-objective robust optimization model for disaster response planning under uncertainties. *Computers & Industrial Engineering*, 155:107213. 14

Sun, X., Wandelt, S., and Stumpf, E. (2018). Competitiveness of on-demand air taxis regarding door-to-door travel time: A race through europe. *Transportation Research Part E: Logistics and Transportation Review*, 119:1–18. 1

Tang, L., Li, Y., Bai, D., Liu, T., and Coelho, L. C. (2022). Bi-objective optimization for a multi-period covid-19 vaccination planning problem. *Omega*, 110:102617. 32

Tiketi (2025). Joby aviation pricing in dubai: What to expect for the future of air mobility. https://tiketi.com/fr-fr/tips-and-inspiration/joby-aviation-pricing-in-dubai/. 39

Tofighi, S., Torabi, S. A., and Mansouri, S. A. (2016). Humanitarian logistics network design under mixed uncertainty. *European Journal of Operational Research*, 250(1):239–250. 11, 93

Tricoire, F., Graf, A., and Gutjahr, W. J. (2012). The bi-objective stochastic covering tour problem. *Computers & Operations Research*, 39(7):1582–1592. 108

Vascik, P. D. and Hansman, R. J. (2018). Scaling constraints for urban air mobility operations: Air traffic control, ground infrastructure, and noise. In *2018 Aviation Technology, Integration, and Operations Conference*, page 3849. 9

Vascik, P. D., Hansman, R. J., and Dunn, N. S. (2018). Analysis of urban air mobility operational constraints. *Journal of Air Transportation*, 26(4):133–146. 9

Veytia, A. M., Badea, C. A., Ellerbroek, J., Hoekstra, J., Patrinopoulou, N., Daramouskas, I., Lappas, V., Kostopoulos, V., De Vries, V., van Ham, J., et al. (2022). Metropolis ii: Benefits of centralised separation management in high-density urban airspace. In *12th SESAR Innovation Days*. 10

Wang, B., Deng, W., Tan, Z., Zhang, B., and Chen, F. (2024). A two-stage stochastic optimization for disaster rescue resource distribution considering multiple disasters. *Engineering Optimization*, 56(1):1–17. 13

Wang, B. C., Qian, Q. Y., Gao, J. J., Tan, Z. Y., and Zhou, Y. (2021a). The optimization of warehouse location and resources distribution for emergency rescue under uncertainty. *Advanced Engineering Informatics*, 48:101278. 3

Wang, D., Yang, K., and Yang, L. (2023a). Risk-averse two-stage distributionally robust optimisation for logistics planning in disaster relief management. *International Journal of Production Research*, 61(2):668–691. 107, 124

Wang, D., Yang, K., Yang, L., and Dong, J. (2023b). Two-stage distributionally robust optimization for disaster relief logistics under option contract and demand ambiguity. *Transportation Research Part E: Logistics and Transportation Review*, 170:103025. 120

Wang, D., Yang, K., Yang, L., and Li, S. (2022a). Distributional robustness and lateral transshipment for disaster relief logistics planning under demand ambiguity. *International Transactions in Operational Research*. 14

Wang, K., Jacquillat, A., and Vaze, V. (2022b). Vertiport planning for urban aerial mobility: An adaptive discretization approach. *Manufacturing & Service Operations Management*, 24(6):3215–3235. 9, 21, 26, 28

Wang, K., Li, A., and Qu, X. (2023). Urban aerial mobility: Network structure, transportation benefits, and sino-us comparison. *The Innovation*, 4(2). 2

Wang, K. and Qu, X. (2023). Urban aerial mobility: Reshaping the future of urban transportation. *The Innovation*, 4(2). 2, 27

Wang, Q. and Nie, X. (2022). A stochastic programming model for emergency supply planning considering transportation network mitigation and traffic congestion. *Socio-Economic Planning Sciences*, 79:101119. 12, 65

Wang, W., Yang, K., Yang, L., and Gao, Z. (2021b). Two-stage distributionally robust programming based on worst-case mean-cvar criterion and application to disaster relief management. *Transportation Research Part E: Logistics and Transportation Review*, 149:102332. 107, 124

Wang, X., Kuo, Y.-H., Shen, H., and Zhang, L. (2021c). Target-oriented robust location–transportation problem with service-level measure. *Transportation Research Part B: Methodological*, 153:1–20. 33

Wang, Z., Delahaye, D., Farges, J.-L., and Alam, S. (2022c). Complexity optimal air traffic assignment in multi-layer transport network for urban air mobility operations. *Transportation Research Part C: Emerging Technologies*, 142:103776. 10

Wang, Z. and Sheu, J.-B. (2019). Vehicle routing problem with drones. *Transportation Research Part B: Methodological*, 122:350–364. 84

Wu, J., Liu, M., Sun, H., Li, T., Gao, Z., and Wang, D. Z. (2015). Equity-based timetable synchronization optimization in urban subway network. *Transportation Research Part C: Emerging Technologies*, 51:1–18. 10

Wu, Y., Wang, S., Zhen, L., Laporte, G., Tan, Z., and Wang, K. (2023). How to operate ship fleets under uncertainty. *Production and Operations Management*, 32(10):3043–3061. 72, 76, 101

Wu, Z. and Zhang, Y. (2021). Integrated network design and demand forecast for on-demand urban air mobility. *Engineering*, 7(4):473–487. 9

Xu, J., Wang, Z., Zhang, M., and Tu, Y. (2016). A new model for a 72-h post-earthquake emergency logistics location-routing problem under a random fuzzy environment. *Transportation Letters*, 8(5):270–285. 140

Yahyaei, M. and Bozorgi-Amiri, A. (2019). Robust reliable humanitarian relief network design: an integration of shelter and supply facility location. *Annals of Operations Research*, 283(1-2):897–916. 14

Yang, K., Lu, Y., Yang, L., and Gao, Z. (2021a). Distributionally robust last-train

coordination planning problem with dwell time adjustment strategy. *Applied Mathematical Modelling*, 91:1154–1174. 33

Yang, M., Kumar, S., Wang, X., and Fry, M. J. (2021b). Scenario-robust pre-disaster planning for multiple relief items. *Annals of Operations Research*, pages 1–26. 155

Yang, Y., Yin, Y., Wang, D., Ignatius, J., Cheng, T., and Dhamotharan, L. (2023). Distributionally robust multi-period location-allocation with multiple resources and capacity levels in humanitarian logistics. *European Journal of Operational Research*, 305(3):1042–1062. 15, 84

Yi, W., Sutrisna, M., and Wang, H. (2021). Unmanned aerial vehicle based low carbon monitoring planning. *Advanced Engineering Informatics*, 48:101277. 3

Yin, F., Chen, Y., Song, F., and Liu, Y. (2019). A new distributionally robust p-hub median problem with uncertain carbon emissions and its tractable approximation method. *Applied Mathematical Modelling*, 74:668–693. 33

Yin, F., Liu, Y., and Chen, Y. (2023a). Distributionally robust optimisation model for multi-objective hub location problem via considering ambiguousness. *Transportmetrica A: Transport Science*, 19(3):2094494. 33

Yin, Y., Yang, Y., Yu, Y., Wang, D., and Cheng, T. (2023b). Robust vehicle routing with drones under uncertain demands and truck travel times in humanitarian logistics. *Transportation Research Part B: Methodological*, 174:102781. 3, 15

Yu, C.-S. and Li, H.-L. (2000). A robust optimization model for stochastic logistic problems. *International Journal of Production Economics*, 64(1-3):385–397. 37

Zahiri, B., Torabi, S. A., and Tavakkoli-Moghaddam, R. (2017). A novel multi-stage possibilistic stochastic programming approach (with an application in relief distribution planning). *Information Sciences*, 385:225–249. 13

Zhang, G., Zhu, N., Ma, S., and Xia, J. (2021). Humanitarian relief network assessment using collaborative truck-and-drone system. *Transportation Research Part E: Logistics and Transportation Review*, 152:102417. 2, 15

Zhang, P., Liu, Y., Yang, G., and Zhang, G. (2022). A multi-objective distributionally robust model for sustainable last mile relief network design problem. *Annals of Operations Research*, pages 1–42. 14

Zhao, Y. and Feng, T. (2025). Commuter choice of uam-friendly neighborhoods. *Transportation Research Part A: Policy and Practice*, 192:104338. 2

Zhao, Y., Hu, Y., and Feng, T. (2025). Exploring the integration of urban air mobility into mobility-as-a-service: A stated preference analysis of commuters. *Travel Behaviour and Society*, 39:100990. 2

Zhong, S., Cheng, R., Jiang, Y., Wang, Z., Larsen, A., and Nielsen, O. A. (2020). Risk-averse optimization of disaster relief facility location and vehicle routing under stochastic demand. *Transportation Research Part E: Logistics and Transportation Review*, 141:102015. 106

Zhu, S. and Fukushima, M. (2009). Worst-case conditional value-at-risk with application to robust portfolio management. *Operations Research*, 57(5):1155–1168. 107, 124, 172

Zhu, T., Boyles, S. D., and Unnikrishnan, A. (2022). Two-stage robust facility location problem with drones. *Transportation Research Part C: Emerging Technologies*, 137:103563. 16, 69, 84, 112, 129

Ziakkas, D. and Natakusuma, H. C. (2025). Advanced air mobility (aam) and emergency services: The association of southeast asian nations (asean) case study. *Journal of Air Transport Management*, 126:102787. 2

Zografos, K. G. and Jiang, Y. (2019). A bi-objective efficiency-fairness model for scheduling slots at congested airports. *Transportation Research Part C: Emerging Technologies*, 102:336–350. 10, 30, 34